UNIVERSITÉ DE LORRAINE | BIBLIOTHÈQUES UNIVERSITAIRES

AVERTISSEMENT
DROIT D'AUTEUR

Ce document est le fruit d'un long travail approuvé par le jury de soutenance et mis à disposition de l'ensemble de la communauté universitaire élargie.

Il est soumis à la propriété intellectuelle de l'auteur. Ceci implique une obligation de citation et de référencement lors de l'utilisation de ce document. Toute contrefaçon, plagiat ou reproduction illicite encourt une poursuite pénale.

Contact bibliothèque : ddoc-theses-contact@univ-lorraine.fr
(Cette adresse ne permet pas de contacter les auteurs)

Code de la Propriété Intellectuelle. articles L 122. 4
Code de la Propriété Intellectuelle. articles L 335.2- L 335.10

UNIVERSITÉ DE LORRAINE
34 COURS LÉOPOLD — CS 25233
54052 NANCY CEDEX
WWW.UNIV-LORRAINE.FR

UNIVERSITÉ DE LORRAINE

Ecole Doctorale BioSE
Laboratoire IMoPA

Thèse

Présentée et soutenue publiquement pour l'obtention du titre de

DOCTEUR DE l'UNIVERSITE DE LORRAINE

Mention : Sciences de la Vie et de la Santé

par **Mireille TABIKH**

Sous la direction de Laurent KOESSLER

Étude instrumentale et électrophysiologique de l'impact de la stimulation électrique transcrânienne sur la reconnaissance visuelle chez l'être humain

Le 23 Septembre 2025 à Nancy

Membres du Jury :

Directeur de thèse:	**M. Laurent KOESSLER**	**Directeur de recherche, IMoPA, Nancy**
Président de jury: et rapporteur	**M. Jean-Pascal LEFAUCHEUR**	**Professeur, Université de Paris-Est Créteil, Créteil**
Rapporteurs:	**Mme. Andrea ANTAL**	**Professeur, Centre Médical Universitaire De Göttingen, Göttingen**
Examinateurs:	**Mme. Susana FERRAO SANTOS**	**Professeur, Université Catholique De Louvain, Bruxelles**
	Mme. Ghina HARIKA-GERMANEAU	**Maitre de Conférences, Université De Poitiers, Poitiers**
Membre invité:	**M. Bruno ROSSION**	**Directeur de recherche, IMoPA, Nancy**

Instrumental and Electrophysiological studies of transcranial electrical stimulations impact on visual recognition in humans

Acknowledgements

First and foremost, I would like to express my heartfelt gratitude to all the people who helped me, encouraged me, and supported me through this four-year doctoral journey.

To begin with, I would like to express my deepest gratitude to my thesis reviewers, Pr. Andrea Antal and Pr. Jean-Pascale LeFaucheur, for taking the time to examine my manuscript and share their valuable insight. I extend special thanks to Pr. Lefaucheur for his kind, supportive, and motivating remarks during the committee meetings, as well as for the insightful exchanges we had on those occasions. I would also like to warmly thank Dr. Ghina Harika-Germaneau and Pr. Susana Ferrao Santos for accepting the examination of my work and for contributing to the defense of my thesis.

I would like to express my appreciation to my thesis supervisor, Dr. Laurent Koessler, for giving me the opportunity to work on such an interesting and challenging research topic. Thank you for your guidance and your expertise, and your insight throughout the course of this project.

I would next like to express my deepest appreciation to the team of the Epileptology Unit led by Prof. Louis Maillard at the CHRU of Nancy. My gratitude goes to all the physicians, and especially to Prof. Louis Maillard himself, for his guidance and for giving research a prominent place within the unit. I would like to extend my sincerest thanks to the nurses of the unit for their kindness, support, and for always being helpful and welcoming throughout my time at the hospital. I am also deeply grateful to the patients who agreed to participate in my experiments; this project would not have been possible without their contribution.

I would like to express my greatest appreciation to all the ERCN team, especially to Dr. Bruno Rossion, for his insightful guidance in my research. His contributions were instrumental in shaping my critical thinking and deepening my understanding of the field. I would like to thank Jacques Jonas for his valuable support in advancing this work. Thanks to Tal for her constant encouragement and motivation, always celebrating even the smallest wins along the way.

To my colleagues, I am grateful for the endless coffee breaks, valuable discussions, and eternal memories we've created. Without you, this experience wouldn't have been as memorable as it was. A special thanks to Marion and Justine, not only were they my first colleagues but also my first ever friends in the laboratory and in France. Your friendship will always hold a very special place in my heart. Thanks to my office mate, Luna, for patiently listening to my endless complaints and sharing countless wonderful conversations. Thanks to Begüm for being the sweetest heart, your kindness, support, and genuine spirit mean more to me than words can describe. Thanks to Marie-Alphée for your support

and for inspiring me with your elegance and intelligence. Thanks to Marua and Alexandros for the touch of youth they added to the lab, I've known you short but greatly indeed. Thanks to Ridvan for the wonderful scientific discussion we've shared. I would also like to thank my former colleague, Tom, for his invaluable help during the testing and for his continued support throughout this project. I am deeply thankful to Dr. Samuel Louviot for his guidance at the start of my PhD journey. His insights into the field and unwavering support have been invaluable in helping me navigate this path.

I would like to express my sincerest gratitude to the entire team at Bioserenity for their generous financial support, which made this project possible. I extend special thanks to Hélène and Julie for their invaluable guidance and insightful expertise regarding testing with the Neuronaute, as well as for their steadfast assistance throughout the process, even from afar. I am also grateful to my colleagues at Bioserenity for their collaboration, which greatly enriched this experience.

Thanks to all the friends in Nancy who have made this little city feel like home. Thanks to Marilyne for your endless support and wise words, they have been a constant source of comfort and strength. Jana, we walked the same path, shared the struggles, and made plenty of memories along the way. Marie-Paul and Aya, your fun spirits and lighthearted conversations have brightened countless days. To Maeva, thank you for helping me take my mind off work and for always offering a listening ear when I needed it most.

My friends from university who shared my dreams and followed the same path as me. I was honored to watch you become doctors over the years and share your success. To Charbel, thank you for always being there when I needed you, for the long phone calls filled with laughter, tears, and lots of discussions. Johny, seeing you evolve and finding your path has been truly inspiring. To Christine and Baddih, having you in my life has been one of my greatest joys. Thank you for your wise support, your kindness, the countless memories over the years, and the warmth you bring.

To Dado, my sunshine in a human form, we've experienced countless places and new adventures in so little time. I'm truly grateful for every moment, and I can't wait to create many more memories in new places together.

To my childhood friends Issam, Maha, Tatiana, and Ward, whom I've known for over 20 years, thank you for always being there and for your unwavering support. It has truly been one of life's greatest pleasures to walk this journey with you by my side, no matter the distance that separates us.

To Momo, words cannot fully describe how grateful I am to have you in my life. Truly, some of life's greatest blessings come in the form of very special people.

To my family, thank you for being my anchor, the ones I could always lean on when things got tough. My beautiful Mom and Dad, thank you for raising me with so much love and warmth and with values that shape who I am today. Everything I am or ever hope to be, I owe it all to you. To Karim, the warmest and sweetest heart, thank you for never failing to make me laugh and helping me forget all the hard times. To Mahmoud and Farah, and baby Amar, thank you for being my piece of home away from home. Thank you for bringing a little bit of your family's warmth and love wherever you go.

To my family away in Lebanon, Taita, Sousou, Mimo, Maro, Natho, and Zein, thank you for always welcoming me with the warmest hearts and making me feel as if I never left home. To my grandma, thank you for being my second mother. I hope I have made you proud.

And finally, I would like to thank Allah for all the blessings he has given me over these years. I thank Him for it all, the good and the bad, during this journey. Throughout these four years, a verse from the Qur'an has been a constant source of strength whenever I felt weak or doubtful, when I was no longer able to continue: "لا يُكلِّفُ الله نفساً إلا وسعها", which translates to:" Allah burdens no soul beyond that it can bear". I kept reminding myself of another beautiful truth: ما زرعَ اللهُ في قلبِكَ رغبةً في الوصُول لأمرٍ معيَّن إلا لأنه يعلمُ أنك ستصلُ , which translates to: What Allah planted in your heart as a desire to reach something was only because He knows you will get there.

Abstract

Transcranial direct current stimulation (tDCS) is a noninvasive brain stimulation technique that gained prominence for its potential in cognitive rehabilitation. It's based on injecting a direct current of low intensity via two electrodes placed on the surface of the scalp to modulate cortical excitability. Despite its widespread use and accessibility, the efficacy of tDCS in humans remains debated, largely due to uncertainties regarding the ability of the applied current to reach and influence targeted brain structures. Recent *in vivo* human studies combining tDCS with intracerebral EEG (iEEG) recordings have demonstrated that electric fields generated by tDCS can reach both cortical and deep brain regions. Nonetheless, the precise neurophysiological mechanisms underlying tDCS remain unclear, particularly concerning its effects on human electrophysiological activity. To date, a definitive quantification of tDCS-induced electrophysiological modulation in humans is lacking. While Electroencephalography (EEG) offers high temporal resolution to monitor brain activity, studies using scalp EEG and event-related potentials have reported limited reliability and only indirect evidence of tDCS neuromodulation.

The primary objective of this thesis is to address a fundamental gap in the field of tDCS, namely, the limited mechanistic understanding of how low-intensity electric currents modulate the electrophysiological activity in the human brain. To overcome methodological limitations, we utilize the minimally invasive method of intracerebral recording in drug-resistant epileptic patients, in combination with a fast periodic visual stimulation (FPVS) designed to engage face-selective cognitive processes.

We present a novel approach that integrates a single session of low-intensity anodal tDCS, applied using only 2 small High-Definition (HD) electrodes, targeting the ventral occipito-temporal cortex, a region critically involved in face processing. tDCS was combined with simultaneous intracerebral (iEEG) and scalp EEG recording with FPVS paradigm, to assess tDCS-induced neuromodulation both during and after stimulation. Using this unique tDCS-iEEG-FPVS approach, we demonstrate that a single session of anodal tDCS with two HD electrodes significantly neuromodulates cognitive evoked iEEG responses, with effects occurring during tDCS and persisting beyond the stimulation period.

The simultaneous intracerebral and scalp EEG recordings allowed us to further investigate the correlation between the neural activity at two spatial scales. This approach opens the possibility of moving toward less invasive approaches for capturing tDCS-induced effects, potentially bypassing the need for intracerebral recordings in future studies. Combining tDCS with scalp EEG and FPVS revealed that tDCS transiently disrupts the organization of cortical networks near the stimulation site while

concurrently enhancing neural activity in deeper brain regions, as evidenced by iEEG recordings. Although statistical power was limited, our findings demonstrate promising potential for detecting neuromodulatory effects at the scalp level that correspond to those observed intracerebrally.

Monitoring the clinical effects of tDCS can be quite challenging, often requiring advanced EEG setups and expert supervision. As medical technologies increasingly shift toward accessible, home-based applications, developing portable EEG systems capable of reliably recording tDCS-induced neuromodulation is becoming essential. After addressing these challenges in previous chapters, we aim to demonstrate the wireless EEG system Neuronaute, coupled with an ultrathin Icecap, capability in recording cognitive evoked measures. Combining this EEG system with FPVS would enable future investigation of long-term, home-based monitoring of neuromodulation effects. This approach would be valuable for tracking tDCS changes and indicating when the previous effects of tDCS subsided and new stimulation is required.

Key Words: Transcranial Direct Current Stimulation, Fast Periodic Visual Stimulation, Intracerebral and Scalp Electroencephalography, Cognitive Neurosciences, Human in-vivo, EEG Biomarkers.

Résumé en Français

La stimulation transcrânienne par courant direct (tDCS) est une technique de neuromodulation non invasive, reconnue pour son potentiel en réhabilitation cognitive. Elle repose sur l'injection d'un courant continu de faible intensité par deux électrodes placées sur le cuir chevelu, afin de moduler l'excitabilité corticale. Malgré sa large accessibilité, son efficacité chez l'humain reste débattue, en raison des incertitudes concernant la capacité du courant appliqué à influencer les structures cérébrales ciblées. Une étude récente chez l'humain, combinant la tDCS à des enregistrements par électroencéphalographie intracérébrale (iEEG), a montré que les champs électriques générés peuvent atteindre les régions corticales superficielles et profondes. Néanmoins, les mécanismes neurophysiologiques de la tDCS restent toujours incompris, notamment ses effets sur l'activité électrophysiologique humaine. À ce jour, la modulation électrophysiologique induite par la tDCS n'a pas encore été clairement quantifiée. Bien que l'EEG offre une excellente résolution temporelle pour l'observation de l'activité cérébrale, les études de EEG de scalp et les potentiels évoqués montrent une fiabilité limitée et seulement des indices indirects de neuromodulation.

L'objectif principal de cette thèse est de combler une lacune majeure dans le domaine de la tDCS : la compréhension mécanistique limitée des effets des courants de faible intensité sur l'activité électrophysiologique cérébrale. Pour dépasser les limites méthodologiques actuelles, nous avons utilisé une méthode minimement invasive d'enregistrement intracérébral chez des patients épileptiques pharmacorésistantes, associée à une stimulation visuelle périodique rapide (FPVS) ciblant les processus cognitifs sélectifs aux visages.

Nous proposons une approche originale intégrant une session unique de tDCS (+2mA) à faible intensité, appliquée par deux électrodes HD ciblant le cortex occipito-temporal ventral, une région clé de la reconnaissance des visages, combinée à des enregistrements simultanés par iEEG et EEG de scalp au paradigme FPVS. Cette configuration permet d'évaluer la neuromodulation pendant et après la stimulation. Nos résultats montrent qu'une seule session de tDCS suffit à moduler significativement les réponses cognitives évoquées en iEEG, avec des effets persistants au-delà de la stimulation.

Les enregistrements simultanés intracérébraux et de scalp nous ont permis d'explorer la corrélation entre l'activité neuronale à deux échelles spatiales. Cette approche ouvre la voie à des méthodes moins invasives pour détecter les effets de la tDCS, rendant potentiellement les enregistrements intracérébraux non nécessaires dans les études futures. L'association tDCS-EEG-FPVS révèle une désorganisation transitoire des réseaux corticaux proches de l'anode, tout en renforçant l'activité neuronale dans des régions plus profondes, comme le confirment les données iEEG. Malgré

une puissance statistique limitée, nos résultats suggèrent un fort potentiel de détection des effets neuromodulateurs via l'EEG de scalp.

La surveillance des effets cliniques de la tDCS repose souvent sur des dispositifs EEG complexes et une expertise spécialisée. Avec l'émergence de technologies portables et accessibles, le développement de systèmes EEG fiables pour suivre les effets de la tDCS devient essentiel. Après avoir abordé ces enjeux, notre objectif est de démontrer la capacité du système EEG sans fil Neuronaute, associé à la IceCap, à enregistrer les mesures cognitives évoquées. En combinant ce système à un paradigme SVPR, nous visons à terme une évaluation continue et à domicile des effets neuromodulateurs de la tDCS. Une telle approche serait particulièrement utile pour surveiller à distance les effets de la tDCS et identifier le moment où les effets d'une session précédente se sont estompés, signalant ainsi le besoin d'une nouvelle stimulation.

Mots Clés : Stimulation Transcrânienne à Courant Continu, Stimulations Visuelles Périodiques Rapides, Electroencéphalographie Intracérébrale et du Cuir Chevelu, Neurosciences Cognitives, Chez l'humain in vivo, Biomarqueurs EEG.

Résumé Substantiel en Français

La stimulation transcrânienne à courant continu (tDCS) est une technique non invasive de stimulation cérébrale, fondée sur l'application d'un courant continu de faible intensité (entre 0,5 et 2 mA) par deux électrodes ou plus placées sur le cuir chevelu. Le champ électrique induit par ce courant circule de l'électrode stimulante (anode), traverse le cerveau, puis est recueilli par l'électrode de retour (cathode) (Pilloni et al., 2022). Bien qu'une partie importante de ce champ soit déviée par le crâne, une quantité suffisante pénètre dans le cerveau, où elle module l'excitabilité corticale, entraînant des effets à la fois aigus et durables (Reed & Cohen Kadosh, 2018). Facile à utiliser, peu coûteuse et portable, la tDCS est généralement bien tolérée, les effets secondaires non invasifs, se limitant à des sensations légères de picotement (Kessler et al., 2012). Malgré son accessibilité et son application étendue, son efficacité chez l'humain fait toujours l'objet de débats, en raison d'incertitudes sur la capacité du courant appliqué à atteindre et influencer les structures cérébrales profondes (Horvath et al., 2015a, 2015b ; Parkin et al., 2019). Néanmoins, des études récentes in vivo chez l'humain, combinant tDCS et enregistrements intracérébraux (iEEG), ont montré que les champs électriques générés par la tDCS peuvent atteindre les régions corticales et sous-corticales (Louviot et al., 2022). Cette capacité à induire une neuromodulation profonde a suscité un intérêt clinique croissant pour son potentiel thérapeutique dans plusieurs pathologies neurophysiologiques et neurobiologiques, telles que la maladie d'Alzheimer ou la Schizophrénie, ainsi que pour son utilisation dans la modulation des fonctions cognitives telles que la perception, la mémoire ou encore le langage (Lefaucheur et al., 2017).

Malgré cet essor, les mécanismes précis par lesquels une tDCS de faible intensité influence l'activité cérébrale et les fonctions cognitives restent encore mal compris. Le fait que la tDCS puisse induire une neuromodulation significative *in vivo* chez l'humain soulève de nombreuses questions fondamentales. Dans ce manuscrit, nous concentrons notre attention sur la reconnaissance des visages et les avancées récentes quant à la capacité de la tDCS à moduler cette fonction. La neuromodulation de la reconnaissance des visages par la tDCS a été principalement étudiée selon deux approches : des mesures comportementales et des enregistrements électroencéphalographiques. Ces effets ont été investigués aussi selon des protocoles « en ligne », c'est-à-dire pendant la stimulation, que selon des protocoles « hors ligne », examinant les effets après la stimulation. Des études menées chez des sujets sains (Barbieri et al., 2016 ; Brunyé et al., 2017 ; Gonzalez-Perez et al., 2019 ; Manfredi et al., 2017 ; Pisoni et al., 2020 ; Renzi et al., 2015) ainsi que chez des patients (Boggio et al., 2012 ; Diana et al., 2024) ont montré des améliorations notables des performances en perception des visages, en mémoire des visages et en discrimination de visages non familiers après tDCS. Toutefois, ces résultats ont été remis en question, certaines études ne parvenant pas à les reproduire ou rapportant des effets inverses

(Kho et al., 2023 ; Willis et al., 2019 ; Wu et al., 2021 ; Horvath et al., 2015a). Ces divergences pourraient s'expliquer par la variabilité cognitive interindividuelle, par l'implication d'autres processus cognitifs comme l'attention ou la prise de décision (Zorowitz & Niv, 2023), ainsi que par des variations importantes dans les protocoles de tDCS (montage, intensité, durée, etc.) (Vergallito et al., 2022). Bien que les mesures comportementales permettent d'inférer certains effets de la tDCS sur la perception des visages, elles ne suffisent pas à elles seules à révéler les mécanismes neuromodulateurs sous-jacents. Pour approfondir cette compréhension, il est essentiel d'y associer des enregistrements électrophysiologiques, tels que l'EEG de surface, qui fournit des marqueurs neuronaux directs du traitement des visages.

Plusieurs composantes des potentiels visuels évoqués ont été étudiées en lien avec la tDCS, dont la composante N170, spécifique au traitement des visages. Une tDCS anodale appliquée en ligne au niveau du cortex préfrontal dorsolatéral (DLPFC) lors d'une tâche de reconnaissance des visages a entraîné une réduction de l'amplitude du N170 ainsi qu'un allongement considérable des temps de réaction, suggérant une facilitation du phénomène de suppression par répétition. À l'inverse, la stimulation cathodale a induit des effets opposés (Lafontaine et al., 2013). Une autre étude en ligne avec une tDCS anodale ciblant le DLPFC s'est intéressée à l'effet d'inversion des visages. En cohérence avec les résultats comportementaux précédents, elle a mis en évidence une diminution de la latence du N170, reflétant un traitement moins ralenti des visages inversés, et donc une réduction de l'effet d'inversion. Cependant, ce même protocole a aussi montré une augmentation de l'amplitude du N170 pendant la stimulation, indiquant paradoxalement un renforcement de l'effet d'inversion. Cette contradiction pourrait suggérer un basculement d'un traitement configurationnel vers un traitement plus analytique centré sur les traits individuels, comme aux yeux (Civile et al., 2018, 2019, 2020, 2024). Malgré l'intérêt majeur des enregistrements EEG pour quantifier la neuromodulation induite par la tDCS, leur combinaison est simultanée à plusieurs limitations méthodologiques. Deux grandes catégories d'artefacts peuvent apparaître lors des protocoles EEG-tDCS : les artefacts physiologiques, liés à l'interaction entre la stimulation et les tissus biologiques (rythmes cardiaques, respiration, mouvements oculaires), qui altèrent fortement la tension du courant et interfèrent avec les signaux neuronaux. Ces artefacts sont particulièrement difficiles à éliminer avec les techniques conventionnelles de traitement du signal. Les artefacts méthodologiques, causés par des conditions expérimentales imparfaites ou des limitations techniques, comme la fuite de bruit du dispositif tDCS dans les électrodes (Diana et al., 2024 ; Gebodh et al., 2019). Ces artefacts compliquent les processus de débruitage et compromettent une caractérisation précise des effets électrophysiologiques (Faria et al., 2012b ; Mancini et al., 2015 ; D. W. Kim et al., 2019).

Afin de contourner ces limitations, l'étude présentée au chapitre II a combiné une stimulation tDCS contrôlée en aveugle avec un enregistrement iEEG pendant une stimulation visuelle périodique rapide (FPVS). La FPVS, ou « frequency-tagging », est une méthode objective et robuste qui génère des réponses électrophysiologiques à des fréquences précises, avec un excellent rapport signal sur bruit (Liu-Shuang et al., 2014b ; Rossion, 2014). L'activité neuronale étant confinée à des bandes de fréquence spécifiques et connues, cette approche est largement immunisée contre les artefacts induits par la tDCS, la rendant particulièrement adaptée pour étudier les effets de la tDCS sur les réponses intracérébrales évoquées périodiquement. Par ailleurs, notre analyse du bruit a montré que l'amplitude des réponses reste stable et ne varie pas au fil des phases de stimulation. Les paradigmes FPVS sont largement validés pour isoler de manière objective les réponses cérébrales évoquées lors d'enregistrements électrophysiologiques. Dans cette étude, nous avons utilisé la FPVS comme signature objective de la catégorisation des visages, en isolant les réponses sélectives aux visages (1,2 Hz et harmoniques) des réponses visuelles générales (6 Hz et harmoniques). Grâce à la périodicité du paradigme, ces deux types de réponses peuvent être quantifiés dans le domaine fréquentiel des enregistrements intracérébraux (Rossion et al., 2015b).

Les enregistrements iEEG chez des patients atteints d'épilepsie pharmacorésistante ont été obtenus grâce à une procédure rare et peu invasive d'implantation intracérébrale, qui ne modifie pas significativement la conduction volumique dans la tête (pas de fuite de courant ; Koessler et al., 2015). Cette méthode offre une opportunité unique d'explorer la neuromodulation électrophysiologique induite par la tDCS sans introduction d'artefacts dans les signaux iEEG. De plus, l'iEEG permet d'examiner les sources corticales profondes, intermédiaires et superficielles, offrant ainsi un accès direct aux réseaux cognitifs distribués à grande échelle. Dans l'étude présente, nous avons ciblé le cortex occipito-temporal ventral (VOTC), une région contenant un réseau fonctionnellement organisé de régions sélectives aux visages, souvent étudiée chez les patients épileptiques (Rossion et al., 2023).

Dans l'étude du chapitre **I**I, la tDCS anodale a été administrée à l'aide de deux électrodes de haute définition (HD) uniquement, à une intensité de +2 mA, ciblant les structures du VOTC droit. Plusieurs régions telles que l'aire occipitale des visages (OFA) et l'aire fusiforme des visages (FFA), situées dans le VOTC droit, ont été identifiées dans de nombreuses études (Rossion et al., 2024 ; Jonas et al., 2016 ; Haxby et al., 2000) comme des régions clés de l'hémisphère droit impliquées dans le traitement des visages. Le paradigme de stimulation visuelle périodique rapide (FPVS) a été présenté simultanément durant l'enregistrement intracérébrale continu et la tDCS chez des patients pharmacorésistants. Une approche contrôlée par condition Sham a été mise en place selon trois phases afin d'examiner l'influence de la tDCS sur les réponses évoquées intracérébrales, sélectives aux visages et générales. Une stimulation Sham a été administrée avant (Phase 1) et après (Phase 3) une phase

active de tDCS anodale de 20 minutes (Phase 2). Pendant la phase 2, la tDCS dans sa forme active uniquement a été délivrée durant 10 minutes, suivie de 10 minutes supplémentaires de stimulation simultanée à la FPVS. Chaque phase comprenait deux sessions successives de FPVS (6 sessions FPVS au total : 2 par phase : avant, pendant et après stimulation).

Les résultats ont montré que l'application de la tDCS anodale, en simultané avec les enregistrements intracérébraux et la FPVS, induisait une neuromodulation significative des réponses sélectives aux visages dans l'hémisphère droit, le VOTC droit, ainsi que dans ses sous-régions : le lobe temporal antérieur (ATL), le lobe temporal postérieur (PTL) et le lobe occipital (OCC), à la fois pendant et après la stimulation. Concernant les réponses visuelles générales, une neuromodulation significative a été observée après stimulation, comparativement à avant, dans l'hémisphère droit, dans le VOTC droit, et plus particulièrement dans la région occipitale droite. À partir de ces observations dans les trois régions d'intérêt (ROIs) constituant l'ATL, le PTL et l'OCC du VOTC, nous avons examiné les effets neuromodulateurs pendant et après la stimulation dans les dix sous-régions des ROIs. Parmi ces dix sous-régions, les plus fortes réponses intracérébrales pour les trois phases ont été observées dans le cortex occipital ventromédial (VMO) pour les réponses visuelles générales, et dans le gyrus fusiforme latéral (latFG) pour les réponses sélectives aux visages. La neuromodulation la plus significative a été observée dans le gyrus fusiforme médial (medFG), pour les deux types de réponses pendant la stimulation. Il est important de souligner que cette modulation se traduisait par une augmentation des réponses sélectives aux visages dans le medFG, mais par une diminution des réponses visuelles générales. Cependant, cette modulation observée dans le medFG n'était plus significative après la stimulation. Le latFG a montré une neuromodulation significative pendant et après la tDCS pour les réponses visuelles générales. En revanche, pour les réponses sélectives aux visages, il a présenté une tendance à la neuromodulation pendant la tDCS sans atteindre le seuil de significativité. Toutefois, après la stimulation, cette modulation est devenue significative. Par ailleurs, le champ électrique induit par une stimulation transcrânienne à courant alternatif a été évalué dans les contacts intracérébraux implantés dans les sous-régions du VOTC. Le gyrus occipital inférieur (IOG) dans l'OCC et le gyrus temporal moyen antérieur (antMTG) dans l'ATL ont présenté les valeurs de champ électrique les plus élevées parmi l'ensemble des régions du VOTC. Comme attendu, les régions les plus profondes présentaient des valeurs de champ plus faibles que les régions plus superficielles.

Bien que les paramètres de tDCS aient été fixés à une intensité classique (2 mA), une durée standard (20 min) et un montage simple à deux électrodes circulaires HD, la stimulation a significativement modulé les réponses intracérébrales évoquées. Ces paramètres ont été volontairement choisis sans optimisation, dans le but de refléter les conditions les plus couramment rencontrées dans les contextes de recherche et d'application clinique (Lefaucheur, 2016), rendant les

résultats plus largement exploitables. La quantification des effets neuromodulateurs de la tDCS en termes d'amplitude a révélé des augmentations significatives, possiblement liées aux paramètres standard utilisés. Étant donné que la neuromodulation est directement liée à l'intensité du champ électrique intracérébral induit au sein du réseau ciblé, une intensité plus élevée pourrait potentiellement amplifier la neuromodulation induite par la tDCS. Dans une étude combinant tDCS et enregistrements intracérébraux, nous avons démontré une relation linéaire directe entre l'intensité de la tDCS et le champ intracérébral mesuré chez l'humain (Louviot et al., 2022). En s'appuyant sur les résultats prometteurs issus de modélisations computationnelles de la tDCS HD (Alam et al., 2016), cette configuration pourrait permettre une modulation encore plus efficace.

Dans cette étude, bien qu'un seul bloc de stimulation de 20 minutes ait été administré, une neuromodulation électrophysiologique sélective aux visages significatifs a été observée même après la fin de tDCS. Ce résultat rejoint les observations précédentes selon lesquelles la tDCS peut altérer l'excitabilité corticale pendant environ une heure après la stimulation, comme le montrent les analyses de potentiels évoqués en EEG de surface (Nitsche, Nitsche et al., 2003 ; Nitsche & Paulus, 2001). Ici, les effets post-tDCS ont été mesurés dans les minutes suivant la fin de la stimulation. Bien qu'il n'ait pas possible, pour des raisons cliniques, d'étendre l'enregistrement bien au-delà de la stimulation, l'exploration des effets à plus long terme (par ex. plusieurs heures après la tDCS) permettrait de mieux caractériser la durée des effets neuromodulateurs électrophysiologiques induits par une seule session de tDCS à faible intensité, et le temps nécessaire pour un retour à l'activité de base. De telles données seraient essentielles pour optimiser les protocoles incluant des sessions répétées de stimulation.

Grâce à l'analyse des réponses intracérébrales synchronisées en fréquence, nous avons démontré que la tDCS appliquée sur l'hémisphère droit induit une modulation électrophysiologique forte et consistante des réponses sélectives aux visages, qui persiste au-delà de la période de stimulation. Ces résultats suggèrent que le réseau de reconnaissance faciale est particulièrement sensible et réactif à la tDCS. Cette spécificité pourrait s'expliquer par le ciblage fonctionnel du VOTC, une région clé du traitement des visages. Étant donné que la tâche FPVS requiert une reconnaissance rapide des visages (en un seul regard), les réseaux neuronaux sélectifs aux visages localisés dans le VOTC ont été fortement engagés au cours de la tâche.

Contrairement à nos attentes, aucune neuromodulation significative n'a été observée dans le gyrus occipital inférieur (IOG), malgré sa forte sélectivité aux visages et son exposition prolongée aux champs électriques induits par la tDCS. Ce résultat pourrait s'expliquer par un effet plafond ou par la nature non linéaire des réponses neuromodulatrices. En revanche, le gyrus fusiforme médial (medFG) a présenté des effets opposés selon le type de stimulus : les réponses sélectives aux visages ont

significativement augmenté durant la tDCS, tandis que les réponses visuelles générales ont diminué, suggérant une spécificité fonctionnelle et une modulation potentielle d'une région multimodale. Parallèlement, le gyrus fusiforme latéral (latFG) a également montré une modulation significative, particulièrement marquée après la stimulation, probablement en raison de sa localisation superficielle et de sa proximité avec l'anode. Les différences d'effets entre medFG et latFG pourraient résulter de variations dans la profondeur du champ électrique, de la microstructure anatomique et de l'organisation cytoarchitectonique suivant le gradient médial-latéral défini par le sillon fusiforme médian. Ces résultats soulignent l'importance de l'anatomie locale et de la spécialisation fonctionnelle dans les effets régionaux de la tDCS au sein du lobe temporal postérieur.

Dans l'ensemble, les résultats actuels issus de cette investigation intracérébrale chez l'humain constituent une première étape démontrant la capacité de la tDCS à induire des effets électrophysiologiques objectifs, sélectifs et significatifs. Grâce à cette approche originale combinant tDCS, l'enregistrement EEG intracérébrales et FPVS en simultané, des recherches futures pourront répondre à des questions fondamentales pour définir les paramètres de stimulation les plus efficaces, en vue d'obtenir une neuromodulation électrophysiologique optimale et des effets comportementaux durables.

Conscients de l'accessibilité limitée des enregistrements intracérébraux, nous avons utilisé des enregistrement EEG simultané intracérébrales et sur le cuir chevelu, permis par l'exploration clinique chez des patients atteints d'épilepsie pharmacorésistante. Dans le chapitre III, nous avons quantifié les effets électrophysiologiques au cuir chevelu induits par une tDCS anodale en ligne (+2 mA) à l'aide de deux électrodes HD annulaires, appliquées sur le lobe occipito-temporal droit, sur les réponses évoquées visuelles générales et sélectives aux visages.

Les enregistrements EEG simultané intracérébraux et sur le cuir chevelu ont été réalisés en parallèle à la tDCS HD et au paradigme SVPR pour explorer la corrélation entre les effets neuromodulateurs détectés intracérébralement (chapitre II) et ceux observés au niveau du scalp. Les enregistrements EEG ont révélé un profil de variation similaire au cours et après la stimulation, mais sans atteindre de seuil de significativité statistique. Bien que les signaux EEG intracérébraux et sur le cuir chevelu aient été enregistrés simultanément, selon un protocole identique (tDCS anodale sur P10, +2 mA, 20 minutes) et le même paradigme FPVS (localisation des réponses sélectives aux visages), des divergences de résultats apparaissent en raison de différences méthodologiques.

L'enregistrement EEG intracérébrales fournit une résolution spatio-temporelle élevée grâce à l'enregistrement direct des potentiels de champ locaux au sein de régions sélectives aux visages, tandis que l'EEG sur le cuir chevelu capte des signaux provenant de sources cérébrales multiples et distantes,

ce qui réduit sa spécificité spatiale (Koessler et al., 2015). De plus, les signaux EEG sont davantage atténués que les signaux intracérébraux à cause des propriétés résistives du crâne, mal caractérisées et difficiles à estimer in vivo, en particulier chez l'humain (Koessler et al., 2017). En moyenne, l'amplitude corrigée de base des réponses sélectives aux visages est réduite d'un facteur 6,4 entre les enregistrements intracérébraux et ceux du scalp. Par ailleurs, la taille d'échantillon plus faible pour l'EEG de scalp (n=8) par rapport à l'EEG intracérébrale (n=11) a limité la puissance statistique.

La combinaison des électrodes EEG intracérébrales et de scalp pendant la tDCS pose aussi certains défis. Étant donné le schéma d'implantation unique à chaque patient, en fonction de leur profil épileptique, certaines électrodes de scalp ont dû être repositionnées pour minimiser les interférences avec les électrodes intracérébrales et réduire les risques infectieux (Barborica et al., 2021). En fait, une étude sur les décharges épileptiformes à proximité de défauts osseux du crâne a montré une possible altération de la distribution du voltage EEG au scalp à proximité de ces zones (Mader Jr et al., 2018). Bien que les trous induits par la SEEG soient très petits, la possibilité d'une distorsion du signal EEG liée aux implants ne peut être exclue.

En parallèle à l'augmentation d'amplitude du signal enregistré au niveau des électrodes de scalp, le rapport signal/bruit (SNR) a significativement diminué pendant la tDCS, reflétant une augmentation du signal accompagnée d'une élévation proportionnelle du bruit de fond. Cela suggère que la tDCS pourrait avoir modulé à la fois la réponse sélective aux visages et l'activité neurale ou non-neurale environnante (bruit). Bien que la réponse ait été maintenue, sa détection semble avoir été compromise pendant la stimulation, en raison de plusieurs contraintes méthodologiques liées à la combinaison tDCS, EEG de scalp et EEG intracérébrale. Malgré des contrôles méthodologiques rigoureux, certains artefacts induits par la tDCS demeurent inévitables. Le stimulateur tDCS peut générer des artefacts large bande, déviant du courant continu idéal, et injecter du bruit dans le signal enregistré via la mesure d'impédance durant la stimulation (Gebodh et al., 2019). Ces artefacts ont pu être évités avant et après la stimulation, grâce au débranchement du câble de stimulation après la phase de montée, mais pas pendant la stimulation. Ces résultats soulignent l'importance de considérer les caractéristiques du bruit en plus de la force du signal lorsqu'on évalue les effets neuromodulateurs induits par la tDCS.

Pour explorer les effets électrophysiologiques de la tDCS en dehors du contexte clinique, nous avons répliqué le même protocole de stimulation chez 18 adultes sains, en utilisant uniquement l'EEG de scalp (Torro-Alves et al., 2025, soumis). Contrairement à l'étude clinique de EEG intracérébrale et scalp, cette expérience a révélé une réduction significative de l'amplitude et du SNR pendant la tDCS, suivie d'un rebond marqué après la stimulation. Bien que les deux études aient utilisé les mêmes

paramètres de tDCS et un protocole Sham en trois phases, des différences clés liées à l'environnement d'enregistrement et à la taille d'échantillon ont probablement contribué aux résultats divergents. Notamment, l'étude EEG a utilisé un casque à 64 électrodes dans un environnement de laboratoire contrôlé, tandis que notre configuration clinique imposait un placement variable des électrodes en raison des contraintes des électrodes intracérébraux chez les patients. Les différences d'objectif expérimental peuvent également avoir joué un rôle : notre paradigme localisait les réponses sélectives aux visages, tandis que celui de Torro-Alves et al. 2025 ciblait la discrimination d'identité faciale, engageant potentiellement des réseaux neuronaux distincts. Ces divergences pourraient expliquer les effets post-stimulation plus marqués observés dans l'étude utilisant l'EEG de scalp uniquement.

Pris ensemble, les résultats du chapitre III suggèrent que la tDCS anodale perturbe temporairement la synchronisation neuronale à grande échelle mesurée au scalp, tout en renforçant ou réorganisant l'activité localisée dans des régions plus profondes. Ces modifications peuvent conduire à des effets de rebond après stimulation, influencés par la méthode d'enregistrement, la temporalité de la stimulation et la spécificité de la tâche. En appui, des études hémodynamiques ont montré que la tDCS anodale augmente le flux sanguin cérébral régional dans les régions ciblées pendant et après stimulation (Zheng et al., 2011), ce qui est compatible avec une désynchronisation neuronale suivie d'une reconfiguration fonctionnelle dans le cortex occipito-temporal.

Surveiller les effets cliniques de la tDCS peut s'avérer complexe, nécessitant souvent des dispositifs EEG sophistiqués et une expertise technique avancée. Dans les chapitres précédents, nous avons contourné ces limitations par une approche simple combinant EEG de scalp, tDCS et FPVS. Ainsi, cette étude vise à évaluer le Neuronaute®, un système EEG sans fil, facile d'utilisation et cliniquement efficace, couplé à une IceCap® ultrafine, comme solution pratique pour mesurer de façon fiable les marqueurs cognitifs électrophysiologiques. L'objectif principal était d'évaluer la capacité de ce système à suivre les effets neuromodulateurs dans le temps, dans une perspective de monitoring longitudinal à domicile. Une telle capacité serait précieuse pour identifier quand les effets post-tDCS commencent à s'estomper, et où une nouvelle session serait nécessaire.

Pour valider ce système, nous avons caractérisé la qualité (amplitude, topographie, SNR) des biomarqueurs EEG évoqués enregistrés chez des adultes sains avec le Neuronaute couplé à l'IceCap, comparé au Neuronaute associé à une coiffe EEG de référence, l'Electrocap®, largement utilisée en recherche clinique. Pour évaluer objectivement la performance des deux systèmes d'électrodes de scalp, nous avons utilisé la méthode du frequency-tagging, qui consiste à présenter un stimulus à une fréquence rapide et régulière, et à analyser les réponses EEG dans le domaine fréquentiel (SSVEP, Regan, 1966). Les caractéristiques robustes de cette approche (sensible, implicite, objective) offrent

des avantages clés pour les mesures EEG en neurosciences cognitives, notamment lorsqu'il s'agit de comparer des populations ou de valider des systèmes, puisqu'elle permet d'obtenir des réponses neuronales à fort SNR, identifiables et quantifiables de façon objective à la fréquence de stimulation (Norcia et al., 2015 ; Rossion et al., 2015a ; Regan, 1989).

Dans l'étude présentée au chapitre IV, nous avons utilisé un paradigme rapide de type "Oddball" spécifiquement validé au cours de la dernière décennie pour mesurer la reconnaissance de l'identité faciale (inconnue) (étude originale : Liu-Shuang et al., 2014a ; voir aussi Rossion et al., 2020 pour une revue ; Hagen et al., 2024). Ce paradigme de discrimination de l'identité faciale permet d'isoler la réponse à une nouvelle identité faciale insérée entre des images de la même identité, reflétant ainsi un traitement visuel de haut niveau.

Nos résultats ont démontré que le système combinant l'ultrafine IceCap® et le Neuronaute®, un EEG sans fil, permettait d'enregistrer de manière fiable et rapide (en quelques minutes) les marqueurs EEG cognitifs évoqués, en comparaison avec le système de référence bien validé Electrocap. Des amplitudes similaires ainsi que des SNR élevés ont été observés pour les réponses neuronales à l'identité faciale, localisées dans les mêmes régions cérébrales avec les deux systèmes de coiffes. De plus, les topographies d'amplitude au scalp étaient comparables entre les deux systèmes d'électrodes et les différents participants. Dans la littérature, les réponses EEG de discrimination de l'identité des visages ont été régulièrement rapportées dans les régions occipito-temporales avec une dominance hémisphérique droite, que ce soit avec des mesures ERP classiques (Caharel et al., 2009 ; Jacques et al., 2007) ou avec le paradigme FPVS (Liu-Shuang et al., 2016). Dans notre étude méthodologique, les réponses EEG étaient systématiquement localisées dans les régions occipito-temporales, soulignant la fiabilité et la sensibilité de cette méthode combinant Neuronaute et paradigme FPVS pour évaluer le traitement de l'identité des visages. Ces résultats indiquent également que l'IceCap assure une couverture suffisante du scalp ainsi qu'une distance inter-électrodes adaptée pour l'évaluation électrophysiologique cognitive. Les fortes corrélations obtenues dans les analyses de fiabilité intra- et inter-coiffe confirment la stabilité des mesures de potentiels évoqués entre les deux systèmes, renforçant la robustesse des réponses indépendamment du type de cap utilisé. De plus, la corrélation significative entre l'IceCap et l'Electrocap soutient l'utilisation de l'IceCap comme alternative viable pour les recherches futures, tout en garantissant la précision et la reproductibilité des mesures électrophysiologiques.

Une différence majeure entre l'IceCap et l'Electrocap réside dans la répartition des électrodes : l'Electrocap comprend des électrodes latérales occipito-temporales supplémentaires (P10/P9), connues pour leur sensibilité au traitement des visages. Malgré l'absence de l'électrode P10 sur

l'IceCap, des amplitudes de réponse similaires pour la discrimination faciale ont été observées à l'électrode P8, probablement en raison de sa proximité avec P10 et de sources corticales sous-jacentes telles que le gyrus occipital inférieur. Cela suggère que même des montages minimaux, comme celui proposé par l'IceCap, peuvent capter efficacement les réponses à l'identité faciale, à condition que les électrodes soient positionnées de manière stratégique. La cohérence des résultats entre les deux coiffes, notamment la détection de l'effet d'inversion des visages, renforce la validité de l'IceCap pour l'enregistrement EEG cognitif.

Par ailleurs, les participants ont globalement rapporté une préférence pour l'IceCap en termes de confort, grâce à sa légèreté, sa flexibilité et l'absence de sangle mentonnière. Toutefois, le temps de mise en place de l'IceCap était significativement plus long, en partie à cause de sa structure moins familière et du gel conducteur plus épais nécessitant une application manuelle minutieuse. Des améliorations pourraient inclure la proposition de tailles variées de cap et l'utilisation d'un gel plus facile à appliquer pour optimiser l'ergonomie. Malgré des valeurs moyennes d'impédance similaires entre les deux coiffes, le système Neuronaute a présenté un taux élevé d'erreurs de mesure d'impédance, pouvant affecter la qualité du signal. Ce problème était plus fréquent avec l'Electrocap, notamment à cause des connexions individuelles de ses électrodes. Ces constats soulignent la nécessité d'optimiser le placement des électrodes, la conception des caps et la compatibilité des systèmes pour garantir un enregistrement EEG fiable, en particulier dans des contextes d'utilisation à distance ou à domicile.

Rendre l'utilisation de l'EEG et des neurotechnologies associées accessible à domicile constitue une avancée majeure pour élargir l'accès au suivi et à l'intervention cérébrale. Cette transition ouvre la voie à l'intégration d'outils comme la tDCS dans des applications à distance et sur le long terme. Toutefois, elle nécessite des protocoles clairs, des systèmes faciles à utiliser et des procédures robustes pour garantir l'efficacité en dehors des environnements cliniques. Le suivi à distance pourrait permettre des diagnostics plus précoces, des traitements personnalisés et un suivi continu de pathologies comme la maladie d'Alzheimer, l'épilepsie ou la dépression, dans lesquelles des sessions répétées de tDCS associées à des biomarqueurs objectifs pourraient améliorer les résultats cliniques.

En conclusion, nos travaux fournissent les premières preuves électrophysiologiques directes d'une neuromodulation induite par la tDCS au sein du cerveau humain à l'aide d'enregistrements intracérébraux. L'intégration multimodale de la tDCS avec les enregistrements intracérébraux et la SVPR, réalisée chez des patients épileptiques, permet de combler un fossé ancien entre les recherches animales et les protocoles humains, en démontrant clairement les effets de la tDCS sur l'activité neuronale in vivo dans le cerveau humain. Les résultats présentés dans cette thèse font avancer le

champ en montrant que : 1) Un champ électrique de faible intensité appliqué en une seule session de tDCS peut induire des modifications significatives et durables des fonctions neuronales ; 2) Deux petites électrodes HD suffisent à cibler de manière fonctionnelle l'activité neuronale évoquée dans des régions cérébrales sélectives aux visages ;3) Les profil différenciés de neuromodulation observés dans le gyrus fusiforme médian reflètent l'influence de caractéristiques neuroarchitectural sous-jacentes ; 4) L'efficacité des paramètres standards de tDCS utilisés en clinique (20 minutes, 2 mA) est validée ; 5) Ces résultats offrent une base électrophysiologique aux effets comportementaux de la tDCS largement rapportés dans la littérature ; 6) Le paradigme SVPR émerge comme un outil robuste et fiable pour capter des effets neuromodulateurs sélectifs et objectifs chez l'humain.

Conscients des contraintes d'accessibilité liées aux enregistrements iEEG, nous avons utilisé des enregistrements EEG simultanés intracérébraux et de scalp, associés à la tDCS HD et au SVPR, pour évaluer si les effets neuromodulateurs intracérébraux se reflètent également au niveau du scalp. Cette approche multimodale unique, combinant enregistrements EEG intracérébraux et de scalp avec la tDCS et SVPR, nous a permis de montrer que : 1) Malgré la couverture limitée du scalp et la petite taille d'échantillon, l'EEG de scalp présente un fort potentiel pour détecter les effets neuromodulateurs de la tDCS observés en intracérébrale ; 2) Contrairement aux enregistrements EEG intracérébraux, les effets d'une seule session de tDCS sur les signaux EEG de scalp sont transitoires; 3) Pendant la stimulation active, la tDCS module temporairement à la fois le signal neuronal et le bruit de fond, rendant difficile l'interprétation des variations d'amplitude induites par la tDCS ; 4) La tDCS désorganise temporairement le réseau cortical autour du site de stimulation tout en renforçant l'activité neuronale dans les régions plus profondes.

Enfin, dans une perspective d'élargissement de l'application méthodologique de l'approche tDCS–SVPR à des contextes accessibles à domicile, nous avons validé l'utilisation du système Neuronaute–IceCap pour l'enregistrement de biomarqueurs EEG cognitifs. Cette configuration a révélé : 1) Des mesures électrophysiologiques fiables, significatives et objectives de la discrimination de l'identité faciale ; 2) Le design ergonomique de la cap facilitant le confort des utilisateurs ainsi qu'une application et un retrait simplifiés ; 3) Une transmission sans fil des données et une possibilité de suivi à distance qui soutiennent son potentiel d'utilisation dans les environnements domestiques.

En conclusion, nous avons significativement approfondi la compréhension des mécanismes électrophysiologiques de la neuromodulation induite par la tDCS chez l'humain. Nous avons posé les bases de futures investigations multimodales (EEG intracérébral, EEG de scalp, SVPR) pour des applications à la fois en neuro-réhabilitation chez les patients et en modulation de l'activité cérébrale chez les individus sains. Nous avons également fourni des mesures objectives et quantifiables de la

neuromodulation induite par la tDCS à différentes échelles d'enregistrement. L'approche par balisage fréquentiel (frequency-tagging) s'est avérée être un outil puissant pour suivre de manière fiable les changements dynamiques du traitement cognitif dans les régions cérébrales ciblées pendant la stimulation. Enfin, nous apportons une validation solide de l'utilisation des paramètres minimaux standards de la tDCS (2 mA, 20 minutes, 2 électrodes HD) et établissons un cadre pour de futures recherches visant à appliquer ces protocoles ou à explorer les effets de la tDCS sur d'autres fonctions cognitives.

Table of Contents

Acknowledgements I

Abstract V

Résumé en Français VII

Résumé Substantiel en Français IX

Table of Contents 1

List of Figures 5

List of Tables 7

List of Abbreviations 9

Chapter I: Introduction 13

I. Non-Invasive Brain Stimulation 13

II. History of Transcranial Direct Current Stimulation 14

III. Lack of Standardized tDCS Protocols 16

IV. tDCS application and parameters 17

IV.1. Electrodes montage: placement and size 19

IV.2. Duration of the stimulation 22

IV.3. Intensity of stimulation and Safety 23

IV.4. Electric field induced by tDCS 25

IV.4.1 Effect of The Type of TES on The Induced EF 27

IV.4.2 Effect Of Electrode Montage on the Induced EF 28

a. Electrode placement on the scalp 28

b. Inter-electrode distance 30

c. Electrode's montage 31

d. Electric field components 32

IV.4.3 tDCS-Induced EF Interaction with the Brain's Anatomy 32

a. Skull resistance 32

b. Cortical gyrification 33

IV.5. Can tDCS-Induced EF Reach Deep Brain Structures? 34

V. tDCS mechanism of action 36

V.1. Influence of Neuronal Orientation and Morphology on tDCS effects 38

V.2. Long-term effects of tDCS: influence on synapses and plasticity 39

V.3. tDCS Influence on Brain Networks and Cellular Activity 40

VI. Effect of tDCS on Cognition and Perception 43
VII. tDCS and Visual Perception 45
VII.1. Organization of Face Recognition Regions 45
VII.2. tDCS Neuromodulation of Face Recognition 46
VIII. Scalp Electroencephalography investigation 49
IX. tDCS electrophysiological effect on scalp EEG recordings 50
X. Intracerebral investigation 54
XI. Fast Periodic Visual Stimulation to measure face recognition 57
XII. Measuring FPVS responses with intracerebral EEG recording 61
XIII. Thesis objectives 66
Chapter II: Transcranial Direct Current Stimulation Neuromodulates Intracranial Cognitive Evoked Activity in Human 69
I. Introduction 70
II. Aims of the study 72
III. Materials and Methods 72
III.1. Participants 72
III.2. Transcranial electrical stimulation 73
III.3. Fast Periodic Visual Stimulation 74
III.4. Intracranial EEG 75
III.5. Experimental procedure 77
III.6. Intracranial neuromodulation investigation 79
IV. Results 81
IV.1. Effects of Right-Hemispheric tDCS on Ipsilateral Cortical Excitability 81
IV.1.1 tDCS significantly neuromodulates face-selective and general visual responses 81
IV.1.2 HD electrodes targeted regions of the VOTC 83
IV.1.3 HD electrodes spatially targeted medial and Lateral FG in VOTC 86
IV.1.4 Electric Field Investigation in the Different Brain Structures 89
IV.1.5 Frequency Dependent Influence of tDCS on Individual Harmonics 90
IV.2. Effects of Right-Hemispheric tDCS on Contralateral Cortical Excitability 92
V. Discussion 95
V.1. Significant neuromodulation using low-intensity, -duration and -resolution tDCS configuration. 95
V.2. Significant neuromodulation maintained after a single-tDCS session 96
V.3. Functional targeting and specific neuromodulation 97
V.4. tDCS Spatially Target Deep Medial Fusiform Gyrus 99
V.5. Harmonic-Specific Analysis of tDCS Neuromodulation 102

V.6. Hemispheric Differences and Lateralized Neuromodulation Effects....103
V.7. tDCS induced EF....103
VI. Perspectives and conclusion....105
VII. Supplementary Materials....108
Chapter III: Correlation Between Intracerebral and Scalp EEG Responses During and After Simultaneous tDCS....115
I. Introduction....116
II. Main objectives....118
III. Materials and Methods....119
III.1. Participants....119
III.2. EEG recording....119
III.3. Transcranial electrical stimulation....120
III.4. Fast Periodic Visual Stimulation....121
III.5. EEG analysis....122
III.6. Statistical analysis....124
IV. Results....125
IV.1. Effect of tDCS on the face-selective response....125
IV.2. Effect of tDCS on the general visual response....128
V. Discussion....130
V.1. Attenuation of face-selective responses detectability during tDCS in scalp EEG....130
V.2. Comparison between iEEG results to Scalp EEG....131
V.3. tDCS disrupts surface synchrony while enhancing deep neural activity....132
V.4. Reconsidering stimulation sites in face recognition: VOTC or DLPFC?....135
V.5. Effects of tDCS on the contralateral hemisphere....136
VI. Perspectives and Conclusion....138
VII. Supplementary Materials....139
Chapter IV: Cognitive EEG Biomarkers recorded with Wireless Neuronaute and Icecap: A frequency-tagging Validation Study....142
I. Introduction....143
II. Main Objectives....144
III. Materials and Methods....145
III.1. Participants....145
III.2. EEG Acquisition....145
III.2.1 Neuronaute: a Wireless EEG System....145
***a.* Icecap: An Ultrathin EEG Net....146**
***b.* Electrocap: a widely clinically used EEG cap....147**

III.3. Fast Periodic Visual Stimulation 147
III.4. Experimental Procedures 148
III.5. EEG Analysis 149
III.6. Statistical Analysis 151
IV. Results 152
IV.1. Face Identity Discrimination EEG Responses Across Systems 152
IV.2. Face Identity Discrimination Inversion Effect 154
IV.3. Face Identity Discrimination at the Individual Level 155
IV.4. Intra And Inter-Cap Reliability 155
IV.5. General Visual Base Frequency Response 156
IV.6. Set Up Time and Comfort 157
IV.7. Impedance Measurement 158
V. Discussion 160
V.1. Icecap Reveals Comparable Cognitive Evoked EEG Measures to Electrocap 160
V.2. Comfort, Setting Up Time, and Remote Usability of Icecap 161
V.3. Assessment of Face Discrimination with FPVS 162
V.4. Impedance Measurement with Icecap and Neuronaute 163
V.5. Future Applications of the Icecap-Neuronaute System 164
VI. Conclusion and Perspectives 165
VII. Supplementary Materials 168
Chapter V: General discussion and Perspectives 170
I. tDCS and Intracerebral Investigation 171
II. tDCS and Scalp EEG 175
III. Icecap and Neuronaute 177
General Conclusion 180
References 182
Appendix 212

List of Figures

Figure 1. The different types of transcranial electrical stimulation waveforms.....14
Figure 2. Electroshock experiments performed by Aldini with different patients, ...16
Figure 3. Application of tDCS.....18
Figure 4. Conventional and HD tDCS configurations. 20
Figure 5. Influence of the electrode's placement on the scalp. 21
Figure 6. Influence of stimulation duration on anode and cathodal (1mA) tDCS after-effects. 23
Figure 7. Influence of stimulation intensity on tDCS after-effects. 24
Figure 8. A. Macro-to-microscopic presentation of the induced EF using a finite element model. ...26
Figure 9. Distribution of common tDCS and tACS montages on the electric field propagation. 27
Figure 10. Influence of modifying electrode position on EF distribution in cortical and subcortical region. 29
Figure 11: Influence of electrode placement on the induced EF. 30
Figure 12. Influence of electrode types and configurations on the distribution of the EF. 31
Figure 13. Impact of Skull Thickness and Spongy Bone Tissue on EF Distribution.....33
Figure 14. Effect of white matter fiber orientation on skull resistivity and current density. 34
Figure 15. tDCS mechanism on neuronal membrane potentials. 37
Figure 16. Influence of neurons' morphology and orientation on tDCS effects. 39
Figure 17. tDCS impacts neuronal plasticity through LTP and LTD. 40
Figure 18. Proposed mechanisms of LTP enhancement by tDCS. 41
Figure 19. Effects of tDCS on Functional Connectivity and Astrocytic Activity. 42
Figure 20. Impact of tDCS on different cognitive functions. 44
Figure 21. The cortical face recognition network in humans. 46
Figure 22. tDCS modulation of face perception. 47
Figure 23. The N170 face-selective ERP.....50
Figure 24. tDCS impact on evoked responses recorded by EEG in the human brain. 52
Figure 25. Influence of tDCS on FIE measured by the N170 amplitude and latency. 53
Figure 26. Figure of ECoG and SEEG implantation methods. 55
Figure 27. Development of the FPVS approach. 58
Figure 28. Experimental FPVS paradigm and its corresponding responses recorded using scalp EEG. 59
Figure 29. Face categorization paradigm and analysis procedure for face-selective responses recorded in a single contact in the fusiform gyrus. 60
Figure 30. Map of face-selective regions in the VOTC brain with intracerebral recordings and FPVS. 62
Figure 31. Effective connectivity of functional brain regions through concurrent intracerebral DES and FPVS. 63
Figure 32. Bidirectional and unidirectional connections between the core cortical face network. ..64
Figure 33. Design of the study protocol with tDCS, FPVS, and iEEG. 74
Figure 34. Fast Periodic Visual Stimulation paradigm used in this tDCS-iEEG experiment. 75
Figure 35. Overview of the combined iEEG-FPVS-tDCS protocol. 78
Figure 36. Overview of the iEEG data analysis.....80
Figure 37. Spatial distribution of the iEEG contacts and the HD-ring tDCS electrodes in MNI space.81

Figure 38. Neuromodulation of iEEG general visual and face-selective responses across the three phases of the tDCS experiment in the right hemisphere and in the right VOTC. 83
Figure 39. Neuromodulation of iEEG general visual and face-selective responses in the right VOTC. 85
Figure 40. Neuromodulation of iEEG general visual and face-selective responses across the three phases of the tDCS experiment in the ten face-selective regions of the right VOTC. 88
Figure 41. Detailed neuromodulation across the first twelve consecutive significant face-selective harmonics during the three tDCS experiment phases in the right hemisphere. 91
Figure 42. Detailed neuromodulation across the first five consecutive significant general visual responses harmonics during the three tDCS experiment phases in the right hemisphere. 92
Figure 43. Neuromodulation of iEEG general visual and face-selective responses across the three phases of the tDCS experiment in the left hemisphere and in the left VOTC. 94
Figure 44. Anatomical characteristics of the middle fusiform gyrus separating the LatFG and medFG. 102
Figure 45. Study design combining tDCS, FPVS, and iEEG to test tDCS On/Off effects on electrophysiological responses. 105
Figure 46. Scalp EEG electrodes positioning according to the 10–20 international system. 120
Figure 47. Design of the study protocol with tDCS, FPVS, and iEEG. 121
Figure 48. Fast Periodic Visual Stimulation used in tDCS-EEG-FPVS experiment. 121
Figure 49. Frequency spectrum of the averaged SNR quantified at the right occipitotemporal regions across three experimental phases for the FPVS paradigm. 125
Figure 50. Baseline-corrected amplitudes and SNR of the face-selective responses across phases. 126
Figure 51. Histograms of the baseline-corrected amplitudes and SNR of the face-selective responses across phases. 127
Figure 52. Frequency spectrum of the averaged SNR quantified at the middle occipital (MO) regions for each stimulation phase. 128
Figure 53. Baseline-corrected amplitudes and SNR of the general visual responses across phases. 129
Figure 54. Face-identity discrimination responses at Bilateral OT regions across tDCS phases. 133
Figure 55. A. Schematic representation of the Neuronaute. 146
Figure 56. Schematic presentation of both EEG recording caps.....147
Figure 57. Representation of the experimental design paradigm.....149
Figure 58. Frequency spectrum of SNR at right occipito-temporal electrode P8 and 3D scalp map topographies.....152
Figure 59. Baseline-corrected amplitudes of the summed harmonics for both caps. 154
Figure 60. Face identity discrimination inversion effect 155
Figure 61. Intra and inter-cap reliability 156
Figure 62. Baseline-corrected amplitudes of the general visual response for both caps.....157
Figure 63. Box plots of setup time for Icecap and Electrocap. 158
Figure 64. Box plots of scalp-electrodes impedances for Icecap and Electrocap. 159
Figure 65. Experimental Words paradigm. 166
Figure 66. Proposed protocol for Investigating tDCS' duration effects and post-stimulation dynamics.....175

List of Tables

Table 1. Studies Investigating the Electric Field Inside the Human Brain: 35
Table 2. Number of contacts implanted in each of the ten face-selective regions for both responses. 86
Table 3 Electric field values in each region of interest: 89

List of Abbreviations

AC	Alternating Currents
AMG	Amygdala
antCoS	Anterior Collateral Sulcus
antFG	Anterior Fusiform Gyrus
antMTG	Anterior Middle Temporal Gyrus
antOTS	Anterior Occipito-Temporal Sulcus
AP	Action Potential
ATL	Anterior Temporal Lobe
BBB	Blood-Brain Barrier
BDNF	Brain-Derived Neurotrophic Factor
CoS	Collateral Sulcus
CREB	Camp-Responsive Element Binding Protein
CSF	Cerebrospinal Fluid
DBS	Deep Brain Stimulation
DC	Direct Current
DES	Direct Electrical Stimulation
DLPFC	Dorsolateral Prefrontal Cortex
DMO	Dextromethorphan
ECoG	Electrocorticography
EEG	Electroencephalography
EF	Electric Filed
ERP	Event-Related Potentials
fEPSP	Field Excitatory Postsynaptic Potentials
FFA	Fusiform Face Area
FFT	Fast Fourier Transform
FIE	Face Inversion Effect
FIR	Face Identity Recognition
fMRI	Functional Magnetic Resonance Imaging
FPVS	Fast Periodic Visual Stimulation,
FU	Follow-Up
GABA	Gamma-Aminobutyric Acid
HD	High-Definition
HIP	Hippocampus
ICA	Independent Component Analysis
iEEG	Intracerebral EEG
IFG	Inferior Frontal Gyrus
IOG	Inferior Occipital Gyrus
kΩ	Kilohms
LatFG	Lateral Fusiform Gyrus
LOT	Left Occipitotemporal
LTD	Long-Term Depression
LTP	Long-Term Potentiation
MDD	Major Depressive Disorder
MedFG	Middle Fusiform Gyrus
MEP	Motor Evoked Potentials
MFS	Medial Fusiform Sulcus
MO	Middle Occipital
ms	Milliseconds
MTG	Mesial Fusiform Gyrus
NHP	Non-Human Primates
NIBS	Non-Invasive Bran Stimulation
NMDA	N-Methyl-D-Aspartate
OCC	Occipital Lobe
OFA	Occipital Face Area
OTS	Occipito-Temporal Sulcus
P1	Phase 1
P2	Phase 2
P3	Phase 3
PD	Parkinson's Disease
PET	Positron Emission Tomography
POS	Posterior Collateral Sulcus
PTL	Posterior Temporal Lobe
rCBF	Regional Cerebral Blood Flow
ROI	Region Of Interest
ROT	Right Occipito-Temporal
RT	Reaction Time
SEEG	Stereoelectroencephalography
SEM	Standard Error of the Mean
SNR	Signal To Noise Ratio
SO	Supra Orbital
SSVEP	Steady State Visual Evoked Responses
STS	Superior Temporal Succus
tACS	Transcranial Alternating Current Stimulation
tDCS	Transcranial Direct Current Stimulation
TES	Transcranial Electrical Stimulation
TMS	Transcranial Magnetic Stimulation
TP	Temporal Pole
TrkB	Tropomyosin receptor kinase B
tRNS	Transcranial Random Noise Stimulation
VEP	Visual Evoked Potential
VMO	Ventromedial Occipital Cortex
VOTC	Ventral Occipito Temporal Cortex
WM	White Matter



Stand at the edge of the dream and fight.

Chapter I: Introduction

I. Non-Invasive Brain Stimulation

Over the past twenty years, the use of non-invasive brain stimulation (NIBS) techniques has gained the attention of neuroscientists in the field, especially for rehabilitating and boosting functions of the human brain. The non-invasive nature common to all NIBS tools has contributed to their widespread recognition and adoption in clinical neuroscience research. Transcranial Electrical Stimulation (**TES**) and Transcranial Magnetic Stimulation (**TMS**) are among the most widely used NIBS techniques, each modulating neural activity through different electromagnetic mechanisms (Antal et al., 2022).

TMS is a safe and painless method of stimulation. It's based on the principle of electromagnetic induction, where an electric current passes through a copper-wired coil placed on the scalp. The resulting magnetic field passes through the skull and induces an electric current in the targeted cortical regions, resulting in modulation of their neuronal firing activity (O'Shea & Walsh, 2007).

TES is a term that refers to NIBS methods that apply an electric current to the scalp's surface. Depending on the type of current used (**Figure 1**), it includes: transcranial direct current stimulation (tDCS), transcranial alternating current stimulation (tACS), and transcranial random noise stimulation (tRNS).

tDCS is an easy-to-use, low-cost, and portable tool that noninvasively stimulates the brain using a direct electrical current. It neuromodulates cortical excitability, resulting in both acute and long-term effects (Nitsche et al., 2005). It gained widespread interest for its clinical application and therapeutic potential for neurophysiological and neurobiological disorders such as Alzheimer's and Schizophrenia, as well as its ability to modulate cognitive functions like perception, memory, and language (Lefaucheur et al., 2017). Despite extensive exploration of its mechanisms, a clear understanding of tDCS's electrophysiological impact on the human brain remains unclear.

tACS utilizes the same setup as tDCS, but applies an alternating current between the 2 electrodes, which switches polarity in a sinusoidal pattern. Unlike tDCS, it does not polarize the membrane potential but influences the brain activity by modulating and entraining neuronal oscillations. This can lead to synchronization or desynchronization of neuronal networks. **tRNS** is a variant of tACS that applies a randomized current fluctuating between 0.1 and 640 Hz (Paulus et al., 2016; Yavari et al., 2018) .

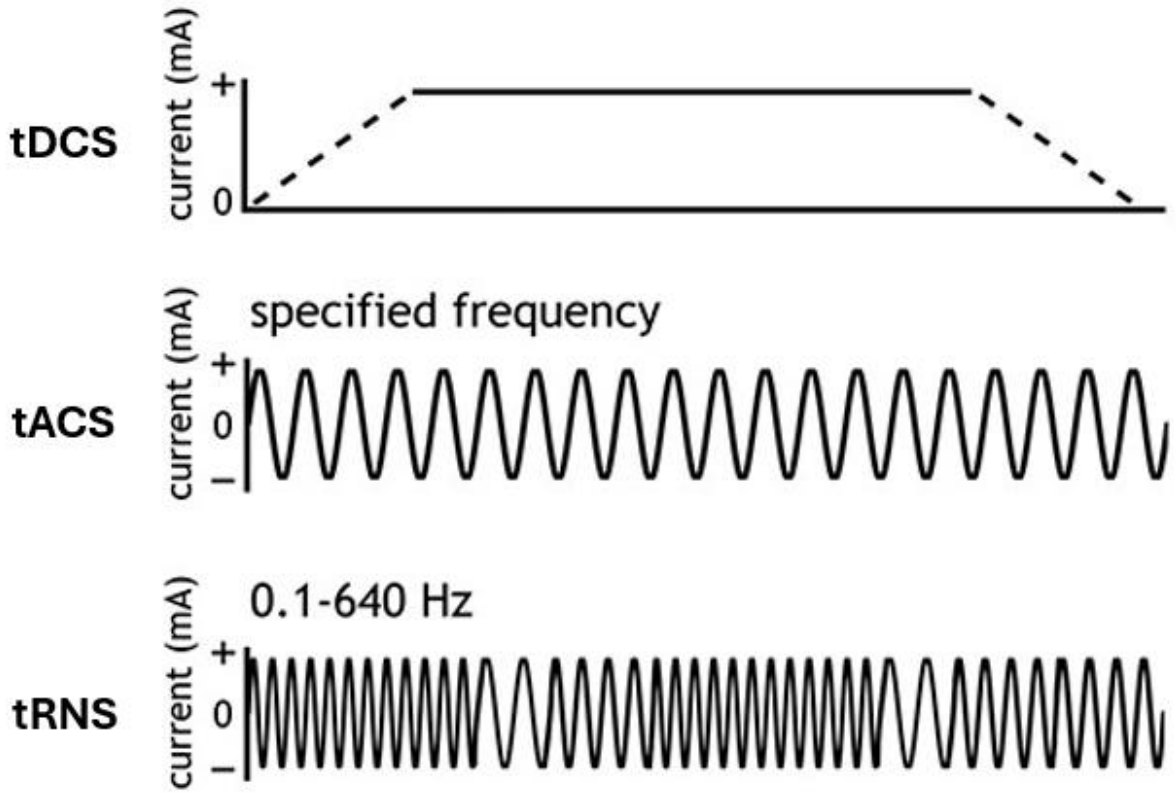

Figure 1. **The different types of transcranial electrical stimulation waveforms**.
Adopted from Park & Thompson, 2024.

In this chapter, we first present a brief history of tDCS application and the current regulations governing its use. Then we examine the key characteristics of tDCS application, its underlying mechanisms of action, and its effects on cognitive functions, with a particular focus on visual perception. We specifically discuss the behavioral and electrophysiological influence of tDCS on facial recognition, as assessed through cognitive tasks and scalp EEG recordings in humans. Furthermore, we introduce the emerging robust approach of periodic visual stimulation combined with intracerebral recordings to investigate face-selective regions in the human brain and propose its advantages for potentially assessing the electrophysiological effects of tDCS. We finally present the objectives of this thesis manuscript in exploring tDCS electrophysiological effects by means of intracerebral and scalp recordings on evoked visual responses.

II. History of Transcranial Direct Current Stimulation

The therapeutic use of electricity is not a modern concept; its potential for treating illnesses has been explored for centuries. One of the earliest recorded instances of electrical phenomena being harnessed for medical purposes is the discovery of "animal electricity." This was observed as early as the ancient Egyptian empire, where reports of electrical fish, such as the torpedo fish, were recorded.

These fishes possess specialized electric organs capable of generating short and powerful, high-voltage pulses of electric current under neural control to stun their prey (Hopkins, 2009).

The use of electric fish for medical treatments has long been used in ancient civilizations. The Romans employed them for therapeutic purposes, where they placed the fish on the forehead to relieve headaches and migraines. Furthermore, in the late 11th century, the Arab physician Ibn-Sidah used them in attempts to treat epilepsy patients. However, it was not until the discovery of electricity in the 17th and 18th centuries and its growing integration into everyday life that researchers began to explore how this newfound phenomenon could be further harnessed for the benefit of human health.

More systematic and scientific applications of electrical stimulation emerged later on, with the first proposition for its medical use in 1743. Johan Gottlob Krüger, a professor of medicine in Germany, was the first to suggest the use of electricity for treating medical conditions. He suggested that it might be particularly beneficial for individuals with palsied limbs, theorizing that electrical stimulation could alleviate muscle contraction (Sarmiento et al., 2016). In 1757, Benjamin Franklin, inspired by Krüger's ideas, utilized the Leyden jar, the first capacitor capable of storing and discharging electrical charges, to treat various ailments. Franklin's experiments involved applying electricity to limbs suffering from movement and brain diseases, such as epilepsy and depression (Beaudreau & Finger, 2006).

The 18th century saw further breakthroughs in the understanding of bioelectricity, particularly through Luigi Galvani's invention of the galvanic battery, which generates direct current (DC) electricity. His experiments with frog muscle contraction under electric stimulation laid the foundation for the development of modern electrophysiology and provided early insights into understanding bioelectric signals in nerve and muscle functions. Giovanni Aldini, his assistant and nephew, expanded on his work by applying galvanic current in electrotherapy. Aldini notably used a Volta pile (an early battery) to administer a galvanic current to the skull to stimulate the brain transcranially in the treatment of conditions such as melancholia (now recognized as major depression) (**Figure 2**). Aldini's self-experimentation led him to report intense sensations and temporary insomnia, further illustrating the profound effects of electrical stimulation on the nervous system (Parent, 2004).



Figure 2. Electroshock experiments performed by Aldini with different patients,
From Aldini's 1804 Essai théorique et expérimental sur le galvanisme.

The pioneering work of Galvani and Aldini significantly contributed to the development of electrical stimulation techniques for the treatment of neurological and psychiatric disorders. These early electrotherapies gained popularity in the 19th century. However, the use of DC stimulation, particularly tDCS, faced criticism due to inconsistent results and variability in stimulation parameters, which led to its decline in clinical and research settings until its resurgence in the mid-20th century.

Over the past two decades, researchers such as Nitsche and Paulus have pioneered our understanding of the modern tDCS and its mechanism of action. Their investigations revealed the importance of various tDCS factors, like duration and intensity, and emphasized the need to consider the outcomes of the different polarities when applying tDCS to a targeted neuronal population (Nitsche et al., 2008). Additionally, current ongoing refinements to tDCS features include developing portable devices for remote at-home application and combining tDCS with advanced neuroimaging techniques to enhance both its precision and applicability (Truong & Bikson, 2018)

III. Lack of Standardized tDCS Protocols

Despite the exponential advancements in the field of NIBS over the years, particularly in tDCS, clear guidelines about the proper application protocols, such as electrode montage and size, current intensity, duration of stimulation, and adverse effects assessment, are still lacking. As of now, no clinical indication for tDCS has received a Level A recommendation indicating its efficacy based on well-conducted randomized controlled trials or consistent findings from multiple studies (Lefaucheur et al., 2017).

For the European Union, the regulation of tDCS devices has undergone significant changes, particularly with the introduction of the Medical Device Regulation 2017/745 on May 26, 2021. It reclassified repetitive TMS and low-intensity tES as Class III medical devices *without an intended medical purpose* (class of high risk, the same category that includes invasive neurosurgical procedures

like Deep Brain Stimulation (DBS)). Although in previous years it was considered as Class IIa, i.e., a category of manageable risk. This reclassification imposes strict requirements on manufacturers, including extensive clinical evaluations and enhanced safety and performance standards. It's been a subject of debate within the scientific community, with concerns that it may hinder the development and accessibility of tDCS, potentially delaying its integration into clinical practice (Antal et al., 2024).

IV.tDCS application and parameters

tDCS is a neuromodulation technique based on applying a direct current of low intensity (order of 0.5 to 2mA) via two or more electrodes placed on the scalp. The electric field induced by the DC flows from the stimulating electrode (anode), traverses the brain, and is received by the return electrode (cathode) (**Figure 3A**). While a large portion of the tDCS-induced electric field (EF) is shunted through the skull, the remaining current is conducted in the brain, where it modulates the cortical excitability, resulting in acute and long-term effects (Reed & Cohen Kadosh, 2018). It's an easy-to-use, low-cost, and portable tool that is generally well-tolerated, with minimal side effects typically limited to mild sensations such as tingling or itching at the electrode sites (Kessler et al., 2012).

tDCS operates using a battery-powered device that delivers a direct current (DC) of low intensity to the brain via electrodes placed on the scalp. Modern tES devices can deliver several types of electric currents, including DC, for applying tDCS and alternating currents (AC) with different sine waves for applying tACS. A positive (anodal stimulation) or a negative current (cathodal stimulation) can be delivered through scalp electrodes. At the onset and offset of stimulation, the current is gradually increased and decreased using a ramp-up and ramp-down procedure to ensure a smooth transition and to avoid abrupt current surges that can harm the skin (**Figure 3B**).

tDCS devices allow the application of sham stimulation: a placebo tDCS consisting of only applying a ramp up and ramp down before and after a specific period that usually matches the period of active tDCS (**Figure 3B**). This procedure is designed to blind participants to the stimulation condition by mimicking the initial physical sensations, such as tingling or itching, associated with active tDCS, without delivering a current long enough to induce neuromodulatory effects (Woods et al., 2016a). Although some studies reported that stronger stimulation intensities, especially during repeated sessions, can increase sensitivity and compromise the blinding, these results don't seem to be consistent (O'Connell et al., 2012; Russo et al., 2013). In some cases, applying a double blinding for both the experimenter and the participant can be useful to avoid experimental bias.

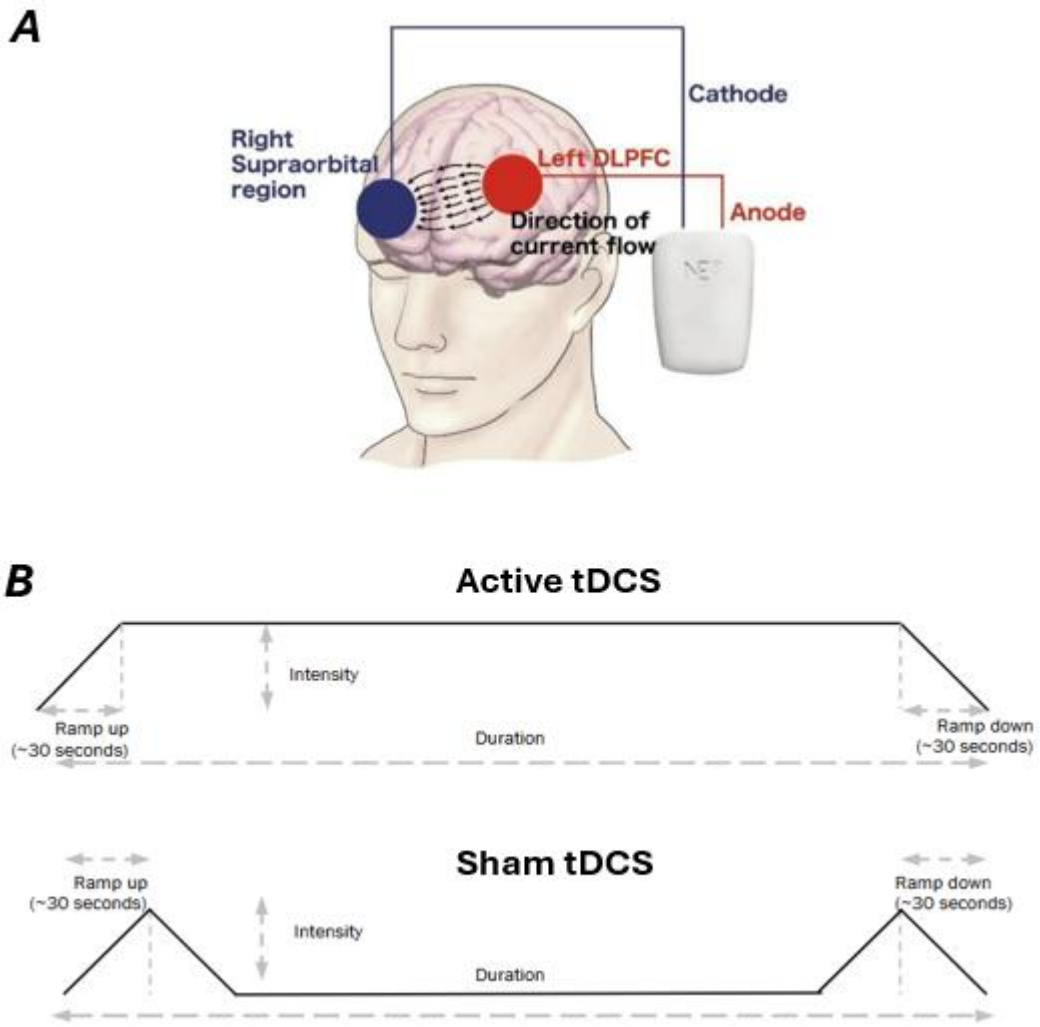

Figure 3. Application of tDCS.
A. Schematic example of tDCS application using two electrodes placed on the frontal lobe. Adopted from Wang et al., 2023. **B.** Active and sham tDCS waveforms illustrations. During active tDCS, the intensity is gradually ramped up over 30 seconds, followed by a sustained intensity at 2mA during the period of stimulation, followed by a gradual ramp down over 30 seconds to reach 0mA again. During sham tDCS, the intensity also ramps up to 2 mA for 30 seconds, then immediately ramps down to 0 mA at the beginning and end of the stimulation period. Adopted from the Soterix website.

Additionally, most devices include real-time impedance monitoring, which refers to the resistance of the materials within the electrical circuit to current flow. Higher impedance indicates greater resistance; therefore, it reduces the efficiency of current delivery to the brain. To assess impedance during stimulation, a small alternating pulse is delivered on top of the DC. This feature enables continuous assessment of the circuit quality during stimulation and facilitates adjustments, such as adding gel to the electrodes, to maintain optimal electrode-skin contact (Reinhart et al., 2017).

Unlike pharmacotherapy, tDCS allows for anatomically specific brain activation and precise temporal control, making it customizable for individual brain targets. Thus, the application of tDCS can

be personalized to target specific brain regions, and therefore specific cognitive functions, in order to optimize particular rehabilitation outcomes (Bikson et al., 2012). Evidently, the effective application of tDCS requires controlling several factors depending on the specific targeted function. In the following section, we discuss these different factors: choice of electrode configuration, duration, polarity, and intensity of stimulation to ensure participants' safety. We will also discuss the various methodological and anatomical factors that can directly influence the flow and the strength of an EF induced by tDCS.

IV.1. Electrodes montage: placement and size

The type, size, shape, and montage of electrodes used during tDCS are detrimental factors of the magnitude and distribution of the tDCS-induced EF in the brain. In conventional tDCS protocols, electrode sizes typically range between 25 to 35 cm2. These large, spongy electrodes target broader cortical areas and tend to generate a more diffuse EF distribution. Moreover, their size may result in an edge effect, where current density is concentrated at the edges of the electrode. To address these concerns, smaller circular ring electrodes have been used, particularly in high definition (HD) tDCS montages. Due to their small size, these electrodes are capable of producing a more focal and spatially restricted EF, thereby improving the precision of neuromodulation (**Figure 4 A,B and 5Ac ,d**: Solomons & Shanmugasundaram, 2020).

Therefore, we can distinguish two types of tDCS:

1. **Conventional tDCS:** Involves applying a direct current of low intensity to the scalp using two spongy rectangular pad electrodes, where the anode is placed over the targeted region and the cathode over another brain region or an extracephalic region. This type of large and separated electrodes results in a widespread stimulation over the surface of the cortex, with a non-focal EF distribution within the brain (Datta et al., 2009).

2. **High-definition tDCS:** This configuration utilizes concentric ring configurations (e.g., 4x1 ring), where, in total, 5 small ring electrodes are used. The anode is placed over the targeted region, surrounded by the other 4 return electrodes. The montage's radius is approximately 3 cm. The sum of the current density in each electrode corresponds to the total applied current (e.g., 1 or 2 mA). This configuration results in an enhanced spatial focality, with the region of modulation being constrained to the perimeter between the anode and the return electrodes (Edwards et al., 2013). The appropriate placement of the electrodes on the scalp, along with the number, type, and size of the electrodes, plays a critical role in the generation and magnitude of the EF and its influence on targeted cortical areas. See the 4x1 and the MXN HD configuration shown in **Figures 5Ac and 5Ad.** (for the influence of the electrode montage on the induced EF modulation, detailed in section **IV.4.2.c**).

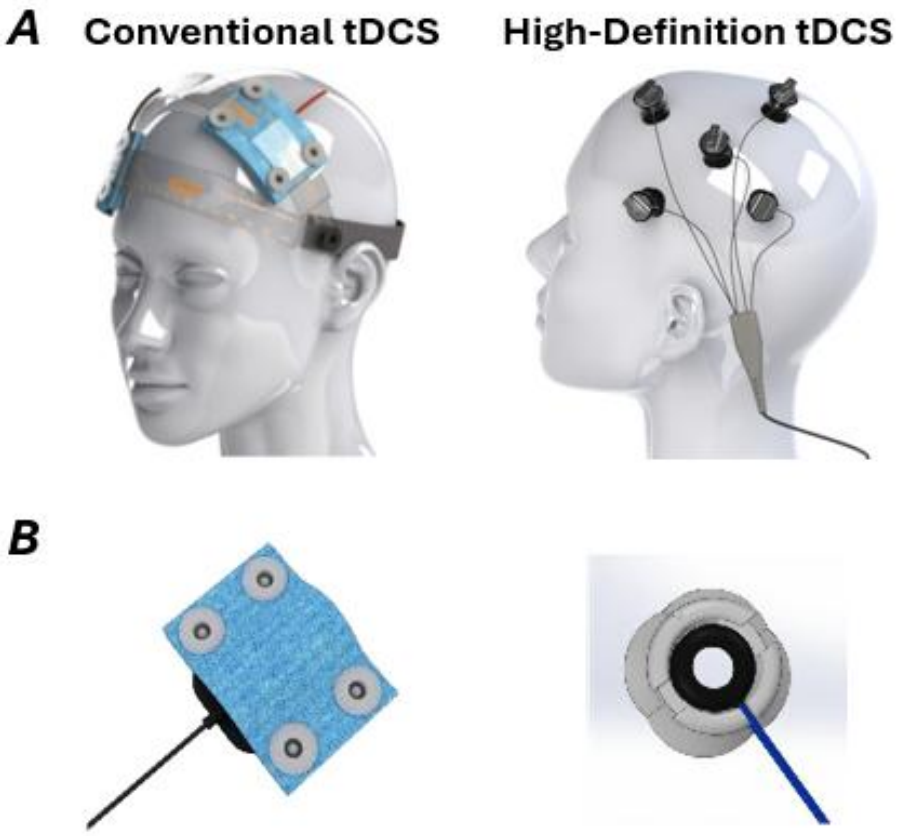

Figure 4. Conventional and HD tDCS configurations.
A. Head models of Conventional and HD-tDCS montages. **B.** Close-up view of the sponge electrodes and the HD ring electrode in the electrode holder base. Adopted from the Soterix website.

The proper placement of the electrodes on the surface of the scalp, especially the location of the stimulating electrode (anode), is determined by the functional targeting during the stimulation. Commonly, tDCS electrode montage follows the International 10/20 EEG system for electrode placement. For instance, a tDCS montage targeting the primary Motor cortex (M1) and the Supraorbital region, using C3 and F2 scalp positions respectively, appears to be the optimal configuration for stimulating the motor cortex and elucidating significant changes in motor evoked potentials (MEP). Notably, other tDCS montage combinations failed to demonstrate significant changes in the MEP amplitudes (**Figure 5B**: Nitsche et al., 2008; DaSilva et al., 2011). For more focal montages (HD-tDCS), neuronavigation software can be employed to incorporate individual MRI head models, allowing for more precise targeting of specific brain regions (Niemann et al., 2024).

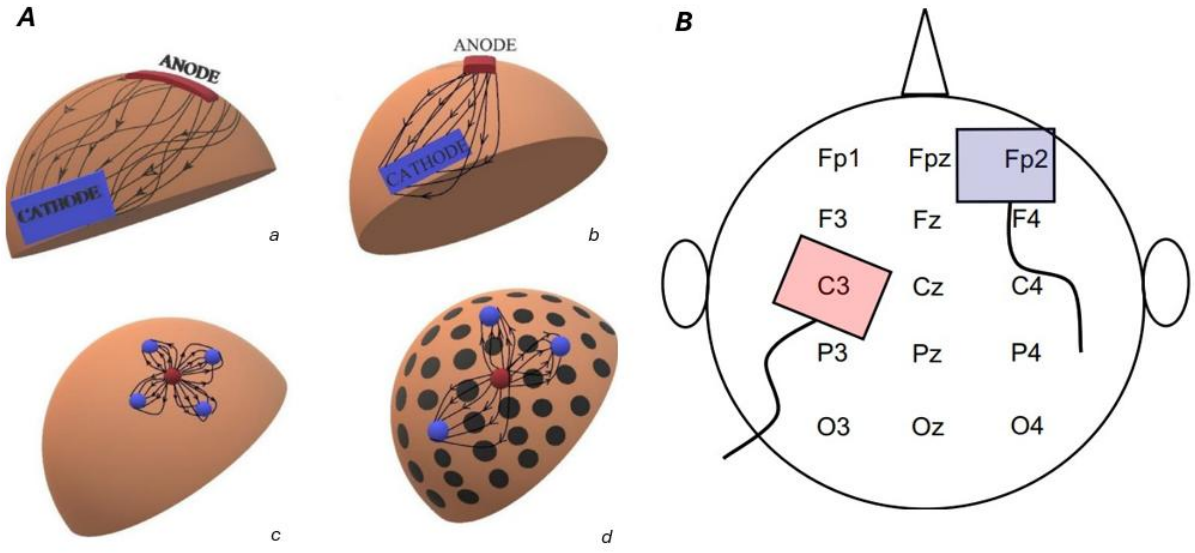

Figure 5. Influence of the electrode's placement on the scalp.
A. Illustration of the current flow in different electrode configurations. a) tDCS with large sponge electrodes, b) small anode electrode, large cathode electrode, c) HD-tDCS 4 ×1 ring electrode configuration, anode (red) in the center and four cathodes (blue), d) HD-tDCS MXN configuration allows for various combinations of anode and cathode electrodes, the example here shows one anode and three return electrodes. Adopted from Solomons & Shanmugasundaram, 2020. **B.** Schematic drawing of the optimal anode and cathode positions for tDCS of the primary motor cortex; anode (red) over the primary motor cortex (C3) and the cathode (blue) over the supra-orbital (Fp2), according to the 10-20 system. Adopted from Nitsche et al., 2008.

Notably, experimental evidence revealed the potential superiority of HD-tDCS montages in eliciting significant neuromodulatory effects in comparison to conventional tDCS configurations (Morya et al., 2019). For example, in heathy participants, tDCS was applied using both a conventional electrode setup (35 cm2 electrode) and an HD-tDCS configuration employing a 4 × 1 ring montage. Stimulation was applied at 2mA for 10 min over the motor cortex, and its effects were assessed on MEPs. Findings revealed a greater modulation of the MEP with HD-tDCS than with convention tDCS montages, with effects persisting for more than two and less than 6 hours post-stimulation. Notably, the peak effect of HD-tDCS was delayed and reached maximum magnitude approximately 30 minutes after the end of the stimulation. Thus, these findings underscore the importance of electrode placement and montage design in targeting specific neural functions during therapeutic applications, particularly in light of the relatively transient and diminishing effects observed with conventional tDCS (H.-I. Kuo et al., 2013).

Furthermore, it's important to mention the important role the placement of the return electrode plays in the distribution of the field and, consequently, the outcome of the stimulation. The cathode can be placed on the scalp or extracephalically (for example, on the arm) to increase the inter-electrode distance and reduce the shunting effect at the scalp. Modifying the return electrode placement can lead to distinctly different outcomes in terms of cortical excitability and evoked potential. For example, implementing a tDCS montage with the anode placed over the motor cortex

and cathode over the chin, in contrast to its typical placement over the contralateral orbit, did not reveal a clear modulation of the MEP. However, when anodal tDCS was preceded by a cathodal session in the same setup, it counterintuitively reduced the MEP amplitude (Masina et al., 2021; Nitsche et al., 2008; Priori et al., 1998). Therefore, these findings suggest that the direction and magnitude of excitability shifts depend not only on the stimulation polarity but also on the specific electrode configuration. Adjusting both the stimulating and return electrodes' positions directly alters the distribution of the EF in the brain, which in turn influences the efficacy of stimulation, the targeted brain regions, and the overall physiological response to tDCS. Thus, careful consideration of electrode placement is crucial for achieving optimal neuromodulatory and therapeutic outcomes with tDCS.

IV.2. Duration of the stimulation

The duration of the stimulation is a critical parameter for tDCS strength. It can last from a couple of seconds to several minutes, during one or multiple sessions. The most commonly adopted duration of stimulation for clinical therapy is around 20 minutes (Lefaucheur, 2016). Varying this duration can influence the direct acute outcomes and long-term after-effects of tDCS. Short-duration (minimum of 3 min) anodal or cathodal tDCS over the primary motor cortex modulates the amplitude and endurance of MEPs, with anodal stimulation increasing excitability and cathodal stimulation decreasing it (**Figure 6A:** Nitsche & Paulus, 2000). However, these effects are limited to the stimulation period and do not induce lasting after-effects. For longer stimulation durations, at least 13 minutes for anodal and 9 minutes for cathodal, tDCS elicited lasting after-effects that persist for approximately 90 and 60 minutes, respectively (**Figure 6 C,D** :Nitsche & Paulus, 2001; Nitsche, et al., 2003, 2005, 2008). Interestingly, extending the stimulation duration without interruptions may shift the excitability enhancement induced by anodal tDCS into a reduction (Monte-Silva et al., 2013). This underscores the importance of choosing the appropriate stimulation duration based on the targeted function.

Repeated sessions of tDCS are performed to stabilize and prolong the stimulation's after-effects. For most disorders like Chronic pain, Parkinson's disease, Stroke, Epilepsy, Alzheimer’s disorder, Depression, and others, patients receive one or several tDCS sessions every day for a couple of weeks or months (Antal et al., 2010; Lefaucheur et al., 2008, 2017). For example, consecutive daily sessions of anodal tDCS have been shown to enhance motor functions in stroke patients more effectively than weekly spaced sessions (Boggio et al., 2007). Notably, the duration between sessions plays a crucial role in determining tDCS influence. A short inter-session interval, varying between 3 to 20 minutes, seems to combine simulation’s after-effects and maintain them for more than 24 hours. However, a long interval (3 to 24 hours) between sessions has been shown to abolish the after-effects (**Figure 6B,** Monte-Silva et al., 2013).

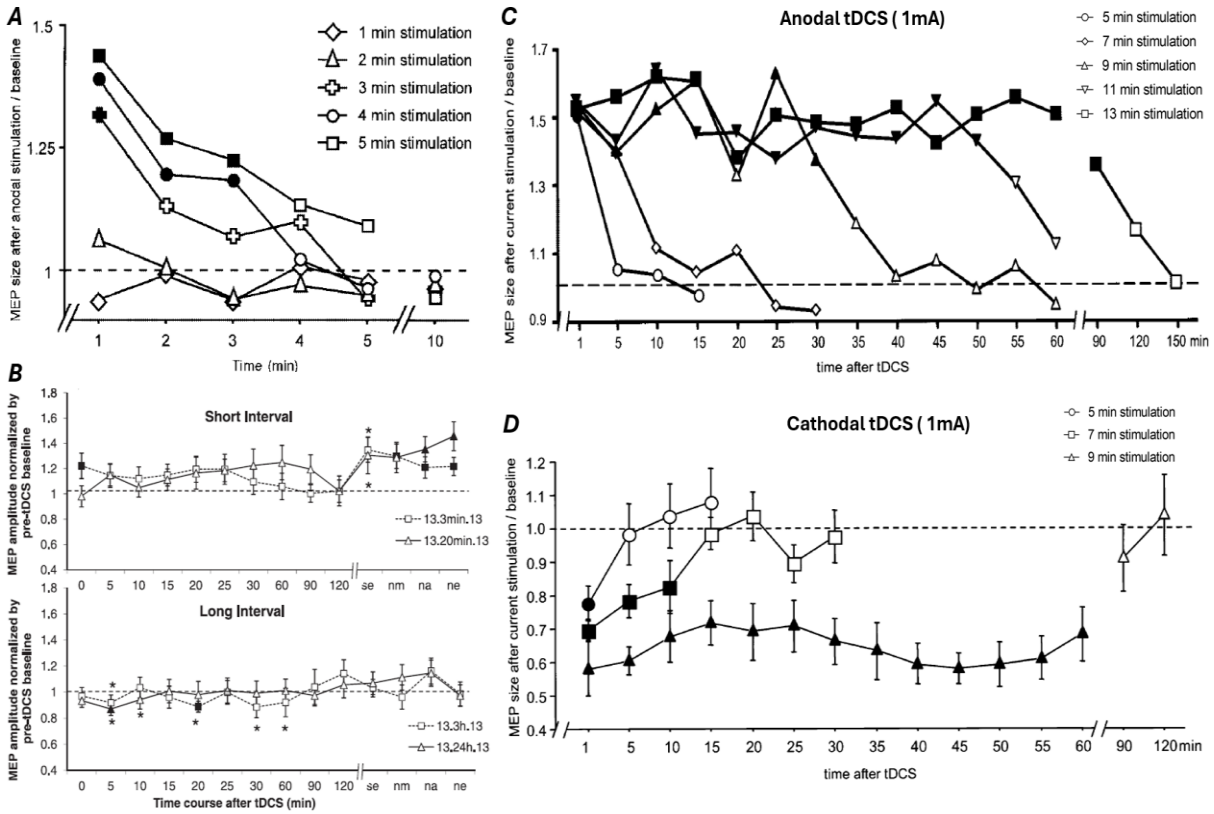

Figure 6. Influence of stimulation duration on anode and cathodal (1mA) tDCS after-effects.
A. A minimum of 3 min stimulation duration was needed to induce significant changes in the size of the MEP after anodal tDCS. Adopted from Nitsche & Paulus, 2000. **B.** Influence of inter-tDCS interval duration. For a short interval (3 to 20 min) between two 13 min anodal tDCS sessions, the MEP amplitude is reduced until 90 min post-tDCS, followed by a significant increase in the next morning (nm), afternoon (na), and evening (ne). The effect is more pronounced with a 20-minute inter-tDCS interval. Moreover, long intervals (3 to 24 hours) between tDCS sessions completely abolished anodal tDCS excitability enhancements. Adopted from Monte-Silva et al., 2013. **C.** After 5 and 7 min of anodal stimulation, MEP amplitudes return to baseline within 5 min. In contrast, tDCS applied for 9 to 13 minutes produces after-effects that persist for up to 1.5 hours post-stimulation. **D.** After 5 and 7 mins of cathodal tDCS, MEP amplitudes return to baseline within minutes, whereas 9 minutes of tDCS leads to after-effects lasting up to 1-hour post-stimulation. Adopted from Nitsche, et al., 2003; Nitsche & Paulus, 2001.

IV.3. Intensity of stimulation and Safety

tDCS is considered a noninvasive and well-tolerated stimulation technique, with little to no adverse side effects. The most common side effects reported from a large sample (n=131) and sessions (277) size were tingling, burning, itching, and tolerated pain sensations under or near the stimulating electrodes (Kessler et al., 2012). Mild skin redness is common during tDCS and resolves shortly after stimulation. Notably, it doesn't damage the blood-brain barrier (BBB) or brain tissue as detected by MRI investigation, and cumulative exposure from multiple tDCS sessions doesn't give rise to additional adverse effects (Bikson et al., 2016).

The intensity of tDCS is one of the most critical parameters to adjust in order to achieve effective stimulation of a specific brain region. Several intensities, varying from 0.2 to 1mA, were used to investigate the minimal intensity that induces tDCS after-effects in humans. A minimum 0.6 mA

intensity, during 5 min of stimulation, seems to be the lowest range at which tDCS induces significant excitability changes on MEP (**Figure 7A:** Nitsche & Paulus, 2000). It's important to mention that increasing stimulation intensity can sometimes reverse tDCS effects. For instance, during a sustained stimulation duration of 20 minutes, cathodal tDCS, which typically induces inhibition at 1 mA, may instead lead to excitation when applied at 2 mA (**Figure 7B:** Batsikadze et al., 2013). In addition, anodal tDCS applied at an intensity threshold ≥ 1 mA during 26 min can reverse the excitatory neuronal plasticity induced by tDCS, helping to prevent excessive brain excitation (Hassanzahraee et al., 2020).

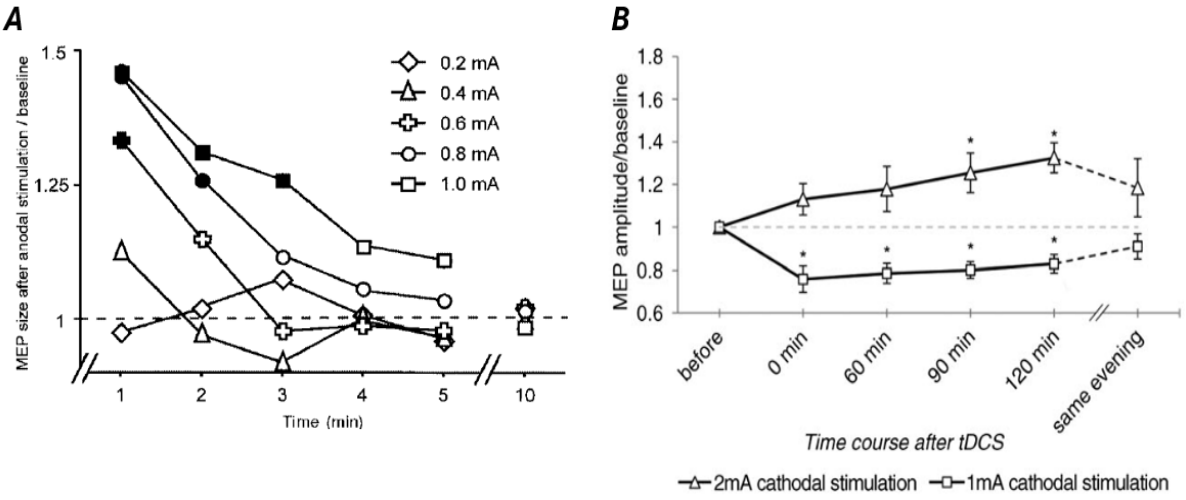

Figure 7. Influence of stimulation intensity on tDCS after-effects.
A. A minimum of 0.6 mA stimulation intensity during 5 min of anodal tDCS was needed to significantly change the size of the prolonged MEP post-stimulation. Adopted from Nitsche & Paulus, 2000. **B**. Cathodal tDCS at 2 mA significantly increased the MEP amplitudes at 90- and 120-minute post-stimulation, whereas at 1 mA, cathodal tDCS significantly decreased the MEP amplitudes throughout 0 to 120 min after stimulation (n = 9). Adopted from Batsikadze et al., 2013.

For clinical investigations, the most common intensities applied are around 2mA (Lefaucheur et al., 2017, for review), but also, intensities as high as 4mA have been applied without reports of adverse effects (Nitsche & Bikson, 2017). A direct correlation between tDCS intensity and the induced EF in the human brain exists: when the intensity of tDCS is increased twofold, the EF is also doubled (Louviot et al., 2022). A potential way to increase the efficacy of the simulation is to increase its intensity from the standard 2mA. This can be achieved by using larger rectangular pad electrodes or applying a more focal HD-configuration with smaller electrodes (Dmochowski et al., 2011). However, the assumption that higher intensities, leading to higher currents, improve clinical outcomes remains largely unexplored (Nitsche & Bikson, 2017). Research that explored the impact of varying tDCS intensities on human cortical excitability showed that while the induced EF correlates linearly with current intensity, neurophysiological responses are complex, non-linear, and state-dependent. This indicates that simply increasing the intensity does not consistently enhance cortical excitability and may sometimes diminish tDCS effects (Esmaeilpour et al., 2018). Notably, the induction of tDCS after-

effects is both intensity- and duration-dependent, with these two factors being interrelated. Increasing the intensity should consider the duration, and vice versa, to prevent reverse tDCS effects and ensure individuals' safety.

IV.4. Electric field induced by tDCS

One of the most detrimental aspects of tDCS application is the generated EF, particularly its direction and magnitude within the brain. During tDCS, a direct current is delivered between two electrodes, which induces a bipolar EF across the scalp and underlying brain regions. It represents the voltage gradients generated inside the head as current passes through the brain, leading to the polarization of neuronal membranes and affecting various functional and cellular properties (Datta et al., 2009). More specifically, the EF flows from the anode to the cathode and modulates neuronal excitability by inducing membrane polarization: neurons located near the anode tend to become depolarized, increasing their excitability, while those near the cathode undergo hyperpolarization, leading to reduced excitability. Notably, different compartments of a single neuron can experience both depolarization or hyperpolarization simultaneously when exposed to an EF (Reato et al., 2019; Datta et al., 2008; Nitsche & Paulus, 2000; Bindman et al., 1962; Creutzfeldt et al., 1962).

The generated EF during the stimulation is composed of two components: tangential and radial (**Figure 8Ab, 8Ba, b**). The radial EF component is parallel to the somatodendritic axis of the pyramidal neurons in layer 5 and primarily affects the somas and the dendrites following the somatic doctrine (detailed in section **V.1**). During anodal stimulation, the radial EF tends to depolarize the soma, enhancing neuronal excitability. Whereas cathodal stimulation causes hyperpolarization and reduces their excitability. Notably, due to the spatial orientation of the field, neurons closer to the positive pole are hyperpolarized, and the ones closer to the negative pole are depolarized. Interestingly, pyramidal neurons in layers 2/3 display a more complex response pattern due to their morphology, with their distal dendritic terminals reaching peak depolarization independently of the somatic membrane potential (**Figure 8Ca**). In contrast, the tangential EF component is perpendicularly oriented to the somato-dendritic axis and seems to be the component predominantly generated by tDCS. Tangential EF influences axonal terminals and alters synaptic efficacy and transmission. This polarization effect is most pronounced in neuronal processes aligned with the direction of the field (**Figure 8Cb** : Rahman et al., 2013).

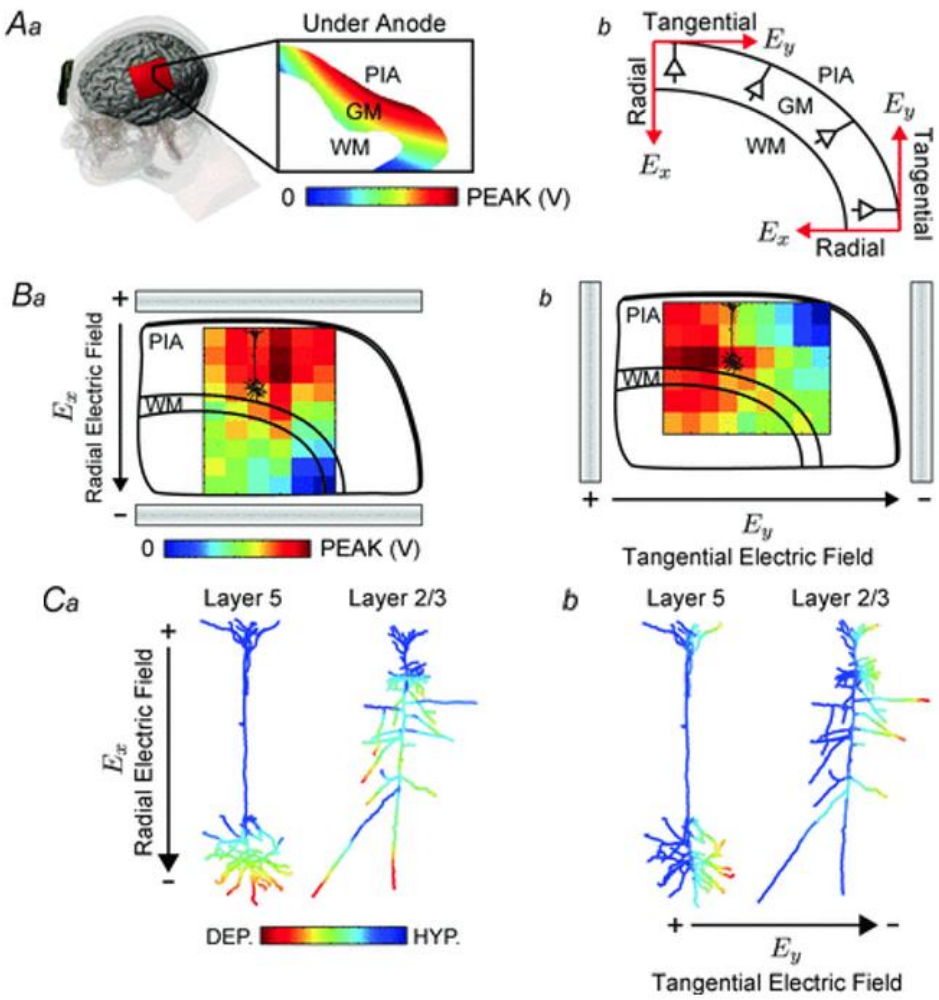

Figure 8. A. Macro-to-microscopic presentation of the induced EF using a finite element model.
Aa. Modeled electric current in the cortical gyri, showing a uniform voltage gradient in the grey matter under the stimulating electrode. **Ab.** tDCS induced EF in the cortex decomposed into a radial (Ex) and tangential (Ey) components parallel and orthogonal to the somato-dendritic axis, respectively. **B.** Schematic presentation of a rat brain slice of the primary motor cortex preparation between two wires during both radial **(a)** and tangential **(b)** induced field potentials. **Ca.** Polarization pattern of a layer V pyramidal neuron in a radially directed uniform EF, showing soma depolarization (red) and apical dendrite hyperpolarization (blue). Pyramidal neurons in layer II/III exhibit a more complex pattern, with long terminals reaching peak depolarization regardless of the soma **Cb.** Under a tangential EF, polarization primarily affects neuronal processes aligned with the field direction. Adopted from Rahman et al., 2013.

Current knowledge from direct intracranial recordings provides evidence that EFs generated by tES in the human brain typically fall within the range of 0.02–0.36 mV/mm for common used stimulation intensities (1-2 mA) (Guidetti et al., 2022). These fields are in the ranges that enable subthreshold neuromodulation inside the brain, as reported in animal studies (<1mV/mm) (Ranieri et al., 2012). Nevertheless, a proper estimation of the exact EF induced by tDCS inside the human brain is still lacking.

Although properties of the induced EF appear well-defined, their effects on the brain are far more complex due to various methodological and biological factors that can modulate their influence. Methodological variables, such as the type of tES used, the electrode montage implanted, and their

characteristics, directly influence the strength and directionality of the EF. Furthermore, the interaction between the EF with the brain's anatomical properties has significant implications on the effects of stimulation, especially in terms of its ability to influence deeper brain regions. This interaction determines the electrical dose delivered, which in turn influences the underlying neurobiological responses and, ultimately, behavioral outcomes (Peterchev et al., 2012).

IV.4.1 Effect of The Type of TES on The Induced EF

Various non-invasive tES techniques, like tDCS and tACS, are designed to modulate neural activity by applying electrical currents to the scalp. Each type can influence the EF in a different manner; therefore, selecting the proper stimulation waveform determines the nature of neuromodulation. tDCS generates a static or direct EF by applying a constant current to the scalp. The polarity of this EF is unidirectional and remains stable over time, resulting in a relatively uniform and steady distribution within the brain (**Figure 9A1, 2:** Datta et al., 2009). The EF generated by tDCS alters the neuronal firing threshold rather than inducing neurophysiological responses like action potentials. Notably, the effects of the EF are transient: once the stimulation is stopped, the induced current ceases immediately, leaving no residual electrical activity in the tissue (Bikson et al., 2012).

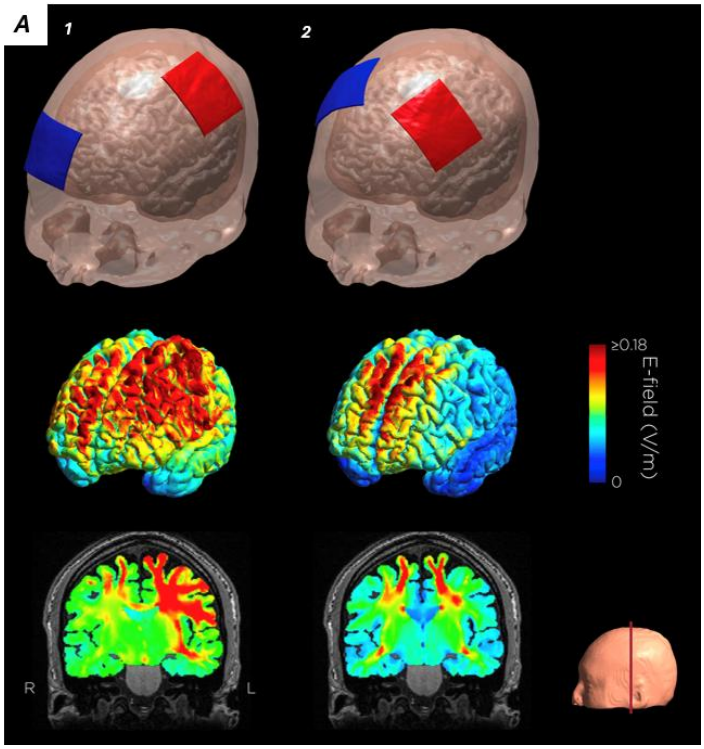

Figure 9. Distribution of common tDCS and tACS montages on the electric field propagation.
A.1. Conventional tDCS applied using rectangular-pad electrodes where the anode was placed over the left primary motor cortex (red) and cathode over the contralateral supraorbital ridge (blue) electrodes. **A.2.** A bilateral dorsolateral prefrontal cortex (DLPFC) setup was used, with sponge electrodes positioned over the F3 and F4 EEG locations. The EF was modeled using a stimulation intensity of 1 mA. Adapted from Bikson et al., 2018.

Meanwhile, tACS generates an oscillating EF by alternating the polarity of the current at specific frequencies, resulting in an EF that follows the sinusoidal waveform of the current. The primary neurophysiological effect of tACS is the entrainment of spontaneous neural oscillations by synchronizing with ongoing brain rhythms at the applied frequency (Antal & Herrmann, 2016). In contrast to tDCS, the oscillatory nature of tACS introduces phase-dependent variations in the EF. In non-human primates (NHP), switching the stimulation phase from 180 to 0 degrees resulted in 1.8-fold and 3.5-fold increases in the EF in deep brain regions for each monkey (Alekseichuk et al., 2019).

The range of the EF magnitude induced by tACS is typically comparable to that of tDCS for similar stimulation intensities (Guidetti et al., 2022). Moreover, biological tissues (white matter and skull bone) present capacitive properties that distort the EF and lead to phase shifts and attenuation, particularly at higher frequencies, as seen in both humans (Huang et al., 2017) and NHP (Opitz et al., 2016). The distribution of the EF produced by both tDCS and tACS is heavily influenced by the configuration of the electrode: size, montage, number, and location, and by the individual's brain anatomy (Guidetti et al., 2022; Bikson et al., 2012).

IV.4.2 Effect Of Electrode Montage on the Induced EF

a. Electrode placement on the scalp

The EF is both montage and dose-dependent; choosing the precise positioning of the stimulating and receiving electrodes is essential to ensure sufficient EF magnitude targets the intended brain regions. Proper placement directly affects the depth, precision, and efficacy of stimulation and determines which cognitive functions are modulated. Using five distinct tDCS montages, DaSilva et al., 2015 employed computational modeling to investigate predicted EF's effects on different cortical and subcortical regions in migraine and chronic pain conditions. A Motor Cortex-Supraorbital (M1-SO) montage produced peak current flow of 0.68V/m in the prefrontal cortex, and in deep brain structures like the anterior and posterior insula, suggesting its preferential use for visceral pain in chronic patients. Conversely, the montage targeting bilateral DLPFC induced peak EF only in the anterior insula, showing its suitability for specifically modulating emotional involvements in chronic pain disorders (**Figure 10**).

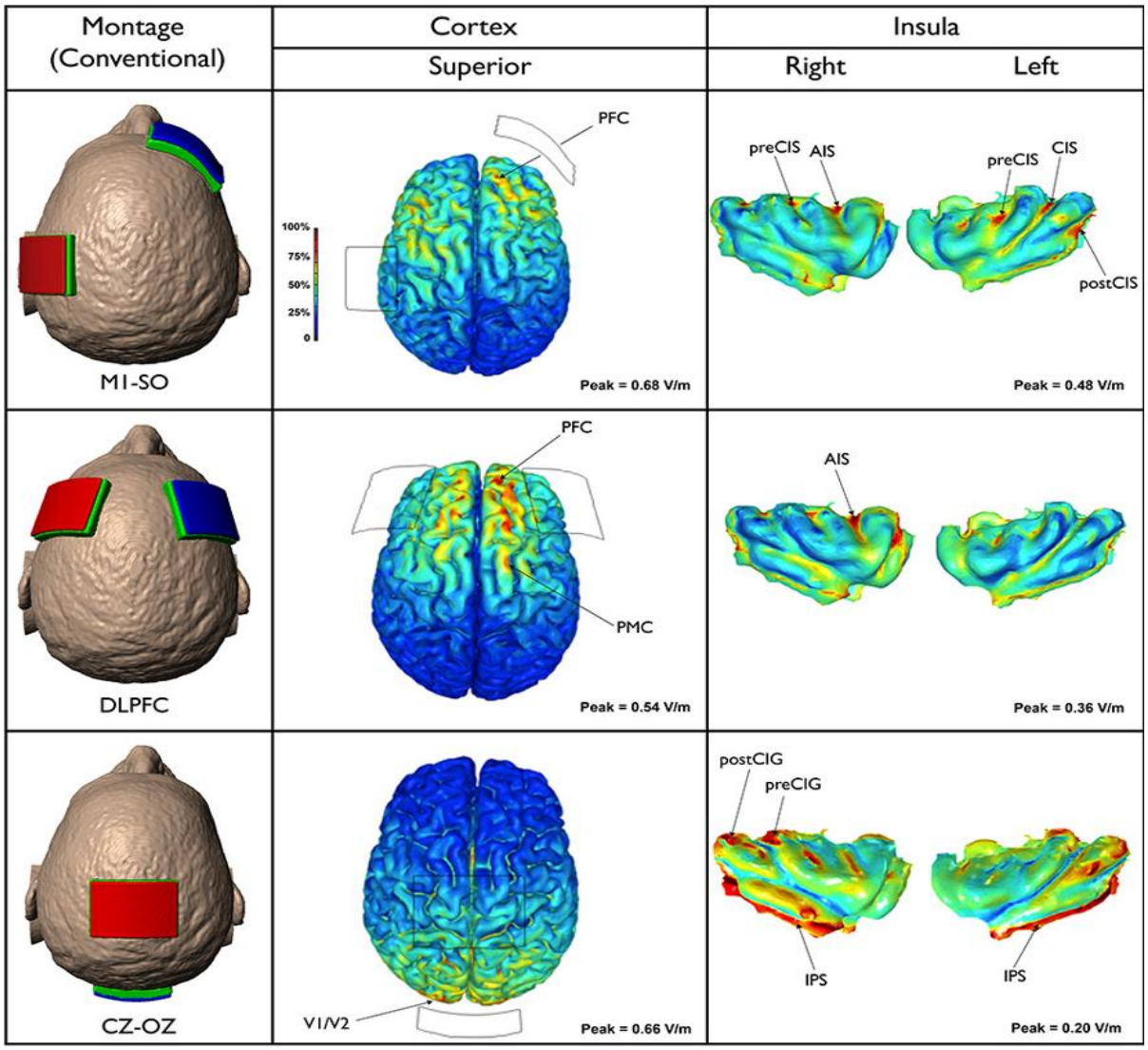

Figure 10. Influence of modifying electrode position on EF distribution in cortical and subcortical region.
Three conventional tDCS montages, shown in the first column, from top to bottom: M1-SO, bilateral DLPFC, and Cz-Oz. The second and third columns show the distribution of the electric field in the cortex and in the right and left insula. Adapted from DaSilva et al., 2015.

Notably, applying an electrode montage for targeting the vertex in two monkeys during 2mA tES resulted in a fourfold increase in intracranial EF intensity when the cathode was placed over the right middle temporal area compared to the mirrored montage (Kar et al., 2017). Moreover, for a fixed montage, the EF density correlates with the stimulation intensity of tDCS (Huang et al., 2017) and tACS (Kar et al., 2017). Research highlights that optimized electrode arrangements can dramatically enhance both focality and intensity of the EF, with improvements of up to 80% and 98%, respectively (Dmochowski et al., 2011; Huang & Parra, 2019).

b. Inter-electrode distance

Proximity in the placement of the electrodes plays a critical role in EF distribution: electrodes placed closer to each other are more prone to current attenuation, resulting in higher currents on the scalp (> 3000 A/m) and reduced EF in deeper brain regions (**Figure 11A, a**). Conversely, it decreased over the lateral sulci to 50 A/m when the distance between the electrodes was increased. Interestingly, spacing the electrodes further apart (sites C3-C4), and especially over areas like the deep sulci, allows the EF to flow in the pathway of the low-resistive cerebrospinal fluid (CSF) and improves the density of the current in deeper brain structures (**Figure 11A,d,** Holdefer et al., 2006).

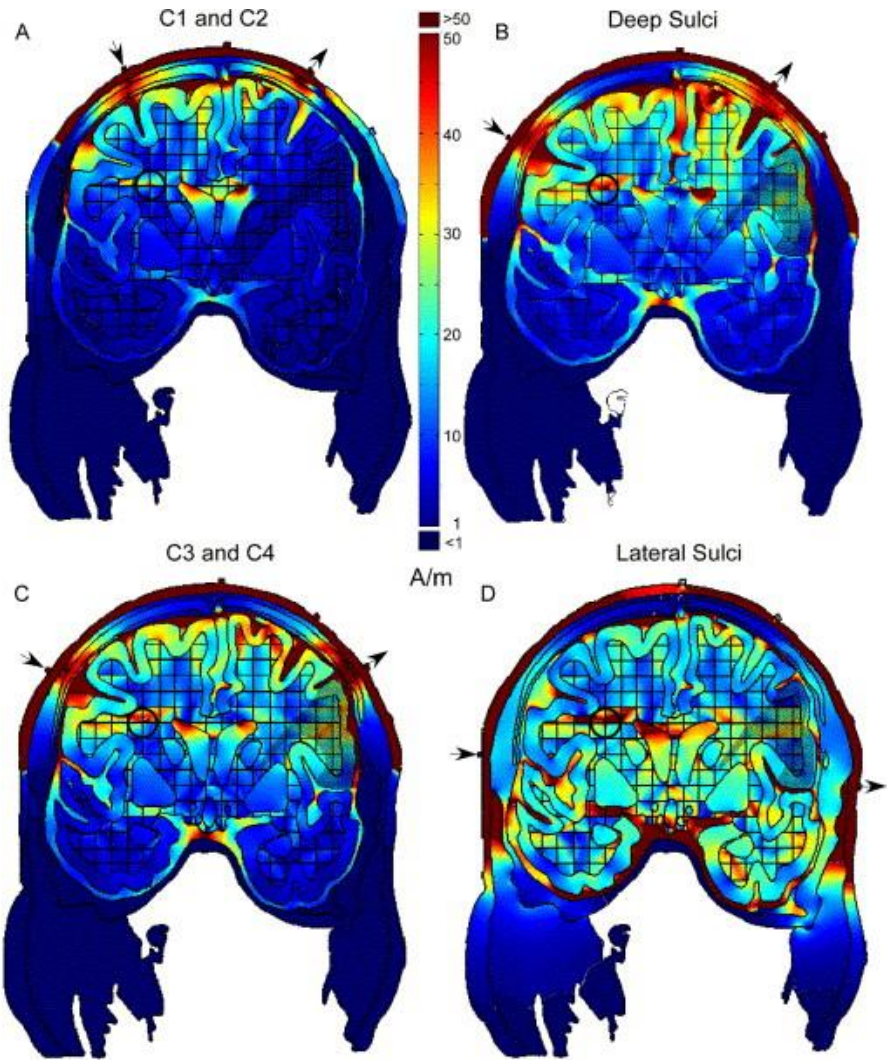

Figure 11: Influence of electrode placement on the induced EF.
Panels A to D present the current density distribution in montages with increasing distance between scalp electrodes (arrows). The greatest current density on the scalp was measured for the stimulation using C1-C2 sites (> 50 A/m) (**A**) and decreased as the distance increased between sites to 50 A/m in the lateral sulci (**D**). In contrast, the current density measured for white matter regions expected to represent face and arms (black circle) peaked in the lateral sulci (89 A/m) (**D**) with comparable densities for the C3-C4 sites (**C**) and in deep sulci (**B**). Adapted from Holdefer et al., 2006

c. Electrode's montage

The size, the type, and the number of electrodes used for stimulation play an important role in delivering sufficient electric current to deeper brain regions. Using a conventional tDCS with two rectangular (ex., 7x5 cm2) pad electrodes results in a diffused EF, with peak magnitudes not necessarily occurring beneath the stimulating electrode but at intermediate regions due to cortical neuroarchitecture and conductivity. Hence, the induced current spreads beyond the montage targeted areas (Datta et al., 2009). However, increasing the number of electrodes and using a smaller electrode in a 4x1 ring arrangement can improve the spatial focality and allow better control of the field's orientation (DaSilva et al., 2015, see **Figure 12**). Peak magnitudes of the induced EF in the HD configuration were observed in the gyri and sulcus directly underneath the anode, and modulated regions were limited to the circular region between the anode and return electrodes (Caparelli-Daquer et al., 2012; Datta et al., 2009).

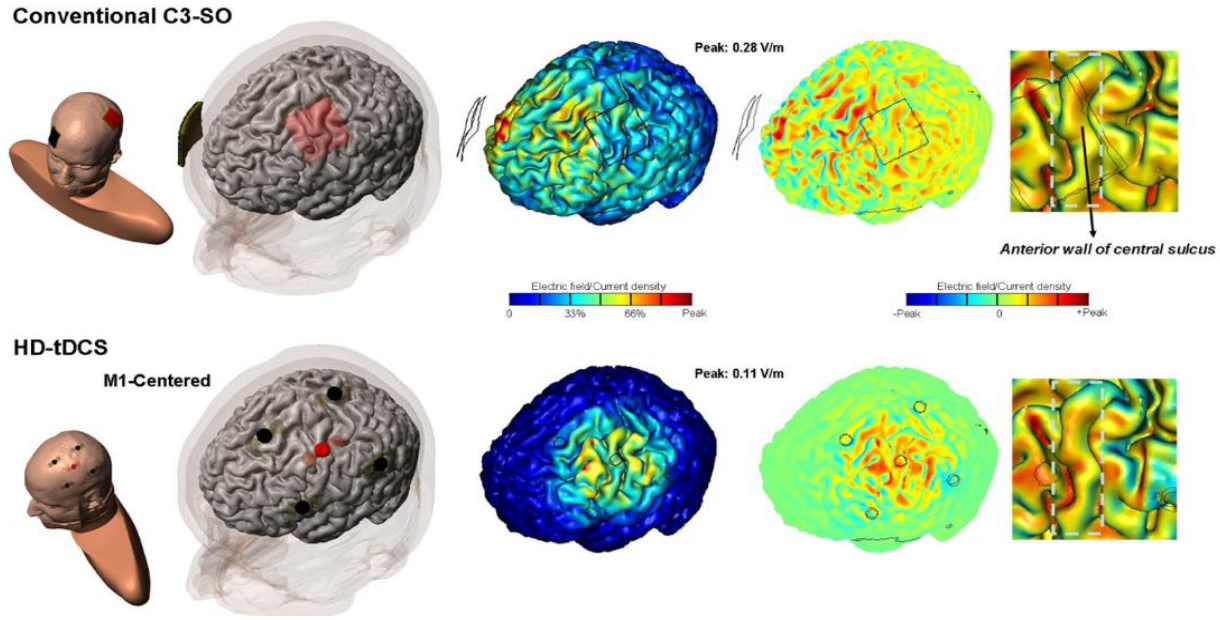

Figure 12. Influence of electrode types and configurations on the distribution of the EF.
Comparison of the predicted EF between conventional and HD 4x1 montage. For the conventional setup with 4x4 cm2 pad electrodes, the anode (red) was placed over C3 and the cathode (black) over the contralateral supraorbital (SO). In the 4x1 montage, the anode was placed centrally over the left central sulcus. The magnitude of the EF (left) and the EF normalized to the cortical surface (right) were presented. HD-tDCS generated a predominantly inward current on the gyri and constrained within the ring perimeter, while conventional tDCS produced a more diffuse bidirectional current flow across the cortex, with clustered peaks. Adopted from Caparelli-Daquer et al., 2012.

d. Electric field components

As mentioned earlier, optimized configurations consider not only the trade-off between focality and intensity, but also the ideal orientation of the targeting EF. Tangential EF ideally targets regions positioned between the 2 electrodes. However, radial EF is better achieved through a focal 4x1 electrode configuration. For achieving maximum intensity with a tangential field, the most efficient approach is to place both electrodes at a distance from the targeted region, along the direction of the desired EF, with the targeted region in between the two electrodes. In contrast, for radial EF computational models, reveal maximum intensity is revealed with the electrode positioned directly over the targeted region, with the return electrode placed at a distance (Dmochowski et al., 2011).

Hence, in clinical applications, identifying the target regions and the orientation of the induced EF is essential for employing optimal electrode montages. This allows for more precise and efficient stimulation tailored to the individual brain, thereby enhancing the effectiveness of the intervention and its outcomes.

IV.4.3 tDCS-Induced EF Interaction with the Brain's Anatomy

The distribution and strength of the EF in the brain depend not only on methodological factors but also on its interaction with the brain's anatomy. Several anatomical factors influence its distribution: the skull thickness and composition, the thickness of the CSF, and the sulcal depth.

a. Skull resistance

The skull's resistivity is the primary factor responsible for the attenuation of the EF induced by TES. Approximately 75% of the current applied by tDCS is shunted by the skull and the soft brain tissues, as reported in rodent and cadaverous brains (Vöröslakos et al., 2018). It may vary between subjects and, in the same individual, can vary between brain regions (Holdefer et al., 2006). This resistivity depends on the skull's thickness and bone type, which influences the distribution and intensity of the EF and leads to inconsistencies. Regions where the skull is thinner (near the temporal lobes) or have higher conductivity and may allow stronger EF to pass, while thicker or less conductive regions further weaken the field's strength (**Figure 13A, B**). Interestingly, regions of spongy but thick composition allow for enhanced radial EF conductivity (**Figure 13:** Opitz et al., 2015). This variability influences the accuracy and overall effectiveness of tDCS.

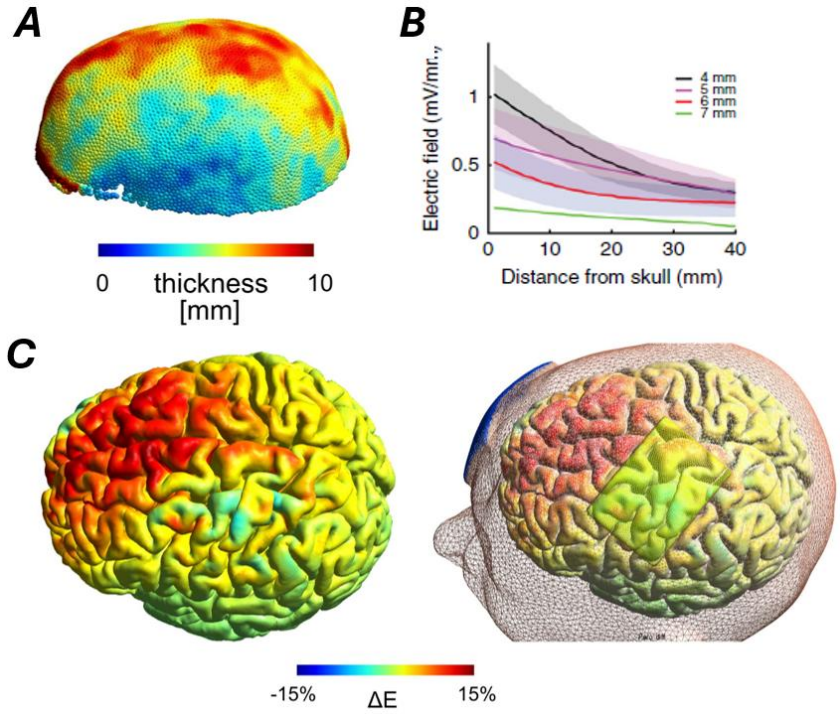

Figure 13. Impact of Skull Thickness and Spongy Bone Tissue on EF Distribution.
A. A head model showing the variation of the skull thickness across the brain, where thinner tissue regions occur on the temporal lobe. **B.** Influence of skull thickness (millimeters) on the induced EFs (in 8 cadavers). Adopted from Vöröslakos et al., 2018. **C.** Percentage of the differential maximum EF between models with (right) and without (left) spongy bone. Modeling spongy skull tissue improves the EF strength between the anode and cathode. Adopted from Opitz et al., 2015.

b. Cortical gyrification

The gyrification of the cortical sheet, folding of the cortex into gyri and sulci, affects the EF distribution and causes variations in its density. In a computational model investigating the complex cortical geometry, EF density underneath the stimulating electrode was simulated and found unexpected peak values in the sulcus, rather than in gyral structures closer to the electrode. Due to its conductive nature, the CSF in the deep sulci acts as a preferential current pathway, allowing more efficient flow into specific cortical regions (Miranda et al., 2013). However, when accounting for the anisotropic nature of the white matter (WM), showing realistic non-uniformity of fibers' directions, simulated current density peaked particularly in the neck regions of cortical gyri bordered by deep sulci, where CSF helped guide current inward (**Figure 14D**). Anatomical structures like CSF and white matter act as current sinks, where the electric current tends to accumulate or flow easily due to their conductive nature. Exploiting these pathways of low resistivity by strategically placing the stimulation electrodes over deep sulci regions, for instance, could allow for better focus of the induced currents on the regions of interest (**Figure 14,** Holdefer et al., 2006).

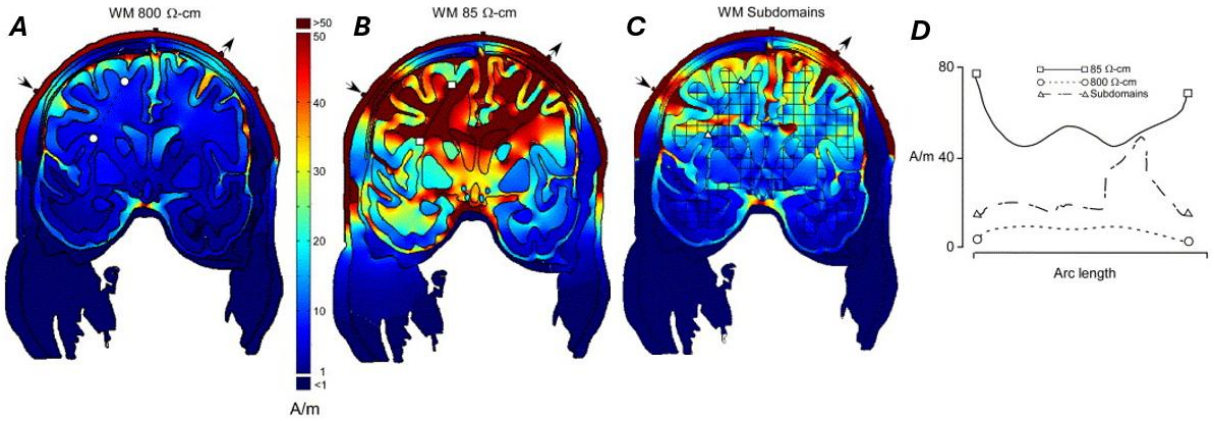

Figure 14. Effect of white matter fiber orientation on skull resistivity and current density.
A. Modeling of the current flow in an isotropic model with high resistivity (800 Ω cm), where current flows across the WM fiber. **B.** Modeling of the current flow in an isotropic model with low resistivity (85 Ω cm), where current flows along the fibers. **C.** realistic anisotropic model of WM containing subdomains of fiber orientations. **D.** Line plots of current density across a slice of white matter from each of the 3 WM conditions. High EF densities were shown when the WM was oriented parallel (WM 85 Ω cm) to the current (>50A/m), with the greatest peaks at the neck of the cortical gyri. Realistic model of the WM anisotropy showed peak current density of 49 A/m in the section through WM. Adopted from Holdefer et al., 2006.

Hence, combining computational models of the EF with individualized head models while systematically addressing the various inter- and intra-individual variabilities (e.g., skull anatomy, CSF, tissue composition and depth, electrode montage) offers a robust approach to achieving precise and optimal EF magnitudes in targeted brain regions, especially in deeper ones (Guidetti et al., 2022).

IV.5. Can tDCS-Induced EF Reach Deep Brain Structures?

One of the major issues with using tES is knowing whether its EF reaches deep brain structures. This stems from a lack of understanding of its neuromodulatory mechanism in deeper regions and its ability to bypass the thick skull and the various tissue types. Over the past few years, direct intracranial recordings have played a crucial role in quantifying these EFs, allowing advancements in our understanding of tES mechanisms and guiding the development of more effective neuromodulation therapies. Various intracranial recording techniques, such as DBS, Stereoelectroencephalography (SEEG), and Electrocorticography (ECoG), have been instrumental in quantifying EFs in deep brain regions *in vivo* in the human brain. Studies using SEEG during tACS, through intracerebral electrodes implanted for epilepsy intervention, found peak EF values ranging from 0.07 to 0.4 V/m in deep brain structures like the peri-ventricular white matter, the hippocampus, the cingulate gyrus, and the amygdala (Huang et al., 2017; Louviot et al., 2022; Opitz et al., 2015). Similar values were found in a DBS investigation in subcortical regions such as the subthalamic nuclei, with a peak EF of 0.3 V/m (Ruhnau et al., 2018). In 2017, Chhatbar et al., 2018 were the first to directly measure the EF during tDCS, in regions such as the ventral intermediate and subthalamic nucleus and the globus pallidus.

Notably, applying a simple tES montage utilizing only 2 HD ring electrodes can generate an EF in deep brain structures like the hippocampus (Louviot et al., 2022). In line with other EF assessments (Huang et al., 2017), intracerebral recordings revealed the correlation between the EF magnitude and the stimulation intensity; the EF doubles when the intensity is doubled, depending on the applied electrode montage. Additionally, the EF magnitude decreased proportionately as the depth of the intracerebral electrodes increased, due to the biophysical properties of the brain (Louviot et al., 2022). Although these techniques serve as empirical tools for measuring the EF in vivo, they still present some drawbacks. Measuring the EF in humans using implanted electrodes does not account for the directionality of the EF or optimize the electrode placement. Consequently, it results in discrepancies between the predicted and the recorded values of the EF due to the lack of consideration for the paths of best conductivity into deeper brain regions (Salimpour et al., 2017).

Table 1. Studies Investigating the Electric Field Inside the Human Brain:

Study	**Location of EF measured, (tES, Max E-Field*)**
(Louviot et al., 2022)	Right and Left amygdala, hippocampus, cingulate gyrus (tACS; 0.49 mV/mm)
(Huang et al., 2017)	Right and left, lateral and medial frontal, parietal, occipital, and Temporal cortex ; hippocampus (tACS ; 0.38 mV/mm)
(Salimpour et al., 2017)	Right primary motor cortex (M1) and right primary sensory cortex (tDCS)
(Esmaeilpour et al., 2017)	Right and left, nucleus accumbens, subthalamic nucleus, Right motor cortex (tDCS; 5.06 mV/mm)
(Lafon, Henin, et al., 2017)	Right and left lateral and medial frontal, parietal, occipital, and temporal cortex, hippocampus (tACS; 0.16 mV/mm)
(Opitz et al., 2015)	Right-lateral and left-medial orbitofrontal area; Right and left superior, inferior, and temporal area, Left entorhinal area and cerebellum (tACS; 1.17 mV/mm)

All in all, adjusting tES parameters like current intensity, duration, and electrode configuration seems to be a critical step to modulate the brain's excitability and induce the desired acute and long-term effects. Notably, considering individual differences in skull anatomy and brain tissue through personalized brain models can enhance the precision and strength of the stimulated EF, particularly in targeting deep brain regions. These biophysical and methodological factors influence neural activity at multiple levels, i.e., neuronal, synaptic, and network, which we will explore in the following section.

V. tDCS mechanism of action

tDCS operates similarly to a battery, with two poles: an anode (+), which injects current into the brain, and a cathode (-) that draws it out. This setup generates an EF that guides the current flow through neural tissue, modulating neuronal activity depending on the properties and orientation of the cells relative to the EF. In particular, near the anode, positively charged ions (like K^+, $Na^{+,}$ and Ca^{2+}) are pushed away, and the negatively charged ions (Cl^-) are attracted, leading to the depolarization of the neuronal membrane and increased excitability. In contrast, near the cathode, the ion movement induces hyperpolarization, decreasing neuronal excitability and reducing the likelihood of action potential generation. Thus, the strategic placement of both electrodes is essential in tDCS experiments (**Figure 15A**: Reinhart et al., 2017).

Several foundational studies using animal models (rats and cats) (Bindman et al., 1962, 1964; Creutzfeldt et al., 1962) and humans (**Figure 15C:** Nitsche & Paulus, 2000; Priori, 2003) have established the widely recognized polarity-dependent effects of tDCS. Anodal tDCS enhances cortical excitability and neural activity, while cathodal tDCS induces the opposite effects. These effects are believed to be linked to tDCS modulation of the neuron's membrane potential, leading to the generation of an action potential. It's important to note that, unlike TMS, tDCS does not induce an action potential. Experimental studies revealed that anodal tDCS depolarizes the membrane and brings it closer to its firing threshold, therefore increasing the likelihood of firing an action potential and its spike timing. While cathodal tDCS tends to hyperpolarize neurons, reducing excitability by moving the membrane potential further from the firing threshold (**Figure 15B*:*** Yamada & Sumiyoshi, 2021; Radman et al., 2007; Bikson et al., 2004). These findings highlight the ability of sub-threshold tDCS to modulate both spontaneous neural activity and evoked responses.

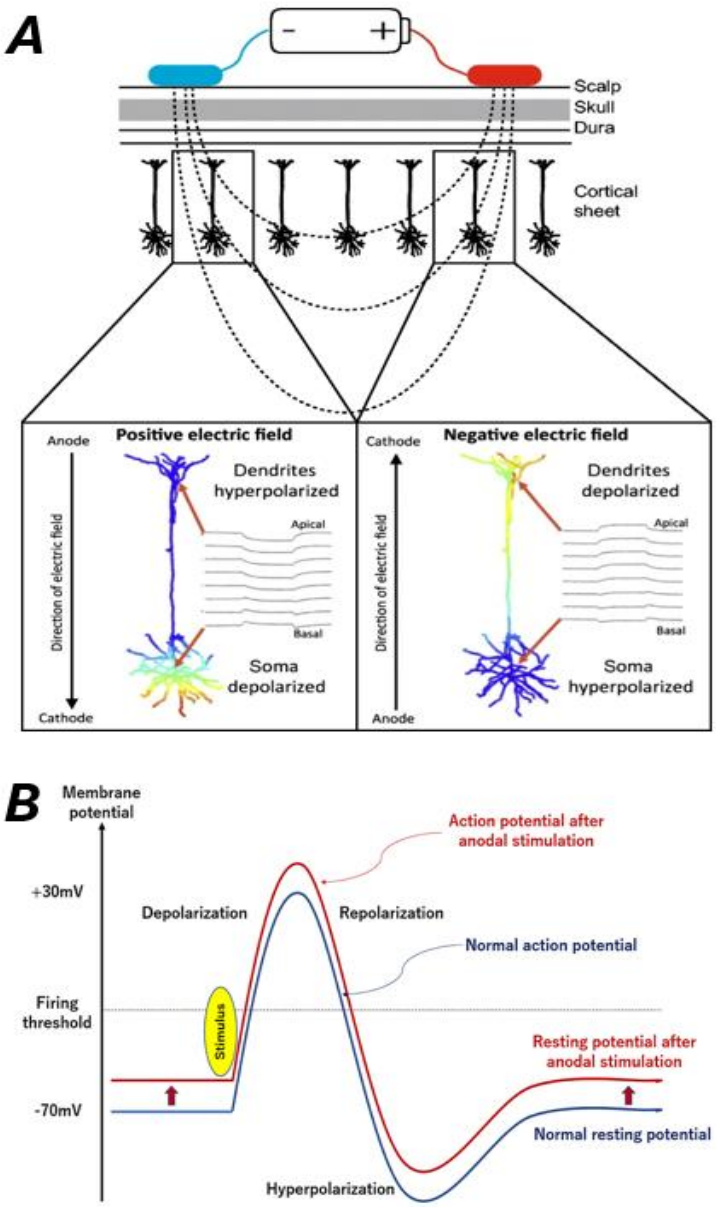

Figure 15. tDCS mechanism on neuronal membrane potentials.
A. Illustration depicting the effects of the bipolar EF on neurons adjacent to the anode (blue) versus near the cathode (red). This EF depolarizes the soma of the neurons close to the anode, bringing them closer to their action potential firing threshold. In contrast, near the cathode, the ionic gradients produce an opposing effect. Adopted from Reinhart et al., 2017. **B.** Schematic representation of neuronal potential changes induced by tDCS. Anodal tDCS (1–2 mA) doesn't induce an action potential but depolarizes the resting membrane potential, thereby bringing it closer to the firing threshold and increasing the likelihood of action potential generation. Adopted from Yamada & Sumiyoshi, 2021.

Nitsche's pioneering study (Nitsche & Paulus, 2000) examined tDCS-induced excitability in the primary motor cortex (M1) by applying anodal or cathodal stimulation over M1 in the healthy brain, followed by TMS to assess MEPs. tDCS produced polarity-dependent effects where anodal tDCS increased MEP amplitude, while cathodal tDCS decreased it. The effects were influenced by stimulation duration, with brief sessions inducing immediate polarization. Short stimulations (5–7 min) led to transient after-effects, whereas prolonged stimulation (9–13 min) resulted in sustained after-effects (

Nitsche, et al., 2003; Nitsche et al., 2005; Nitsche & Paulus, 2000, 2001; Priori, 2003). Acute polarity-specific tDCS changes have also been found in rat brain slices after direct stimulation (Bikson et al., 2004; Lafon, Rahman, et al., 2017).

V.1. Influence of Neuronal Orientation and Morphology on tDCS effects

At the neuronal level, specifically in pyramidal neurons, the orientation of the cell relative to the applied EF determines the direction of the polarization. Apical dendrites aligned with the anode are hyperpolarized, leading to the depolarization of the soma. Conversely, if the apical dendrite faces the cathode, the soma is hyperpolarized (**Figure 15A**). This is likely due to the local redistribution of charges, regions near the anode attract negative charges, creating a positively charged environment around the soma that promotes its depolarization *(somatic doctrine)* (Das et al., 2016; Radman et al., 2009)**.** According to Nitsche, and colleagues (2003) these acute tDCS effects seem to be directly related to sodium and calcium voltage-gated ion channels in humans. Sodium-gated channels seem to play a predominant role in controlling membrane polarization, modifying the presynaptic release of Ca2+ in the synapse, and resulting in increased firing rate (Bindman et al., 1964; Pelletier & Cicchetti, 2014).

However, it is now apparent that the effects of tDCS on excitability are more complex than initially believed. Prolonged anodal tDCS may reduce excitability (Monte-Silva et al., 2013), while increasing the intensity of cathodal tDCS can enhance it (Batsikadze et al., 2013). Notably, neurons are not uniformly affected by tDCS-induced EF, the morphology (structure, orientation, size) of their compartments (dendrites, axons, soma) can influence the degree and direction of polarization **(Figure 16B:** A. Liu et al., 2018). The dendritic polarization approach suggests that dendrites polarize in the same direction as the soma, while apical dendrites exhibit the opposite effect (Bikson et al., 2004; Rahman et al., 2013). Moreover, axons are extremely sensitive to EFs, with polarization dynamics depending directly on their morphology and function. Although the initial axon segment polarizes concordantly with the soma, this doesn't necessarily apply to distal regions of long axons. The orientation of an axon relative to the electric field is a key determinant of whether DCS produces excitatory or inhibitory effects. In hippocampal brain slices, the vector of the EF induced by DCS was approximately aligned with the direction of action potential (AP) propagation in the Schaffer collaterals (**Figure 16Aa**) but opposed to that in the mossy fibers (**Figure 16Ab**). DCS significantly inhibited evoked field excitatory postsynaptic potentials (fEPSPs) in CA1 neurons while leaving fEPSPs of the CA3 unaffected (**Figure 16Ac**). Conversely, when the DC vector was oriented opposite to the Schaffer collateral AP direction but parallel to the mossy fiber AP direction, DCS induced significant inhibition of CA3 fEPSPs without affecting CA1 fEPSPs (**Figure 16A:** Kabakov et al., 2012).

Due to the cortical folding of the cortex and the different influence of the two components of the EF (tangential and radial fields), under its stimulating electrode, tDCS produces mixed direct currents in the brain (Rahman et al., 2013). This, in turn, results in mixed polarization in the different neuronal compartments (see Bikson et al., 2019 for a review).

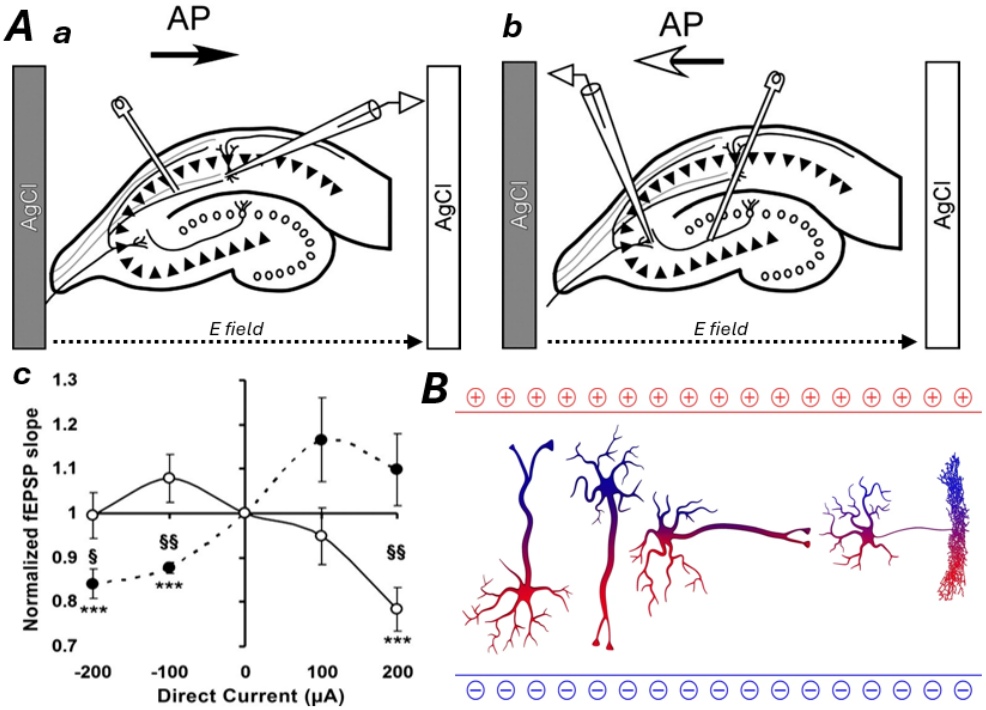

Figure 16. Influence of neurons' morphology and orientation on tDCS effects.
Aa, b. Effect of DC on evoked fEPSP recorded in the apical dendrites of CA1 and CA3. EF in the same orientation as the AP propagation for the Schaffer collaterals (black head arrow) and opposite to the AP propagation in the mossy fibers (white head arrow). **Ac**. DCS effect on fEPSPs differs between apical dendrites of CA1 and CA3 neurons, with fEPSPs in CA1 neurons (filled circles) responding oppositely to those in CA3 (open circles). Adopted from Kabakov et al., 2012. **B.** Schematic illustration of four neurons, each has a different orientation relative to the induced EF. Whether a neuron becomes depolarized or hyperpolarized depends on the alignment of the EF vector with the neuron's morphology and the compartment's orientation. Adopted from A. Liu et al., 2018.

V.2. Long-term effects of tDCS: influence on synapses and plasticity

tDCS influences brain plasticity by modulating synaptic efficacy during ongoing activity. In rat brain slices, DCS facilitated neuromodulation and potentially reversed synaptic depression through postsynaptic and axonal polarization (**Figure 17B**: Rahman et al., 2017). This coactivation is analogous to combining tDCS with a cognitive task to co-activate a targeted region. As evidenced in synapses of rats' hippocampal slices, tDCS is a major modulator (rather than inducer) of long-term potentiation and depression (LTP and LTD). The direction and magnitude of its modulation of LTP and LTD depend on the type and location of the targeted dendrites (apical or basal) and the properties of the endogenous synaptic activity. Both stimulation polarities influence LTP depending on the dendritic compartments. Anodal DCS enhances LTP in the basal dendrite while cathodal stimulation enhances it in the apical

dendrites (**Figure 17A**: Bikson et al., 2019; Stagg et al., 2018; Kronberg et al., 2017). LTP and LTD are mediated through the N-methyl-D-aspartate (NMDA) receptors, which are directly involved with calcium influx and subsequent modulation of synaptic strength. Interestingly, tDCS induced-plasticity effects like LTP increased the intracellular calcium in stimulated rat brain (Islam et al., 1995). In humans, the administration of a calcium channel blocker abolished the tDCS-induced acute and long-term effects, while NMDA receptor blocker dextromethorphan (DMO) eliminates the lasting effects during repeated tDCS sessions (**Figure 17C**: Monte-Silva et al., 2013; Stagg & Nitsche, 2011; Liebetanz et al., 2002). Subsequently, through the modulation of the calcium influx, the application of a prolonged tDCS session can induce the switch from LTP to LTD excitability changes.

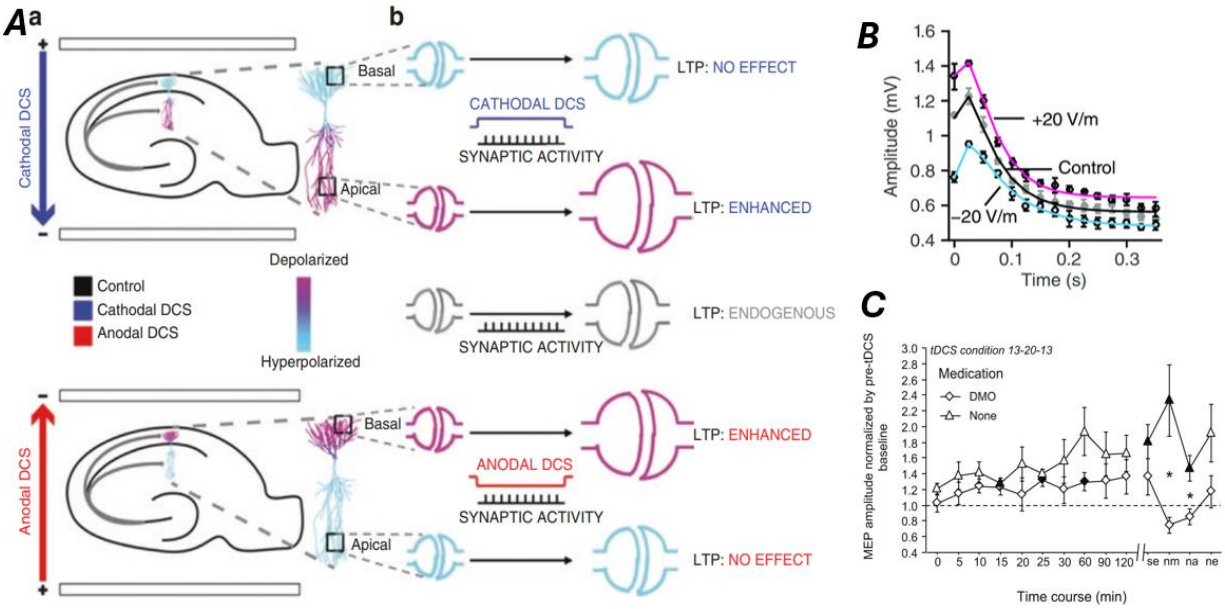

Figure 17. tDCS impacts neuronal plasticity through LTP and LTD.
A. Modulation of LTP and LTD by tDCS depends on the dendritic compartment location. **A.a** Schematic presentation of a hippocampal slice showing the CA1 pyramidal neuron with both dendritic compartments (basal and apical) during each stimulation polarity (cathodal and anodal). **A.b** Changes in synaptic strength and plasticity induction during DCS on basal and apical compartments. Adopted from Bikson et al., 2019. **B.** DCS affects synaptic strength during ongoing input from afferent neurons, even when synaptic depression occurs due to the depletion of neurotransmitter vesicles in the presynaptic terminals. Adopted from Rahman et al., 2017. **C.** Influence of DMO, NMDA blocker, on MEP during repeated tDCS (13 min) sessions with a short interval (20 min). Administration of DMO 2 hours pre-simulation significantly modulated anodal tDCS (1 mA) late-onset excitability enhancement in MEP. Adopted from Monte-Silva et al., 2013.

V.3. tDCS Influence on Brain Networks and Cellular Activity

The action potential propagation resulting from tDCS can also influence the rate of neurotransmitters released, like dopamine, serotonin, and gamma-aminobutyric acid (GABA) in synapses (Yamada & Sumiyoshi, 2021). Plasticity induced by tDCS and paired associative stimulation was abolished by dopamine antagonists, especially when mediated through D2 receptors (M.-F. Kuo et al., 2008; Nitsche et al., 2012). GABA receptor agonist, Lorazepam, delayed anodal tDCS

effects followed by selective enhancement, while anodal tDCS itself decreased GABA levels in the motor cortex (Nitsche et al., 2004; Stagg & Nitsche, 2011). The alteration in the concentration of these systems can directly impact tDCS-induced effects on plasticity. Subsequently, the variation in the activation and inhibition of neurotransmitters leads to a cascade of intracellular signaling pathways, including the upregulation of the brain-derived neurotrophic factor (BDNF) expression and activation of Tropomyosin receptor kinase B (TrkB), critical for synaptic plasticity and neural network remodeling (**Figure 18**: Yamada & Sumiyoshi, 2021; Fritsch et al., 2010).

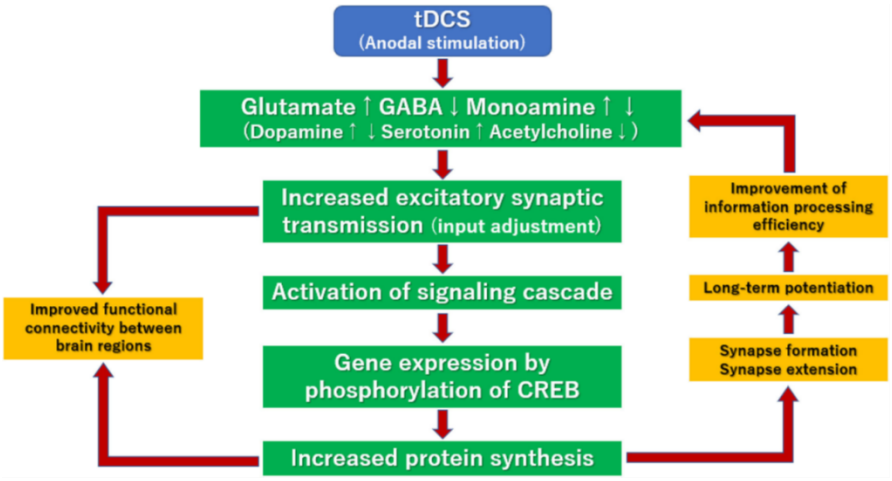

Figure 18. Proposed mechanisms of LTP enhancement by tDCS.
The activation or inhibition of various neurotransmitters, which interact with G-proteins or ion channels, triggers signaling cascades that lead to the phosphorylation of cAMP-responsive element binding protein (CREB) and the activation of specific genes in the neuronal nucleus. These signaling pathways facilitate the synthesis of key proteins, including neurotransmitter synthases, receptors, ion channels, and intracellular signaling proteins. The roles of these proteins in regulating the efficiency of neurotransmission within cortical circuits may help explain tDCS's capacity to induce LTP. Adopted from Yamada & Sumiyoshi, 2021.

Beyond modulating neurotransmission and synaptic plasticity, tDCS also influences several intracellular mechanisms, including galvanotropism (growth induced by electric stimulation), cell death, neurogenesis, and cell growth (Das et al., 2016; McCaig et al., 2005). Additionally, tDCS can influence other brain cells like astrocytes and endothelial cells, which could potentially contribute to tDCS-related neuromodulation. Astrocytes, integral to the tripartite synapse, play a crucial role in synaptic modulation. In mice study, tDCS over the primary visual cortex induced calcium influx in astrocytes, leading to modifications in the visual evoked response, while neurons didn't exhibit significant changes in activity (**Figure 19B**: Monai et al., 2016). Furthermore, endothelial cells that form the BBB may channel tDCS currents to modulate vascular responses. Polarity-specific changes in blood perfusion and increased permeability suggested tDCS influence on the BBB neurovascular dynamics (Lopez-Quintero et al., 2010).

The neuromodulatory effects of tDCS, including both acute and long-lasting changes in synaptic plasticity, extend beyond the neuronal level to influence the broader brain networks. When applied to the human brain, tDCS polarizes the network coherently, enhancing its connectivity and leading to changes in oscillatory dynamics (Reato et al., 2013, 2015). It is noteworthy to mention that tDCS effects are not strictly confined to the stimulated hemisphere; regions isolated from the stimulation might also be recruited in response to tDCS. They can extend to the contralateral hemisphere via transcallosal connections, enabling network-level interactions or changes in overall excitability (see Morya et al., 2019, for review). Also, functional connectivity studies during and after tDCS using scalp EEG revealed inter-hemispheric and intra-hemispheric connections in all frequency bands, especially for theta and gamma over the sensory motor brain network (**Figure 19A***:*Hordacre et al., 2018; Polanía et al., 2011).

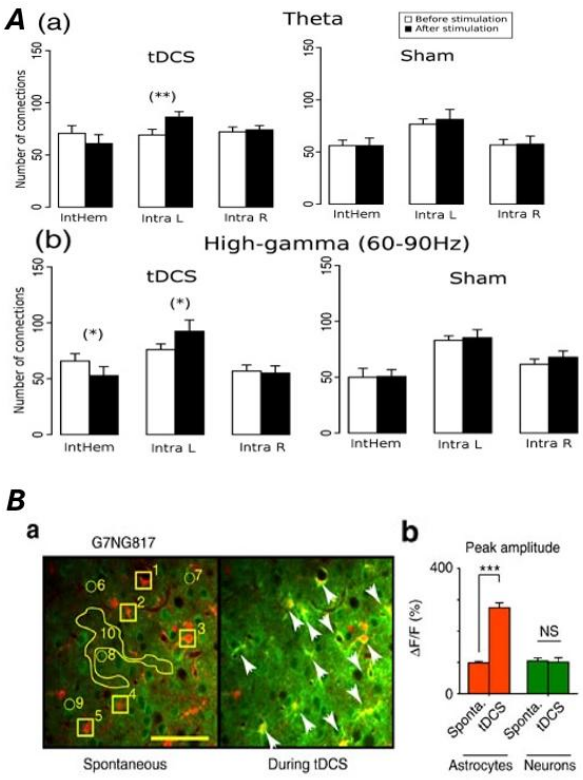

Figure 19. Effects of tDCS on Functional Connectivity and Astrocytic Activity.
A. Influence of tDCS on the number of connections for inter-hemispheric (intHem) and right (intra R) and left intra-hemispheric (intra L) connections before (white) and after (black) 10 minutes of 1 mA tDCS and sham. Effects are shown for theta and high-gamma frequencies during a motor task. Adopted from Polanía et al., 2011. **B.a** Intracranial fluorescent imaging of layer 2/3 in the primary visual cortex during tDCS in urethane-anesthetized mice. Astrocytes (red) during spontaneous activity and tDCS, with arrows pointing to those with increased Ca2+. **B.b** tDCS significantly increased astrocytic signal amplitude (▲F/F) in comparison to spontaneous activity. Adopted from Monai et al., 2016.

Despite advancements *in vitro, in silico, and in vivo* (animal and human) studies, the precise mechanisms of action of tDCS remain poorly understood, largely due to the inherent challenges in investigating its effects on the human brain. Consequently, integrating new methods and advanced

technologies is essential to understanding the proper electrophysiological influence of tDCS in the human brain. Nevertheless, it is well documented that tDCS modulates cortical excitability and influences synaptic plasticity, leading to measurable changes in cognitive and behavioral performance. Moreover, current evidence, despite variability in reliability across studies, supports the therapeutic potential of tDCS for cognitive and motor neurorehabilitation, particularly in neurological and psychiatric conditions such as stroke, spinal cord injuries, Parkinson's disease, and Depression (Begemann et al., 2020; Flöel, 2014; Morya et al., 2019). In the following section, we will discuss the impact of tDCS on different cognitive functions, especially on visual perception.

VI. Effect of tDCS on Cognition and Perception

Currently, treatment options for cognitive impairments in neurological and psychiatric disorders remain limited to insufficient drugs, physical exercise, and cognitive rehabilitation methods. As a result, the application of NIBS techniques has emerged as a promising approach for rehabilitating neural activities and addressing cognitive dysfunctions.

tDCS has been applied to improve different functions in ***neurological*** disorders such as dementia, Parkinson's disease (PD) (Doruk et al., 2014), acute and chronic pain (Antal et al., 2008) and epilepsy (Begemann et al., 2020). Interesting, short (10 days) and long-term (8 months) sessions during 20 minutes of anodal tDCS (+2mA) revealed the effectiveness of tDCS as a treatment to slow the progression of dementia (Gangemi et al., 2021). Many researchers have opted for NIBS techniques like tDCS as a painless alternative therapy to DBS for treating PD. Various tDCS protocols have demonstrated benefits in executive functions like working, processing speed and visual attention, and have been associated with a significant decrease in Bradykinesia (slowness of movement), one of the cardinal symptoms of PD. For instance, anodal tDCS (2 mA,20min) applied to the right and left dorsolateral prefrontal cortex (DLPFC) significantly decreased the time to accomplish the Trail making test in PD patients, with effects persisting for up to 2 weeks and still observable 1 month after stimulation. However, further clinical research is needed to ensure tDCS's clinical applicability (**Figure 20A:** Doruk et al., 2014; Benninger et al., 2010). tDCS has also been applied as an analgesic in managing refractory chronic pain, particularly in fibromyalgia and neuropathic pain of the lower limbs. The use of anodal tDCS over the left primary motor cortex and the cathode over the right orbitofrontal region has been recommended for treating patients suffering from fibromyalgia (LeFaucheur et al., 2017).

The applications of tDCS extend beyond this scope to include various ***neuropsychiatric*** disorders as well, including major depressive disorder (MDD), schizophrenia, obsessive-compulsive disorder, autism, and substance use disorder (Kekic et al., 2016). MDD is one of the most extensively

studied disorders with tDCS. To date, no definite indication for the use of tDCS for depression treatment has been recommended. However, the level B recommendation, indicating probable efficiency, of tDCS has been proposed by Lefaucheur et al., 2017, where they suggested the antidepressant effect of anodal tDCS (+2mA) for non-drug-resistant major depressive episodes when the anode is applied over the left DLPFC and the cathode over the right orbitofrontal region for at least 10 daily sessions, for 20-30 min per session.

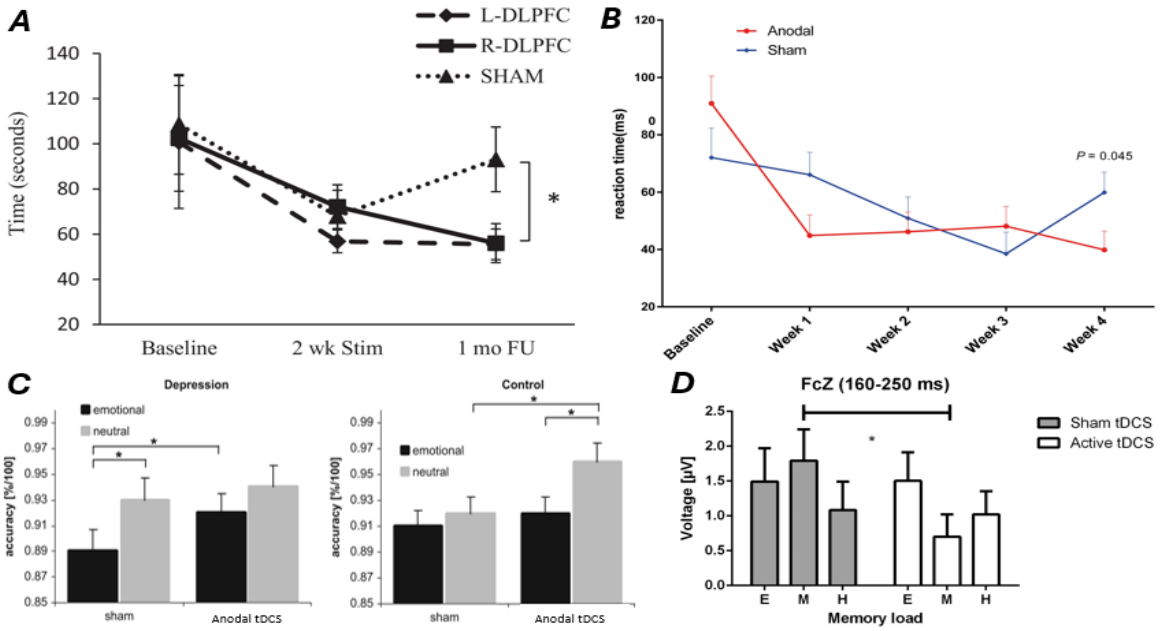

Figure 20. Impact of tDCS on different cognitive functions.
A. tDCS at 2 mA applied during 20 min to the right (R) and left (L) DLPFC significantly decreased the mean time required to accomplish the Trail making test in PD patients (n=18). The tDCS-induced improvement in performance was maintained after 2 weeks and 1 month of follow-up (FU). Adopted from Doruk et al., 2014. **B.** Attention network test during anodal 1.5-mA HD-tDCS showed a significant decrease in reaction time from baseline to week 4 in comparison to sham in healthy participants (n=39). Adopted from Lu et al., 2020. **C.** Permeance accuracy assessed in 22 MDD patients and control subjects in a delayed working memory task involving neutral and emotional distractors during anodal tDCS and sham conditions. Anodal tDCS showed a threefold enhancement, indicating that MDD patients provided more correct responses in the emotional condition. Adopted from Wolkenstein & Plewnia, 2013. **D.** Assessment of 20 min tDCS (2 mA) effect on the N200 evoked potential, recorded at FcZ, during retrieval of a memory load task produced at different levels (E: easy, M: medium, H: hard) in 14 MDD patients. A significant reduction of the N200 voltage was revealed during anodal tDCS (white bars) compared to sham (grey bars). Adopted from Powell et al., 2014.

tDCS has also been employed to further study and enhance cognitive functions in healthy individuals, as well as to alleviate cognitive impairments in neurological and neuropsychiatric disorders, thereby helping mitigate its impact on patients' daily life (Antal et al., 2014). Prefrontal lobe tDCS has been investigated in healthy participants for its ability to enhance learning, as well as to improve both working and long-term memory (M.-F. Kuo & Nitsche, 2012), as further seen with increased gamma activity in schizophrenic patients (Hoy et al., 2015). Additionally, multiple tDCS sessions over several

days have been shown to improve language learning and attention in healthy individuals (**Figure 20B**: Lu et al., 2020; Brunyé et al., 2017). Although no recommendation for clinical application has been proposed, the use of tDCS to alleviate cognitive deficits associated with MDD symptoms has been investigated. A single session of anodal tDCS to the DLPFC significantly improved working memory in MDD (**Figure 20C**: Wolkenstein & Plewnia, 2013). In line with these results, Powell et al. (2014) evidenced the notable reduction in N200 amplitude and frontal theta activity during a visual working memory task after a single tDCS session over the DLPFC (**Figure 20D**).

In the following section of this manuscript, we will mainly focus on the role of tDCS in modulating a specific cognitive function: visual perception, especially facial recognition in humans.

VII. tDCS and Visual Perception

VII.1. Organization of Face Recognition Regions

Facial perception is one of the most essential cognitive functions in our daily life. It allows the recognition and interpretation of facial features, expressions, and cues, contributing to our understanding of interpersonal communication. This intricate process is grounded in a network of brain structures, extending its involvement not only to facial processing but also to emotions and memory (Atkinson & Adolphs, 2011).

Pioneering studies using Positron emission tomography (PET) scans identified several brain regions in the ventral occipito-temporal cortex (VOTC) that respond to face stimuli (Sergent et al., 1992). Early lesion studies in prosopagnosia patients further demonstrated the involvement of VOTC regions in facial processing, especially in the right hemisphere (Rossion et al., 2012). From then on, neuroimaging research using functional magnetic resonance imaging (fMRI) utilized the functional localizer, an approach based on presenting a series of face images with non-face images (e.g., objects, animals) to investigate face processing regions. A pillar face recognition region in the right VOTC was identified: the ***Fusiform gyrus***, also called the ***fusiform face area (FFA)*** (FFA1 in **Figure 21A**) (Kanwisher et al., 1997). It's now widely known, through the progress of fMRI studies, that face recognition is based on an interconnected network of regions, in addition to the FFA, including the inferior region of the fusiform gyrus, aka. ***Inferior frontal gyrus (IFG***), a region in ***the inferior occipital gyrus (IOG)*** also called the ***Occipital Face Area (OFA),*** and the ***Superior temporal Succus (STS)*** (**Figure 21A, B** : Weiner & Grill-Spector, 2015; Grill-Spector et al., 2017). Recent studies revealed the role of the ***Anterior temporal lobe (ATL)***, in the anterior inferior temporal cortex, in facial selectivity (Rossion et al., 2024).

Neuroimaging techniques and prosopagnosia patients' investigations combined with tasks like face matching, were carried out to identify the functional role of each region for face identity recognition. fMRI studies suggest that dorsal face-selective regions in the STS are involved in processing dynamic facial features like expressions, eye gaze, and head orientation, while those in the VOTC seem to play a greater role in recognizing more stable traits such as identity and gender. Based on their functions regarding face recognition, they were classified into 2 streams: the dorsal (STS) and the ventral (VOTC) stream. Therefore, based on this functional division, Haxby and colleagues (2000) proposed a hierarchical, evolutionary, and complex posterior-to-anterior organization of face-selective regions. In this model, the core visual system (STS, OFA, and FFA) is involved in the initial analysis of visual perception, from which extends anteriorly further processing into the ATL for the extraction of face-identity related information, as well as to other neural systems involved in attention, speech, emotion processing, and memory (**Figure 21C**:Haxby et al., 2000).

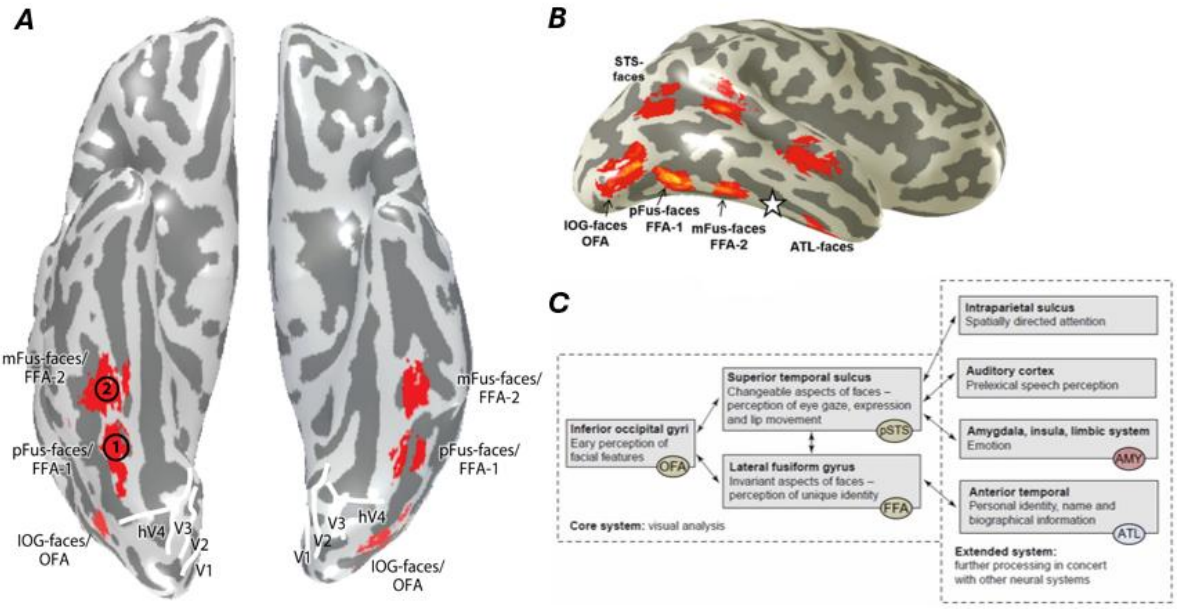

Figure 21. The cortical face recognition network in humans.
A-B. Inflated ventral views of the VOTC in humans depicting the typical locations of face-selective regions identified as clusters of voxels measured by fMRI using a functional localizer. Adopted from Grill-Spector et al., 2017; Weiner & Grill-Spector, 2015. **C.** Haxby's model of the organization of the human neural system for face perception. The core system consists of the OFA, FFA, and ST (yellow) for analysis of visual face stimuli. The OFA is believed to be the gateway to this system. The latter interacts with regions in the extended system, including the anterior regions of the temporal and parietal lobes for processing spatially directed attention, speech perception, emotion, and facial identity and expression. Adopted from Haxby et al., 2000.

VII.2. tDCS Neuromodulation of Face Recognition

The neuromodulatory effects of tES on facial perception have been extensively investigated using both *online* protocols, assessing influences during stimulation, and *offline* protocols, examining

effects after stimulation. In one of the first studies to neuromodulate the visual cortex, tDCS was applied during a short session (7 min) at 1mA over the primary visual cortex to assess the perception of static and dynamic contrast sensitivity. Anodal stimulation showed no significant effect, although contrast perception was diminished during and immediately after cathodal tDCS (**Figure 22A**: Antal et al., 2001). However, another study applying anodal tDCS at a relatively longer stimulation duration (15 min) revealed a transient significant increase in contrast sensitivity (Kraft et al., 2010).

tDCS applied over visual areas implicated in face perception alters the processing of various visual stimuli, like faces and objects. Offline anodal tDCS applied over the right occipitotemporal cortex (PO8 scalp EEG) before the task boosts performance during face and object perception and during memory tasks, in comparison to sham and online tDCS (**Figure 22D** : Barbieri et al., 2016). Additionally, 10 minutes of anodal tDCS has been reported to alter the robust face inversion effect (FIE), when applied over the frontal brain regions (Fp3 scalp EEG), where it significantly reduces recognition for upright faces (**Figure 22C** : Civile et al., 2018, 2019). Considering the brain state during stimulation can have an important effect on the outcome of tDCS (Antal et al., 2007)When targeting the fusiform gyrus, online anodal tDCS (0.5 mA) placed over the occipitotemporal lobe improved aspects of face memory, particularly by increasing the number of items retained at higher memory loads. The greatest benefits were observed in participants who initially exhibited lower performance (Brunyé et al., 2017).

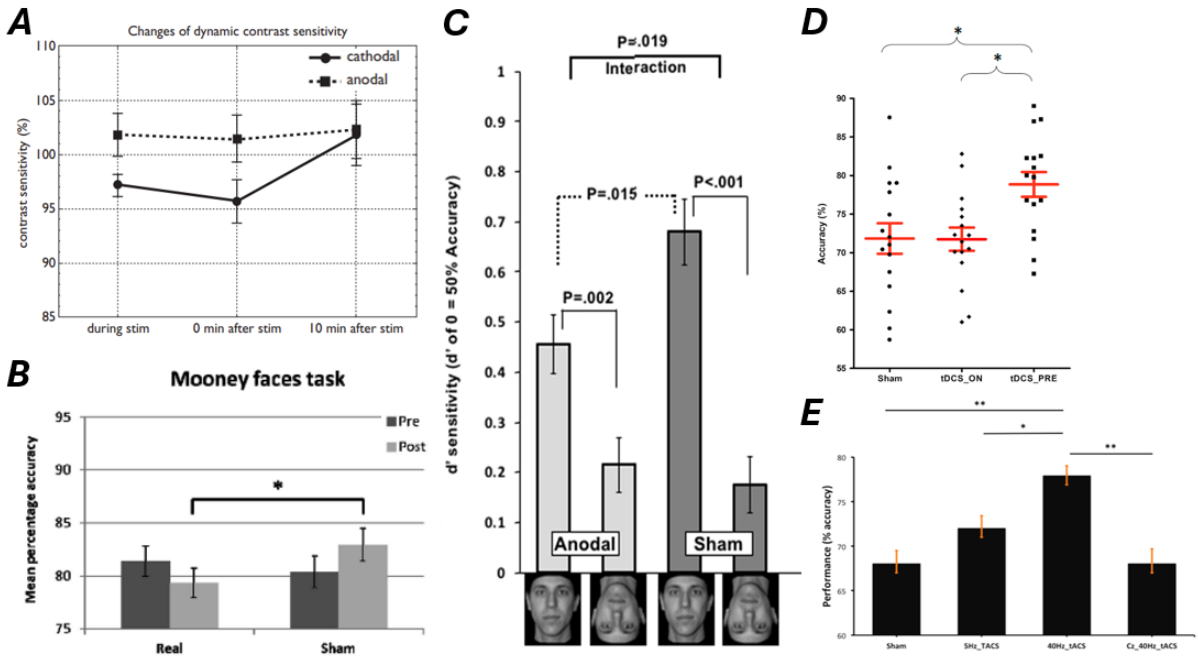

Figure 22. tDCS modulation of face perception.
A. Cathodal tDCS (7 min, 1mA) significantly reduced dynamic contrast sensitivity during and immediately after stimulation. Anodal tDCS exhibited no significant effects. Adopted from Antal et al., 2001. **B.** Participants' accuracy was significantly lower following real tDCS (20 min, 2mA) in comparison to sham when viewing money faces. Adopted from Renzi et al., 2015. **C.** Anodal tDCS (1.5mA) applied over Fp3 on the scalp for 10 min significantly reduced the face inversion effect, by reducing the sensitivity to upright faces. Adopted from Civile et al., 2018. **D.**

Offline tDCS (tDCS_PRE) significantly enhanced performance accuracy for four tasks (face and object perception, Cambridge Memory Face and object tasks) in comparison to sham and online tDCS (tDCS_ON). Adopted from Barbieri et al., 2016a. ***E.*** tACS at 40 Hz applied over the right lateral occipital cortex enhances perception of both faces and objects, specifically when applied to the right occipital cortex. Adopted from Gonzalez-Perez et al., 2019.

tDCS has also been used to explore and improve the functions of various regions involved in face processing. A stimulation targeting the OFA during 20 min of 2mA tDCS disrupted the learning effect for Mooney faces while leaving the composite face effects unaffected, suggesting the implication of the OFA in facial detection under noisy visual conditions (**Figure 22B:** Renzi et al., 2015). The application of tDCS to the STG improved its ability to recognize and appreciate humor during a comic judgment task (Manfredi et al., 2017). Notably, tDCS was used to investigate the role of right and left ATL in famous face recognition and naming, where it revealed a significant improvement in naming accuracy associated with the left ATL and enhanced non-famous face discrimination linked to the right ATL (Pisoni et al., 2020). Another form of TES, tACS, has been used to explore facial recognition processing. tACS applied at 40 Hz in the gamma band for 20 to 25 min to stimulate the right lateral occipitotemporal cortex (PO8) enhanced face and object perception, and interestingly, increased face pareidolic illusion in healthy controls (**Figure 22E**: Gonzalez-Perez et al., 2019; Palmisano et al., 2023).

Various disorders exhibit impairments in visual perception, with current treatments being limited to resistance or absence of drugs and insufficient rehabilitation methods. TDSC has been employed as a noninvasive therapy to alleviate some of these symptoms. In Alzheimer's disease patients, tDCS applied over the temporal cortex daily for 5 days improved visual recognition memory, persisting 4 weeks post-stimulation (Boggio et al., 2012). Furthermore, occipital tDCS combined with multisensory training for patients suffering from visual deficits after traumatic brain injury revealed significant enhancement in performance during visual tasks (Diana et al., 2024).

In contrast, the effectiveness of tDCS in modulating facial processing, particularly in healthy individuals, has been met with considerable skepticism. Several studies, including both offline and online protocols, have reported difficulties in replicating earlier findings or have even observed opposite effects following stimulation (Kho et al., 2023; Willis et al., 2019; Wu et al., 2021; Horvath et al., 2015a). This inconsistency in outcomes raises concerns about the reliability and robustness of tDCS effects. However, it might arise from inter-individual variability in cognitive functions, but also from other cognitive processes such as baseline performance levels, attention, and decision-making (Zorowitz & Niv, 2023). Additionally, methodological discrepancies in tDCS protocols across studies, such as variation in electrode montage, current intensity, and duration of stimulation, can directly impact the neuromodulatory effects and magnitude of the stimulation (Vergallito et al., 2022).

While behavioral measures provide useful insight into the effects of tDCS on face perception, they are insufficient to fully capture its underlying neuromodulatory mechanisms. Given the variability and limitations observed in behavioral outcomes, it becomes even more critical to rely on reliable direct and objective measures of brain activity. To better understand the tDCS effects, it is therefore necessary to complement behavioral findings with electrophysiological recordings, such as scalp EEG, which offers direct neural markers of face processing.

VIII. Scalp Electroencephalography investigation

Electroencephalography (EEG) is a noninvasive neuroimaging tool that records the postsynaptic electrical brain activity via electrodes placed on the scalp. An EEG recording system consists of: scalp electrodes with conductive solution, signal amplifiers, an analog-to-digital converter, and a recording device. Electrodes are grouped into caps that usually adopt the standardized international 10-20 system for electrode placement to record multiple brain regions. A conductive medium is used to increase signal transmission and reduce impedance, i.e., the resistance of the current flow between the skin and the electrodes. High impedance values can result in distorted recordings that compromise original neural signal extraction. Some EEG devices have built-in impedance monitors to ensure that impedance is maintained below 5 kilohms (kΩ), which helps maintain good signal quality (Biasiucci et al., 2019). This method is simple enough to be effectively implemented for at-home use, making remote monitoring more accessible and practical. In particular, for Epilepsy patients, using remote EEG devices could allow clinicians to constantly monitor patients' electrical activity and seizure occurrence from a distance (Milne-Ives et al., 2023).

Furthermore, EEG research advanced with the discovery of event-related potentials (ERPs), which reflect the electrophysiological brain activity in response to a specific stimulus. In the context of face perception, the N170 is a large negative ERP that appears over the lateral occipitotemporal regions and peaks approximately around 150 milliseconds (ms) after the presentation of a face image (Caharel & Rossion, 2021; Rossion, 2011; 2000 ; Yovel, 2016). Characterized by its selective response to faces, in face vs. non-face matched stimuli, the N170 has been identified as the earliest indicator of high-level visual processing (Rossion, 2014 for review). Moreover, the N170 component is modulated when the orientation of the presented faces is altered, showing delayed duration and increased amplitude in response to inverted or misaligned faces. This phenomenon, known as the face inversion effect (FIE), shows disruption of face processing by manipulation of orientation. The changes in N170 amplitude could be explained by the additional recruitment of regions involved in object recognition or by a delayed processing due to the complexity of the stimuli (**Figure 23B**: Rossion, 2000).

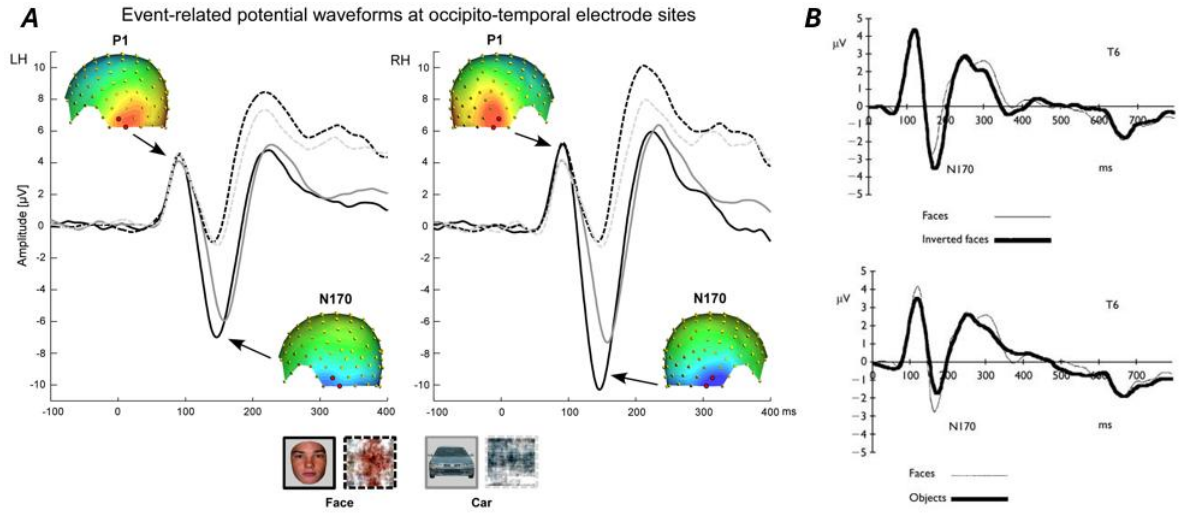

Figure 23. The N170 face-selective ERP.
A. Grand average ERP waveform responses to faces and car images (left and right panels, respectively) and their scrambled versions as recorded at the left and right occipito-temporal electrode sites (red). The N170 component appears between 120 and 200 ms, and presents a large amplitude response for faces, in comparison to non-face (car) stimuli. Note the right hemisphere lateralization and absence of the N170 for scrambled stimuli (grey lines). Face selectivity appears even before the N170 peak, at approximately 80-100 ms after stimulus onset, when the P1 deflection appears in response to faces. Adopted from Rossion & Caharel, 2011. **B.** Grand-averaged ERP responses recorded at electrode T6, positioned over the right occipito-temporal cortex, show a significantly larger and delayed N170 for inverted faces compared to upright ones. Notably, no significant difference is measured for object stimuli. Adopted from Rossion et al., 2000.

The use of scalp EEG provided high temporal resolution information about face processing. Notably, combining EEG with fMRI to determine the spatiotemporal organization of face processing associated the N170 response activity that occurs in the occipitotemporal regions with the activation in the pillar face recognition region of the VOTC, i.e., the OFA, the FFA, and the STS (Yovel, 2016). Despite the valuable insight from combining these techniques, relying solely on fMRI to precisely delineate the dynamics of face-selective processing in the human brain presents significant drawbacks (Rossion et al., 2018). This underscores the need for more precise methods that offer both high temporal and spatial resolution inside the human brain, like intracerebral investigations.

IX. tDCS electrophysiological effect on scalp EEG recordings

The works of Antal and colleagues (2004) aided in one of the first electrophysiological characterizations of the effect of tDCS on visual perception. Their findings demonstrated that tDCS modulates the amplitude of visual evoked potential (VEP) in a polarity-dependent manner. Cathodal tDCS reduced, meanwhile, anodal tDCS enhanced the amplitude of the N70. Similar polarity-dependent effects were also observed in oscillatory brain activity, with a reduction in gamma and beta power

following cathodal stimulation that persisted for 10 and 20 minutes, respectively, indicating a sustained neuromodulatory influence of tDCS on visual cortical activity. (**Figure 24A**: Antal, Varga, et al., 2004). Conversely, applying identical tDCS parameters, cathodal stimulation led to a stronger reduction than anodal enhancement, likely due to the asymmetry in neuroplasticity and the visual system already being optimally tuned, limiting the potential for further excitatory enhancement by anodal tDCS (Antal et al., 2006).

Several visual ERP components have been explored with tDCS, including the face-selective N170 and the P3a, which reflects attentional activity. When anodal tDCS was applied to the DLPFC during a face recognition task, researchers observed a reduction in N170 amplitude alongside an increase in P3a amplitude, as well as a tenfold increase in reaction times, suggesting a facilitation of repetition suppression. In contrast, cathodal stimulation of the same region produced opposite effects, an increased N170 amplitude and reaction time, coupled with a delay in P3a latency. These results demonstrate that tDCS-induced modulation of DLPFC excitability in a polarity-dependent manner and affects the early visual encoding of unfamiliar faces (**Figure 24B**: Lafontaine et al., 2013).

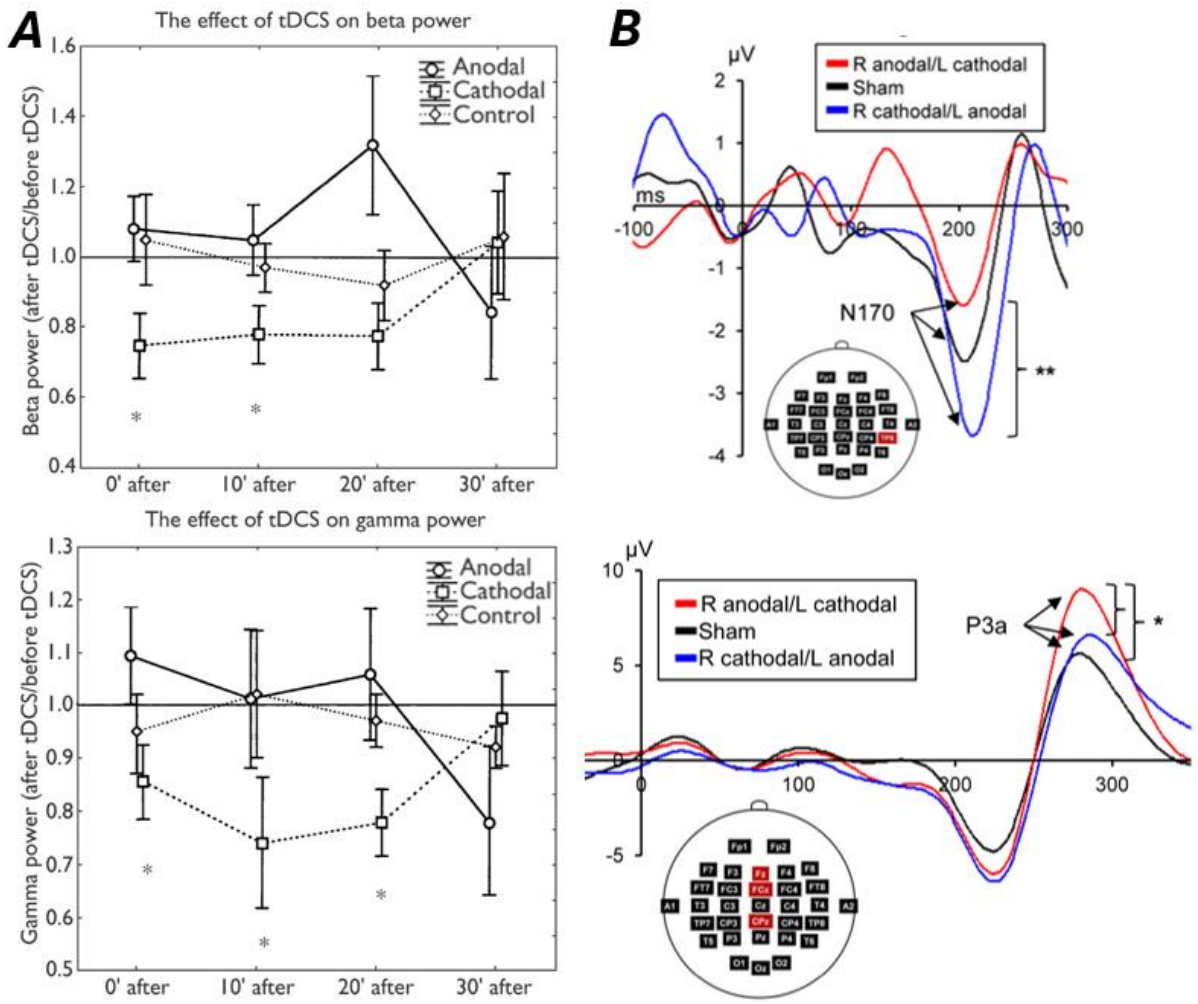

Figure 24. tDCS impact on evoked responses recorded by EEG in the human brain.
A. Influence of 10 min tDCS on beta (top) and gamma (bottom) power. Cathodal tDCS significantly reduced beta and gamma powers immediately after the stimulation and persisted for 10- and 20-minute post-stimulation, respectively. Anodal stimulation presented a trend toward an increase in beta and gamma power, but no significant changes. Adopted from Antal, Varga, et al., 2004. **B.** Effects of tDCS on grand average of N170 (top) and P3a (bottom) power amplitude over right occipito-temporal cortex in response to repeated presentation of unfamiliar faces. Anodal tDCS significantly suppressed the N170 amplitude, while cathodal tDCS enhanced it. The opposite effect was observed for P3a, as right anodal tDCS enhanced P3a amplitude in comparison to right cathodal tDCS. Adopted from Lafontaine et al., 2013.

An online anodal tDCS investigation by Civile and colleagues (2020) further examined the influence of electrically stimulating the DLPFC on the FIE. In line with previous behavioral investigations, they found a decrease in the latency of the N170 component, reflecting less delay in the N170 peak for inverted faces, and therefore decreased FIE (**Figure 25A, B**). The authors suggested that tDCS modifies the configural face processing by enhancing the perceptual similarity among faces, making upright faces harder to differentiate and resulting in a reduced inversion effect. In contrast to latency, the same tDCS procedure also found an increase in the inversion effect as seen by an increased amplitude of the N170 component during stimulation (**Figure 25C**). This contradictory result could potentially indicate a

switch from configural processing to a more feature-based processing, with a more enhanced focus on the eyes of the face. In contrast, at a stimulation intensity of 1.5 mA, offline tDCS targeting the parietal and lateral occipitotemporal regions, whether anodal or cathodal, reduced the distinctiveness of upright faces, as indicated by changes in N170 amplitude and latency in the right hemisphere, thereby diminishing the typical inversion effect (Yang et al., 2014).

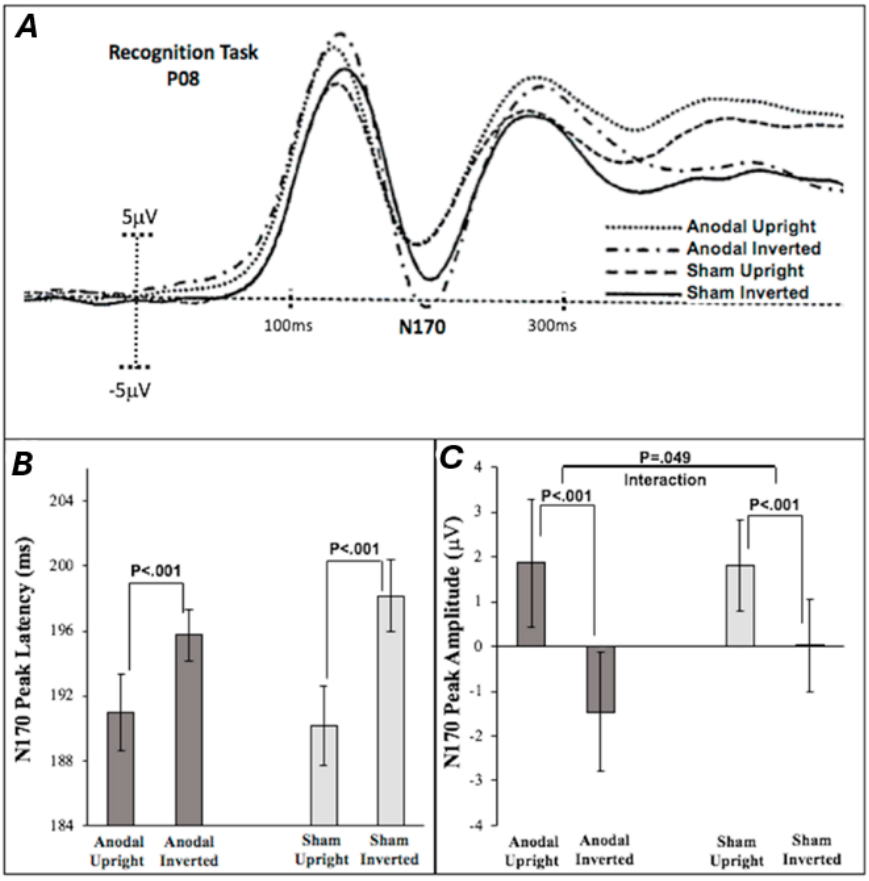

Figure 25. Influence of tDCS on FIE measured by the N170 amplitude and latency.
A. Waveform of the N170 after face stimulus (upright and inverted faces) at electrode P08 during anodal and sham tDCS in the recognition phase. **B.** The mean peak latency of the N170 significantly increased between upright and inverted faces for both stimulations. **C.** Mean peak amplitude of the N170 was significantly decreased between upright and inverted faces, and a trend towards a significantly increased face inversion effect was measured. Adopted from Civile, Waguri, et al., 2020a

Despite the valuable insight scalp EEG recordings provide to measure the neuromodulation induced by tDCS and understand its mechanism in the human brain, this simultaneous application is hindered by several methodological limitations that lead to controversies. Two types of artifacts can be distinguished during online tDCS-EEG protocols: 1) ***Physiological artifacts*** arise from the interaction between stimulation and biological tissue, including motion, cardiac, respiratory, and ocular distortions. These artifacts strongly modulate DC voltage and overlap with neural responses, making them difficult

to remove using conventional signal processing techniques. 2) ***Methodological artifacts*** caused by imperfect experimental conditions or inadequate equipment performance, such as leaked noise by the tDCS system into the electrodes (Diana et al., 2024; Gebodh et al., 2019). These artifacts on scalp EEG signals, specifically during tDCS, induce challenging denoising processes (Faria et al., 2012b; Mancini et al., 2015) and imprecise characterization of the electrophysiological effects (D. W. Kim et al., 2019).

Overall, the lack of artifact-free techniques for electrophysiological recordings during tDCS contributes to interpreting its effects as placebo or indirect (e.g., metabolic) influences. Although several studies have attempted to quantify the electrophysiological effects of tDCS, methodological limitations, particularly the difficulty of recording artifact-free data during stimulation, have made it challenging to obtain consistent and direct evidence of neuromodulation. High-resolution methods such as intracerebral EEG, which allow for artifact-free, spatially and temporally precise recordings, remain rare and are typically limited to specific clinical populations.

X. Intracerebral investigation

Employing intracranial electrodes to record electrophysiological activity provides a key insight for comprehending how the human brain functions. Clearly, this approach is uncommon and is only applied in clinical settings for drug-resistant epileptic patients. Among these cases, temporal lobe epilepsy is the most prevalent, accounting for approximately 30% of patients (Maillard et al., 2004). Intracranial implantations are especially valuable for drug-resistant epileptic patients when non-invasive methods such as scalp EEG and neuroimaging fail to precisely localize the epileptogenic zones, allowing for more accurate diagnosis and treatment planning.

Two surgical procedures are adapted for intracranial recordings (**Figure 26**):

1) Electro-CorticoGraphy (ECoG) is based on removing a part of the skull, in order to apply a subdural strip of electrodes on the surface of the cortex, between the dura mater and the brain (Wyler et al., 1984). Although ECoG provides valuable spatial coverage for recording intracranial activity, its recording area is limited to the gyral surface (**Figure 26A**).

2) Stereo-Electroencephalography (SEEG) is based on inserting multi-contact depth electrodes that penetrate the cortex and reach deeper brain areas like the mesial cortex and the medial temporal lobe. It relies on a stereotactic frame, a tool that utilizes a 3D coordinate system originally developed in 1973 by Talairach to precisely localize brain sections while the head is fixed for electrode implementation (**Figure 26C**: Talairach & Bancaud, 1973). For SEEG recording, each electrode consists of 8–15 consecutive contacts responsible for independent recording of the local field potential

positioned along the medio-lateral axis (**Figure 26B**). Minimally invasive, this method presents several advantages: a) Intracerebral EEG (iEEG) recording of direct neural activity inside white and grey matter, b) Exploring activity of deep brain regions in the medial temporal lobe, like amygdala and hippocampus. c) Recording local field potentials by multi-contact depth electrodes, as well as electric fields at various distances along a single electrode. d)Intracerebral bipolar stimulation through adjacent contacts, aiding clinicians in accurately assessing epileptic cases and investigating network connectivity (**Figure 25B**). e) Radiofrequency thermocoagulation to treat pathological regions (Rossion et al., 2023).

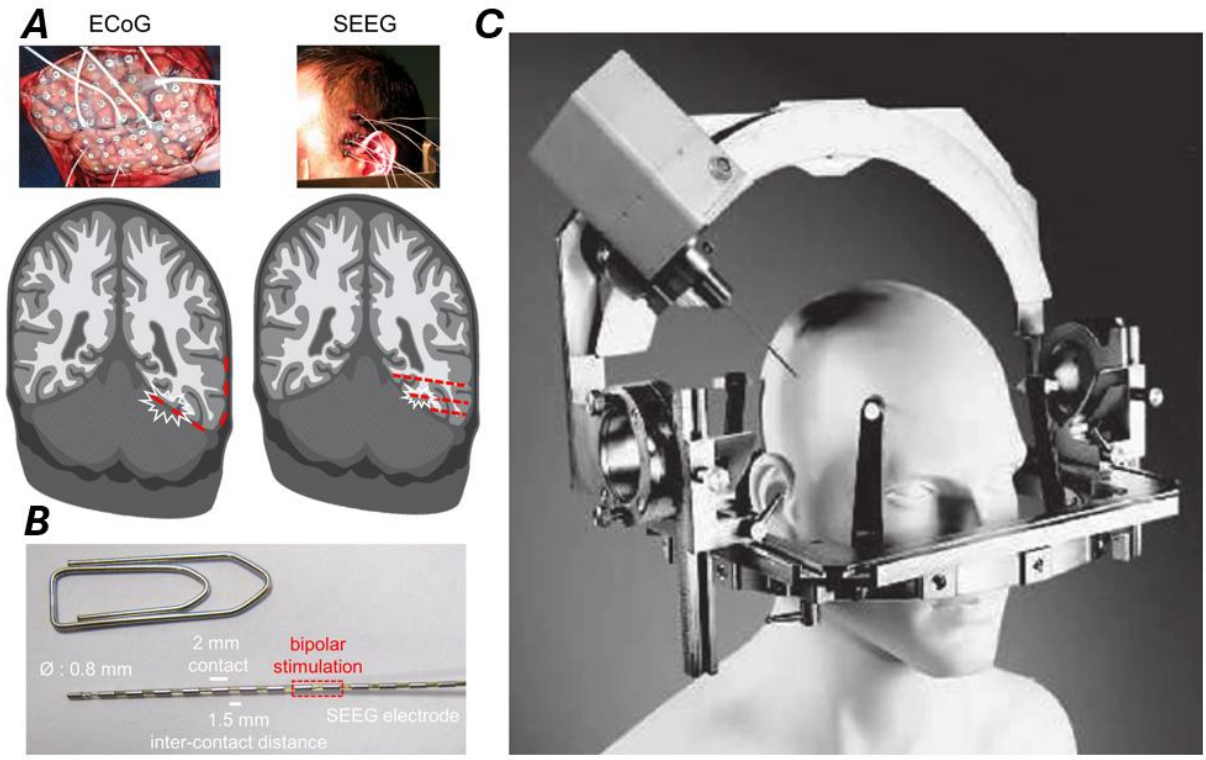

Figure 26. Figure of ECoG and SEEG implantation methods.
A. Figure illustrates two intracranial EEG techniques used for recording and stimulation: ECoG and SEEG. Top images: surgical procedures for electrode placement. In ECoG, a portion of the skull is removed to position electrode grids directly on the cortical surface. In SEEG, narrow depth electrodes are inserted through small openings carefully drilled into the skull. Bottom panel: a coronal schema illustrating intracranial electrodes in the middle fusiform gyrus, where electrodes (in red) are used for bipolar stimulation (in white), applied between two adjacent recording sites. **B**. Photograph showing a typical SEEG electrode, placed next to a paperclip for size comparison. It consists of a 0.8 mm diameter cylinder containing 8–15 independent recording contacts, each 2 mm in length, spaced 1.5 mm apart and 3.5 mm center-to-center. The dotted rectangular area shows the section involved in bipolar stimulation. Adopted from Jonas & Rossion, 2021**. C.** Stereotactic head frame. Adopted from Zanotto et al., 2011

This type of procedure is carried out over the course of several days (5 days), to weeks in some cases. The implantation is planned and carried out by a multidisciplinary group of clinicians, taking into consideration the suspected location of the epileptogenic zone. The exact implantation coordinates in the brain are predetermined and tailored for each patient. After the implantation, patients are placed under supervision, stripped of their medications, and monitored for spontaneous seizure occurrence

to assess the localization of the epileptogenic zone. This approach allows direct exploration of brain activity, as well as the behavior of patients, in response to epilepsy (Paredes-Aragon et al., 2022). Additionally, patients implanted with intracerebral electrodes sometimes volunteer for cognitive clinical research, providing a rare and valuable opportunity to study human brain functions.

In some cases, the epileptogenic zone is in a critical vital location, for example, close to the hippocampus, the visual or the respiratory cortex, making it difficult to operate. Clinicians are faced with these complicated cases and can sometimes opt for NIBS methods like tES, TMS, and vagus nerve stimulation to help alleviate the seizures and decrease their risk. In line with scalp EEG studies applying tDCS during various periods of time (San-juan et al., 2015, 2017), iEEG recording (using SEEG) during tDCS revealed a reduction in interictal epileptiform discharges that occur between seizures (Koessler et al., 2023). In addition to recurrent seizures, epileptic patients also struggle with cognitive impairments that impact their quality of life, highlighting the need for a more comprehensive approach to symptomatology management.

Intracerebral stimulation has provided valuable insights into the role of various brain regions and their link to specific behavioral and electrophysiological responses, particularly in facial perception. Intracerebral stimulation via adjacent SEEG contacts (from 0.8 to 2 mA) revealed an impairment in face identity recognition that resulted in prosopagnosia, the inability to recognize faces, when regions in the VOTC, like the OFA and the FFA, were stimulated (Jonas et al., 2012, 2014, 2015; see Jonas & Rossion, 2021 for a review). In line with these results, TMS targeting regions of the VOTC, directly or indirectly, revealed significant neuromodulation of face processing, as shown by EEG recordings (Mattavelli et al., 2013, 2016, 2019) and fMRI responses (Pitcher et al., 2007, 2011, 2014, 2017; Pitcher, 2024 for review).

Both ECoG and SEEG enable intracranial recordings of local potentials with millisecond resolution, providing stable and high signal-to-noise ratio (SNR) measurements, revealing key face-selective electrophysiological responses. Particularly, the intracerebral face-selective ERPs, like the N200 and AP350, have been identified over the IOG and fusiform gyrus using ECoG (Allison et al., 1999). Additionally, SEEG recordings further revealed distinct face-evoked potentials in the fusiform gyrus, characterized by a triphasic pattern consisting of the N130, P180, and N240 components (Halgren et al., 1994). Notably, simultaneous scalp EEG and iEEG recordings revealed the functional correspondence between the N170 face-ERP recorded over the occipitotemporal region and the intracranial face-selective N200 recorded in the lateral occipital cortex, in terms of both latency and amplitude modulations for face inversion (Rosburg et al., 2010).

Despite their advancements, iEEG studies investigating face-selective cortical responses have yet to establish a comprehensive large-scale map of the VOTC in humans. A relatively novel approach that has been adopted since the early 2010s to precisely distinguish face-selective responses and identify the brain regions involved in visual processing using intracerebral recordings. This approach is based on the "frequency-tagging" method and will be explained in detail in the following section.

XI. Fast Periodic Visual Stimulation to measure face recognition

Fast periodic visual stimulation, or FPVS, is a relatively novel approach based on the generation of steady-state visual evoked responses (SSVEP). When a visual stimulus, a luminance flicker, is presented periodically, it generates an electrophysiological response at the same frequency as the representation of the stimulus. In essence, this method evokes a continuous, frequency-tagged neural response. Notably, the brain synchronizes its activity to the stimulus frequency, generating highly stable and measurable SSVEPs (Regan, 1966). Due to their periodic nature, SSVEPs are analyzed in the frequency domain. In this manuscript, we disregarded the term SSVEPs and used FPVS or frequency-tagged, as it's the generic term defining the approach.

SSVEPs have been mostly investigated for low-level visual stimuli, like luminance and color periodicity changes (Regan, 1966, 1974). Rossion & Boremanse, (2011) were the first to implement the frequency-tagging approach for high-level visual stimuli to assess face discrimination. In their approach, identical or different face images were presented periodically at a rate of 3.5Hz during short sequences of 60s, which elicited a response at the same frequency of presentation (**Figure 27A**). The frequency-tagged responses showed a larger response for different faces than for the same face repeated at the frequency of presentation (**Figure 27B**). The differential response between the 2 responses at 3.5 Hz was the largest over the bilateral occipitotemporal regions, especially in the right hemisphere, and can be considered as an objective measure for individual face discrimination(**Figure 27Bb**).

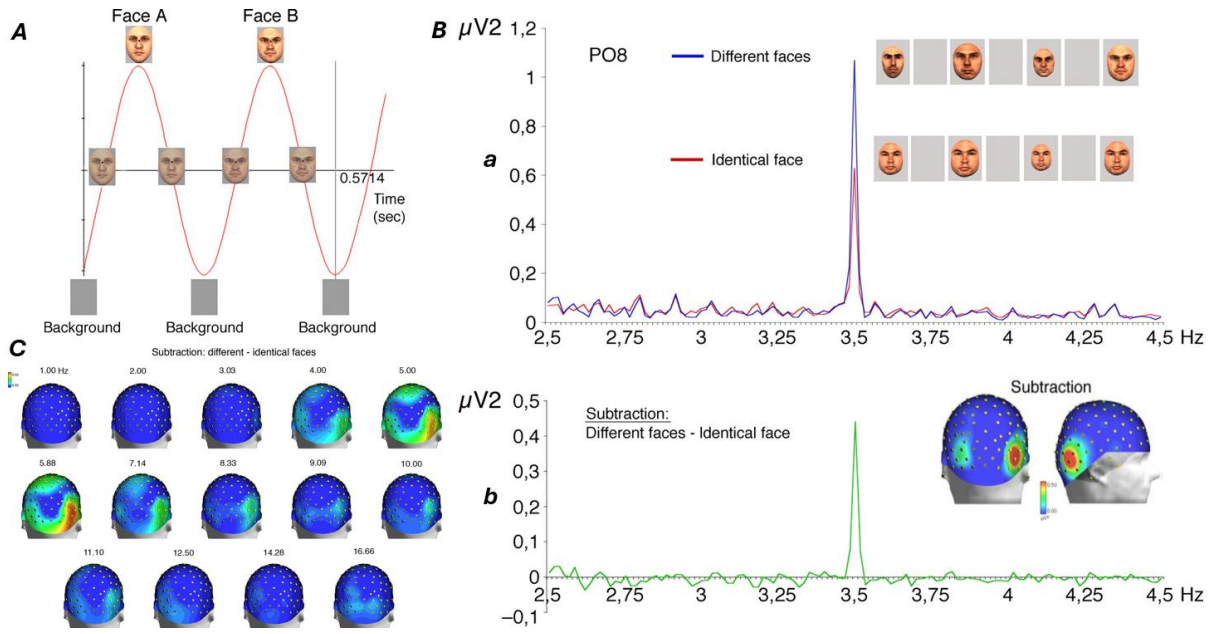

Figure 27. Development of the FPVS approach.
A. Visual stimulation used in Rossion & Boremanse, 2011. Sinusoidal stimulation at different contrasts (0 to 100%) of different face identities presented at a frequency of 3.5Hz (3.5 cycles/s, here only showing 2 cycles). A new face identity appears each cycle. **B.** Grand average of the EEG power spectrum from 12 participants, recorded at the PO8 electrode using scalp EEG. **B, a.** Notably, responses to different faces elicited larger response amplitude than identical faces (the two conditions shown next to the peak). **B, b.** The subtraction between the 2 conditions of interest arises only at 3.5Hz, the frequency of stimulation. Topographic maps of the subtracted response show right hemispheric dominance. Adopted from Rossion & Boremanse, 2011. **C.** Topographical maps of the differential SNR (different faces vs identical face) at the different frequencies of stimulation. Note that the 5.88Hz elicits the highest SRN response on the maps for the subtracted response. Adopted from Alonso-Prieto et al., 2013.

To identify the frequency that elicits the highest face recognition response, several frequencies were tested with both conditions, and the maximal difference between the conditions was measured. It was revealed that the frequency of 5.88Hz or a temporal rate of 170ms (6 faces/s) is the fundamental frequency rate at which faces are clearly discriminated in the occipitotemporal cortex (**Figure 27C**: Alonso-Prieto et al., 2013). This discovery influenced the design of FPVS paradigms for studying facial recognition, where faces were presented at a frequency of 6 Hz. At this relatively fast rate, each stimulus is processed within a single fixation, minimizing contamination from eye movements. Furthermore, measuring face discrimination by subtracting from the different versus identical faces conditions risks the assumption that participants sustain the same level of attention across both sequences while also introducing the concern that noise may affect each condition differently. To enhance the efficiency of this method, both conditions (different vs same face) were integrated in the same sequence using the FPVS approach (**Figure 28**:Liu-Shuang et al., 2014), instead of using a subtraction method.

Hence, the FPVS paradigm is based on presenting two stimuli, the base and the oddball, within the same sequence at different periodicities to measure face discrimination between them. In this context, the first stimulus is presented at a base frequency of 6Hz and a second stimulus at an oddball frequency every fifth frame, at 6/5=1.2Hz. The oddball response represents the subtracted response we were to see if the subtraction method was still used (**Figure 28**: Liu-Shuang et al., 2014). This paradigm is also called the *Identity Discrimination paradigm,* as it aids the discrimination of a new face identity (i.e., oddball, 1.2Hz) between same face identities (i.e., base, 6Hz).

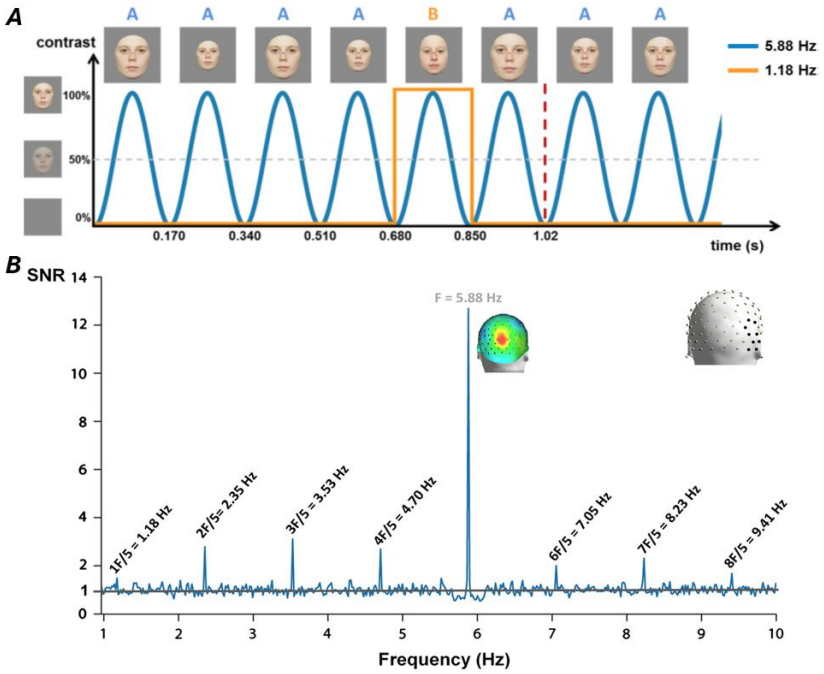

Figure 28. Experimental FPVS paradigm and its corresponding responses recorded using scalp EEG.
A. Schematic presentation of the FPVS paradigm using face stimuli. FPVS paradigm design involves base same identity face images (A) presented by sinusoidal contrast modulation at 5.88 Hz, with oddball new identity faces (B) presented every 5th stimulus, at 5.88/5Hz = 1.2Hz. Each trial includes a fixation period (2–5 s), a 60-s stimulation sequence, and a 5-s fade-out phase. Participants focus on the fixation cross and respond to rare color changes. Face sizes were randomly varied between 74 to 120 % every cycle of stimulation to avoid pixel overlapping. **B.** SNR spectrum at the occipitotemporal regions of interest for face discrimination. The oddball face discrimination responses were clearly defined and significant at the fundamental frequency (1.18 Hz) and its harmonics up to the 8th harmonic (9.41 Hz). While the amplitude of the 1.18 Hz response appears small, it corresponds to an SNR of 1.49, indicating a 49% increase relative to noise. The base response is clearly defined at 5.88Hz. Adopted from Liu-Shuang et al., 2014a.

Rossion et al. (2015) were the first to apply this FPVS approach to measure face categorization. They presented participants with sequences of 70 s featuring a diverse range of natural images from various non-face ***object*** categories, shown at a fast periodic rate of 6 images/second (6 Hz). Images of ***faces*** were presented every fifth stimulus, at 5.88 Hz / 5 = 1.18 Hz. The brain's activity synchronizes with the frequency of presentation of the images, resulting in a ***face-selective response*** at the frequency of presentation of face images and ***general visual response*** at the frequency of presentation

of non-face object images (and faces as 6Hz is a harmonic of 1.2Hz) (**Figure 29A**)**.** Both responses are distributed across their proper frequency-characterized harmonics. Due to their periodic nature, the EEG responses can be analyzed in the frequency domain, where they present a periodic spread at specific harmonics of the frequencies i.e., 2.4 Hz, 3.6 Hz, 4.8 Hz, 6 Hz for the 1.2Hz face-selective response and 12 Hz, 18 Hz, 24 Hz for the 6Hz general visual response (**Figure 29B**, Retter & Rossion, 2016). This paradigm, *the Face Localizer*, allows discrimination between the general visual response and the brain's face-selective responses, which respond only to face images. The detailed procedure to analyze the electrophysiological face-selective responses (scalp EEG or iEEG) recorded during an FPVS paradigm is shown in **Figure 29**.

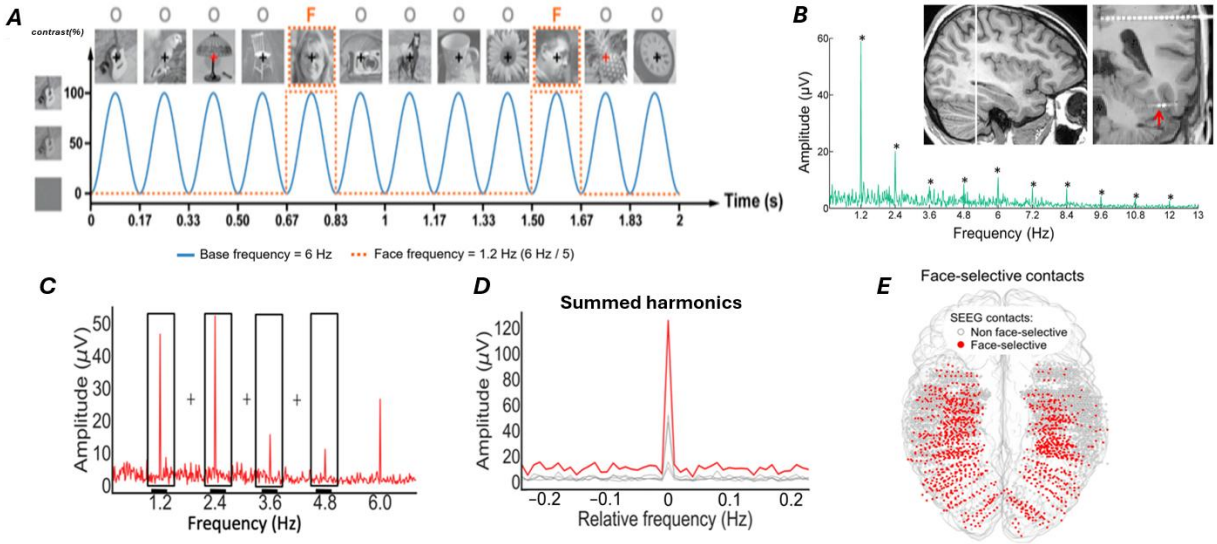

Figure 29. Face categorization paradigm and analysis procedure for face-selective responses recorded in a single contact in the fusiform gyrus.
A. FPVS paradigm to measure face categorization. Object images are presented sinusoidally at a rate of 6Hz (6 images per sec), with face images presented every 5th stimulus (6/5=1.2Hz). **B.** Intracerebral recording from a contact located in the right fusiform gyrus (red arrow), showing significant face-selective responses at the fundamental frequency of 1.2Hz and its harmonics (2.4Hz to 10.8Hz). **C, D.** Procedure to analyze the face-selective responses recorded during FPVS. Top spectrum: Due to their periodicity, iEEG face-selective responses are analyzed in the frequency domain. For each iEEG recording contact, the significance of the response is computed based on its amplitude at the first four harmonics (1.2 Hz to 4.8Hz). The qualification can consider more harmonics (> 4.8Hz), although the bulk response is usually found at the first four. The frequency spectrum is then divided into four segments containing the amplitude at the specific harmonics and their neighboring frequency bins (black rectangles). Bottom spectrum: each segment containing the signal and the noise around it (grey signal) is summed (red signal). The Z score is then computed at each frequency bin based on the estimated surrounding noise. ***E.*** Significant contacts (Z-score > 3.1) identified across individual brains (N = 84) are mapped onto the Colin27 template brain in Talairach space. Adopted from Rossion et al., 2018, 2023d.

This FPVS approach is an (1) ***objective*** tool to identify a signature of face categorization, incorporating both visual discrimination (from non-face objects) and generalization (across widely variable face exemplars). The visual response is measured (2) ***implicitly and automatically*** without any behavioral task that might contaminate the response through decision making. It also results in a

significant, quantifiable response with (3) ***high SNR*** (signal to noise ratio) in a few minutes of stimulation (or less)**.** The periodicity (frequency-locked) of this approach in presenting the visual response allows for a high test-retest-reliable method to measure the responses (Dzhelyova et al., 2019; Liu-Shuang et al., 2014b).

XII. Measuring FPVS responses with intracerebral EEG recording

The robustness of this approach facilitated its application beyond scalp EEG recordings, extending to intracerebral investigations of face-selective brain regions (**Figure 29**). In a large cohort of epileptic patients (n=28) implanted with depth electrodes (SEEG) (**Figure 30A**), Jonas et al. (2016) adopted the same FPVS paradigm, the Face Localizer, to comprehensively map visual face-selectivity across the entire human VOTC through direct brain activity measurements. Face-selective regions were scattered throughout the whole VOTC, forming clusters in specific brain areas extending from the occipital to the anterior pole (**Figure 30B**). The right lateral part of the middle fusiform gyrus (**latFG**) showed the most consistent and pronounced face-selective response, corresponding to the predominant face-selective area, the ***right FFA,*** as identified in MRI studies. The ***right IOG***, corresponding to the cortical region of the ***OFA,*** and the anterior fusiform gyrus (***antFG***) exhibited the second most prominent face-selective responses (**Figure 30C**). Interestingly, three distinct face-selective regions were identified in the right anterior temporal lobe (***ATL***), a region that's often undersampled in neuroimaging due to magnetic susceptibility artifacts. Face-selective regions also include the anterior fusiform gyrus ***antFG***, the anterior segment of the collateral sulcus (***antCoS***), and the region along the anterior section of the occipito-temporal sulcus (***antOTS***) (**Figure 30D, b**)**.** Additionally, face-exclusive regions, regions that respond only to face stimuli without any general visual response, were also identified. These regions' responses increased according to a posterior-to-anterior selectivity axis in the VOTC, increasing from the posterior temporal lobe (PTL) to peak response in the ATL (**Figure 30**: Jonas et al., 2016; Rossion et al., 2018).

The benefits of this approach allowed its application to isolate high-level visual responses as seen by scalp EEG and SEEG recordings. Additionally, it's been used in multiple other settings to discriminate landmark images (Hagen et al., 2020) and to investigate other cognitive functions like language processing (Rossion & Lochy, 2022), semantic categorization (Volfart et al., 2021), and auditory selectivity (Barbero et al., 2021). This approach has also shown significant electrophysiological biomarkers to predict diseases like Alzheimer's disorder (David et al., 2025) and enabled assessment of social orientation and communication levels in young individuals with autism spectrum disorder (Vettori et al., 2020; Vettori, Dzhelyova, et al., 2019; Vettori, Jacques, et al., 2019).

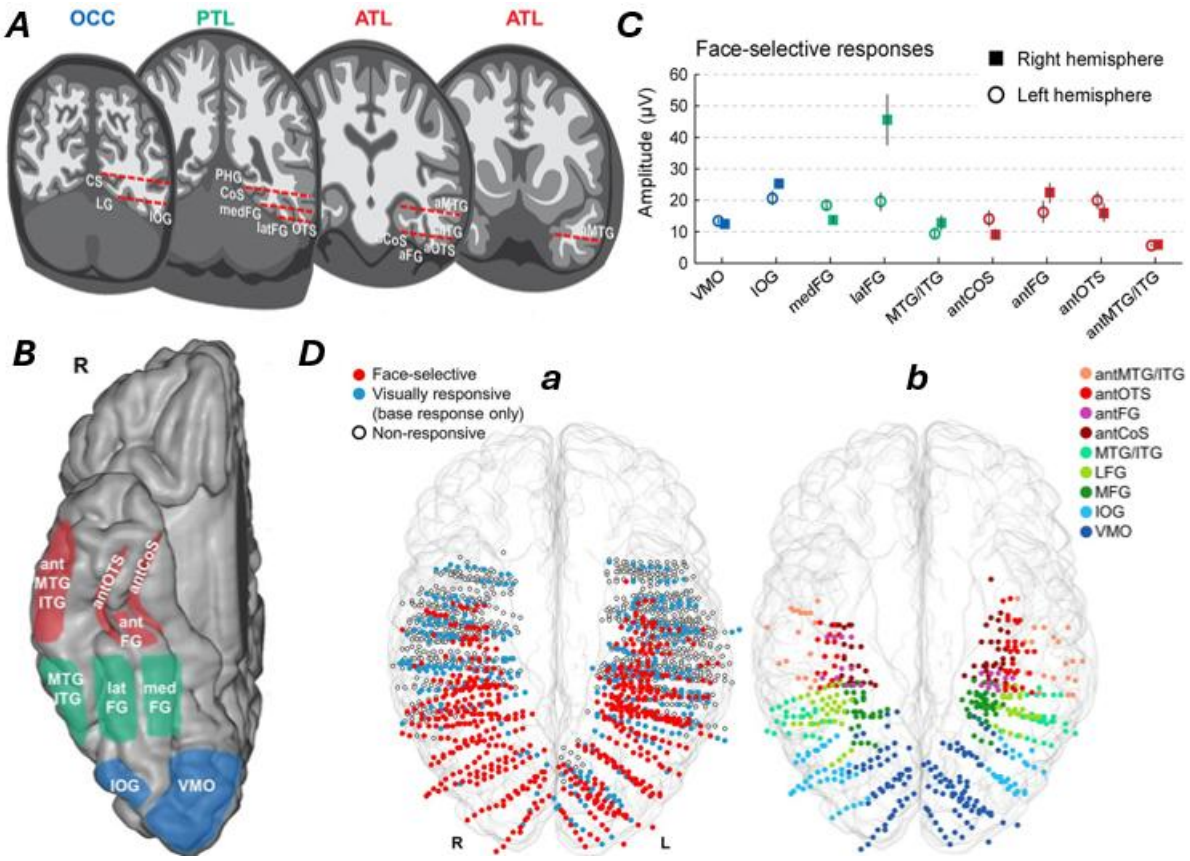

Figure 30. Map of face-selective regions in the VOTC brain with intracerebral recordings and FPVS.
A. Schematic illustration of typical trajectories of SEEG depth electrodes implanted in the right VOTC, in the occipital (OCC), posterior (PTL), and anterior temporal (ATL) lobes. Red rectangles on coronal schematic slices show electrode placement across gyral and sulcal cortical regions. **B.** Reconstructed cortical surface of the Colin27 brain illustrating the anatomical locations of face-selective regions. While the regions are displayed on the cortical surface for visualization purposes, the corresponding responses were recorded intracortically. **C.** Quantification of the average face-selective response amplitudes in each region across contacts in the left and right hemispheres. Note the particularly large amplitude of the face-selective response recorded in the right latFG, followed by a lesser extent in the IOG compared to other regions. **D, a.** Maps of the spatial distribution of the 3 types of responses recorded in all 1678 VOTC recording contacts (n=28 participants). Each contact is represented by a circle. Face-selective contacts are shown in red, with visually responsive contacts (respond only to base) in blue and nonresponsive contacts (no face-selective or general visual responses) in white. A higher number of contacts in the right hemisphere (988) in comparison to the left (690). **D, b.** Face-selective contacts are color-coded according to their individual anatomical location. Adopted from Jonas et al., 2016.

Combining SEEG with the FPVS approach provides not only a measure of face-selectivity at each region but also a measure of the functional connectivity between them. Direct electrical stimulation (DES) can be applied between two adjacent pairs of contacts in a SEEG depth electrode while participants view sequences of an FPVS paradigm. In a case study, DES was applied using typical SEEG stimulation parameters for 10 s using a bipolar stimulation at 1.0 mA (using biphasic square wave electrical pulses with 1050 μs width at 55 Hz). A behavioral impairment in face identity recognition was induced by intracerebral DES of the right latFG/FFA combined with famous and unfamiliar face matching tasks. The patient mentioned seeing all the faces looking similar during DES (Volfart et al., 2023). Interestingly, in the same patient, DES of the right latFG/FFA during a frequency-tagging with

familiar faces (**Figure 31A**) significantly reduced the activity of face-selective regions in the bilateral ATL regions, especially in the right antFG, resulting in impairment in face identity recognition (**Figure 31 B, C**). These findings highlight the effective functional connectivity between face-selective regions within and beyond the same hemisphere (**Figure 31**: Angelini, Volfart, et al., 2024).

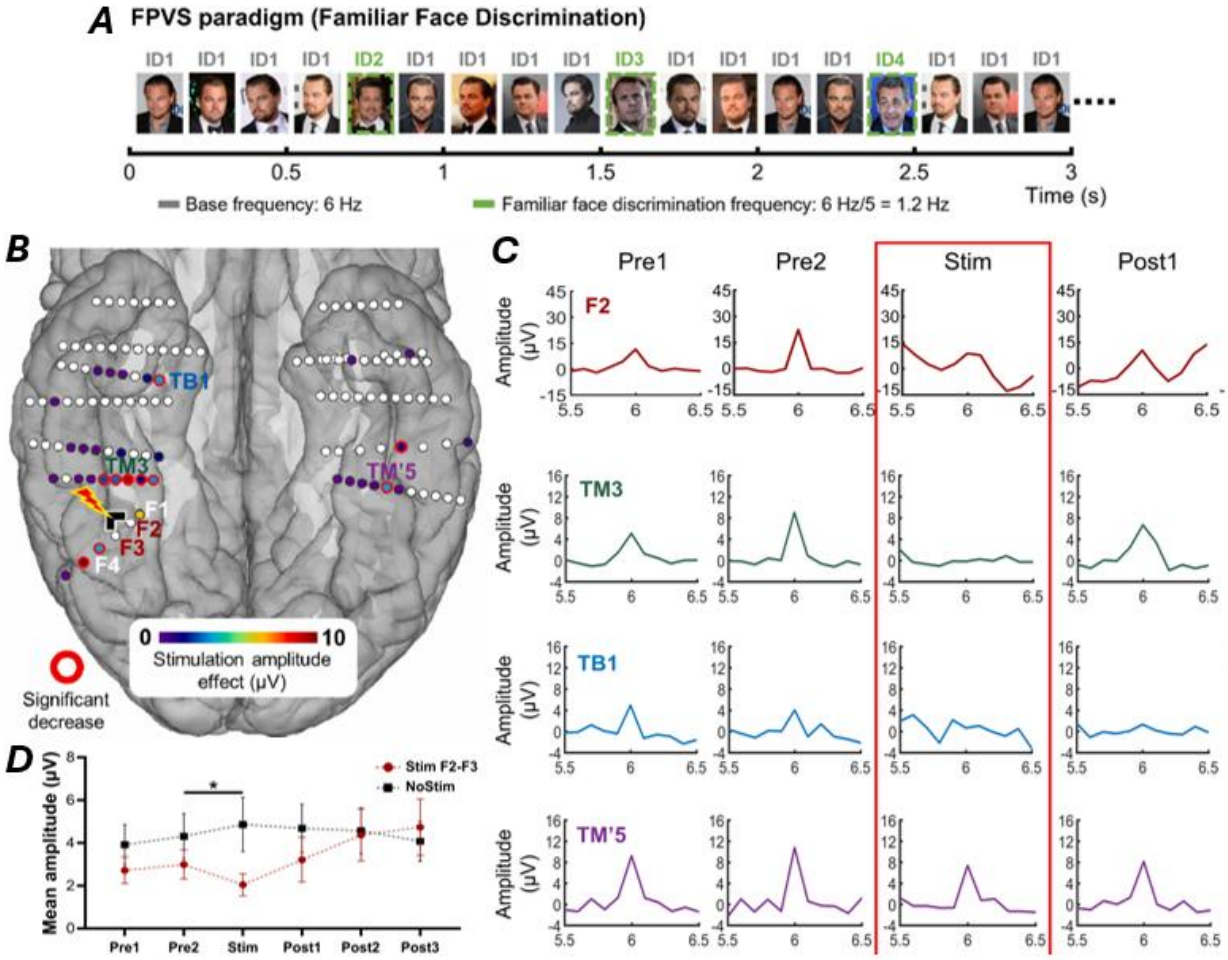

Figure 31. Effective connectivity of functional brain regions through concurrent intracerebral DES and FPVS. **A.** Familiar face discrimination FPVS paradigm administered outside and during DES, composed of familiar face images presented periodically at 6Hz for 70s. It is typically used to record responses that reflect the discrimination between different familiar face identities every 5th image. However, in this case, the most reliable face response at 6 Hz was analyzed. **B, C.** DES was applied for 10s to the right FFA (F2-F3 stimulation site) after 20s of FPVS presentation. SEEG recordings corresponding to the FPVS sequences were divided into epochs of 10s each: before (Pre 1, 2), during (Stim), and after (Post1, 2, 3) the stimulation. For each epoch and contact, the face response at 6Hz was analyzed in the frequency domain. **B.** Reconstructed cortical surface of the patient's CJ brain with the stimulation site (F2–F3) and its corresponding local and distant 6Hz face response. The contacts of interest (n=33), exhibiting a 6 Hz response outside stimulation, are color-coded based on the amplitude difference between Pre2 and the stimulation periods, i.e., stimulation amplitude effect. Contacts circled in red show a significant decrease. **C.** Display of the temporal variation in the amplitude of the 6 Hz response in the frequency domain for the stimulated contact (F2) and remote contacts (TM3, TB1, and TM'5), which exhibited a reduction or even suppression of the 6 Hz face response during stimulation. **D.** Average amplitudes of the 6 Hz response across selected contacts of interest to compare between stimulated and non-stimulated sequences, segmented into 6-time windows. Significant differences were identified for the stimulation amplitude effect (Pre2 minus Stim) between both conditions. Adopted from Angelini, Volfart, et al., 2024.

Furthermore, in another case study, bidirectional effective connectivity was found between the IOG/OFA and latFG/FFA within the face recognition network. The intracerebral DES applied to a face-selective region, during FPVS, led to the reduction or abolition of the activity of another face-selective region (**Figure 32A**). These results also emphasize the inter-hemispheric interaction between the regions of the face processing network. Classical models of visual recognition propose a feedforward progression from posterior (IOG/OFA) to anterior regions (latFG/FFA). However, the evidence they provided for direct, reentrant connectivity shows that higher-level regions also provide feedback to lower-level areas, creating an interactive system that enhances the processing of complex stimuli like faces (**Figure 32B**: Angelini, Jacques, et al., 2024).

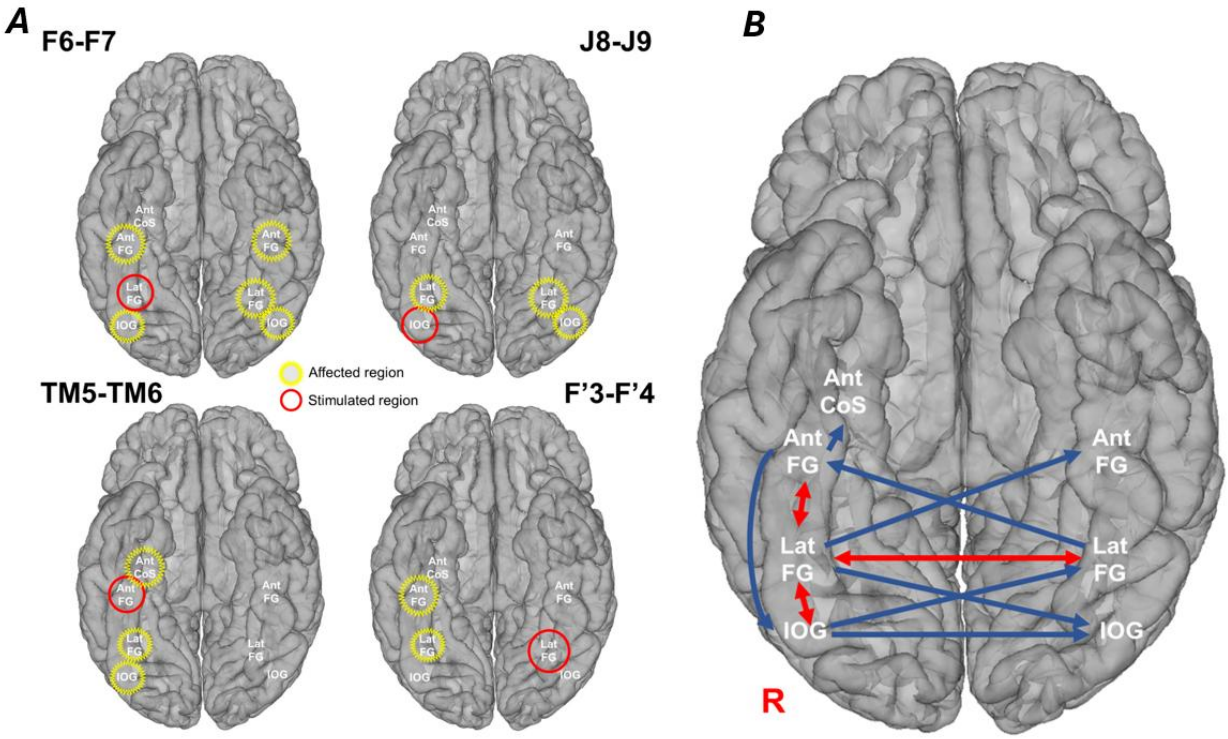

Figure 32. Bidirectional and unidirectional connections between the core cortical face network.
A. Schematic representation of the stimulation effect on the main face-selective regions in the reconstructed cortical surface of subject YR's brain. The stimulated regions (right Lat FG, IOG, Ant FG, and left Lat FG) corresponding to the stimulated sites (F6-F7, J8-J9, TM5-TM6, F'3-F'4) colored in red circles. Their affected local and remote regions, circled in yellow, showed decreased amplitude for the face-selective responses during intracerebral stimulation. **B.** Schematic representation of the bidirectional connectivity between the core face-selective areas in the right hemisphere and the bidirectional inter-hemispheric connectivity relative to core face-selective areas in the bilateral VOTC (in red). In blue, the unidirectional inter- and intra-hemispheric connectivity between the face-selective regions. Adopted from Angelini, Jacques, et al., 2024.

As SEEG is inevitably a minimally invasive approach, the correlation between the intracerebral and scalp EEG recordings has been investigated in the hopes of bridging the gap between local neural populations and scalp EEG. Simultaneous intracerebral and scalp EEG recordings of an epileptic patient's brain activity during an FPVS paradigm generated objective and robust frequency-domain

responses in both recordings. Correlation analysis revealed a significant correlation between intracerebral regions of the lateral IOG and the regions of the right occipitotemporal cortex (electrodes O2, PO8, P10, and P4) specific to face stimulation. Evidently, the amplitude of scalp response was 10 times smaller than the one recorded intracerebrally (Jacques, Jonas, et al., 2020). In line with these findings, a previous simultaneous scalp and intracerebral recording study identified the IOG as a major cortical generator of the scalp face-selective N170 (Jacques et al., 2019).

In conclusion, combining a robust approach like FPVS with intracerebral recording, along with scalp EEG recordings, seems to be a well-established method to investigate the visual recognition network and aid the mapping and identification of the face-selective regions in the VOTC in the human brain. Notably, intracerebral investigations using SEEG have been combined with tDCS, particularly to explore the local electric fields EF induced by stimulation (Chhatbar et al., 2018; Huang et al., 2017; Louviot et al., 2022; Opitz et al., 2015). In addition to characterizing local EF, this coupling has also yielded valuable insights into epileptic discharges in patients with epilepsy. While intracerebral recording is minimally invasive, combining tDCS with iEEG recording, especially during cognitive tasks, could provide a unique opportunity to examine the intracerebral electrophysiological effects of tDCS on the human brain. Consequently, it could offer valuable insights into how tDCS modulates cognitive processes involved in face processing and potentially contribute to improving such functions. Overall, the simultaneous application of these three techniques holds significant promise and warrants further exploration. Hence, in the following chapters of this manuscript, we present an exploration of tDCS effects on visually evoked responses, as measured through both intracerebral and scalp recordings.

XIII. Thesis objectives

tDCS application in humans, particularly for clinical purposes, depends directly on the highly interdependent parameters like intensity, electrode montage, duration, and other factors. The absence of a standardized protocol for tDCS application, combined with tDCS's heterogeneous, non-reproducible, and difficult to interpret results, underscores the need for a more comprehensive understanding of its effects on the human brain. Although the mechanisms of tDCS at the neuronal, cellular, and network levels have been extensively investigated *in vitro, in vivo* and *in silico* investigations, current evidence remains insufficient to clearly define its direct impact on the brain's complex electrophysiological activity. tDCS holds a significant therapeutic potential for neurological and neuropsychiatric disorders, as well as for cognitive neurorehabilitation, particularly in the field of visual perception. However, methodological limitations such as reliance solely on unreliable behavioral tasks and constraints of scalp electrophysiological recordings continue to hinder the advancement of tDCS applications. Therefore, addressing these gaps is crucial for optimizing tDCS efficacy and ensuring its safe and effective use in humans.

In this manuscript, we aim to address *three primary scientific questions*:

- *First of all*, we propose that leveraging the use of rare intracerebral recording in vivo in humans during a standard tDCS protocol could provide unique insight into how tDCS neuromodulates ongoing neural responses during a cognitive visual task*. How does tDCS influence intracerebral electrophysiological activity, particularly during the stimulation period? To what extent can anodal tDCS neuromodulate face-selective neural responses in functionally targeted brain regions like the VOTC? Are the effects of tDCS transient, limited to the duration of stimulation, or do they persist afterward, indicating sustained neuromodulatory impact?*
- *Secondly*, intracerebral recordings provide valuable insight into the human brain, but, unlike scalp EEG, they remain an inaccessible and minimally invasive method. *How can the electrophysiological effects of tDCS measured at the scalp be linked to their underlying intracerebral sources evoked during FPVS? To what extent can bridging this scalable gap improve the reliability of scalp EEG in assessing cortical excitability and neuromodulation?*
- *Lastly*, the portability of the tDCS device expanded its accessibility and enabled its self-administration outside traditional clinical settings. Coupling the tDCS-FPVS approach with a reliable remote scalp EEG system (i.e., Neuronaute) could open new avenues for monitoring tDCS effects. *Does the new Neuronaute device reliably capture the ERP limited by an FPVS paradigm? Can it serve as a valid tool for assessing cognitive-induced changes in home-based applications?*

The ***main aim*** of this manuscript is to elucidate the underlying intracerebral electrophysiological effects of tDCS and assess its neuromodulatory influence on the human brain. Specifically, it seeks to bridge the gap regarding anodal tDCS neuromodulation of the brain activity during a cognitive face perception task. In our investigation, we utilize face perception, a well-defined cognitive function, with key regions clearly identified through neuroimaging and intracerebral recordings. In the context of this study, it serves as an initial framework for understanding the effects of tDCS, intending to subsequently correlate these effects to other cognitive functions. In addition, we aim to correlate the intracerebral findings of tDCS on scalp EEG to identify reliable and accessible electrophysiological biomarkers of tDCS effects. Finally, this approach seeks to facilitate the accessibility of tDCS and scalp EEG monitoring for at-home applications through the validation of a novel scalp EEG recording system.

The remainder of this manuscript is organized into four chapters. Chapters **II**, **III,** and **IV** present the experiments carried out to answer the scientific questions posed and the detailed main findings.

- **Chapter II***,* we propose a novel approach to overcome current methodological limitations, where we combine tDCS with a robust periodic visual stimulation during intracerebral SEEG recording. This is the first, to our knowledge, assessment of tDCS effects on the electrophysiological activity inside the human brain during a cognitive task. The novelty of this approach lies in examining intracerebral electrophysiological changes during a standard protocol of 2mA tDCS for 20 minutes with only two small electrodes, replicating clinical parameters for cognitive interventions.
- **Chapter III**, we utilize the scalp EEG data recorded simultaneously with intracerebral EEG during anodal tDCS and face recognition task to translate tDCS findings from intracerebral to scalp EEG recording. This approach disregards the use of an invasive methodology and consequently supports the use of scalp EEG for investigating tDCS neuromodulation effects.
- **Chapter IV**, we validate the use of a new scalp EEG device (*Neuronaute*) for recording event-related potentials during FPVS. The novelty of this device is that it allows wireless remote monitoring of recorded activity for individuals and patients. It could be used in the future to monitor cognitive functions at home.
- **Chapter V**, we finally conclude by discussing the main findings we've conducted in these studies and their possible implication in future noninvasive applications for potential treatment purposes or cognitive rehabilitation.

Chapter II: Transcranial Direct Current Stimulation Neuromodulates Intracranial Cognitive Evoked Activity in Human

- ***Objective:*** Quantify tDCS-induced electrophysiological neuromodulation during and after stimulation in the human brain.
- ***Methods:*** tDCS (2 mA, one session of 20 minutes, 2 HD electrodes), intracerebral EEG recording (453 intracerebral contacts), and FPVS. N= 11 drug-resistant epileptic patients.

Highlights

1. The method of combining tDCS with FPVS during iEEG provides a valid approach to quantify tDCS electrophysiological neuromodulation in the human brain.
2. One session of low-intensity tDCS with 2HD electrodes significantly neuromodulates face-selective responses with effects persisting beyond the stimulation period.
3. Micro-architectural structures in the lateral and medial fusiform gyrus influence tDCS neuromodulatory effects.
4. These findings demonstrate the first evidence of tDCS neuromodulation of human intracerebral electrophysiological activity.

The work described in this chapter has been published as a paper in the Journal of *PNAS, Proceedings of the National Academy of Sciences* (**Appendix I**):

Tabikh M, Quetu T, Maillard L, Colnat-Coulbois S, Rossion B, Koessler L. Transcranial direct current stimulation neuromodulates intracranial cognitive evoked activity in humans. Proc Natl Acad Sci U S A. 2025 Jun 10;122(23):e2416541122. Doi: 10.1073/pnas.2416541122. Epub 2025 Jun 3. PMID: 40460123.

I. Introduction

As mentioned earlier, the development of NIBS techniques has opened new avenues for cognitive rehabilitation in neurological and psychiatric diseases. Among these techniques, tDCS stands out for its potential to modulate neural activity using low-intensity currents and its accessibility with minimal, cost-effective equipment (Pilloni et al., 2022). TDCS is based on injecting a low-intensity direct current (few milliamps) onto the scalp's surface, for several minutes during one or several sessions, using two or more scalp electrodes (Woods et al., 2016a, For review). Since the early 2000s, the use of tDCS as an alternative, or complementary, treatment for different neurological, psychiatric, and cognitive disorders has increased exponentially (Lefaucheur et al., 2017) for review of neurological disease, (Ciullo et al., 2021) for review of psychiatric disease.

Despite its promising effects in humans, tDCS efficacy has long been questioned due to the lack of evidence demonstrating the current's ability to pass through the highly resistive skull and to reach deep brain tissue (Horvath et al., 2015a, 2015b; Parkin et al., 2019). Recently, human in vivo studies using low-intensity NIBS simultaneously combined with intracerebral EEG recordings (iEEG) have shown that a significant EF can reach cortical brain structures as well as deep medial brain structures (such as hippocampi, cingulate gyri, and amygdalae) (Louviot et al., 2022). Ensuring the current's propagation from scalp to cortical and deep brain structures in humans is fundamental to achieving an electrophysiological modulation of brain activity. The next critical aspect, which has yet to be investigated, concerns the ability of low-intensity currents to modulate the electrophysiological cortical activity in the human brain supporting cognitive functions.

Thus far, the precise quantification of electrophysiological modulation due to tDCS remains unexplored in humans. This lack of electrophysiological evidence supports the interpretation of tDCS effects as placebo or indirect (e.g., metabolic) effects. Objective electrophysiological quantifications of tDCS neuromodulation have never been performed previously due to methodological constraints. This is in particular due to the scarcity of access to iEEG recordings, the only reference method for direct recording of cortical brain sources with high spatial and temporal resolution. Interestingly, several previous studies combined scalp EEG recordings with tDCS during cognitive tasks, but several methodological drawbacks led to controversial results (Kho et al., 2023; Willis et al., 2019). In particular, non-physiological artifacts, different from physiological artifacts resulting from the interaction between the stimulation and the biological tissues, affect scalp EEG signals during tDCS (Gebodh et al., 2019). They induce challenging denoising processes (Faria et al., 2012b; Mancini et al., 2015) and an imprecise characterization of the electrophysiological effects (Civile, Waguri, et al., 2020b; D. W. Kim et al., 2019).

In this study, to circumvent these issues, we simultaneously combined a sham-controlled tDCS with iEEG recording during fast periodic visual stimulation (FPVS). FPVS, or 'frequency-tagging', is an objective and robust approach that generates electrophysiological responses at precise periodic frequencies with high SNR (Liu-Shuang et al., 2014b; Rossion, 2014). As the neural activity of interest can be confined to small (known) frequency bins, it is largely immune to tDCS artifacts, making this approach well-suited to perform an intracerebral evaluation for the tDCS-induced neuromodulation of the periodically evoked iEEG responses. Furthermore, noise analysis revealed that the response's amplitude remains stable and does not increase across the different stimulation phases. Moreover, the noise amplitude is weak, being two to three times lower than the signal amplitude during tDCS (**Supplementary Figure S1**). FPVS paradigms are an objective and well-validated tool to isolate an evoked brain response when recording the electrophysiological activity. In this study, FPVS was applied as an objective signature of face categorization to identify selective face categorization responses from the general visual responses. Due to the periodicity of the FPVS, both types of evoked responses (general visual and face-selective) can be quantified in the frequency domain of the iEEG recording (Rossion et al., 2015b).

iEEG recordings in drug-resistant epileptic patients were obtained through a minimally invasive and rare procedure of intracerebral implantation, which does not significantly alter the volume conduction of the head (no current leakage; (Koessler et al., 2015)). It offers the unique ability to investigate electrophysiological neuromodulation during tDCS without introducing artifacts in iEEG signals. In addition, iEEG permits to investigate deep, intermediate, and superficial cortical brain sources relevant to sampling large cognitive networks. In the present study, the VOTC was investigated as it contains a highly functional and distributed network, often explored in epileptic patients (Rossion et al., 2023).

In this study, anodal tDCS was applied using only 2 HD electrodes at + 2mA to target the right VOTC structures. Several regions, like the OFA and the FFA, located in the right VOTC, have been identified in various studies (Rossion et al., 2024; Jonas et al., 2016; Haxby et al., 2000) as the core regions in the right hemisphere are involved in the facial recognition process. The FPVS paradigm was simultaneously applied during continuous iEEG recording and tDCS stimulation in drug-resistant epileptic patients. A sham-controlled tDCS approach was applied in three phases to compare tDCS influence on the face-selective and the general visual evoked iEEG responses. A sham tDCS was delivered before (Phase 1, P1) and after (Phase 3, P3) an active 20-minute anodal tDCS phase (Phase 2, P2). Each FPVS phase contained two successive FPVS sessions (3 phases with 2 sessions each, i.e., 6 FPVS sessions), and each phase was performed before (sham; P1), during (P2), and after (sham; P3) tDCS.

II. Aims of the study

The main objectives of this study were:

(i) Quantify the intracerebral electrophysiological effects induced by anodal (+2mA) tDCS using only two HD ring electrodes, performed over the right occipito-temporal lobe, on both general visual and face-selective iEEG evoked responses, during and after stimulation.

(ii) Address tDCS' anatomical specificity by quantifying the intracerebral electrophysiological effects in the three main anatomo-functional brain regions of the VOTC and their subregions across the three experimental phases.

(iii) Expand harmonic analysis to examine tDCS neuromodulatory effects not only on the averaged harmonics but also on the individual harmonics for each intracerebral response.

(iv) Investigate inter-hemispheric differences by assessing whether a low-intensity tDCS, applied using only two HD) electrodes, is sufficient to modulate VOTC activity in the left hemisphere.

III. Materials and Methods

III.1. Participants

Eleven patients (6 females; mean age: 31 ± 8 years) with focal drug-resistant epilepsy were prospectively included in this sham-controlled tDCS study. Patients gave written consent to participate in the study, which was conducted according to the Declaration of Helsinki and approved by a local ethics committee. All patients were informed of the side effects of tDCS (tingling sensation, headache, etc.) and were instructed to report any discomfort during the experiment.

Their standard presurgical evaluation included: neuropsychological tests and long-term (5-day period) high-resolution EEG video recordings combined with electrical source imaging analysis, PET scans, and high-resolution MRI.

All participants had normal to corrected-to-normal vision and performed the Benton Face Recognition Test (Rossion & Michel, 2018) before the iEEG exploration, with an average score of 43.3 +/- 4.2 (10 patients had a Benton score above 39 of 54, reflecting normal performance in matching individual faces; only 1 patient had a score below 39 of 54, reflecting mild impairment).

To identify the epileptogenic zone and the surrounding functional brain regions, patients were implanted with intracranial multi-contact electrodes (iEEG) in the Epilepsy Unit of the University Hospital of Nancy. In all patients, SEEG allowed for the delineation of a single and spatially limited epileptogenic zone. Due to the right hemispheric dominance of face perception, participants with at least one iEEG electrode implanted in the right hemisphere were included in this study.

III.2. Transcranial electrical stimulation

tACS:

After the tDCS experiment, a session of tACS (0.5 mA, 2 minutes, 7 Hz, P10-FT9 montage) was performed to measure the EFs in the different brain regions of interest. The EF was obtained by calculating the gradient of the voltage measured on each contact of the same SEEG electrode (for detailed information about the EF calculation procedure, see(Louviot et al., 2022)).

tDCS:

Sham-controlled anodal tDCS experiments were performed before the iEEG electrode removal (i.e., on the last day of the iEEG investigation). This timing was decided to avoid tDCS after-effects during the iEEG investigation, which could influence the diagnosis (e.g., brain network instability). TDCS was performed using 2 HD-ring electrodes (12mm external diameter; Soterix Medical®, New York, NY, USA).

Both were inserted using an electrode holder (24mm diameter) filled with a conductive gel, creating a 4.52 cm2 stimulation area on the scalp for each electrode. The impedances were measured before tDCS stimulation and were always less than or equal to 5kΩ during the active stimulation.

According to the HD electrodes' geometry, the current densities generated on site were 0.44 mA.cm-2 for +2 mA intensity. The stimulation was delivered through these electrodes using a multichannel TES stimulator MxN-9 (Soterix Medical®, New York, NY, USA). To target the VOTC, the anodal electrode was placed over the P10 scalp position, and the cathodal electrode over the FT9 scalp position (Koessler et al., 2009, 20).

Two sham sessions were performed before (Phase 1, P1) and after (Phase 3, P3) tDCS in combination with fast periodic visual stimulation (FVPS) (**Figure 33**). During the sham stimulations, amplitude increased from 0 to 2 mA within the first 30 seconds, followed immediately by a decrease from 2 mA to 0 over the subsequent 30 seconds. The active anodal tDCS session (Phase 2, P2) was performed at +2mA for 20min (common tDCS parameters as outlined in (Lefaucheur et al., 2017)). Considering that it could take from five to ten minutes of tDCS to produce persistent changes inside the brain, FPVS started in phase P2 after 10 minutes of active anodal tDCS (Barbieri et al., 2016a; Lefaucheur et al., 2017). Consequently, the P2 session consisted of 10 minutes of active tDCS alone, followed by 10 minutes of concurrent tDCS and FPVS (**Figure 33**).

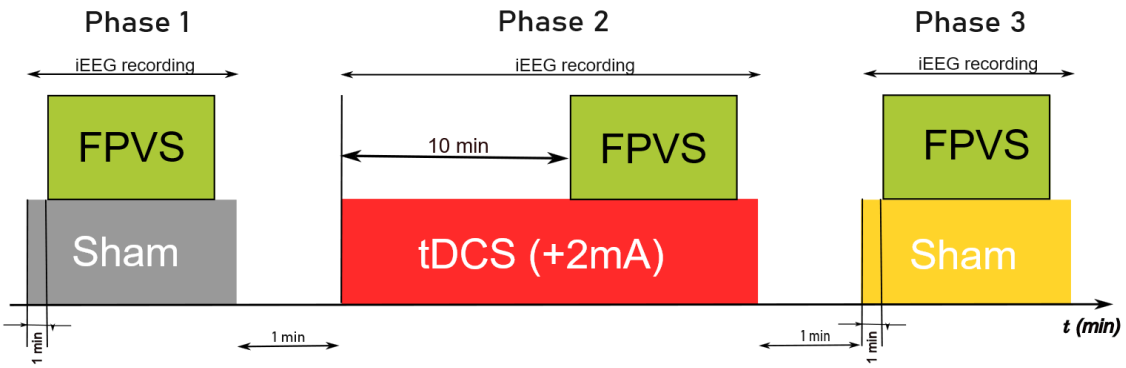

Figure 33. Design of the study protocol with tDCS, FPVS, and iEEG.
During phase 1 (P1) and phase 3 (P3), a sham-tDCS session was performed during fast periodic visual stimulation (FPVS). Between them, phase 2 (P2) was performed with 10 minutes of active +2mA tDCS alone, followed by 10 minutes of active tDCS during FPVS. IEEG recordings recorded brain activity during the three phases.

III.3. Fast Periodic Visual Stimulation

Stimuli. 200 natural images of various non-face objects from 14 non-face categories were used (cats, dogs, vegetables, horses, flowers, birds, fruits, phones...) in addition to 50 natural images of human faces. Each image showcased an unsegmented object or face near the center, varying in size, viewpoint, lighting, and background. All images were standardized for mean pixel luminance and contrast. The same stimuli were used by (Jonas et al., 2016) to find the face-selective ventral occipito-temporal map of the human brain with intracerebral potentials.

Procedure. Participants were shown continuous sequences with highly variable natural images of objects at a frequency of 6 Hz through sinusoidal contrast modulation. Highly variable natural images of faces presented periodically were presented every fifth image (i.e., at 1.2 Hz = 6/5 Hz) (**Figure 34**). Participants were unaware of the periodicity of the faces. A sequence lasted 79 s, including 75 s of stimulation (i.e., 90 images of human faces and 360 images of natural objects) at full contrast, flanked by 2 s of fade-in and 2 s of fade-out, where contrast gradually increased or decreased, respectively. This extended duration of the sequence results in a high-frequency resolution (i.e., 71 seconds so 0.0141 Hz), enabling the isolation of the specific response within a narrow frequency range, significantly improving its SNR. The FPVS paradigm was repeated two times during each phase (i.e., 2 sessions * 3 phases = 6 sessions in all). Throughout the sequences, participants were directed to maintain their gaze on a persistent small blue cross positioned at the center of the stimuli. Their task was only to identify brief color changes (from blue to red) in this central fixation cross, lasting 500ms. In the periodic condition shown here, a different face image was presented every five stimuli (i.e., appearing at the frequency of 6/5 = 1.2 Hz). This stimulation sequence recruits ventral occipito-temporal brain regions and therefore obtains iEEG general visual and face-selective evoked responses.

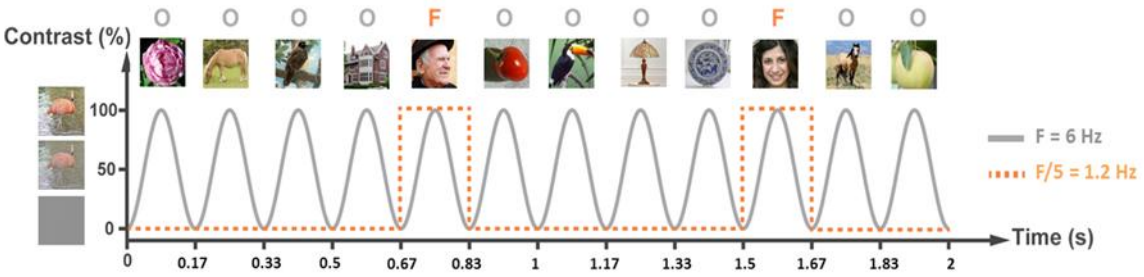

Figure 34. Fast Periodic Visual Stimulation paradigm used in this tDCS-iEEG experiment.
Images of objects were presented by sinusoidal contrast modulation at a rate of six stimuli per second (6 Hz). In the periodic condition shown here, a different face image was presented every five stimuli (i.e., appearing at the frequency of 6/5 = 1.2 Hz). This stimulation sequence recruits ventral occipito-temporal brain regions and therefore obtains iEEG general visual and face-selective evoked responses.

III.4. Intracranial EEG

Recording. For each patient, an individual stereotactic implantation plan was defined according to the presurgical evaluation and epileptogenic zone localization hypotheses. Under general anesthesia, the iEEG electrodes (0.8 mm-diameter, from 5 to 18 Platinum/Iridium contacts with 2 mm length separated by 1.5 mm insulator; Dixi Medical®, Besançon, France) were implanted according to a standard stereotactic procedure (Salado et al., 2018). The SEEG electrodes were inserted through a screw (2.45 mm in diameter) and secured with a tight seal to prevent cerebrospinal fluid leakage. Immediately after the implantation, patients underwent a postoperative CT-scan.

Using a co-registration of the CT-scan with the pre-operation high-resolution MRI (voxel-based registration; SPM 8 toolbox for Matlab; MathWorks, Natick, Massachusetts), the anatomical positions of each electrode's contacts were localized, and potential surgical complications were inspected. Due to the minimally invasive procedure used for SEEG investigation, anatomical structures were not displaced in the intracranial volume (no CSF leakage and no brain swelling), and MR-CT co-registration can be assumed very precise (<1mm). IEEG signals were recorded with a 256-channel (2x128 channels) amplifier with a 1 kHz sampling rate (LTM256, Micromed, Mogliano, Italy). The Fpz scalp electrode was set as the reference electrode for the recording, and a bipolar montage was then computed for each patient. Among 947 iEEG contacts, 67 iEEG contacts showed saturated amplitude during tDCS (Phase P2), so they were excluded from the analysis. No significant general visual or face-selective iEEG responses were found in these contacts before tDCS.

Anatomical localization. The 3D position of each iEEG contact was automatically detected in the individual CT-scan [60] and visually defined using the patient's MRI-CT co-registration. Each brain was subdivided into different brain regions of interest (ROI) using individual anatomical landmarks (i.e.,

gyri and sulci) instead of normalizing all brains, which can blur the individuality of anatomical organization. IEEG contacts were then localized according to these brain ROI and grouped by anatomical localization across all participants. The VOTC was parcellated according to the atlas of Kim et al. (J. J. Kim et al., 2000). The VOTC sulci were used as mesio-lateral landmarks (especially the collateral sulcus and occipito-temporal sulcus), and MR coronal planes gave landmarks for antero-posterior brain structures.

Spectral analysis. Data segments of iEEG signals corresponding to the FPVS sequences were selected (79-s segments, −2 to +81 s) from the recordings. In our main data analyses, we refrained from conducting artifact rejection procedures since intracerebral artifacts, primarily stemming from epileptic spikes, along with electro-oculographic and electro-myographic activities (attributable to our use of a prefrontal scalp Fpz electrode as the reference electrode for most patients), exhibit a more extensive distribution across the frequency spectrum compared to the specific frequencies of interest: 1.2 and 6 Hz, and their corresponding harmonics. The 79s data segments were cropped to contain an integer number of 1.2-Hz cycles beginning 2 s after the onset of the sequence (right at the end of the fade-in period) until ∼77 s, before stimulus fade-out (90 face cycles ∼ 75 s). Sequences were averaged in the time domain separately for each participant. A fast Fourier transform (FFT) was applied to these averaged segments, and then the amplitude spectrum was extracted for all intracerebral contacts (**Figure 36**).

Extraction of iEEG evoked responses. The FPVS sessions applied in this study allow us to identify and separate two different types of iEEG responses:

(i) ***A general visual iEEG response*** occurring at the 6 Hz base stimulation frequency and its harmonics (12Hz, 18Hz, 24Hz...),

(ii) ***A face-selective iEEG response*** at 1.2 Hz and its harmonics (2.4, 3.6 Hz, etc.). Significant face-selective responses at the face stimulation frequency (1.2 Hz) and its harmonics were detected by transforming the frequency spectra to Z scores.

To identify significant responses at the frequency of interest and its harmonics, the *Z-scores* were calculated across contacts on the FFT spectrum for each patient during the three experimental phases:

$$Z\ score = \frac{x - \mu}{\sigma}$$

The Z scores were computed as the difference between the ***x*** amplitude at each frequency bin and $\boldsymbol{\mu}$ the mean amplitude of the corresponding 48 surrounding bins (25 bins on each side of the

frequency of interest, i.e., 50 bins excluding the 2 bins directly adjacent to the bin of interest) divided by the $\boldsymbol{\sigma}$ standard deviation of amplitudes in the corresponding 48 surrounding bins.

Responses were considered significant if the Z-score > 3.1 (i.e., $p < 0.001$, one-tailed: signal > noise), indicating that the response was significantly larger than the noise estimated in the neighboring frequency bins (**Figure 36**).

Characterization of iEEG evoked responses.

Baseline-corrected amplitudes were calculated as the difference between the amplitude at each frequency bin and the mean of 48 corresponding surrounding bins (25 bins on each side of the frequency of interest, i.e., 50 bins, excluding the 2 bins directly adjacent to the bin of interest).

The general visual and the face-selective iEEG responses were then quantified at each iEEG contact as the sum of the baseline-subtracted amplitude across harmonics. Face-selective responses were quantified as the sum of the baseline-subtracted amplitudes at the face-selective frequency harmonics from the 1st until the 12th (1.2 Hz until 16.8 Hz). General visual responses were similarly quantified by summing the amplitudes from the 1st until the 5th base frequency harmonics (6 Hz until 30 Hz). Therefore, for each iEEG contact, we obtained two amplitude values that respectively represented the overall face-selective response and the overall general visual response during each of the 3 phases (before, during, and after tDCS) tested.

Finally, the Signal/noise ratio (SNR) was calculated for each contact and each response as:

$$SNR = \frac{x}{\mu}$$

SNR being the ratio between the $\boldsymbol{x}$ amplitude at the summed frequency bin divided by the $\boldsymbol{\mu}$ average of the corresponding 48 surrounding bins (25 bins on each side of the frequency of interest, i.e., 50 bins excluding the 2 bins directly adjacent to the bin of interest) (**Figure 36**).

III.5. Experimental procedure

Sham-controlled tDCS experiments were prospectively performed in eleven drug-resistant epileptic patients. The experiment contained three consecutive phases of iEEG recordings: P1 with sham tDCS during FPVS; P2 with +2mA tDCS applied over the right VOTC (P10 electrode position) for 10 minutes, followed by 10 minutes of active tDCS during FPVS (i.e., 20 minutes of tDCS in all); P3 with sham tDCS during FPVS. Active tDCS was blinded to the patients. Patients' attention before, during, and after tDCS remained optimal, showing no significant changes in either response accuracy (100% in P1, P2, P3) or response times (mean values for P1: 0.46s, P2: 0.48s, P3: 0.47s; p=0.35) (**Figure 35**).

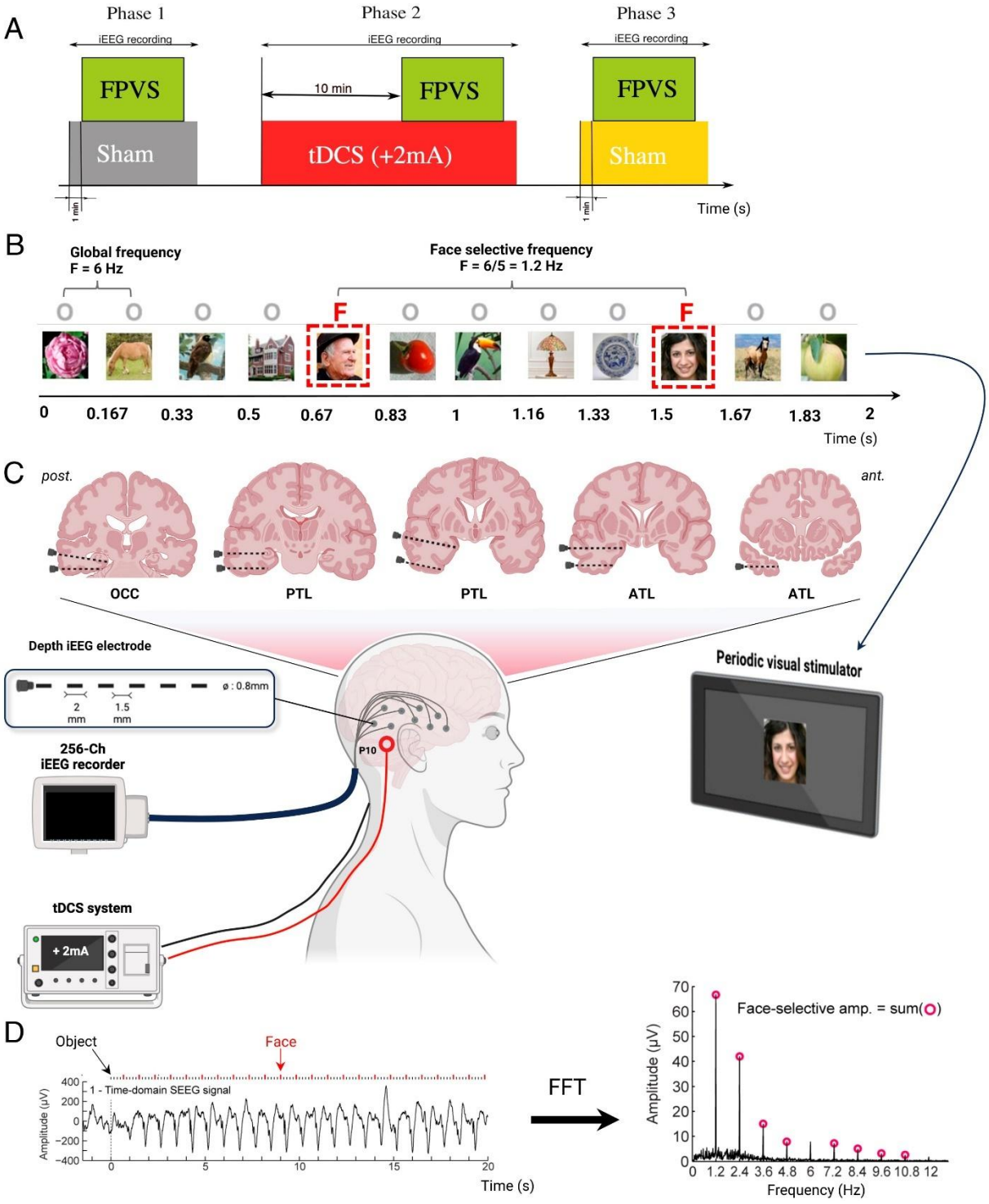

Figure 35. Overview of the combined iEEG-FPVS-tDCS protocol.
A. Timeline of the experiment with the three phases of FPVS-iEEG sessions performed before, during, and after tDCS. **B.** The FPVS paradigm. Images of objects were presented by sinusoidal contrast modulation at a rate of 6 Hz, six stimuli per second. A different face image was presented every fifth stimulus (at 6/5 = 1.2 Hz). **C.** Schematic representation of the patient's setup during the experiment. An average of eight iEEG multi-contact electrodes were implanted in the VOTC from posterior (OCC) to anterior regions (ATL). **D.** iEEG signal analysis. FFT was applied to iEEG signals in the time domain, with amplitude and SNR spectra extracted for all iEEG contacts. Here, face-selective and general visual amplitude responses (peaks) can be seen at 1.2Hz and its harmonics (red dots) and 6Hz and its harmonic (12Hz), respectively. Due to the duration of each FPVS session (71 seconds), the frequency resolution of the signal analysis is very high (i.e., 0.0141Hz).

III.6. Intracranial neuromodulation investigation

Selection of iEEG contacts. To compare the iEEG neuromodulation before, during, and after tDCS, selective iEEG contacts (i.e., contacts that recorded iEEG evoked responses for either general or face-selective responses) were selected. To do so, during the two days leading up to the tDCS experiment (D-2 and D-1), two sessions of FPVS were performed without tDCS using the same paradigm as the one used in this study. The analysis of the iEEG signals during D-2 and D-1 led to the identification of a set of iEEG contacts in the right hemisphere that exhibited statistically significant general visual and face-selective responses. Due to the robustness of the FPVS approach in this protocol (Rossion et al., 2015), this set of iEEG contacts was assigned to our study to compute the mean and standard error of the mean (SEM) of the amplitudes and the SNR during the three phases (**Figure 36**).

Neuromodulation according to the time phases. To characterize the tDCS effect over time, means and SEM baseline-corrected amplitudes and SNR of iEEG evoked responses recorded in all the contacts in the right hemisphere, and then in the VOTC, were calculated for both face-selective and general visual responses during P1, P2, and P3 phases.

Repeated measure ANOVA tests with post-hoc comparisons were performed with the null hypothesis that tDCS has no effect on the iEEG evoked responses (i.e., no baseline-corrected amplitude (or SNR) differences between the iEEG responses) for both general and face-selective responses across the different phases of the experiment (alpha risk: 0.05) (**Figure 36**).

Neuromodulation according to the anatomy. To investigate the tDCS effect on the different regions of the VTOC and therefore investigate the spatial targeting of the small ring electrodes, the VOTC was divided into three brain regions of interest (ROI) using the anatomo-functional classification from Jonas et al., 2016: ATL, anterior temporal lobe; PTL, posterior temporal lobe; OCC, occipital lobe. Means and SEM baseline-corrected amplitudes and SNR of iEEG evoked responses recorded in the contacts of the different ROI. Statistical comparisons were performed using repeated measure ANOVA tests with post-hoc comparisons with the null hypothesis that intracranial neuromodulation will be the same in all ROI (**Figure 36**).

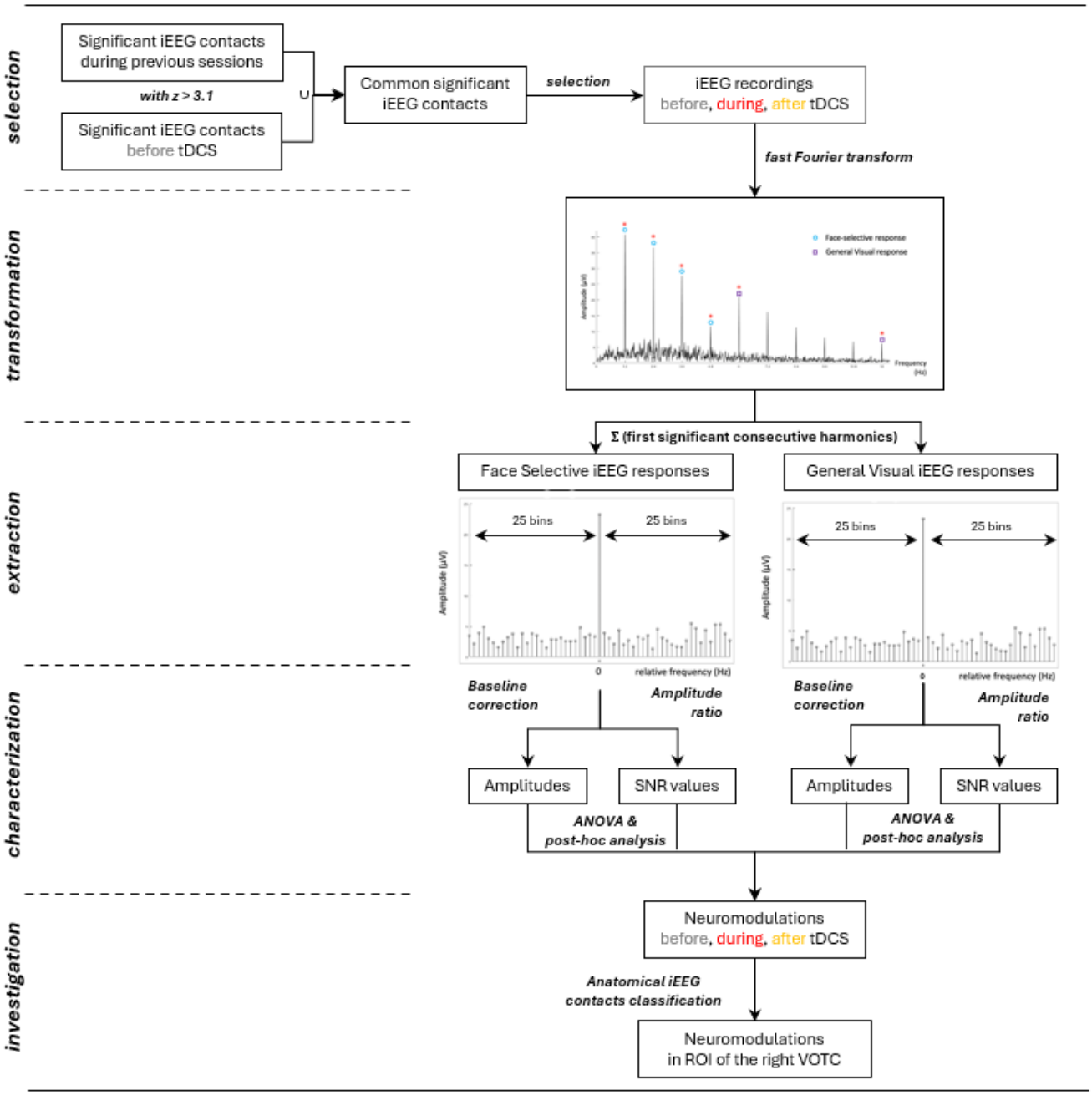

Figure 36. Overview of the iEEG data analysis.
Raw iEEG signals were analyzed in the frequency domain after FFT. A baseline correction was applied to extract the iEEG response amplitudes. Signal-to-noise ratio was also estimated. Then, ANOVA tests with post-hoc comparisons were used to compare the results before, during, and after the tDCS and across the different regions of interest.

IV. Results

IV.1. Effects of Right-Hemispheric tDCS on Ipsilateral Cortical Excitability

In our population, a total of 90 intracranial electrodes were implanted in the right hemisphere, each electrode containing 5-18 contacts for independent recording of the local field potential (947 contacts in total). Then, iEEG contacts within the right hemisphere, where face-selectivity is predominant (Jonas et al., 2016; Puce et al., 1995) were investigated. All iEEG contacts selected in this study recorded significant iEEG evoked responses during previous FPVS sessions (using the same cognitive paradigm, i.e., objects and faces) performed during the week of patients' iEEG investigation.

IV.1.1 tDCS significantly neuromodulates face-selective and general visual responses

Among 453 iEEG contacts in the right hemisphere (**Figure 37A**), 260 and 302 iEEG contacts that showed significant face-selective and general visual iEEG responses were used to compute the means and the SEM of these two types of neural responses, respectively (**Figures 37.B** and **37.C**).

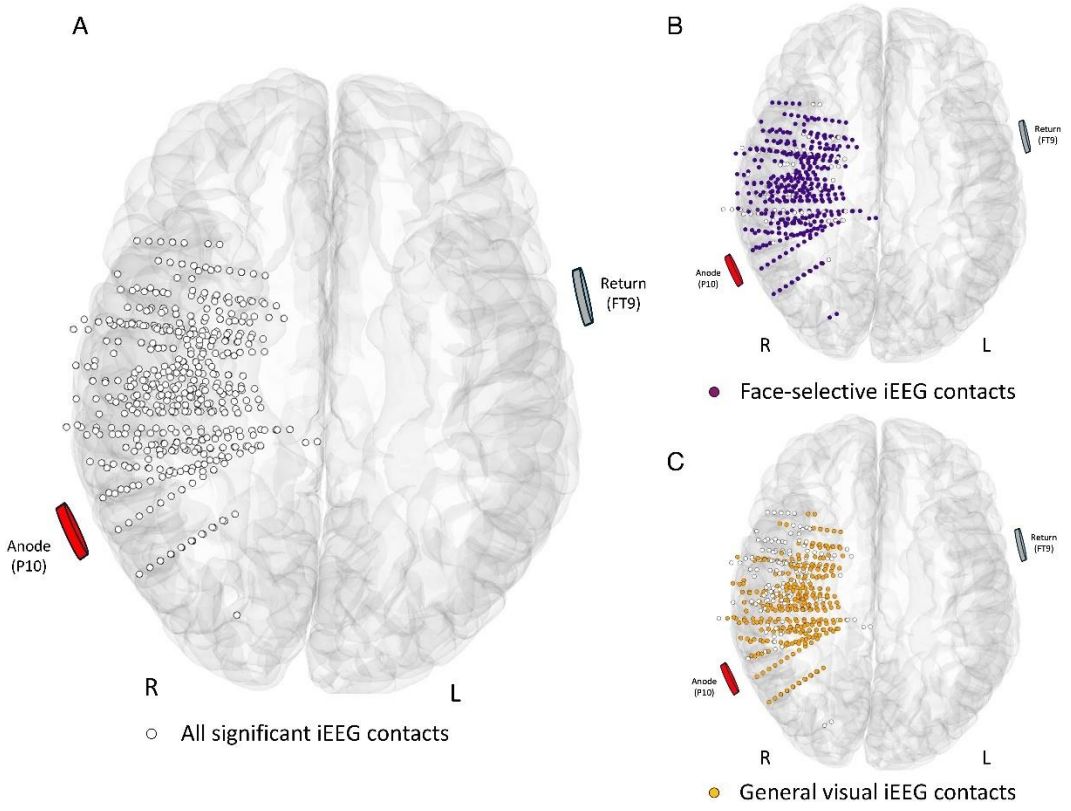

Figure 37. Spatial distribution of the iEEG contacts and the HD-ring tDCS electrodes in MNI space.
A. Maps of all significant iEEG recording contacts (n=452) in the right hemisphere across 11 individual brains are displayed in the MNI space using a transparent reconstructed cortical surface of the Colin27 brain (ventral view). Each circle represents a single iEEG contact. For visualization purposes, individual contacts are displayed larger

than their actual size (2 mm in length). **B.** and **C.** The same display for the iEEG contacts showing face-selective (n=302; violet circles) and general visual (n=260; orange circles) responses, respectively.

For general visual responses, the averaged baseline-corrected amplitudes and SEM recorded in the right hemisphere during the three phases, P1, P2, and P3, were 4.04±0.40, 4.10±0.41, and 4.26± 0.42 µV (i.e., +5.4% with respect to P1), respectively. A significant baseline-corrected amplitude difference was found between the P3 and P1($p<0.01$, Repeated measures ANOVA) (**Figure 38**). The SNR values were 3.62, 3.55, and 3.69 during P1, P2, and P3, respectively (**Supplementary figure S2**).

For face-selective responses, the average baseline-corrected amplitudes recorded in the right hemisphere during the three phases (before, during, and after tDCS) were 10.56±1.27, 13.05±1.41 (i.e., +23.6% with respect to P1), and 13.18± 1.42 µV (i.e., +24.8% with respect to P1), respectively. A significant difference was found between P2 and P1 ($p<0.001$) and between P3 and P1 ($p<0.001$, Repeated measures ANOVA) (**Figure 38**). The SNR values were 2.46, 2.50, and 2.60 during P1, P2, and P3, respectively (**Supplementary figure S2**).

Then, a more restrained iEEG analysis was performed using only the iEEG contacts located in the right VOTC.

For general visual responses, the average baseline-corrected amplitudes recorded in the right VOTC from 147 contacts during phases P1, P2, and P3 were 6.20±0.64, 6.22±0.65, and 6.56±0.67 µV (i.e., +5.8% with respect to P1), respectively. A significant baseline-corrected amplitude difference was found between the P3 and P1 ($p<0.01$, Repeated measures ANOVA) (**Figure 38**). The SNR values during the three phases were 4.57, 4.35, and 4.61, respectively.

For face-selective visual responses, the average baseline-corrected amplitudes recorded in the right VOTC from 181 contacts during phases P1, P2, and P3 were 14.58±1.93, 18.08±2.11 (i.e., +24% with respect to P1), and 18.26±2.14 µV (i.e., +25.2% with respect to P1), respectively. A significant baseline-corrected amplitude difference was found between P2 and P1 ($p=0.002$) and between P3 and P1 ($p=0.003$, Repeated measures ANOVA). The values of the SNR during the 3 respective phases were 2.83, 2.87, and 2.97, respectively (**Figures 38 and supplementary figure S2**).

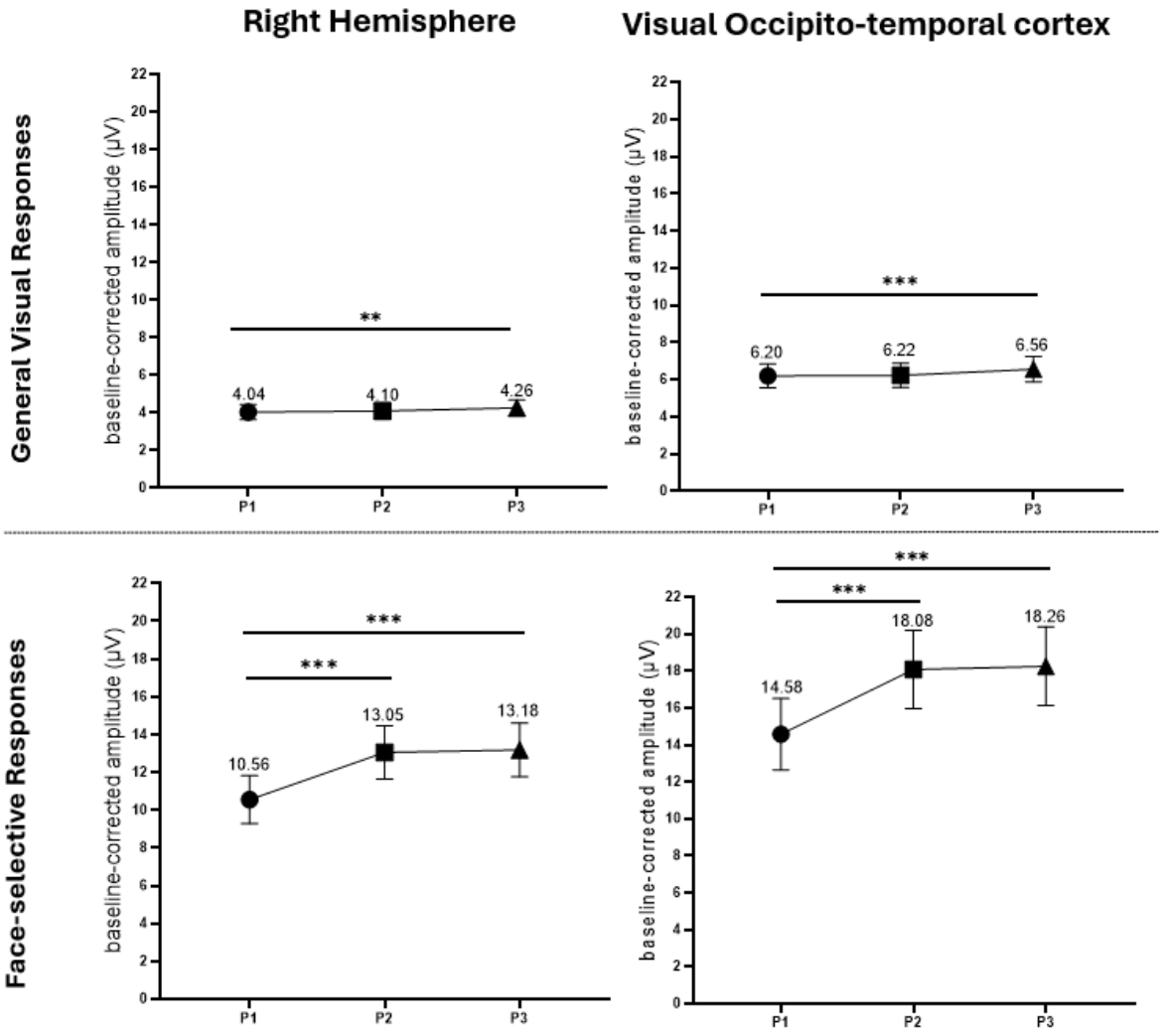

Figure 38. Neuromodulation of iEEG general visual and face-selective responses across the three phases of the tDCS experiment in the right hemisphere and in the right VOTC.
Averaged baseline-corrected amplitudes and standard errors of the mean of the iEEG evoked responses were computed during the three different phases for the eleven patients. In the right hemisphere, 260 and 302 iEEG contacts were used to compute the average baseline-corrected amplitudes, whereas 147 and 181 contacts were selected in the right VOTC for the general visual responses and the face-selective responses, respectively. Face-selective responses were significantly neuromodulated during (P2) and after (P3) tDCS ($p<0.001$) in the right hemisphere as well as in the right VOCT. General visual responses were only significantly neuromodulated after (P3) tDCS in the right hemisphere ($p<0.01$) and in the right VOCT($p<0.001$). Graphs for SNR analysis are presented in supplementary figure **S2**. Phases: ● P1(sham, before tDCS), ■ P2(active, during tDCS), and ▲ P3 (sham, after tDCS).

IV.1.2 HD electrodes targeted regions of the VOTC

To investigate the spatial targeting of tDCS, 328 iEEG contacts in the VOTC for both iEEG responses were classified into three main brain regions of interest (ROI): the anterior temporal lobe (ATL), the posterior temporal lobe (PTL), and the occipital lobe (OCC) (**Figure 39.A**). This anatomical classification was previously defined in an iEEG study exploring the face-selective brain regions in the VOTC (Jonas et al., 2016). The baseline-corrected amplitudes and SNR of the evoked general visual and

face-selective iEEG responses located in the three main ROI of the VOTC were computed in each of the three phases of this study.

For general visual responses, the baseline-corrected amplitudes for the iEEG contacts located in the ATL (n=91) were 3.68±0.47, 3.65±0.43 and 3.83±0.44 µV during the three phases P1, P2 and P3, respectively. In the PTL (n=40), the values were 9.12±1.38, 9.60±1.45 and 9.22±1.39 µV, during the three phases P1, P2 and P3, respectively. Finally, the highest iEEG evoked responses were found in the OCC (n=16) with 13 ±3.14, 13.61±3.45 and 14.48±3.53 µV (i.e., +11.4% with respect to P1) during the P1, P2 and P3, respectively. In the OCC, a significant change was found from P1 and P3, i.e., after the tDCS ($p<0.05$) (**Figure 39.B**). The mean SNR values of the general visual responses were 3.37, 3.25, and 3.35 in the ATL, 5.62, 5.12, and 5.59 in the PTL, and 8.78, 8.72, and 9.32 in the OCC for phases P1, P2, and P3, respectively (**supplementary Figure S3**).

For face-selective responses, the baseline-corrected amplitudes for the iEEG contacts located in the ATL (n=114) were 8.82±1.48, 11.15±1.41 (i.e., +26.4% with respect to P1) and 11.40±1.42 µV (i.e., +29.2% with respect to P1), during the three phases P1, P2 and P3, respectively. In the PTL (n=51), the baseline corrected amplitudes were 25.52±5.45, 29.68±.81 (i.e., +16.3% with respect to P1) and 29.75±5.95 µV (i.e., +16.6% with respect to P1) during the three phases, respectively. In the OCC (n=16), the baseline corrected amplitudes were 20.74±5.41, 30.52±8.91 (i.e., +47.1 % with respect to P1), and 30.49±8.72 µV (i.e., +47% with respect to P1) during the three phases, respectively. The amplitudes of the face-selective responses in the three ROI significantly varied from P1 to P2, i.e., during tDCS (ATL: $p=0.032$, PTL: $p<0.001$, OCC: $p=0.024$), as well as from P1 to P3, i.e., after tDCS (ATL: $p=0.014$, PTL: $p<0.001$, OCC: $p=0.025$) (**Figure 39.B**). The mean SNR values of the face-selective responses were 2.49,2.46, and 2.50 in the ATL, 3.22, 3.37, and 3.22 in the PTL, and 3.96, 4.66, and 5.02 in the OCC, during the 3 phases, respectively (**Supplementary Figure S3**).

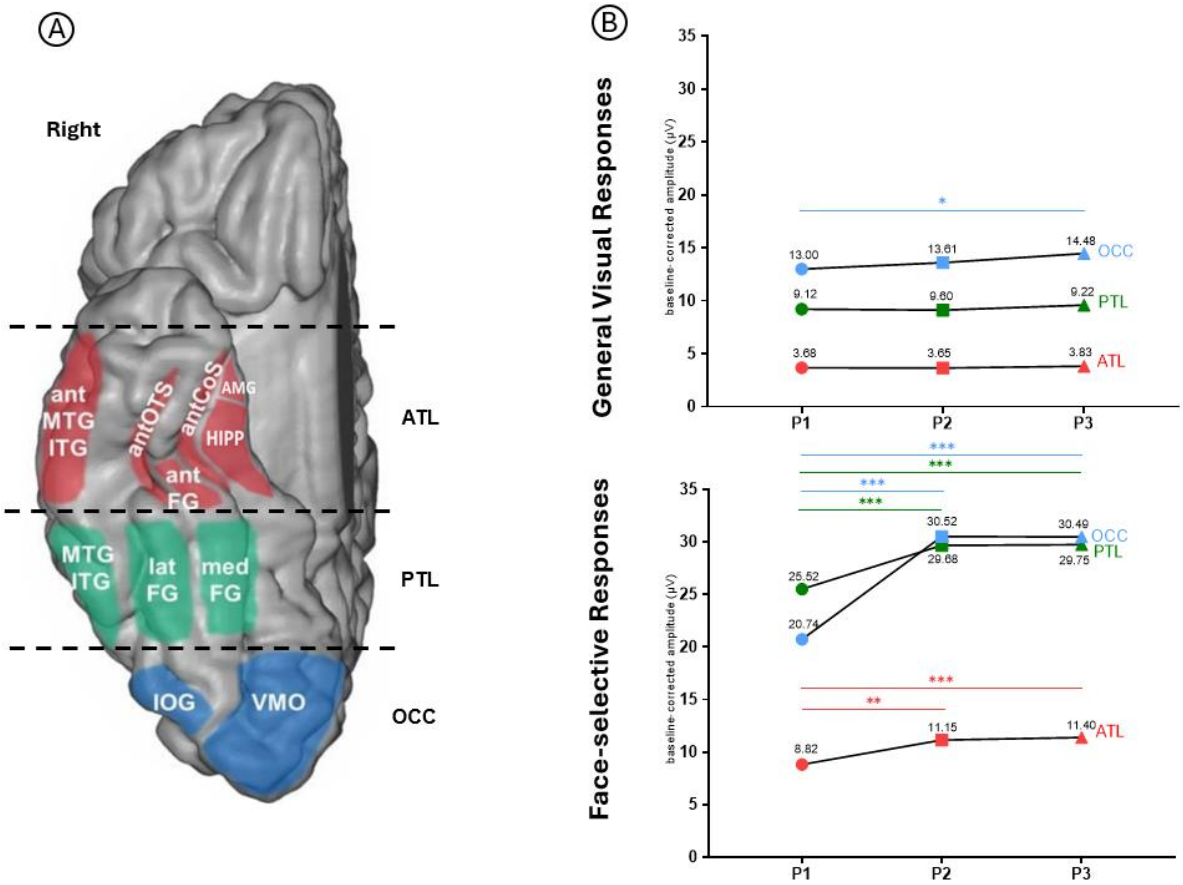

Figure 39. Neuromodulation of iEEG general visual and face-selective responses in the right VOTC.
A. Schematic anatomical view of each brain region of interest in the right VOTC. Brain regions are depicted over the right ventral surface of the Colin27 brain, although the iEEG responses were recorded by intracerebral contacts inside these regions. Three main regions (ATL in red, PTL in green, and OCC in blue) were defined to compare the spatial neuromodulation**. B.** Baseline corrected amplitudes (mean; µV) of the general visual and the face-selective iEEG responses in the three ROIs during the three phases. A significant difference in the baseline-corrected amplitudes of the general visual response was observed in the OCC after the tDCS (P3) in comparison to before tDCS (P1) (p=0.041). For the face-selective response, a significant difference in the baseline-corrected amplitudes was observed for the three brain regions during tDCS (P2) (ATL: p=0.032, PTL: p<0.001, OCC: p=0.024) and maintained after tDCS (P3) in comparison to before tDCS (P1) (ATL: p=0.014, PTL: p<0.001, OCC: p=0.025, repeated measure ANOVA).VOTC: ventral occipito-temporal cortex, ATL: Anterior Temporal Lobe, PTL: Posterior Temporal Lobe, OCC: Occipital Lobe. ● P1(sham, before tDCS), ■ P2(active, during tDCS), and ▲ P3 (sham, after tDCS).

IV.1.3 HD electrodes spatially targeted medial and Lateral FG in VOTC

Given the significant changes in the general visual response in the OCC and in the face-selective response in all three regions of the VOTC, during and after tDCS (i.e., P2 and P3), we examined the neuromodulatory effects during (P2) and after tDCS (P3) in comparison to before (P1) in the ten sub-regions that compose the ATL, PTL, and OCC (**Figure 40**).

The iEEG contacts in the VOTC were classified into ten distinct sub-brain regions of interest (see **Figure 39A**), as defined in a prior iEEG mapping of the face-selective regions according to (Jonas et al., 2016) :

(i) ATL is composed of the anterior collateral sulcus (antCoS), the anterior occipito-temporal sulcus (antOTS), the anterior middle temporal gyrus (antMTG), the anterior fusiform gyrus (antFG), and the Temporal pole (TP),

(ii) PTL is composed of the posterior middle temporal gyrus (MTG), the lateral fusiform gyrus (latFG), and the medial fusiform gyrus (medFG)

(iii) OCC is composed of the ventromedial occipital cortex (VMO) and the inferior occipital gyrus (IOG).

Table 2. Number of contacts implanted in each of the ten face-selective regions for both responses.

Face-selective Regions	antCoS	antOTS	antMTG	antFG	TP	medFG	latFG	MTG	VMO	IOG
# of contacts for Face-selective response	32	34	24	13	9	19	19	13	5	11
# of contacts for General visual response	32	30	10	13	4	20	14	6	5	11

Across the ten ROIs that were individually analyzed, the largest iEEG responses for P1, P2, and P3 were found in the VMO for the general visual responses and in the latFG for the face-selective responses (**Figure 40**). The mean baseline-corrected amplitudes and SEM during P1 , P2 and P3 for VMO (n=13) were 20.17 $\pm$ 8.19 µV, 22.20 $\pm$ 9.15µV, and 22.85 $\pm$ 9.9.29 µV, respectively, and for latFG (n=19) were 46.02 $\pm$ 12.82 µV, 48.83 $\pm$ 13.13 µV, and 50.74 $\pm$ 13.54 µV respectively. All results concerning the SNR differences in the various ROI are reported in **supplementary figure S4**.

Interestingly, the most significant neuromodulation between P1 and P2 was found in the medFG for both general visual and face-selective iEEG responses (p=0.009 and 0.01, respectively). It's

important to note that these neuromodulations corresponded to an increase in the medFG for face-selective responses (from 19.66 to 27.30 μV), whereas for general visual responses, it corresponded to a decrease in the medFG (from 13.16 to 12.40 μV). However, the significance found in the medFG was not maintained after tDCS (P3), for neither the general visual response (12.81 μV) nor the face-selective response (dropped to 25.66 μV).

The LatFG also presented a significant neuromodulation during tDCS, i.e., between P2 and P1 (p= 0.02), as well as after tDCS, i.e., between P1 and P3 (p= 0.01) for the general visual responses. Interestingly, for the face-selective iEEG responses, the LFG presented a trend towards a significant neuromodulation between P2 and P1, i.e., during tDCS, but didn't reach significance. Although after tDCS, i.e., between P1 and P3, the neuromodulation was significantly changed (p=0.041).

Additionally, the antOTS presented a significant neuromodulation between P1 and P3, after tDCS, only for the general visual response (p=0.019). In contrast, the antFG exhibited a trend toward significance in face-selective responses, with neuromodulation observed both during (P1 vs. P2, p = 0.058) and after (P1 vs. P3, p = 0.058) tDCS.

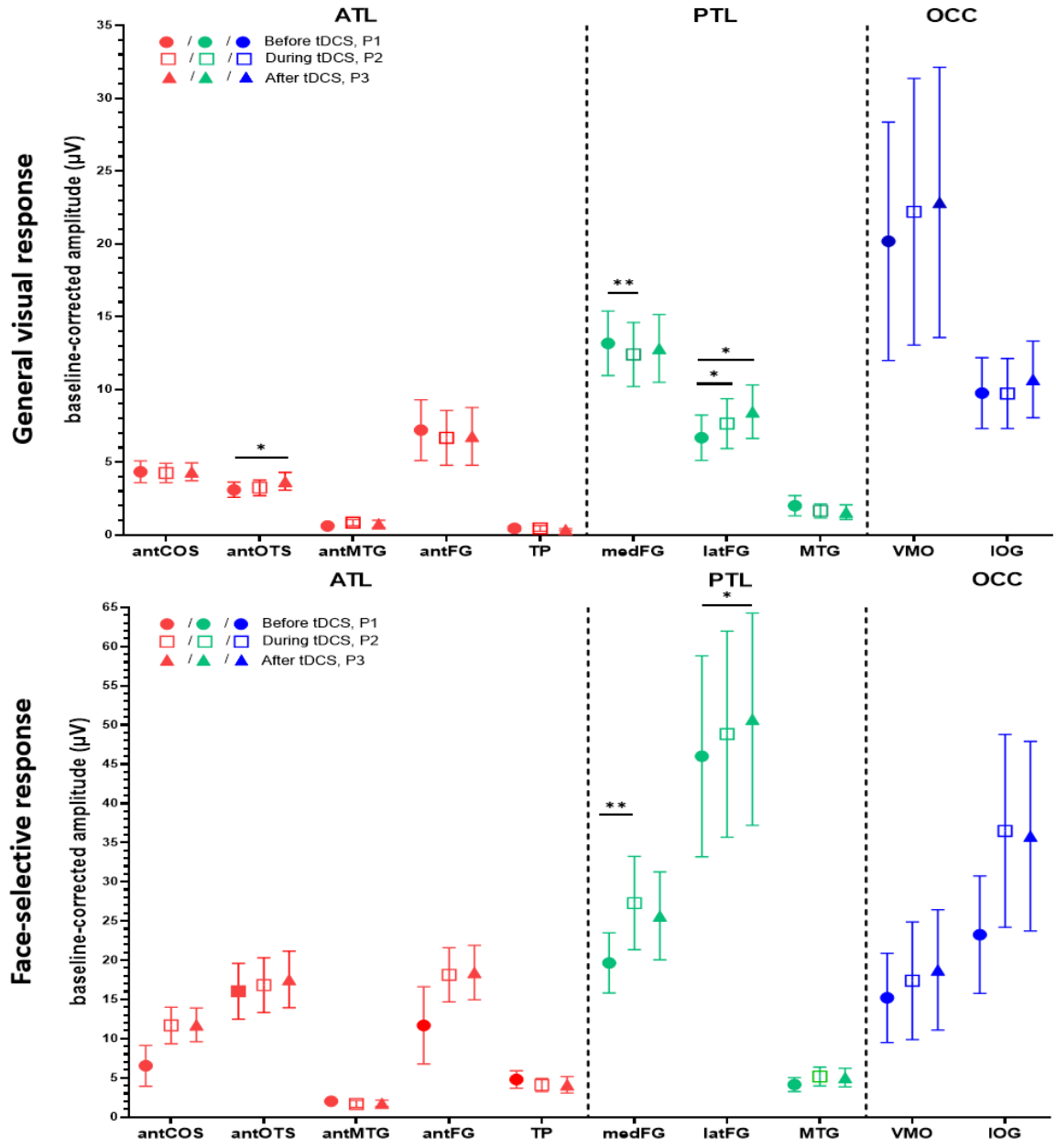

Figure 40. Neuromodulation of iEEG general visual and face-selective responses across the three phases of the tDCS experiment in the ten face-selective regions of the right VOTC.

Averaged baseline-corrected amplitudes and SEM of the iEEG evoked responses were computed during the three different phases (P1, P2, P3) for the contacts in the different regions of the ATL, PTL, and OCC. A significant neuromodulation was observed in the medFG for both the general visual (p=0.009) and face-selective (p=0.012) responses during tDCS (P2) in comparison to before(P1). Notably, these differences exhibited opposite modulation patterns between the two responses, with an increase observed for face-selective responses and a decrease for general visual responses in the MFG. The LFG presented a significant neuromodulation during tDCS (p=0.02), which persisted after the stimulation (p=0.013) for the general visual response. In contrast, for the face-selective response, the LFG showed a trend toward a significant neuromodulation during tDCS (p=0.058), which reached statistical significance after stimulation (p=0.041). The graph for SNR analysis is presented in supplementary figure S4.ATL: Anterior Temporal Lobe, PTL: Posterior Temporal Lobe, OCC: Occipital Lobe, AMG: amygdala, HIPP: hippocampus, antCoS: anterior collateral sulcus, antFG: anterior fusiform gyrus, antOTS: anterior occipito-temporal sulcus, antMTG: anterior middle temporal gyrus, medFG: medial fusiform gyrus, latFG: lateral fusiform gyrus, MTG: middle temporal gyrus, VMO: ventromedial occipital cortex, and IOG: inferior occipital gyrus.

IV.1.4 Electric Field Investigation in the Different Brain Structures

Following the significant neuromodulation of both iEEG evoked responses during and after tDCS, the EF induced by a tACS was investigated for the implanted iEEG contacts in the three regions of interest from the shallowest to the deepest (**Table 3**).

The average EF values were 0.29±0.36 V/m, 0.17±0.11 V/m, and 0.22±0.24 V/m in OCC, PTL, and ATL, respectively. Notably, the IOG in the OCC and the antMTG in the ATL presented the highest EF value among all the regions of the VOTC, of 0.38 V/m and 0.40 V/m, respectively.

As expected, the deepest regions presented the lowest EF values in comparison to the shallowest regions. Specifically, the antFG, the medFG, and the VMO presented EF values of 0.15 V/m, 0.14 V/m, and 0.14 V/m, respectively. In contrast, the more superficial regions, the antMTG, the MTG, and the IOG, which are closer to the stimulating electrode, displayed comparatively higher EF values of 0.40 V/m, 0.23 V/m, and 0.38V/m, respectively.

Table 3 Electric field values in each region of interest:

	ATL	Mean EF values (V/m)	N contacts
shallowest	antMTG	0.40	23
↓	antOTS	0.17	36
	antCOS	0.18	33
deepest	antFG	0.15	13

	PTL	Mean EF values (V/m)	N contacts
shallowest	MTG/ITG	0.23	16
↓	latFG	0.17	16
deepest	medFG	0.14	21

	OCC	Mean EF values (V/m)	N contacts
shallowest	IOG	0.38	11
deepest	VMO	0.14	6

IV.1.5 Frequency Dependent Influence of tDCS on Individual Harmonics

Thus far, we've reported the neuromodulatory changes during and after tDCS based on the mean baseline-corrected amplitudes and SEM of the summed first twelve consecutive significant harmonics of the face-selective responses during the three different phases (P1, P2, P3) (see section III, Characterization of iEEG evoked responses). To further examine the effects of tDCS on the harmonics level, we analyzed the baseline-corrected amplitudes of each of the twelve individual face-selective harmonics, ranging from 1.2Hz to 16.80 Hz, across the three phases in all 302 contacts (**Figure 41**).

For each face-selective harmonic, baseline-corrected amplitudes were averaged across all 302 contacts in the right hemisphere from the eleven tested patients. Nearly all twelve harmonics showed a significant neuromodulation of the averaged baseline-corrected amplitudes during (P2) or/and after tDCS (P3) in comparison to before tDCS (P1) (**Figure 41**).

Notably, seven harmonics (2.4Hz, 3.6Hz, 4.8Hz, 8.4Hz, 9.6Hz, 10.8Hz, 16.80Hz) out of the twelve (i.e., 58%) followed the same pattern of significant changes observed in the averaged harmonics across all 302 contacts in the right hemisphere and the right VOTC (as shown in **Figure 38**). These harmonics showed a significant neuromodulation during (between P1 and P2) as well as after tDCS (between P1 and P3) (**Figure 41**).

Interestingly, certain harmonics exhibited phase-specific effects. For instance, the 1.2Hz and 13.2Hz harmonics presented a significant neuromodulation of the baseline-corrected amplitudes during tDCS (between P2 and P1), while the other 14.40 Hz and 15.60 Hz showed significant change only after tDCS (between P3 and P1). In contrast, no significant modulation was observed for the 7.2 Hz harmonic across phases, with the baseline-corrected amplitude decreasing from 0.60 μV in P1 to 0.55 μV in P2 during tDCS.

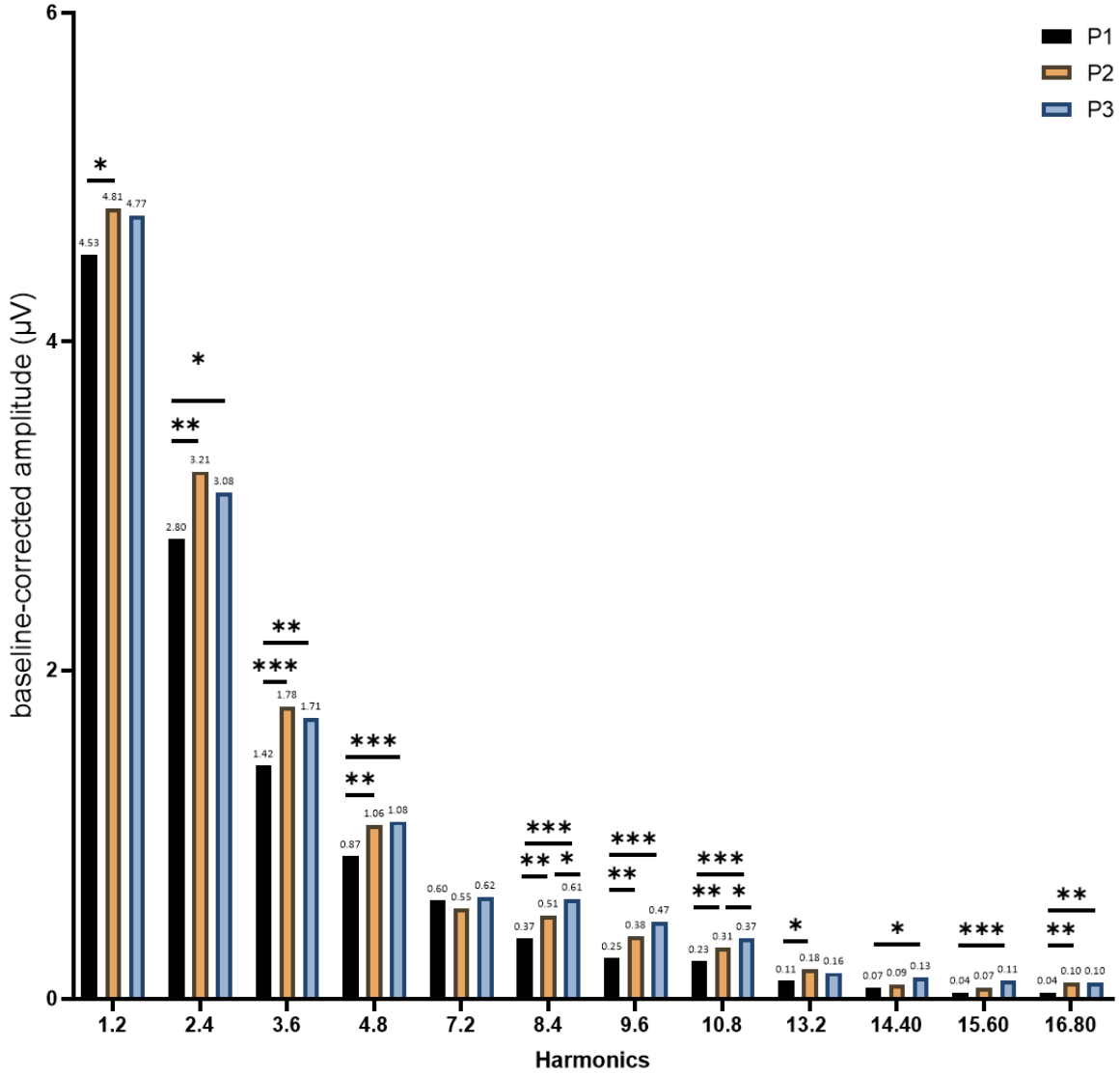

Figure 41. Detailed neuromodulation across the first twelve consecutive significant face-selective harmonics during the three tDCS experiment phases in the right hemisphere.
Averaged baseline-corrected amplitudes and SEM of the 302 iEEG contacts in each individual harmonic (from 1.2 Hz to 16.8 Hz) of the face-selective response were computed during the three phases (P1, P2, P3) for the eleven patients. Almost all face-selective harmonics presented a significant neuromodulation of their baseline-corrected amplitudes during tDCS (P2) (except for 7.2 Hz, 14.40Hz, and 15.60Hz) and after (P3) tDCS (except for 1.2 Hz, 7.2 Hz, 9.6 Hz, and 13.2Hz). P1, before; black; P2, during: yellow; P3, after: blue. Asterisks indicate statistical significance: $p < 0.05$, $p < 0.01$, and $p < 0.001$.

Furthermore, the effect of tDCS on the individual five harmonics of the general visual response, ranging from 6 Hz to 30 Hz, has also been investigated across the three phases in all 260 contacts.

All five general visual harmonics showed significant neuromodulation of the averaged baseline-corrected amplitudes after tDCS (between P1 and P3) (**Figure 42**). Interestingly, during tDCS (between P1 and P2), this effect was observed for all harmonics except the first 6 Hz harmonic, where the baseline-corrected amplitudes during tDCS decreased (from 2.75 µV in P1 to 2.57 µV in P2). This pattern was consistent with the significant changes observed in the averaged harmonics across all 260 contacts in the right hemisphere and the right VOTC (**Figure 42**).

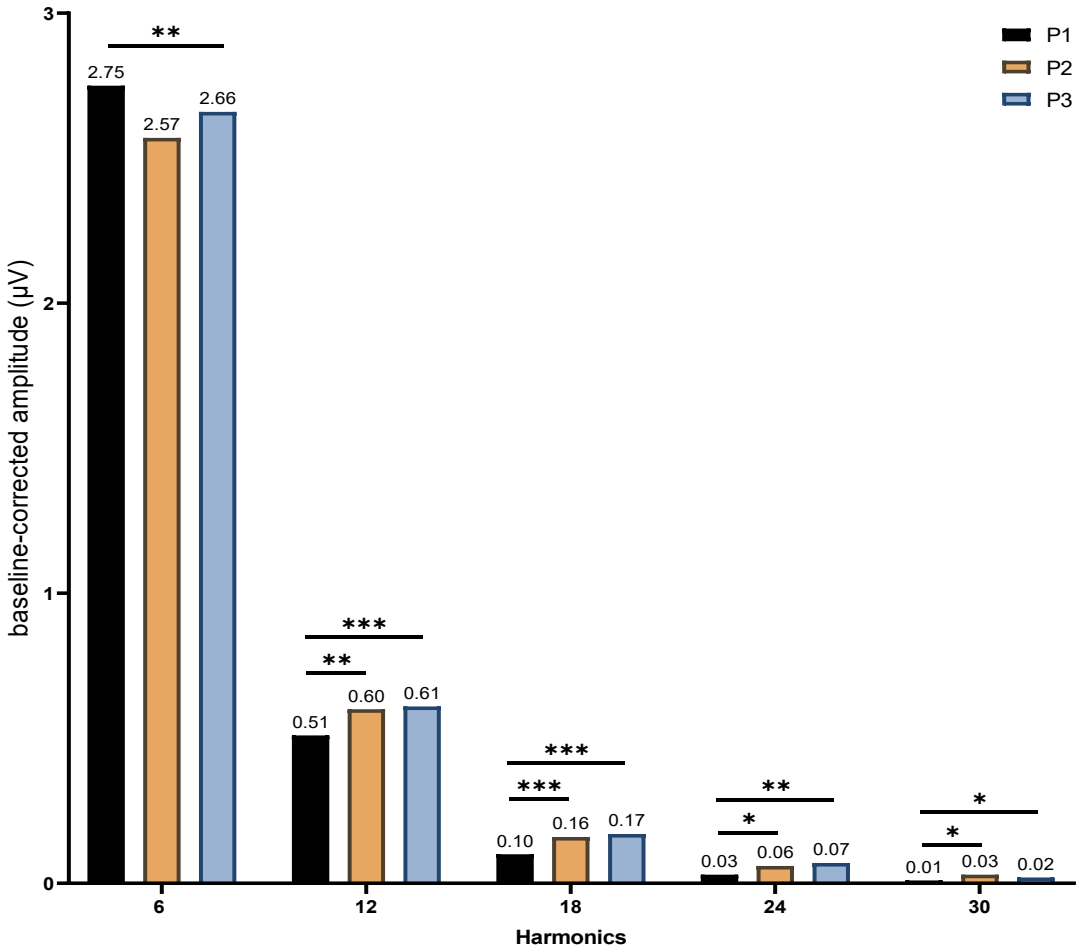

Figure 42. Detailed neuromodulation across the first five consecutive significant general visual responses harmonics during the three tDCS experiment phases in the right hemisphere.
Averaged baseline-corrected amplitudes and SEM of the 260 iEEG contacts in each individual harmonic (from 6 Hz to 30 Hz) of the general visual response were computed during the three different phases for the eleven patients. Baseline-corrected amplitudes of the general visual responses were significantly neuromodulated during tDCS (P2), except for 6 Hz, and after (P3) tDCS across all harmonics. P1, before; black; P2, during: yellow; P3, after: blue. Asterisks indicate statistical significance: $p < 0.05$, $p < 0.01$, and $p < 0.001$.

IV.2. Effects of Right-Hemispheric tDCS on Contralateral Cortical Excitability

Among 249 iEEG contacts in the left hemisphere, 183 and 195 iEEG contacts that showed significant general visual and face-selective iEEG responses were used to compute the means and the SEM of the two types of responses, respectively.

For general visual responses, the averaged baseline-corrected amplitudes and SEM recorded in the left hemisphere during the three phases P1, P2, and P3 (before, during, and after tDCS) were 4.34±7.43, 4.22±7.68, and 4.39± 7.69 µV, respectively. No significant baseline-corrected amplitude difference was found between the different phases (**Figure 43**). The SNR values were 3.86±3.22,

3.51±2.96 (i.e., -35%), and 3.82±3.36 during P1, P2 and P3, respectively. A significant difference in the SNR was found between P2 and P1 ($p<0.05$) (**Supplementary Figure S5**).

For face-selective responses, the average baseline-corrected amplitudes recorded in the left hemisphere during the three phases were 7.13±11.99, 7.84±12.53, and 7.25± 11.69 μV, respectively. No significant difference was found between the different phases (**Figure 43**). The SNR values were 2.04±1.11, 1.96±1.14 (i.e., -8%, P2 in respect to P1), and 1.2±1.16 during P1, P2 and P3, respectively. A significant difference in the SNR was found between P2 and P1 ($p<0.001$) (**Supplementary Figure S5**).

In the left VOTC, tDCS neuromodulated the iEEG responses:

For general visual responses, the average baseline-corrected amplitudes recorded in the left VOTC from 147 contacts during phases P1, P2, and P3 were 6.34±8.82, 6.24±0.64, and 6.52±9.10 μV, respectively. No significant baseline-corrected amplitude difference was observed between the different phases. The SNR values during the three phases were 4.65±3.67, 4.20± 3.39 (i.e., -45%, P2 in respect to P1), and 4.63±3.85, respectively (**Figure 43**). A significant difference in the SNR was found between P2 and P1 ($p<0.001$) (**Supplementary Figure S5**).

For face-selective visual responses, the average baseline-corrected amplitudes recorded in the left VOTC from 181 contacts during phases P1, P2, and P3 were 9.03±12.66, 9.88±12.81, and 9.46±12.37 μV, respectively. No significant baseline-corrected amplitude difference was found between P2 and P1 and between P3 and P1. (**Figure 43**). The values of the SNR during the 3 respective phases were 2.26± 1.14, 2.16±1.18 (i.e., -29%, P2 in respect to P1), and 2.20±1.2, respectively (**Supplementary Figure S5**). A significant difference in the SNR was found between P2 and P1 ($p<0.001$).

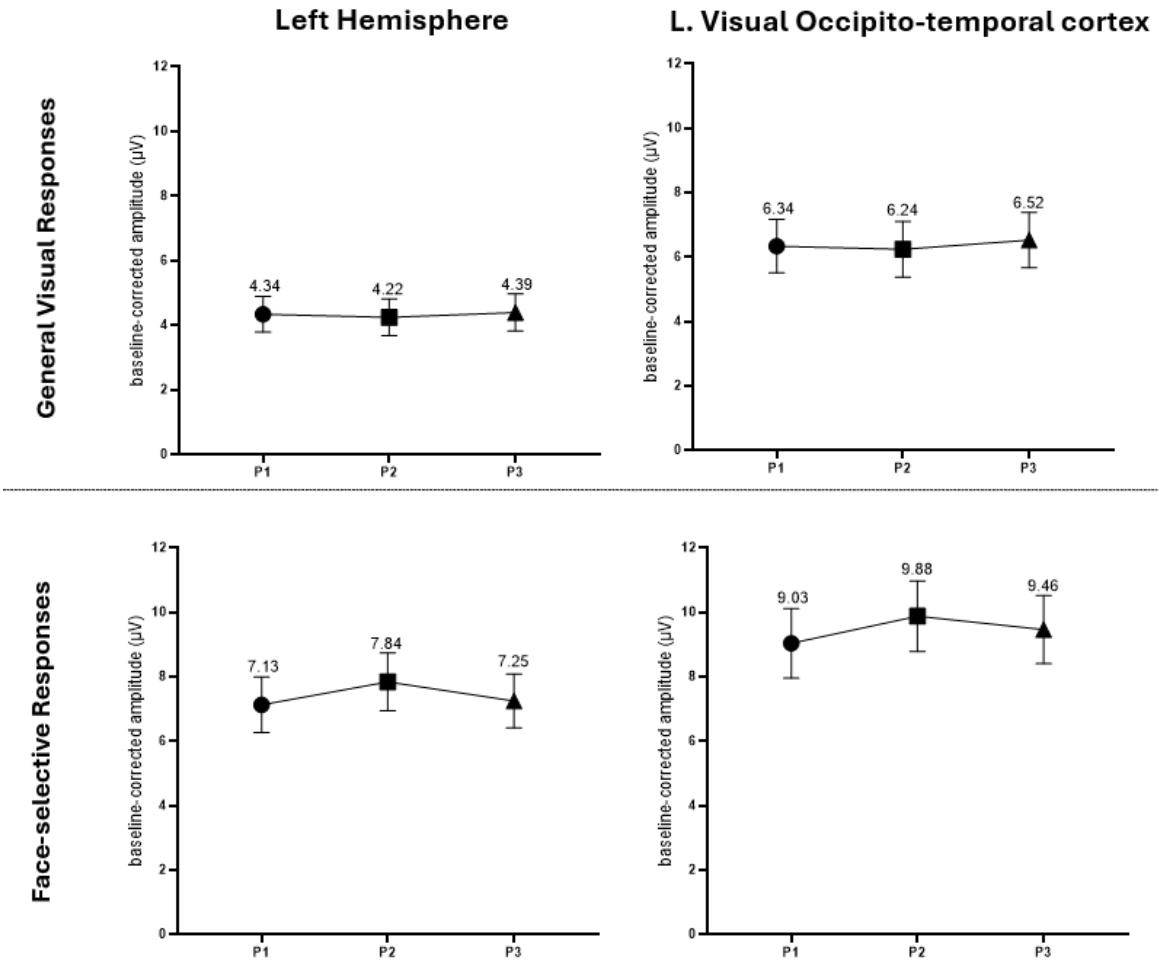

Figure 43. Neuromodulation of iEEG general visual and face-selective responses across the three phases of the tDCS experiment in the left hemisphere and in the left VOTC.

Averaged baseline-corrected amplitudes and SEM of the iEEG evoked responses were computed during the three different phases for the eleven patients. In the left hemisphere, 183 and 195 iEEG contacts were used to compute the average baseline-corrected amplitudes, whereas 113 and 137 contacts were selected for the general visual responses and the face-selective responses, respectively. The average amplitude during stimulation increased, but didn't reach significance for Face-selective responses. No significant neuromodulation was observed for the general visual responses. Graphs for SNR analysis are presented in supplementary figure S5. Phases: ● P1(sham, before tDCS), ■ P2(active, during tDCS), and ▲ P3 (sham, after tDCS).

V. Discussion

V.1. Significant neuromodulation using low-intensity, -duration and -resolution tDCS configuration.

Quantifying the intracerebral neuromodulation induced by NIBS in humans *in vivo* has not been performed before due to methodological and clinical constraints. Here, we overcame these constraints with a simultaneous combination of tDCS with iEEG and FPVS. FVPS and iEEG were used as reference methods since they allow objective measurement of (frequency-tagged) brain activity directly within different brain sources organized in a sparse cognitive network and away from the stimulating scalp electrodes that generate electrical artefacts. In addition, implementing a sham-controlled experiment with iEEG recordings reduced placebo effects and allowed for a thorough investigation of the different tDCS phases (before, during, and after tDCS). The observed intracerebral neuromodulation was obtained in patients with preserved face perception abilities (Volfart et al., 2020) and in cognitive brain networks similar to those previously mapped (Jonas et al., 2016).

Despite setting tDCS parameters at a common intensity (2mA), duration (20min), and using a small number of electrodes (two small HD ring electrodes), tDCS significantly modulated the evoked iEEG responses. Deliberately, these parameters have not been optimized to study tDCS effects under the most frequent conditions encountered in research and clinical use (Lefaucheur, 2016) and consequently, provide findings that would be broadly beneficial to the field. The quantification of iEEG neuromodulation in terms of amplitude showed significant increases (from 5 to 47%), which could be related to the routine tDCS parameters used in the study. Considering that neuromodulation is directly linked to the intracerebral induced EF within the targeted brain network, one method to obtain a stronger EF, and consequently stronger neuromodulation, could be to increase tDCS intensity. In a combined TES-iEEG investigation, we demonstrate that a direct linear relationship exists between the tDCS intensity and the measured intracerebral EF in humans. When tDCS intensity is doubled, the EF is also doubled (Louviot et al., 2022). Yet, increasing the intensity is not without its constraints and dangers. For safety and tolerability considerations, increasing tDCS intensity (e.g., from 2 to 4mA) can be facilitated by using larger electrodes like pads, which distribute the current over a broader area, or by employing a configuration of multiple small HD electrodes, which enhance focality (Nitsche & Bikson, 2017). Considering the promising results of computational studies with HD tDCS (Alam et al., 2016), this configuration could potentially achieve greater neuromodulation.

Our original study, which used small HD ring electrodes instead of the more commonly used large pads, is also a first step in demonstrating that significant neuromodulation can be obtained using

small ring electrodes despite the lack of an HD configuration. In the pre-surgical context of iEEG investigation, small HD electrodes are well-suited to be positioned alongside the iEEG electrodes. This ergonomic aspect, along with their efficiency in distributing currents in the head tissues, is important to highlight, especially for broader clinical use.

Finally, the iEEG neuromodulation induced by tDCS in the VOTC during the face-perception task could objectively explain the behavioral changes (Gonzalez-Perez et al., 2019; Pisoni et al., 2020) and scalp EEG (Civile, Waguri, et al., 2020b; D. W. Kim et al., 2019) and increases observed after tDCS in some studies. The discrepancy with previous literature can stem from variability in the employed tDCS parameters (electrode location, intensity, duration) or the different behavioral tasks implemented in other studies. The methodology employed in this study, combining the robust FPVS approach to activate face-selective regions with tDCS parameters specifically targeting these areas, provides a well-suited framework for investigating the influence of tDCS on face discrimination responses.

V.2. Significant neuromodulation maintained after a single-tDCS session

In this study, a single 20-minute tDCS session was assigned for each participant. Despite this minimal procedure**,** significant face-selective electrophysiological neuromodulation remained after the tDCS session. This finding confirms results showing that tDCS altered cortical excitability for approximately one hour post-stimulation, as demonstrated through scalp EEG evoked potential analysis (Nitsche, Nitsche, et al., 2003; Nitsche & Paulus, 2001). Here, the iEEG after-effects were measured immediately following the tDCS session (within a few minutes). Although extending the investigational period post-tDCS was not feasible within the framework of this study due to clinical constraints (i.e., the removal of iEEG electrodes immediately after the experiment upon completion of the clinical investigation), examining the effects of tDCS over a longer period, such as several hours after stimulation, could provide valuable insights. This approach could help determine the duration for which the electrophysiological neuromodulatory effects of a single 20-minute low-intensity tDCS session persist and the time required for neural activity to return to baseline. Such knowledge could be particularly relevant for optimizing protocols involving repeated tDCS sessions. Furthermore, performing the tDCS experiment earlier in the week isn't feasible either, as tDCS could disorganize the surrounding epileptic brain networks and therefore bias the clinical diagnosis of epilepsy.

In a recent review, Horvath et al. (2015b) concluded that there is insufficient evidence to support any cognitive effects in healthy populations (n=59 analyses) following a single tDCS session. This apparent tDCS inefficacy should not be interpreted as a unique single-session issue, as several

other parameters such as the investigated cognitive networks (language, memory, executive functions, …), the control conditions and the tDCS parameters (montage, duration and intensity) were very different from one study to another and not fully controlled. Here, our findings using a robust methodology, which provides electrophysiological evidence of tDCS effects, open new insights into the link between electrophysiological and behavioral neuromodulation. The implementation of behavioral tasks in this methodology, like face/object recognition (Benton test, Rossion & Michel, 2018), Famous and unfamiliar face matching, and face memory before and after the tDCS experiment, could potentially reveal an enhancement in performance. Indeed, the electrophysiological changes (i.e., the amplitude increases in different VOTC regions) observed are probably not strong enough to induce behavioral changes. Nevertheless, the absence of behavioral changes after a single session must not be interpreted as evidence of tDCS ineffectiveness. Rather, our results suggest that the minimal or absent cognitive effects could be primarily related to methodological aspects such as the moderate neuromodulatory impact of commonly used tDCS parameters.

For therapeutic purposes, more long-lasting aftereffects are desirable. Animal studies indicate that repeating DC stimulation during the aftereffects of an initial session enhances its efficacy (Bindman et al., 1964; Gartside, 1968). Nonetheless, repeated induction of plasticity might also trigger homeostatic counteracting mechanisms (Siebner et al., 2004). Two options were investigated in the literature to induce long-lasting effects. First, extending the duration of stimulation or increasing its intensity, both of which have been employed in clinical settings (Ferrucci et al., 2009; Fregni et al., 2006; Ohn et al., 2008). The alternative method to extend tDCS aftereffects is through the repetition of tDCS sessions. Empirically, repetitive tDCS has been shown to produce cumulative effects when administered once daily in humans (Boggio et al., 2007; Monte-Silva et al., 2010).

The innovative combination of tDCS with iEEG recordings applied here seems to be ideally suited to further investigate the impact of different tDCS parameters, like stimulation polarity (cathodal tDCS, for instance), intensity, montage, duration, and repetition, on electrophysiological responses and human cognition. This tDCS-iEEG-FPVS approach could potentially provide effective technical guidelines to enhance specific cognitive networks. Similarly to the application of the electrodes targeting the VOTC implicated in face processing, modifying the stimulating and return electrodes' positions on the scalp can target other established cognitive functions (e.g., language) and modify their performance.

V.3. Functional targeting and specific neuromodulation

Through the analysis of frequency-tagged iEEG responses, we demonstrate that right hemispheric tDCS has a strong and consistent electrophysiological impact on face-selective responses

that persists beyond the stimulation duration while exerting a mild neuromodulatory effect on the iEEG general visual responses. These findings suggest that the face-recognition network is particularly sensitive and affected by tDCS neuromodulation in the right hemisphere. The specificity of the neuromodulation induced by tDCS can be explained by the functional targeting of the VOTC, a critical region for face processing. Since the FPVS task demands rapid (i.e., single glance) recognition of faces, the face-selective neural networks in the VOTC were more heavily engaged during the task.

The task-specific engagement of face-selective circuits in the right VOTC likely made them more responsive to the effects of tDCS, which modulated their excitability in a task-dependent manner. In contrast, the broader visual networks located posteriorly, closer to the occipital lobe, involved in general visual processing were less engaged by this task, and therefore, less affected by the neuromodulation. Thus, the combined effects of functional targeting and increased neural engagement during face-selective processing could explain why tDCS strongly modulated face-selective responses with less influence on the general visual responses.

In the present study, a P10 (anode) - FT9 (return) tDCS montage was used specifically to target the right VOTC. The choice of the anodal P10 position was driven by previous scalp EEG studies that showed strong face-selective responses in this occipito-temporal scalp region using the same FPVS paradigm (Rossion et al., 2015). The three main structures of the VOTC, the ATL, the PTL, and the OCC, were significantly impacted by tDCS during and after stimulation, with the OCC exhibiting the strongest and most pronounced effect for face-selective responses. The posterior OCC region includes the IOG (OFA), a core region for face-selective activity (Jacques et al., 2019; Jonas et al., 2014; J. Liu et al., 2010; Pitcher et al., 2007) and where a high EF magnitude was observed. Furthermore, the OCC plays a central role in early-stage visual processing before transmitting the information anteriorly to higher-level face-selective regions implicated in memory and attentional functions (Rossion et al., 2015b). These findings suggest that early-stage visual processing regions may be more susceptible to tDCS neuromodulatory effects than anterior high-level face-selective regions. Targeting high-level visual processes might demand an increased stimulation intensity or a more precisely directed EF trajectory, achieved by positioning the anodal electrode further anteriorly or employing a different tDCS montage for increased focality, like the 4X1 HD configuration.

The small HD ring electrodes have the advantage of allowing a precise placement over the right occipito-temporal region without touching the iEEG electrodes that need to be protected (aseptic reasons). The right occipito-temporal cortex was targeted in this experiment as it holds one of the crucial nodes of the cortical face-selective network, as shown with neuroimaging (EEG : (Jacques et al.,

2019), TMS:(Pitcher et al., 2007), and fMRI: (J. Liu et al., 2010)) and direct intracerebral electrical stimulations (Jonas et al., 2014). This original tDCS montage, with only two small HD ring electrodes, enabled significant neuromodulation. It is the first evidence in the literature showing that this montage can yield effective results. Usually, small ring electrodes are used in HD-tDCS with a montage of 4x1, i.e., one center-anode or -cathode and four return electrodes around. In the present study, it is interesting to note that HD electrodes can also be used in a "conventional" tDCS montage with only two electrodes.

Additionally, the small HD ring electrodes were certainly the key element to precisely target face-selective responses in the IOG with a sufficient EF (0.38 V/m). Computational studies with 4x1 HD montage demonstrated that small ring electrodes can focus and increase the intracerebral EF on the brain target compared to a bipolar sponge montage (Villamar et al., 2013).

The face-selective electrophysiological neuromodulation is also crucial and important evidence of functional targeting that considering that cognitive brain networks already activated by a task become more sensitive to direct constant current stimulation (Bikson & Rahman, 2013; Bradley et al., 2022). An in-vitro study showed that only synapses already experiencing plasticity would be influenced by DCS, while inactive synapses remained unmodulated (Kronberg et al., 2017). The dependence of tDCS on brain state has been mainly investigated using non-invasive neuroimaging (e.g., scalp EEG (Petti et al., 2017) and fMRI (L. M. Li et al., 2018)). Our results provide the first evidence of functional targeting in humans using intracranial EEG recordings.

V.4. tDCS Spatially Target Deep Medial Fusiform Gyrus

Contrary to our expectations, no significant neuromodulation was observed in the IOG (i.e., OFA), which is believed to be the gateway to the face perception system (Haxby et al., 2000; Rossion et al., 2012). It's important to note that the latFG presented during the first phase of the experiment with the highest amplitude for the face-selective response, followed by the right IOG and the right medFG. For the general visual response, the VMO presented the highest amplitude responses, followed by the medFG and the IOG. These results are in accordance with Jonas *et al.* (2016) intracerebral mapping for face-selective regions. The presence of these brain regions also demonstrated that our cohort presented regular face perception and no deficit due to their pathology (i.e., no reorganization).

The IOG received the second-highest tDCS-induced EF magnitude among the ten ROI (0.38V/m). Delineated by several sulci: medially by the collateral sulcus (CoS) and the transverse

posterior collateral sulcus (POS), laterally by the inferior occipital sulcus, and anteriorly by the pre-occipital notch, one would expect the formation of EF hotspots around the sulcus contributing to the elevated EF observed in the IOG (**Figure 44.A**). Additionally, the IOG's posterior location within the VOTC and its relatively lateral position to the P10 scalp stimulating electrode suggest that it may be strongly influenced by the tangential EF induced by tDCS. However, despite these factors, the IOG was not significantly affected by tDCS. This lack of significant neuromodulation in the highly face-selective IOG could be attributed to a ceiling effect, where the structure is already maximally engaged by face stimuli before tDCS, limiting the potential for further modulation. Moreover, even a high EF magnitude may not necessarily translate to proportionally larger neuromodulatory effects, as neural responses often follow nonlinear dynamics.

The medial fusiform gyrus (medFG) revealed contrasting patterns of neuromodulation between the two responses during tDCS. Specifically, active tDCS (during stimulation) led to a significant enhancement in the amplitude of face-selective responses, while it induced a significant attenuation in the amplitude of general visual responses. Firstly, this significant neuromodulation could be related to the employed tDCS montage, where the stimulating electrode is close to the PTL, and certainly to the corresponding intracerebral EF in this region. Secondly, this neuromodulation relies on the functional role of the medFG. A previous intracerebral investigation with FPVS combined both face and house stimuli demonstrated that the medFG was activated by both stimuli, but more pronounced for house perception (Hagen et al., 2020). These results suggest that medFG is a multimodal brain region that can respond to several items of perception. In this study, medFG activation before tDCS was expected according to the face processing literature, and we could imagine that during tDCS, the medFG was potentiated and so responded more to face stimuli. In contrast, the significant reduction in the medFG for the general visual response during tDCS may reflect a compensatory mechanism in response to the heightened activation associated with face perception. Notably, intracerebral electrical stimulation of face-selective regions resulted in either abolished or reduced activity in both local and distant regions following stimulation(Angelini, Jacques, et al., 2024). Although the stimulation was applied at a low intensity (1 mA), it was paired with biphasic square wave electrical pulses (1050 µs) and a high frequency (55 Hz), suggesting the possible contribution to the observed reduction in the medFG activity post-stimulation.

In the PTL, two primary face-selective regions, the medFG and the LatFG, presented significant neuromodulatory effects due to tDCS. While neuromodulation persisted in the LatFG after the stimulation period (P3), it was only significant during the stimulation phase (P2) in the medFG for both face-selective and general visual responses. This difference may be attributed to the tDCS parameters applied in our study, with the anode placed over P10, closer to the LatFG than the deeper region of the medFG. As evidenced in Louviot *et al.* (in 2022, the EF magnitudes exhibited a depth-dependent reduction, decreasing from the more superficial cortical regions (MTG) to the deeper ones (medFG). In addition to tDCS technical parameters, the interaction between the induced EF and the biophysical properties of the tissue in the PTL may contribute to the variability in tDCS effects across these regions. In this study, the medial fusiform sulcus (MFS) was used as a guide to functionally divide the middle FG longitudinally into the medial (medFG) and the Lateral regions (LatFG). However, these functional segregations by the MFS have been directly linked to the underlying neuroanatomical features of these regions. The MFS acts as a lateral–medial microarchitectural transition between the two cytoarchitectural regions (FG1 and FG2, **Figure 44.B**) of the ventral temporal cortex on the fusiform gyrus, where the medial FG1 cells present a columnar arrangement of their pyramidal cells in layer IV, while lateral FG2 cells present a higher cell density (Caspers et al., 2013). Furthermore, the MFS highlights the transition in white matter connections, receptor arrangement (acetylcholine receptor type 3), and tissue contrast related to myelination (Grill-Spector & Weiner, 2014a). Variations in the different anatomical characteristics generating this lateral-medial gradient may have differentially modulated the influence of the tDCS-induced EF in a region-specific manner, leading to the divergent effects between the medFG and the LatFG.

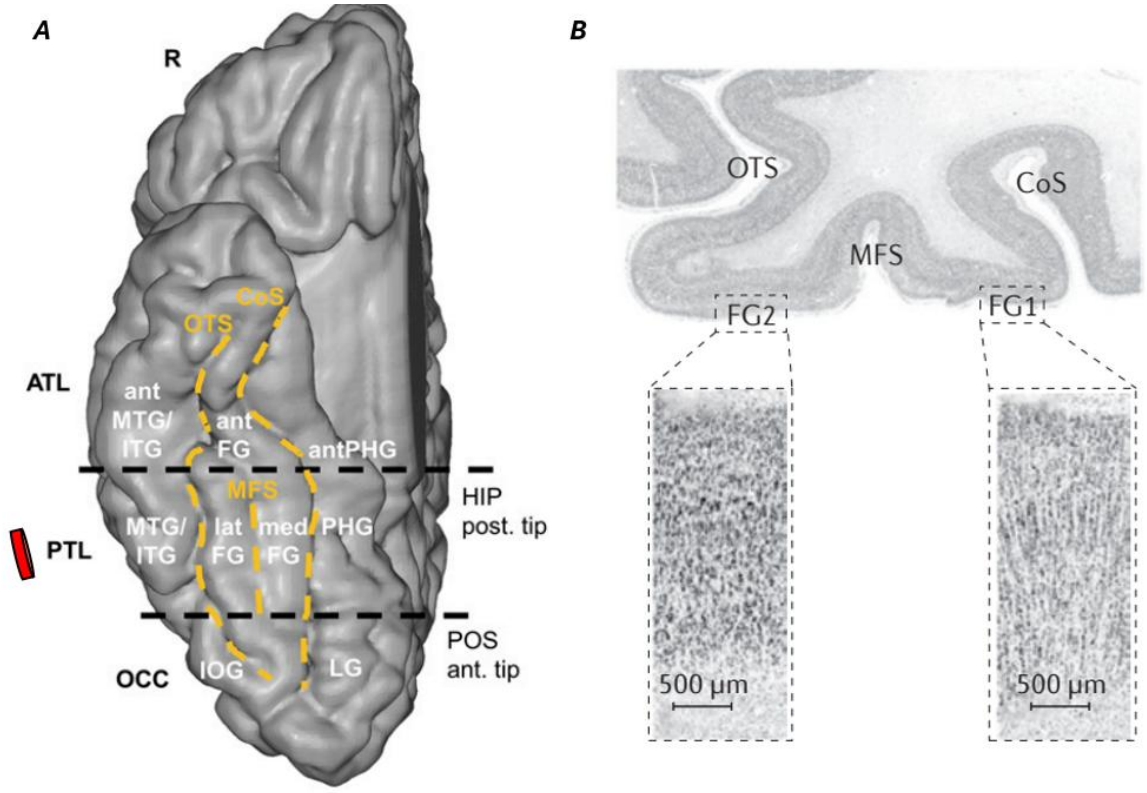

Figure 44. Anatomical characteristics of the middle fusiform gyrus separating the LatFG and medFG.
A. A Colin27 brain schematic illustration depicts the parcellation approach used to assign anatomical labels to face-selective contacts. Major anatomical landmarks were used to define the regions. The ventral temporal sulci (i.e., collateral sulcus (CoS), the anterior segment of the occipito-temporal sulcus (OTS), and midfusiform sulcus (MFS) serve as medial and lateral boundaries. Two coronal reference planes aligned with key anatomical regions (posterior extremity of the hippocampus (HIP) and anterior end of the parieto-occipital sulcus (POS)) define the anterior-posterior boundaries for each region. Adopted from Jonas et al., 2016. **B**. Cell body-stained histological coronal sections through the fusiform gyrus of the adult brain show that the boundary between FG1 and FG2 cells is in the MFS. MFS is a minor sulcus best described as a longitudinal sulcus dividing the FG into lateral and medial partitions with a distinctive "ω" pattern on single coronal slices. Below: Cytoarchitectonical variability of areas FG1 and FG2. Adopted from Grill-Spector & Weiner, 2014b**.**

V.5. Harmonic-Specific Analysis of tDCS Neuromodulation

In this study, we primarily reported the amplitudes and the SNRs for face-selective and general visual responses as the averaged sum of their respective twelve and five harmonics. Moreover, analyzing the harmonic-specific sensitivity to tDCS provided insights into the frequency-dependent nature of neuromodulation. The tDCS effect was almost uniform across most harmonics, presenting the same pattern of variation observed in the averaged sum of harmonics for both response types. Some harmonics of the face-selective response showed stronger neuromodulation (e.g., 3.6Hz, 4.8Hz, 8.4Hz, 9.6Hz, and 10.8Hz) while others showed weaker (e.g., 1.2Hz, 13.2Hz, and 14.4Hz) to no neuromodulation (7.2Hz). These findings suggest that the neural activity at certain frequencies is more or less susceptible to tDCS, which could indicate that tDCS preferentially influences specific processing stages or neural populations that resonate at particular frequencies.

Notably, we previously reported in (Tabikh et al., 2025) finding from the sum of only four harmonics for each response, which limited the sensitivity of our analysis, potentially underestimating the full extent of tDCS neuromodulatory effects. This restriction occurred because neuromodulatory changes manifest across a broader range of harmonics that contributed meaningfully to the overall response. In contrast, the current approach, which includes a more comprehensive summation of harmonics, allows for a more accurate and complete evaluation of tDCS-induced effects.

V.6. Hemispheric Differences and Lateralized Neuromodulation Effects

tDCS induced lateralized neuromodulatory effects in favor of the right hemisphere. These findings indicate the dependence of tDCS impact on the preexisting functional specializations of the face processing network, wherein the right hemisphere plays a predominant role in face perception, while the left hemisphere is more involved in other networks, such as visual word recognition (Rossion & Lochy, 2022). Notably, the baseline activity for the amplitude of the face-selective responses was clearly lower in the left hemisphere compared to the right.

Furthermore, the tDCS parameters used in this study, specifically the low stimulation intensity and the distance from the anodal electrode on P10, were likely insufficient to induce significant neuromodulation in the left hemisphere, or to replicate the inter-hemispheric effects previously reported with intracerebral stimulation (Angelini, Jacques, et al., 2024). Moreover, the electrode contacts in the left hemisphere were relatively distant from the expected EF propagation trajectory between P10 and FT9, further limiting the potential for effective modulation. A tDCS montage mirroring the one applied in this study (anode on P9 and cathode on FT10) seems to be more adaptable to understand tDCS modulation of the left hemisphere. This configuration allows for assessing tDCS ability in enhancing face processing in the left region or to suppress it in favor of other preexisting dominant cognitive functions. Analyzing hemispheric differences in tDCS-induced neuromodulation can contribute to a better understanding of how cortical excitability and network interactions shape face-selective processing.

V.7. tDCS induced EF

Given that all regions of interest exhibited the same range and non-null averaged EF values (0.14–0.40 V/m), the contribution of an indirect neuromodulation, defined here as the physiologically evoked neuromodulation within the highly connected VOTC, cannot be assessed in this study, as it was not influenced by the tDCS-induced EF(Angelini, Jacques, et al., 2024). Addressing this question would require at least one ROI showing significant iEEG responses but a null EF value. Here, all ROIs were influenced by the induced electric fields to varying extents

Furthermore, our data indicates a clear gradient in EF values, exhibiting higher values in more superficial regions (antMTG and IOG) and lower EF values in deeper regions (latFG and medFG). These findings are consistent with computational models predicting that tDCS-induced EFs are stronger near the cortical surface and attenuate with depth (Datta et al., 2009). This gradient could differently influence tDCS neuromodulatory effects across cortical layers, where tDCS is more directly influencing superficial layers and potentially affecting their local processing more than deep layers' signaling. However, indirect neuromodulation effects mediated through network connectivity cannot be ruled out, as deeper brain regions exhibited significant neuromodulation despite weak EF. For instance, we can hypothesize that the high EF in the IOG may have modulated both local visual processing and its projections to more anterior regions in the PTL, resulting in a potentially enhanced activity in the fusiform gyrus' subregions (latFG and medFG). As evidenced by intracerebral electrical stimulation (Angelini, Jacques, et al., 2024), the bidirectional effective connectivity between the IOG (OFA) and the LatFG (FFA) could induce a negative feedback loop. Specifically, increased latFG activity may have led to an attenuation of face-selective responses in the IOG during stimulation, therefore modulating face processing dynamics during tDCS.

Although our study provides valuable insights into the electrophysiological effects of tDCS, it is important to shed light on a potential limitation regarding the EF measurement using tACS after the tDCS experiment. Applying tACS to measure the EF post-tDCS might not have clearly reflected the direct impact of tDCS on the neural activity due to fundamental performance discrepancies, where phase-locking resulting from tACS might not accurately reflect tDCS excitability modulation. Furthermore, tDCS modulates broad neural excitability while tACS targets specific frequency bands, which could lead to different electrophysiological modulations. In this study, the lack of a significant correlation between the EF values and the neuromodulatory effects during and post-tDCS could be explained by the temporal mismatch between measuring EF during tACS after the tDCS experiment. In particular, the application of a tACS protocol in this study (previously reported in the same experimental environment with (Louviot et al., 2022)) was adopted to align with our main goal of applying an EF strong enough to reach the deep brain region and quantify tDCS neuromodulatory effects. Indeed, a better-suited EF measurement approach would incorporate a real-time intracranial EF recording during the tDCS experiment. By capturing the direct effects of tDCS-induced EF on neural activity during stimulation, this approach would help understand tDCS modulation in different brain regions and the interaction between induced EF and brain anatomy.

VI. Perspectives and conclusion

All in all, the current evidence provided by this intracerebral investigation in humans represents the first milestone demonstrating the ability of tDCS to induce objective, selective, and significant electrophysiological effects. By using this original method of simultaneous tDCS-iEEG-FPVS, future research could address important questions to define the most effective tDCS parameters for achieving the highest electrophysiological neuromodulation and, ultimately, sustainable behavioral changes.

The innovative combination of tDCS with iEEG recordings applied here seems to be ideally suited to further investigate the impact of different tDCS parameters, like stimulation polarity (cathodal tDCS), intensity, montage, duration, and repetition, on electrophysiological responses and cognition. Systematically varying the duration of tDCS stimulation could help determine how brief versus prolonged exposure to tDCS influences acute neural excitability, long-term plasticity, and the persistence of its modulatory effects on cognitive processing. This original methodology also allows researchers to explore several scientific doubts related to the minimum duration required for tDCS to induce an electrophysiological change inside the brain, to confirm the works of Nitsche & Paulus, 2000 about the minimum duration required to induce persistent after-effects and long-term effects.

In an approach to understand the direct electrophysiological effect of tDCS on the neural excitability, i.e., to investigate tDCS On/Off effects, we applied tDCS for 10 minutes directly after the first sham phase (phase 1) during FPVS and intracerebral recording (**Figure 45**). Utilizing this methodology would help clarify the temporal evolution of the neuromodulatory effects, therefore distinguishing whether tDCS produces immediate or delayed changes in brain activity. In the meantime, only 5 drug-resistant epileptic patients have been tested with this protocol, leading to insufficient data for a conclusion. Future work needs to include more patients for a clearer understanding of tDCS's direct electrophysiological effects.

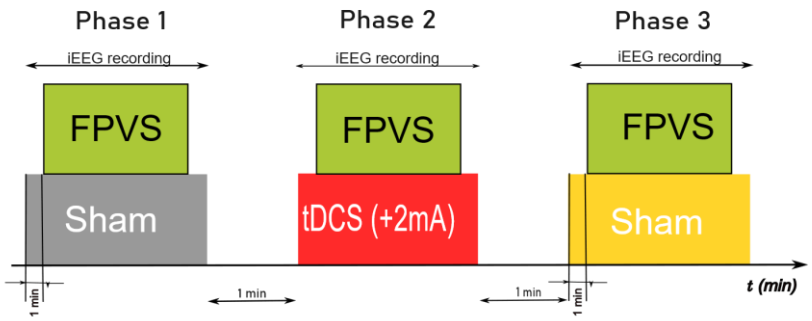

Figure 45. Study design combining tDCS, FPVS, and iEEG to test tDCS On/Off effects on electrophysiological responses.
During phases 1 and 3, a sham-tDCS session was performed during FPVS. Between them, phase 2 was performed during 10 minutes of active +2mA tDCS during FPVS. IEEG recordings recorded the electrophysiological brain activity during the three phases.

Furthermore, implementing this combined tDCS-iEEG-FPVS methodology provides the foundation for testing the acute and long-term influence of different stimulation intensities on the brain electrophysiology and their further implications on cognitive processes. Interestingly, in this study, when applying an anodal (+2mA) stimulation, we observed both increases and decreases in the recorded activity. Although tDCS is producing a positively charged EF, its interaction with the brain anatomy can influence the neuromodulation output. Further research should be carried out concerning the interaction of the induced EF with the specific anatomical properties of the VOTC with participant-specific MRI modeled montages, as well as to test the impact of a cathodal tDCS at the same intensity.

This study introduces a novel methodology for assessing tDCS effects by using a robust and objective FPVS approach. The FPVS paradigm employed here specifically targeted generic face recognition. Moreover, it's a versatile approach adapted to target various cognitive functions, including the human face identity recognition (FIR), i.e. ability to discriminate familiar from unfamiliar face identities. FIR has been investigated through an identity discrimination paradigm (see **Figure 28** in Chapter **1**) during tDCS and intracerebral recording in drug-resistant epileptic patients. In this procedure, 12 patients underwent the same experimental protocol described earlier in this chapter (see *Materials and Methods*, **Figure 33**), with the modification of incorporating the Identity discrimination paradigm. However, no findings have been concluded from this dataset as it currently lacks a dedicated analysis process. Nevertheless, applying this paradigm has the potential to reveal valuable insights into the neural mechanisms underlying FIR, a particularly complex, cognitively demanding task that relies on fine-grained visual discrimination processes to distinguish between highly similar facial features. Investigating FIR with combined iEEG and tDCS could help disentangle the neuromodulatory effects of tDCS on high-level visual processing and provide a more detailed understanding of how electrical stimulation influences the neural substrates involved in identity discrimination.

Additionally, an exploratory investigation was also carried out using our original protocol, which combined iEEG recordings, FPVS (**Figure 29**), and tDCS over the left hemisphere. In this experiment, the anodal electrode was positioned over the left VOTC at P9, with the return electrode placed at FT10. The main objective of this methodological variation was to investigate whether tDCS could enhance face-selective activity in the left hemisphere, which is typically less active in visual face processing. Furthermore, it could pave the way for inter-hemispheric and functional connectivity investigations during tDCS. Overall, our original methodology offers a powerful and versatile tool for investigating various cognitive functions, therefore enabling research exploration of neural mechanisms underlying perception, memory, and decision-making.

As mentioned earlier in this discussion, one of the limitations of this study was the lack of a behavioral assessment of the visual face recognition function before and after tDCS intervention. It's important to mention that patients underwent several behavioral performance assessments in the framework of the clinical assessment of their epilepsy, like the Benton Facial Recognition Test, Electronic version, BFRT-c (Rossion & Michel, 2018), which helped assess a normal baseline facial recognition performance. However, no assessment of this performance was directly done before and after tDCS due to methodological and clinical constraints. Future studies combining the electrophysiological investigation conducted in this study with pre- and post-experiment behavioral assessments would offer a comprehensive framework for linking the recorded neural effects to tangible behavioral outcomes of tDCS. This approach would bridge the gap between neuromodulatory changes observed at the electrophysiological level and their functional behavioral relevance, offering a more complete understanding of how tDCS influences both brain activity and behavior.

To conclude, our novel multimodal approach, which integrates simultaneous tDCS with an FPVS paradigm during intracerebral EEG recordings in humans, provides the first direct evidence of tDCS-induced electrophysiological neuromodulation in the human brain. This method paves a robust foundation for future research to investigate the effect of the various tDCS parameters on intracerebral activity, to explore the influence of tDCS on different cognitive functions, and evidently provide the optimized stimulation settings to achieve optimal behavioral changes. Importantly, this approach facilitates advancements in NIBS interventions, particularly for patients suffering from cognitive impairment.

This approach establishes the foundation for investigating tDCS electrophysiological neuromodulation using intracerebral recordings that are minimally invasive and rarely accessible, only to a specific population (drug-resistant epileptic patients). Therefore, translating these findings from iEEG to non-invasive EEG recording could enable the reliable detection of tDCS effects with a more accessible and user-friendly methodology. In the following Chapter **III**, we discuss this investigation by examining the effects of tDCS combined with the FPVS paradigm during scalp EEG recordings in the same patients with drug-resistant epilepsy. Ultimately, this could support the development of safe and effective at-home tDCS applications, improving accessibility for patients.

VII. Supplementary Materials

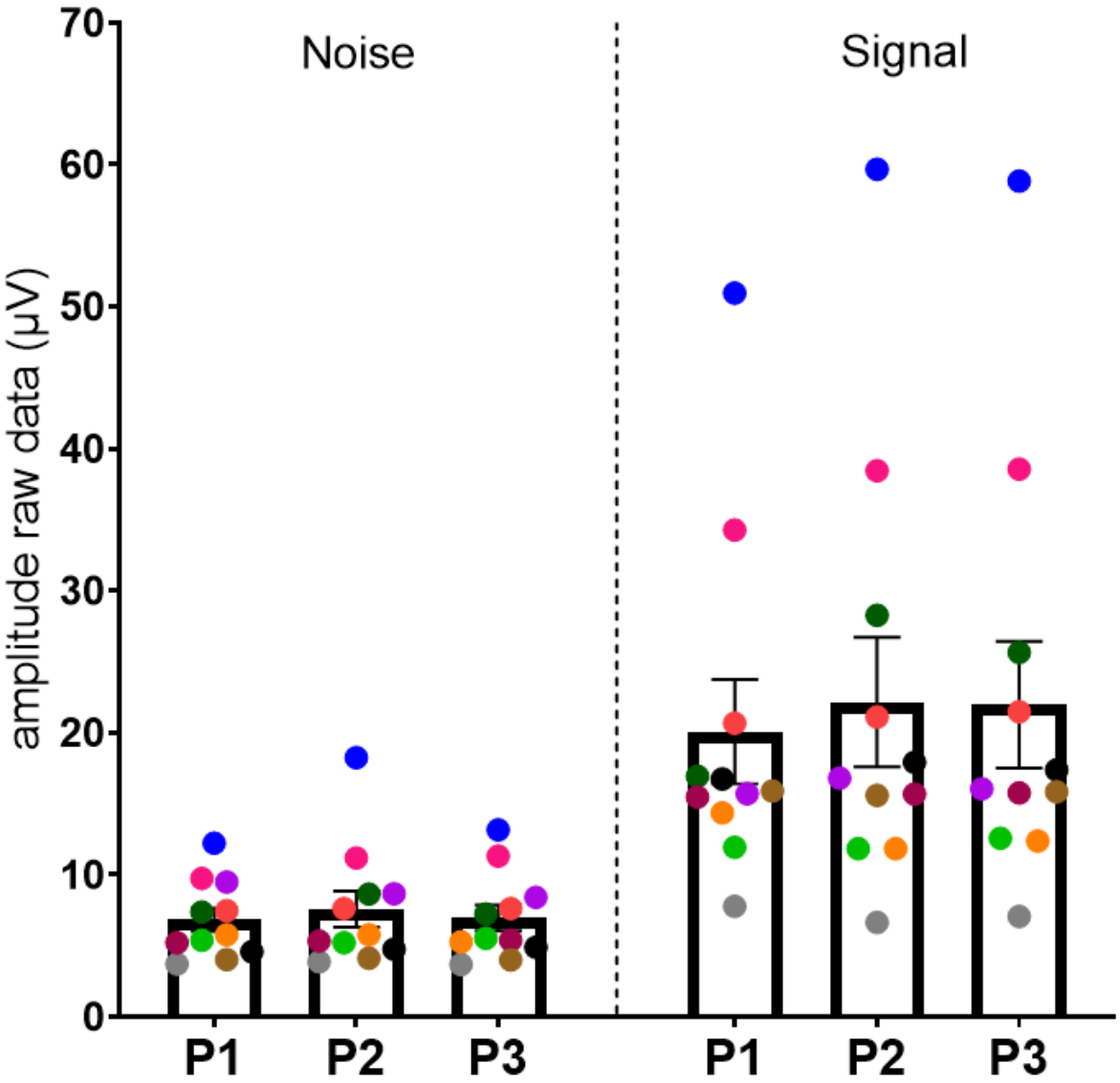

Supplementary Figure S1. Raw iEEG signals for both signals (i.e., the face-selective responses at 1.2Hz and harmonics) and noise (i.e., the surrounding frequency bands around face-selective responses). Average amplitudes of the raw iEEG signals (i.e., without baseline correction) for both signals (i.e., the face-selective responses at 1.2Hz and harmonics) and noise (i.e., the surrounding frequency bands around face-selective responses) before (P1), during (P2), and after tDCS. No noise amplitude increase, and weak amplitude value (by comparison to the signal) were observed in our cohort during tDCS. Each dot represents the average amplitudes of iEEG signals for each patient.

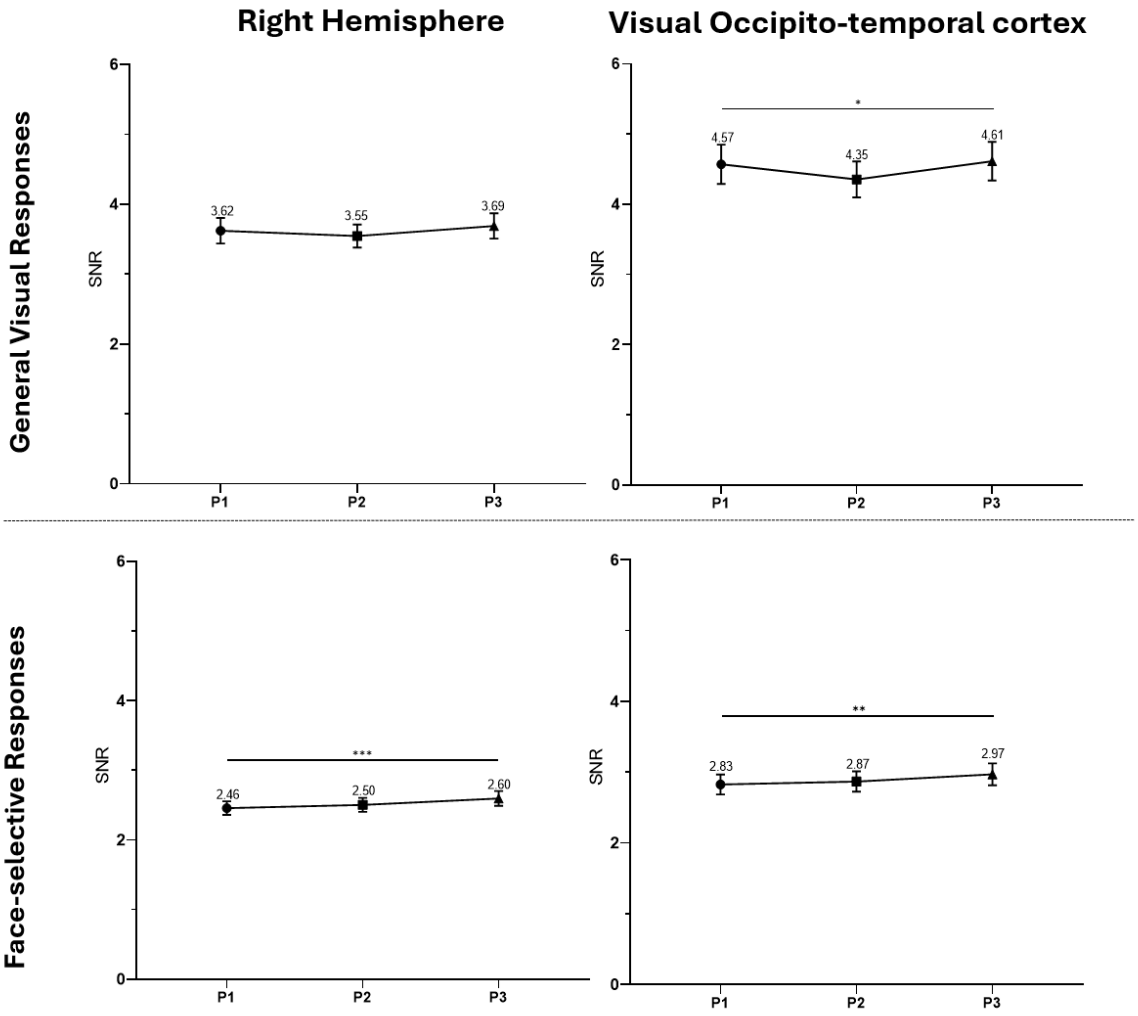

Supplementary Figure S2. **Neuromodulation of iEEG general visual and face-selective responses in terms of SNR across the three successive experimental phases in the right hemisphere and VOTC.** Averaged SNR and SEM of the iEEG evoked responses were computed during the three different phases for the eleven patients. In the right hemisphere, 260 and 302 iEEG contacts were used to compute the average baseline-corrected amplitudes, whereas 147 and 181 contacts were selected in the right VOTC for the general visual responses and the face-selective responses, respectively. No significant neuromodulation was observed for both responses ($p>0.5$) between the three different phases (P1, P2, P3). Phases: ● P1 (sham, before tDCS), ■ P2 (active, during tDCS), ▲ P3 (sham, after tDCS).

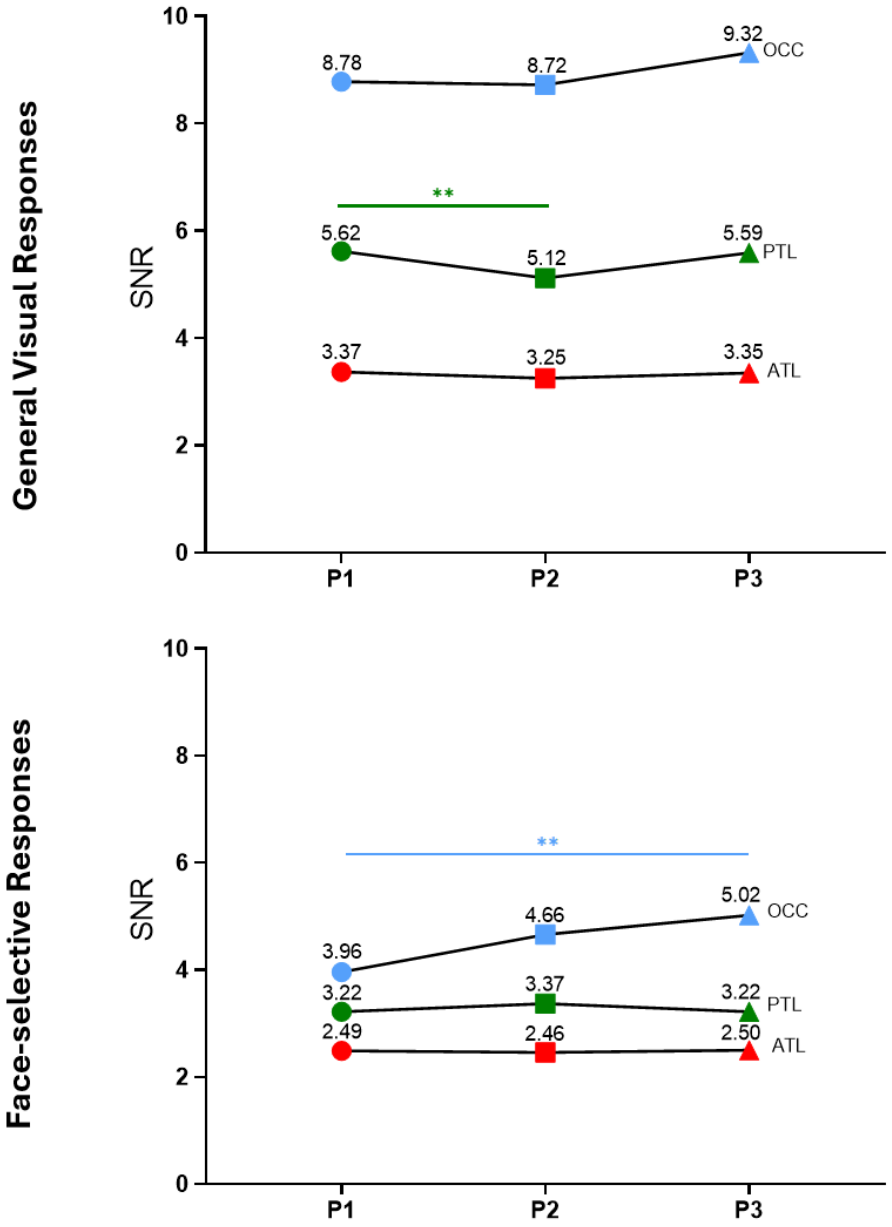

Supplementary Figure S3. Neuromodulation of iEEG general visual and face-selective in terms of SNR in the right ventral occipito-temporal cortex (VOTC).

SNRs of the general visual and the face-selective iEEG responses in the three ROIs during the three phases. No significant difference was found in any of the 3 regions in the VOTC for both types of responses between the three different phases (P1, P2, P3). VOTC: ventral occipito-temporal cortex, ATL: Anterior Temporal Lobe, PTL: Posterior Temporal Lobe, OCC: Occipital Lobe. ● P1(sham, before tDCS), ■ P2(active, during tDCS), and ▲ P3 (sham, after tDCS).

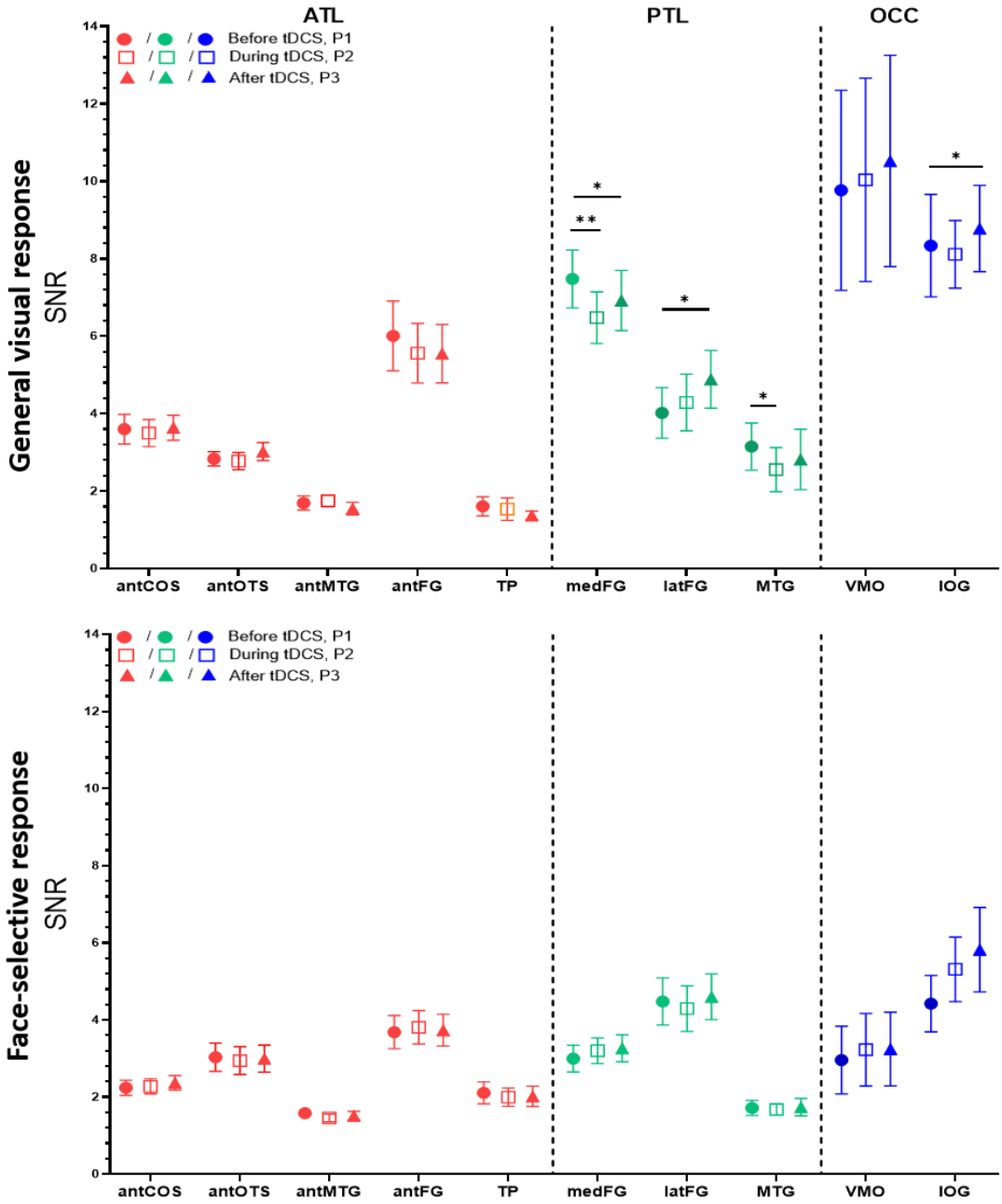

Supplementary Figure S4. Neuromodulation of iEEG general visual and face-selective responses in terms of SNR across the three tDCS phases in the ten face-selective regions of the right VOTC.
Averaged SNR and SEM of the iEEG evoked responses were computed during the three different phases for the contacts in the different regions of the ATL, PTL, and OCC. A significant neuromodulation was observed in the three regions of the PTL for the general visual response: In the medFG (p=0.002) and the MTG (p=0.04) presented a significant neuromodulation was observed after tDCS (P3) in comparison to before(P1). Additionally, the medFG (p=0.01) and the latFG (p=0.01) presented neuromodulatory changes that outlasted the stimulation period between after tDCS (P3) and before (P1).ATL: Anterior Temporal Lobe, PTL: Posterior Temporal Lobe, OCC: Occipital Lobe, AMG: amygdala, HIPP: hippocampus, antCoS: anterior collateral sulcus, antFG: anterior fusiform gyrus, antOTS: anterior occipito-temporal sulcus, antMTG: anterior middle temporal gyrus, medFG: medial fusiform gyrus, latFG: lateral fusiform gyrus, MTG: middle temporal gyrus, VMO: ventromedial occipital cortex, and IOG: inferior occipital gyrus.

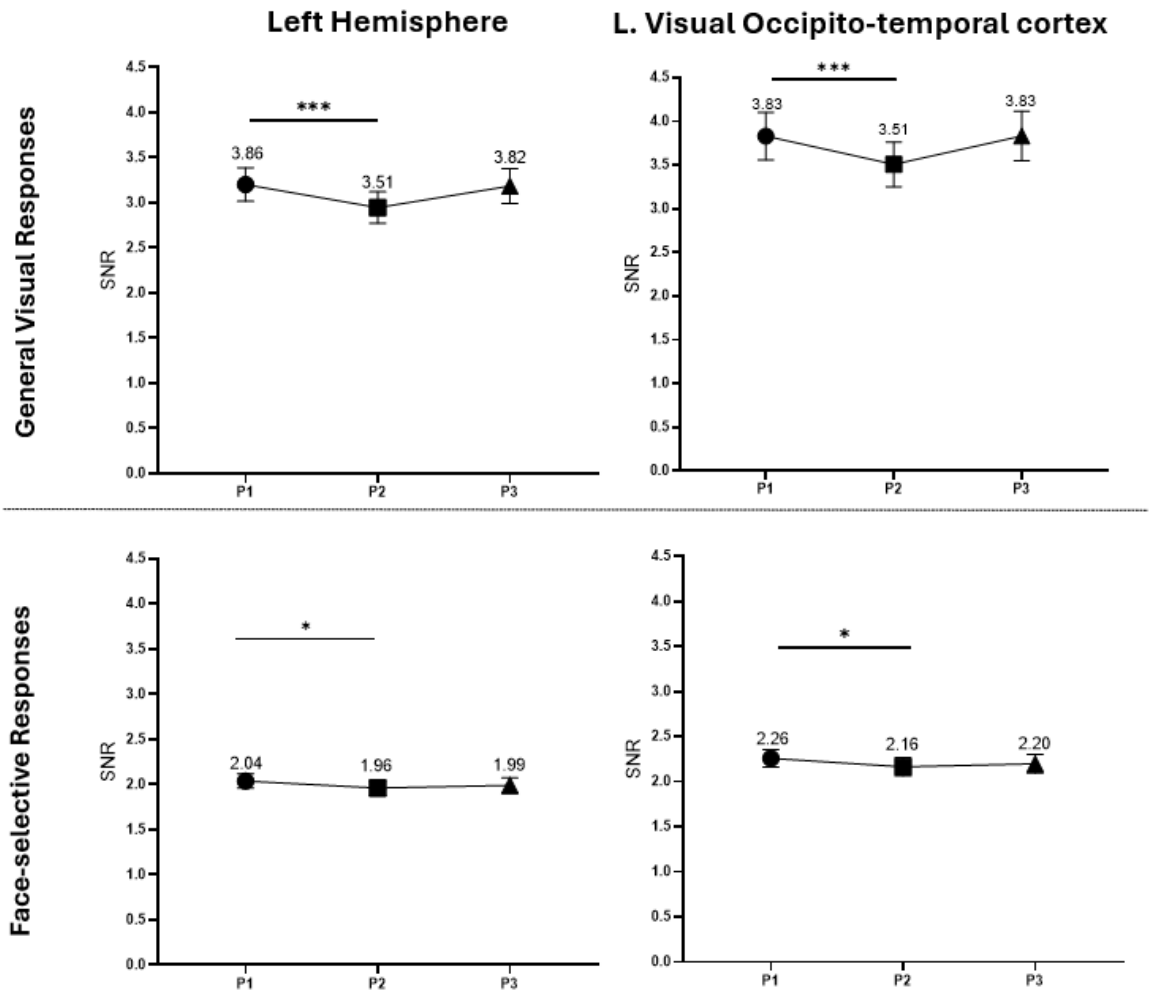

Supplementary Figure S5. Neuromodulation of iEEG general visual and face-selective responses across the three phases of the tDCS experiment in the left hemisphere and left VOTC in terms of SNR. Averaged SNR and SEM of the iEEG evoked responses were computed during the three different phases for the eleven patients. In the left hemisphere, 183 and 195 iEEG contacts were used to compute the average baseline-corrected amplitudes, whereas 113 and 137 contacts were selected in the left VOTC for the general visual responses and the face-selective responses, respectively. No significant neuromodulation was observed for both responses ($p>0.5$) between the three different phases (P1, P2, P3). Phases: ● P1 (sham, before tDCS), ■ P2 (active, during tDCS), ▲ P3 (sham, after tDCS).

Chapter III: Correlation Between Intracerebral and Scalp EEG Responses During and After Simultaneous tDCS

- ***Objective:*** Investigate the electrophysiological correlation between intracerebral and scalp EEG recorded responses during and after simultaneous tDCS.
- ***Methods:*** tDCS (2 mA, one session of 20 minutes, 2 HD electrodes), scalp EEG (26 scalp electrodes), and FPVS, n=8 drug-resistant epileptic patients.

Highlights

1. Scalp EEG combined with FPVS holds considerable potential for detecting at the scalp surface the neuromodulatory effects of tDCS observed in intracerebral recordings.
2. During stimulation, tDCS transiently modulated both face-selective signal and background noise, potentially obscuring the interpretation of amplitude changes.
3. Following one session of stimulation, tDCS revealed a reversible effect on neural signal quality, rather than a sustained neuromodulatory impact.
4. tDCS may transiently disorganize the cortical network near the stimulation site and simultaneously enhance neural activity in deeper brain regions
5. These findings help clarify the differential sensitivity of scalp EEG recordings in detecting tDCS-induced neuromodulation of electrophysiological responses.

I. Introduction

In the previous chapter, we established, for the first time, a combined methodology where tDCS can have a significant neuromodulatory impact on intracerebral electrophysiological responses in the human brain. Although this methodology is an essential tool for our discovery, utilizing intracerebral EEG (through SEEG exploration) remains an invasive tool to explore tDCS effects. The dual recording of iEEG and scalp EEG in drug-resistant epileptic patients for clinical investigation provides us with the means to bridge intracerebral tDCS findings with their scalp EEG correlates. Hence, it enables the translational insights into non-invasive approaches. In this chapter, we delve into the application of the accessible and user-friendly scalp EEG recording with tDCS and FPVS in drug-resistant epileptic patients.

The application of tDCS as a therapeutic noninvasive tool has increased exponentially over the past years for neurological and neuropsychiatric disorders in humans, especially for cognitive neurorehabilitation (Ciullo et al., 2021; Lefaucheur et al., 2017). Despite the advancement in this field, the efficacy and reliability of both its immediate and after-effects remain subject to ongoing debate, with growing skepticism surrounding the reported benefits and its potential for future applications (Filmer et al., 2020). The quantification of tDCS effects on human cognition, particularly in face perception, has been investigated using only two primary methodological approaches.

Firstly, behavioral assessment is one of the most used methods for evaluating tDCS effects. The impact of tDCS is either measured offline, i.e., after one or several tDCS sessions, or online during tDCS, while applying facial behavioral tasks (e.g., face perception task, Cambridge face memory task…). Findings showed an enhancement in face perception and face memory performance after tDCS (Barbieri et al., 2016b; Gonzalez-Perez et al., 2019; Pisoni et al., 2020). However, these effects were questioned as other studies could not replicate the results or observed a contrary effect (Kho et al., 2023; Willis et al., 2019; Civile et al., 2018; Brunyé et al., 2017; Renzi et al., 2015). The inconsistency in tDCS-induced behavioral effects might arise from inter-individual cognitive variabilities in response to stimulation. Closely linked to this replicability issue is the use of explicit behavioral tasks, whose outcomes rely on several cognitive processes beyond facial recognition, such as attention, decision-making, and response strategies. This complexity makes it particularly challenging to compare the effects of tDCS across individuals and over long periods. Additionally, poor methodological approaches contribute to a lack of specificity and consistency in tDCS outcomes, especially those using suboptimal tDCS montages targeting regions like the DLPFC (Civile et al., 2024, 2020, 2019, 2018; Lafontaine et al.,

2013). Therefore, this method does not address the question of tDCS neuromodulation due to the indirect and multifactorial characteristics of behavioral measurements.

A more direct and quantitative method utilizes task-related EEG recordings to measure tDCS effects in the brain. Scalp EEG involves recording electrical activity from various brain sources on the scalp's surface (Koessler et al., 2015), while tDCS involves applying electrical current to the scalp. The simultaneous application of tDCS during EEG can lead to interference, resulting in both montage-related and physiological artifacts. Unavoidable stimulator artifacts, which arise from the imperfect DC generated by a stimulator, introduce unintended and broadband device-specific frequencies into the recordings. Additional noise can also be injected while the stimulating device is actively measuring the impedance of the DC. Poor set-up conditions can also result in artifacts like the saturation of the amplifier and EEG signal distortion due to large DC potentials. We can also distinguish inherent (unavoidable, like DC shifts due to skin impedance changes, cardiac and blink artifacts) and non-inherent physiological artifacts (i.e., muscle and motion artifacts) that result from the interaction between the stimulation-evoked voltage and the biological tissue (Gebodh et al., 2019; Woods et al., 2016b). These EEG artifacts generated during tDCS are complex, dynamic, and share significant overlap with neurogenic frequencies, making it difficult to effectively eliminate them with standard signal processing methods (Gebodh et al., 2019; Lafontaine et al., 2013).

These methodological issues often resulted in the investigation of post-tDCS effects, rather than acute effects during tDCS. The investigation of the electrophysiological influence of anodal tDCS on ERP analysis showed an increase in the amplitude of the N170, an ERP highly sensitive to face stimuli (D. W. Kim et al., 2019; Lafontaine et al., 2013). Simultaneous EEG and tDCS also showed a reduction in the latency of the N170 in response to inverted faces, reflecting a modulation in configural processing (Civile, et al., 2020). ERPs extracted in the time domain, like the N170, present several limitations, especially a low SNR despite the long duration of the experimentation with numerous stimulating events. This extended testing duration also decreases the subjects' attention, and the visual expertise required for precisely quantifying tDCS-induced neuromodulation on amplitude and latency, compromising the reliability of the analysis. Additionally, the measurement error of ERP components varies significantly depending on the component of interest, the number of trials, and the method of amplitude (or latency) estimation, which underscores the complexity in precise quantification in a time domain analysis (Cassidy et al., 2012).

To overcome these limitations in the present study, we apply a novel approach to measure the online effects of tDCS on facial recognition by combining tDCS with FPVS and scalp EEG recording. The

use of frequency tagging method allows us to overcome the previously mentioned restraints and provide an objective, automatic, and robust method to quantify the periodically evoked face-selective responses in the frequency domain. Since the FPVS approach is implicit (i.e., automatic, without explicit instruction to categorize), no assessment of participants' behavioral face categorization is needed alongside EEG recording. Additionally, the orthogonal task involved in the paradigm (detection of a cross changing color) doesn't interfere with the periodic face-selective response of interest. FPVS provides a high SNR, resulting from the relatively short acquisition period (each testing sequence of 79 sec), and the activity of interest is confined to specific and small defined frequency bins that are largely unaffected by typical EEG artifacts (Rossion et al., 2015b, 2014; Norcia et al., 2015; Regan, 1989). The characteristics of the FPVS approach, combined with scalp EEG and online tDCS, make this methodology well-suited to evaluate tDCS-induced neuromodulation of the periodically evoked EEG responses. It allows the comparison between tDCS effects from intracerebral to scalp EEG, and consequently disregards the use of this invasive methodology to investigate tDCS neuromodulation.

II. Main objectives

The main objectives of the study in Chapter **III** were:

(i) Quantify the scalp electrophysiological effects induced by online anodal (+2mA) tDCS using only 2 HD-ring electrodes (same tDCS protocol and patients as chapter **II**), performed over the right occipito-temporal lobe, on both general visual and face-selective EEG evoked responses.

(ii) Compare the findings from intracerebral assessment of tDCS-induced neuromodulation on face-selective responses with those observed in scalp EEG recordings, evaluating the potential for non-invasive scalp EEG to reflect the changes seen in a more localized intracerebral signal.

(iii) Investigate whether scalp EEG, which captures signal from multiple brain sources, can detect acute and after-tDCS neuromodulatory effects induced by a low-intensity tDCS.

(iv) Validate the use of the combined tDCS, FPVS, and scalp EEG system to quantify the electrophysiological neuromodulation induced by tDCS using scalp EEG recording.

III. Materials and Methods

The experimental procedure described here, including the epileptic patients tested with the sham-controlled tDCS study and the recording settings, is *identical* to the methodology outlined in Chapter **II**. As a result, only a brief summary of the methods is provided in this section.

III.1. Participants

From the eleven drug-resistant epileptic patients (same cohort as chapter II), eight patients (5 females; mean age: 32.5 ± 8.4 years) have been prospectively included in this simultaneous scalp EEG and tDCS investigation during an FPVS task. Of the eleven epileptic patients in our cohort (chapter **II**), three were not included in this study because they did not have scalp EEG recordings. Patients gave written consent to participate in the study, which was conducted according to the Declaration of Helsinki and approved by a local ethics committee. All patients were informed of the side effects of tDCS and were instructed to report any discomfort during the experiment.

All participants had normal to corrected-to-normal vision and performed the Benton Face Recognition Test (Rossion & Michel, 2018) before the iEEG exploration week, with a mean score of 43.3 +/- 4.2, reflecting normal performance in matching individual faces from all patients (expect for one patient reflecting mild impairment, score below 39 of 54).

III.2. EEG recording

All patients underwent *simultaneous* intracerebral EEG (iEEG) and scalp EEG recordings. Findings from the iEEG recordings during anodal tDCS investigation and FPVS have been reported in ***Chapter II***. In this chapter, we only report the effects of tDCS on the scalp EEG recordings during FPVS.

Scalp EEG recordings were performed using **26** Ag/AgCl electrodes of 10 mm diameter, which were taped onto the scalp following the 10–20 international system (Koessler et al., 2009) under sterile procedures. The placement of the electrodes was guided by anatomical landmarks, including the nasion, inion, and left and right pre-auricular points. The electrode placement ensured a dense, comprehensive coverage of the bilateral occipitotemporal regions, including sO1, sOz, sO2, sPO7, sPO8, sP9, sP10, sP8, and sP7. Due to the presence of depth electrodes, some posterior electrodes were slightly adjusted from their standard 10–20 positions.

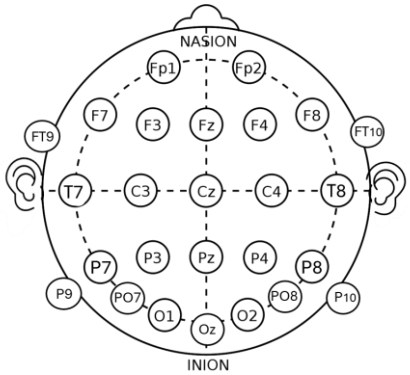

Figure 46. Scalp EEG electrodes positioning according to the 10–20 international system.

Scalp EEG signals were recorded at a 512 Hz sampling rate using a 128-channel amplifier (LTM256, Micromed, Mogliano, Italy). A prefrontal midline scalp electrode (sFPz) served as the reference. As scalp electrodes were placed three days before our experiment, before setting up the tDCS instruments for the experiment, a conducting gel (ECI Electro-Gel, Electro-cap International, Inc., USA) was reapplied to all scalp electrodes for each patient to optimize signal quality. The patient's scalp was then covered with a bandage to maintain a sterile environment and minimize contact. Scalp EEG recordings were simultaneously recorded with iEEG during FPVS. Given the small diameter of the skull defect at the intracerebral electrode penetration sites (1.2 mm) and the low electrical conductivity of the titanium guidance screw, no current leakage was detected in the scalp EEG recordings (Louviot et al., 2019).

III.3. Transcranial electrical stimulation.

The *same* sham-controlled anodal tDCS approach applied in Chapter II was adopted for the scalp EEG recording. As previously mentioned, tDCS was performed on the last day of the iEEG clinical investigation, just before the removal of intracerebral electrodes. This timing was determined to avoid tDCS after-effects during the iEEG investigation, which could influence the diagnosis.

The stimulation was delivered through 2 HD-ring electrodes (12mm external diameter) using a multichannel TES stimulator MxN-9 (Soterix Medical®, New York, NY, USA). Both electrodes were inserted in an electrode holder (24mm diameter) filled with a conductive gel, creating a 4.52 cm2 stimulation area on the scalp for each electrode. tDCS ring electrodes and electrode holders were carefully positioned on the scalp. The impedances were measured before tDCS and were always less than or equal to 5kΩ during the active stimulation phase.

To target the VOTC, the anodal electrode was placed on the P10 scalp position, and the common electrode on the FT9 scalp position (Koessler et al., 2009). Due to the presence of depth electrodes, the stimulating and return electrodes were slightly adjusted from their standard 10–20 positions.

The stimulation procedure was divided into three phases: Two sham (placebo) sessions were performed before (phase P1) and after (phase P3) tDCS in combination with FVPS (**Figure 47**). The active anodal tDCS session (Phase P2) was performed at +2mA (P10) for 20min (common stimulation duration as outlined in (Lefaucheur et al., 2017)). Considering that it could take from five to ten minutes of tDCS to produce persistent changes inside the brain, FPVS was started in phase P2 after 10 min of active anodal tDCS (Barbieri et al., 2016; Lefaucheur et al., 2017). Consequently, the P2 session consisted of 10 minutes of active tDCS alone, followed by 10 minutes of concurrent tDCS and FPVS.

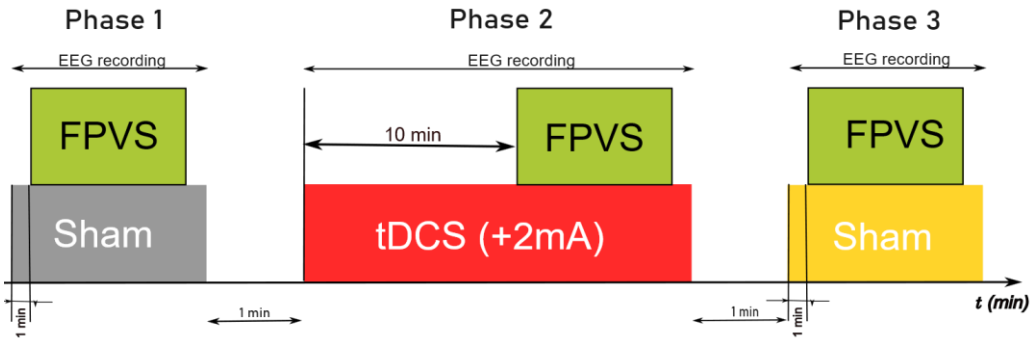

Figure 47. Design of the study protocol with tDCS, FPVS, and iEEG.
During phase 1 (P1) and phase 3 (P3), a sham-tDCS session was performed during FPVS. Between them, phase 2 (P2) was performed with 10 minutes of active +2mA tDCS alone, followed by 10 minutes of active tDCS during FPVS. Scalp EEG recordings were acquired during the three phases.

III.4. Fast Periodic Visual Stimulation

Responses from iEEG and scalp EEG recordings were acquired during the same FPVS sessions and tDCS phases. ***Stimuli.*** 200 natural images of various non-face objects from 14 non-face categories were used (flowers, birds, fruits...) in addition to 50 natural images of human faces. Each image showcased an unsegmented object or face near the center, varying in size, viewpoint, lighting, and background. All images were standardized for mean pixel luminance and contrast. The paradigm was the same as in Jonas (2016).

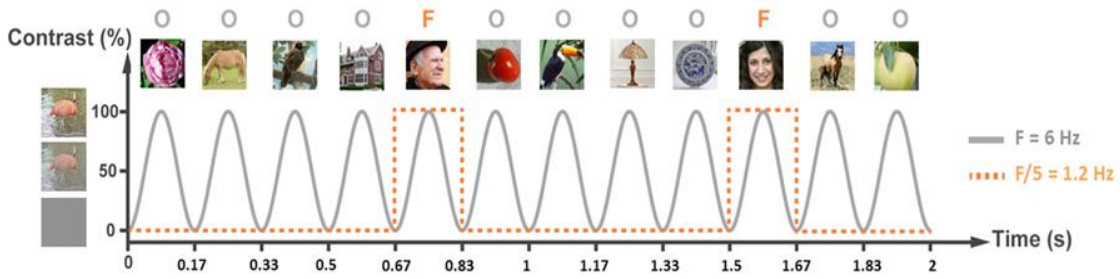

Figure 48. Fast Periodic Visual Stimulation used in tDCS-EEG-FPVS experiment.
Images of objects were presented by sinusoidal contrast modulation at a rate of six stimuli per second (6 Hz). In the periodic condition shown here, a different face image was presented every five stimuli (i.e., appearing at the frequency of 6/5 = 1.2 Hz). This stimulation sequence recruits ventral occipito-temporal brain regions and therefore obtains scalp EEG general visual and face-selective evoked responses.

Procedure. Participants were shown continuous sequences with highly variable natural images of objects at a frequency of 6 Hz through sinusoidal contrast modulation. Highly variable natural images of faces presented periodically were presented every fifth image (i.e., at 1.2 Hz = 6/5 Hz) (**Figure 48**). A sequence lasted 79 s, including 75 s of stimulation (i.e., 90 images of human faces and 360 images of natural objects) at full contrast, flanked by 2 s of fade-in and 2 s of fade-out, where contrast gradually increased or decreased, respectively. This extended duration of the sequence results in a high-frequency resolution (i.e., 71 seconds, so 0.0141 Hz), enabling the isolation of the specific response within a narrow frequency range, significantly improving its SNR. The FPVS paradigm was repeated two times during each phase (i.e., 2 sessions * 3 phases = 6 sessions in total). Throughout the sequences, participants were directed to maintain their gaze on a persistent small blue cross positioned at the center of the stimuli. Their task was only to identify brief color changes (from blue to red) in this central fixation cross, lasting 500ms.

III.5. EEG analysis

Analyses of scalp EEG recordings were conducted using Letswave 6, an open-source toolbox (https://www.letswave.org/) running on MATLAB R2022a (MathWorks, USA). Data processing procedure followed previously established methodologies (Rossion et al., 2015a; Jacques et al., 2016; Retter & Rossion, 2016) and is described in detail below.

Preprocessing and denoising

Firstly, for each patient, a single EEG data file was imported. The data were filtered using a Butterworth band-pass filter with a cut-off value of 0.1-30 Hz, to remove some periodically occurring tDCS artifacts above 30Hz. A FFT multi-notch filter with a 0.5 Hz bandwidth to remove electrical noise at 50 Hz frequency and its two harmonics (100 and 150 Hz) was applied. Then, the data were segmented by sequence, covering the 2 seconds before and after the sequence (-2 to 64 sec). A correction for eyeblink was applied to participants during the sequence for at least one recording (Retter & Rossion, 2016) using independent component analysis (ICA). One clear component was removed in 5 patients for their corresponding three EEG recordings during the three tDCS phases. For individual channels with artifacts due to noisy recording or tDCS-induced interference (two channels for four patients and one channel for two patients), interpolation was carried out with a linear combination of the three neighboring channels. All EEG channels were re-referenced to a common average reference.

Data segmentation

Each sequence was then re-segmented to an integer number of 1.2 Hz cycles, with exclusion of fade-in and fade-out stimulation portions. The resulting cropped epochs were 76.17 seconds long, corresponding to exactly 37980 bins in total. Epochs of the same experimental phase were then averaged in the time domain separately for each patient. Then, an FFT was applied, and the amplitude spectra were extracted, with a high frequency resolution of 0.0135 Hz (1/74.179 seconds).

Regions of interest

To compare the scalp EEG responses (for both face-selective and general visual responses), different ROI were defined using visual inspection of the topographical maps (**Figure 49**) and the results from previous studies, while taking into account the difference in the number of scalp electrodes (26 channels here vs, 128 in Rossion et al., 2015a;160 in Jacques et al., 2016; 128 in Retter & Rossion, 2016). The ROI for face-selective responses (at 1.2 Hz and harmonics) included the right occipito-temporal (ROT) regions composed of five contiguous channels (P8, P10, PO8, Oz, and O2). Regions in the left hemisphere were also investigated for inter-hemispheric comparison; five contiguous channels in the left occipitotemporal (LOT) regions were included (P7, P9, PO7, Oz, and O1). The ROI for general visual responses (at the base rate 6Hz and harmonics) was in the middle occipital (MO) included three contiguous right and left occipital channels (Oz, O1, and O2 channels).

Z-score quantification:

To identify significant responses at the frequency of interest and its harmonics, the Z-scores were calculated across the ROI, and the average of all 26 electrodes on the FFT spectrum was averaged across individuals for each experimental phase (P1, P2, and P3).

$$Z\ score = \frac{x - \mu}{\sigma}$$

$\boldsymbol{x}$ being the amplitude at the bin of the frequency of interest, $\boldsymbol{\mu}$ the baseline noise based on the average amplitude calculated within the 24 surrounding bins before and after the frequency of interest excluding the immediately adjacent bins (i.e., 10 frequency bins on each side, corresponding to a frequency range of 0.302 Hz) and $\boldsymbol{\sigma}$ the standard-deviation calculated within the 24 bins before and after the frequency of interest (or its harmonic). On a chosen intracerebral contact, a z-score > 3.1 at the frequency of interest suggests that a statistically significant response ($p < 0.001$) is recorded on that contact (Jonas et al., 2016).

Responses were considered significant if the Z-score > 1.64 (p<.05, one-tailed, i.e., signal>noise), indicating that the response was significantly larger than the EEG noise estimated in the neighboring frequency bins.

To quantify the EEG responses, the significant harmonics of the frequency of interest identified previously were summed (Retter et al., 2021; Retter & Rossion, 2016). For that, the EEG spectrum was segmented into successive chunks centered on the bin containing the face-selective frequency (1.2 Hz, 2.4 Hz, 3.6 Hz, etc.), and the chunks of significant harmonics were summed. Each chunk contained 25 bins (i.e., a chunk length of 0.728 Hz). For the Face-selective responses, 12 consecutive significant harmonics of the 1.2 fundamental frequency of interest were summed. For the general visual responses, 5 significant consecutive harmonics of the base frequency at 6Hz and its harmonics were summed.

Two methods were used to quantify the summed EEG responses:

(1) Baseline correction of amplitude spectrum:

Subtraction of the baseline noise from the signal (corrected amplitude in µV) for quantification,

(2) Signal/noise ratio (SNR) for optimal visualization:

$$SNR = \frac{x}{\mu}$$

SNR being the division of the $\boldsymbol{x}$ amplitude at the (summed) frequency bin divided by the $\boldsymbol{\mu}$ baseline noise amplitude calculated as the average of the 24 surrounding bins, excluding the immediately adjacent bins and the local maximum and minimum amplitude bins (i.e., 10 frequency bins on each side).

The Grand averages were computed to display results at the group level across experimental phases.

III.6. Statistical analysis

To assess the effects of tDCS on scalp EEG recordings over time, the mean baseline-corrected amplitudes and SNRs of both scalp EEG face-selective and general visual responses recorded were calculated within their respective ROIs across the three experimental phases (P1, P2, and P3).

To evaluate face-selective responses differences across phases, repeated-measures ANOVA tests were conducted for the ROI, followed by post-hoc comparisons to test whether tDCS influenced the evoked responses, with the null hypothesis that there were no differences in baseline-corrected amplitude (or SNR) between phases (alpha = 0.05). The same statistical approach was applied to general visual responses.

IV.Results

IV.1. Effect of tDCS on the face-selective response

Across the three stimulation phases, clear response peaks were observed for the face selective response frequency (1.2 Hz) and its harmonics (2.4Hz, 3.6Hz, 4.8Hz...) at bilateral occipitotemporal electrode sites, with right hemispheric dominance evident for most harmonics and across the majority of phases (**Figure 49**).

On the average of all 26 electrodes for the first phase before tDCS (P1), the amplitude of the responses was significant for all harmonics of the face-selective 1.2Hz until the 12th harmonic excluding the 6Hz and the 12Hz, corresponding to the general visual response frequency and its harmonic, (i.e. 1.2 Hz, 2.4Hz, 3.6Hz, 4.8Hz,7.2Hz, 8.4Hz, 9.6Hz, 10.8Hz, 13.2Hz, 14.4Hz, 15.6Hz and 16.2Hz; Z >1.64, p<0.05). In contrast, the computation of the Z score of the face-selective response's harmonics for the second and the third phases of the study, during and after tDCS (P2 and P3), revealed significant harmonics until the 9th (i.e., 10.8Hz) and the 12th (i.e., 14.4Hz) harmonics, respectively. Consequently, twelve harmonics were considered for the summation of the face-selective response in all three phases (P1, P2, and P3) according to the first highest significant consecutive harmonics.

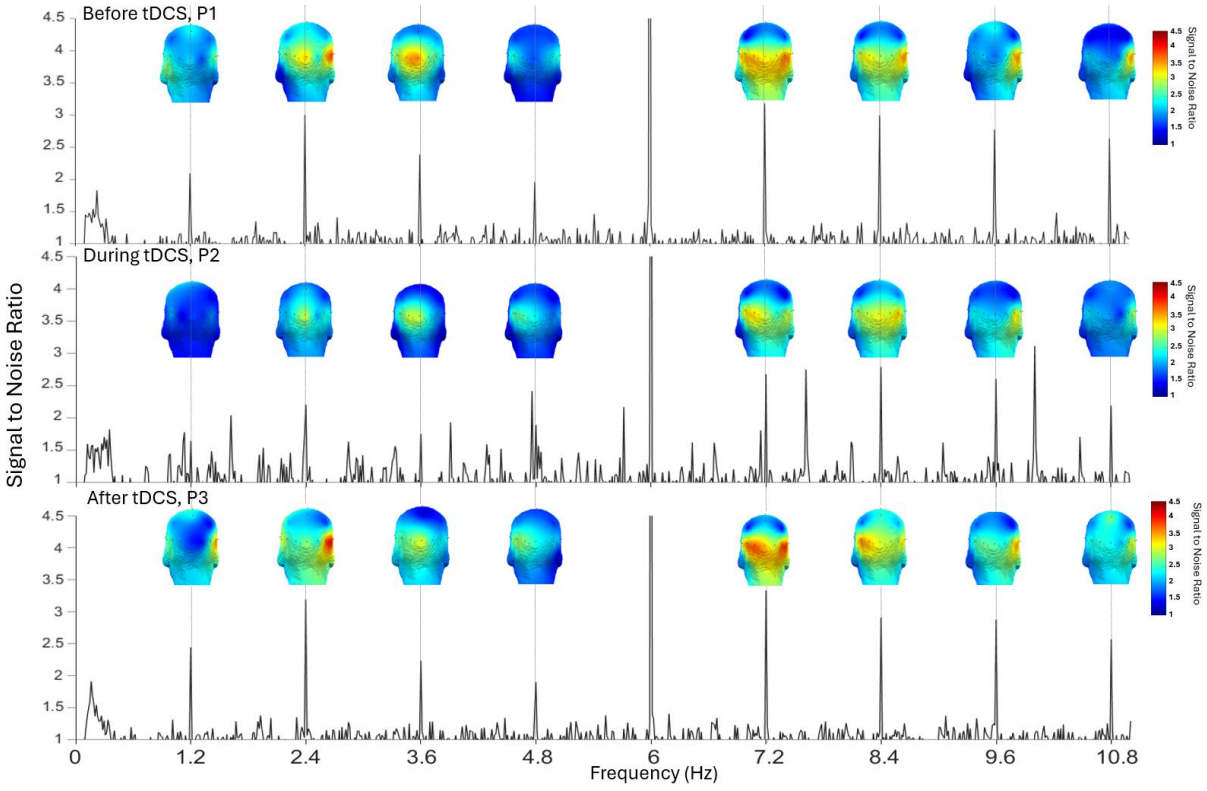

Figure 49. Frequency spectrum of the averaged SNR quantified at the right occipitotemporal regions across three experimental phases for the FPVS paradigm.
Clear significant face-selective responses were observed at the fundamental face-selective frequency of 1.2Hz and its harmonics (2.4Hz, 3.6Hz...) for each experimental phase: before (P1), during (P2), and after (P3) tDCS. 3D Scalp map topographies of the SNR are presented above each face-selective frequency (1.2Hz and harmonics). During tDCS, the SNR is decreased as shown by the smaller peaks for each harmonic. This is followed by an

increase in the SNR after tDCS in P3. Note, the 6 Hz cutoff frequency, which corresponds to the general visual response, is excluded here and is detailed in a separate figure.

Scalp topographies of the face-selective response showed an overall maximal amplitude over the right occipito-temporal regions (ROT) for most harmonics, especially before and after tDCS (P1 and P3). Accordingly, the face-selective responses' baseline-corrected amplitudes and SNRs were quantified in these ROT. The mean amplitude of the face-selective responses, after baseline correction, showed a gradual increase over the three stimulation phases. Before tDCS, the baseline-corrected amplitude of the face-selective response was 1.90 ± 0.53 µV, then increased to 1.93 ± 0.68 µV during tDCS and 1.96 ±x 0.71 µV after tDCS (**Figure 50.A**). No significant change in terms of amplitude was detected between during (P2) and after tDCS (P3) in comparison to before tDCS, P1 (p= 0.916) (**Figure 51.A**). Interestingly, the SNR variation did not follow the same trend as the amplitude (**Figure 50.B**). Repeated measures ANOVA showed a significant reduction of the SNR values between before tDCS (P1: 2.25 ± 0.35) and during tDCS (P2: 1.89 ± 0.35) (p=.0003), indicating decreased signal strength and increased noise during tDCS. Following stimulation, the SNR increased in P3 to reach 2.33 ± 0.61; however, this increase was not statistically significant in comparison to P1 (p=0.798) (**Figure 51.B**).

Furthermore, during tDCS, the amplitude of the noise increased in comparison to before and after tDCS and followed the same trend of variation as the signal. Notably, during tDCS, the noise amplitude reached approximately half the magnitude of the signal (**Supplementary Figure S6**).

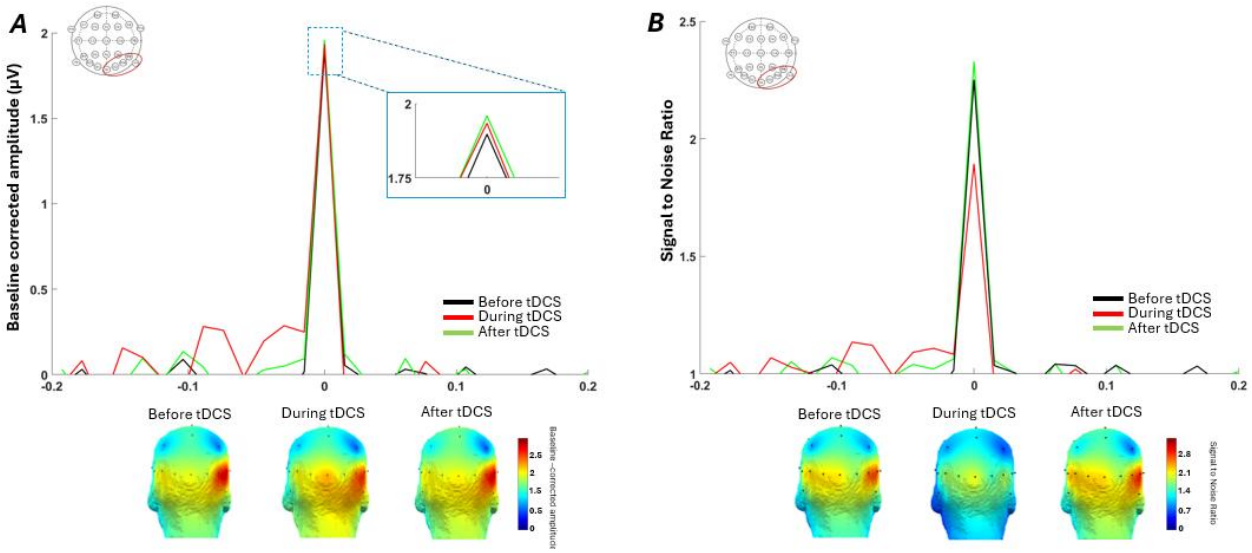

Figure 50. Baseline-corrected amplitudes and SNR of the face-selective responses across phases.
Graphs presenting the baseline-corrected amplitudes (A) and SNR (B) peaks at the sum of the first twelve face-selective (1.2 Hz) harmonics at right occipito-temporal regions before (black), during tDCS (red), and after tDCS (green). The spectrum is centered on the frequency bin of interest. A. A zoomed-in view is provided to improve the visualization of the baseline-corrected amplitude peaks in the three phases (P1, P2, and P3). B. The SNR during tDCS significantly decreased in comparison to before tDCS. Below are presented the 3D scalp map topographies of the baseline corrected amplitude and SNR of the summed face-selective response across the three phases in the ROT regions.

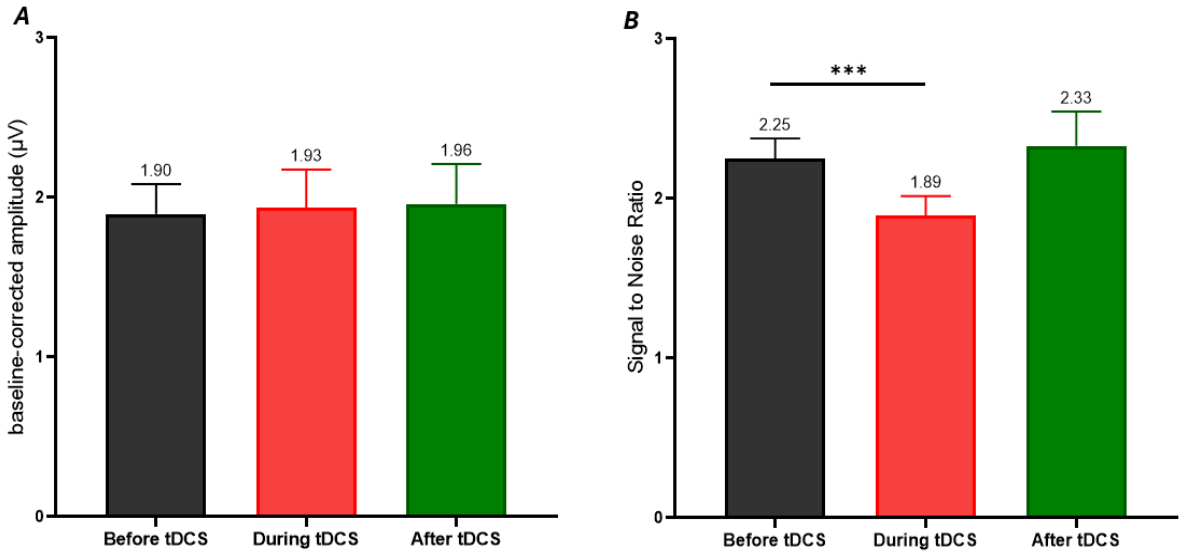

Figure 51. Histograms of the baseline-corrected amplitudes and SNR of the face-selective responses across phases.

Histogram of the baseline-corrected amplitudes (A) and the SNR (B) of the face-selective responses across the different experimental phases before (black), during tDCS (red), and after tDCS (green). The two graphs represent the average in all eight patients in the right occipito-temporal regions. Baseline corrected amplitude of the summed harmonics presents no significant neuromodulation during (P2) and after (P3) tDCS in comparison to before tDCS (P1) (p= 0.916). Notably, the SNR was significantly reduced during tDCS in comparison to before (p=0.0003), then increased after tDCS (P3), but didn't show any significance (p=0,798, repeated measure ANOVA). Bars represent standard mean errors, and the mean is reported on top of each bar.

To investigate tDCS influence on the left hemisphere, the face-selective responses baseline-corrected amplitudes, and SNRs were quantified in the left occipitotemporal (LOT) regions. Similar to the ROT regions, the scalp topographies presented a clear maximal amplitude over the LOT across all three stimulation phases. The average baseline-corrected amplitudes of the face-selective responses in the LOT regions were 1.54± 0.18 µV, 1.53± 0.17 µV, and 1.61 ± 0.20 µV during the three phases (before, during, and after tDCS), respectively. Although there was a slight decrease in amplitude during tDCS, repeated measures ANOVA showed no significant changes between before and during tDCS (p=0.99), or between before and after tDCS (p=0.74). The SNR investigation across the three phases also showed a similar trend, with values varying from 2.15± 0.19 before tDCS, to 1.87 ± 0.13 during tDCS, and 2.23 ± 0.24 after tDCS, but no significant differences were detected across phases (p = 0.059 for P1 vs. P2, p = 0.45 for P1 vs. P3).

IV.2. Effect of tDCS on the general visual response

High significant amplitude responses were observed for the general visual frequency (6Hz) up to the 5th harmonic (6Hz, 12Hz,18Hz, 24Hz, and 30Hz, Z>1.64, p <.05) across all three stimulation phases (P1, P2, and P3) on the average of all scalp electrodes. Therefore, the sum of the first five harmonics was used in all three phases to quantify the general visual response. The general visual response was maximal over the middle occipital (MO) regions of interest (**Figure 52**).

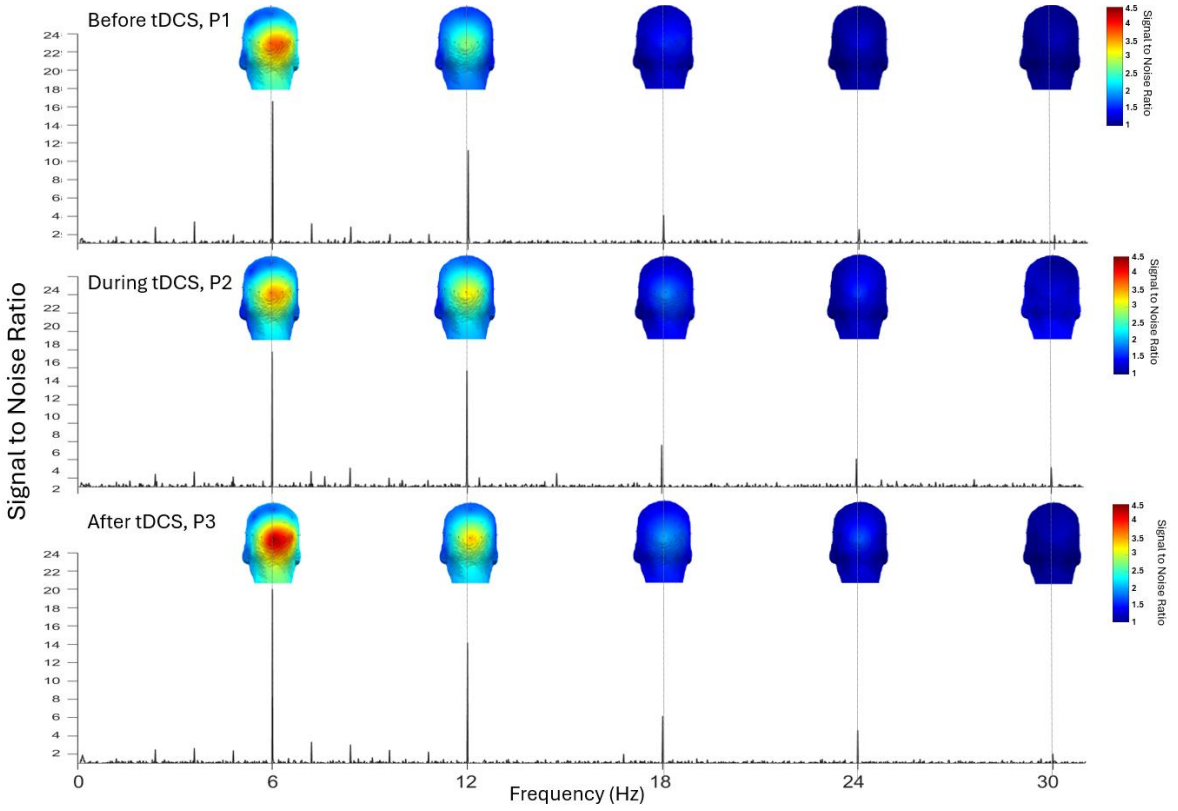

Figure 52. Frequency spectrum of the averaged SNR quantified at the middle occipital (MO) regions for each stimulation phase.
Clear significant face-selective responses were observed at the base general visual frequency of 6 Hz and its harmonics (12Hz, 18Hz...) for each experimental phase: before (P1), during (P2), and after (P3) tDCS. 3D Scalp map topographies of the SNR are presented above each general visual frequency.

The middle occipital regions showed the maximal amplitude for the summed harmonics of the general visual responses over the middle occipital (MO) regions across all three stimulation phases. The average baseline-corrected amplitudes of the general visual responses progressively increased from 3.19±0.64 μV, to 3.56±0.43 μV, and 3.90 ±0.72 μV across the three phases, respectively. Although there was a slight decrease in amplitude during and after tDCS, repeated measures ANOVA showed no significant changes between before and during tDCS (p=0.43), or between before and after tDCS (p=0.11). Similarly, the SNR presented a progressive increase from 9.99 ± 1.77 before tDCS, to 10.48 ±

1.49 during tDCS, and 12.10 ± 1.87 after tDCS, but no significant differences were detected across phases (p = 0.72 for P1 vs. P2, p = 0.14 for P1 vs. P3) (**Figure 53**).

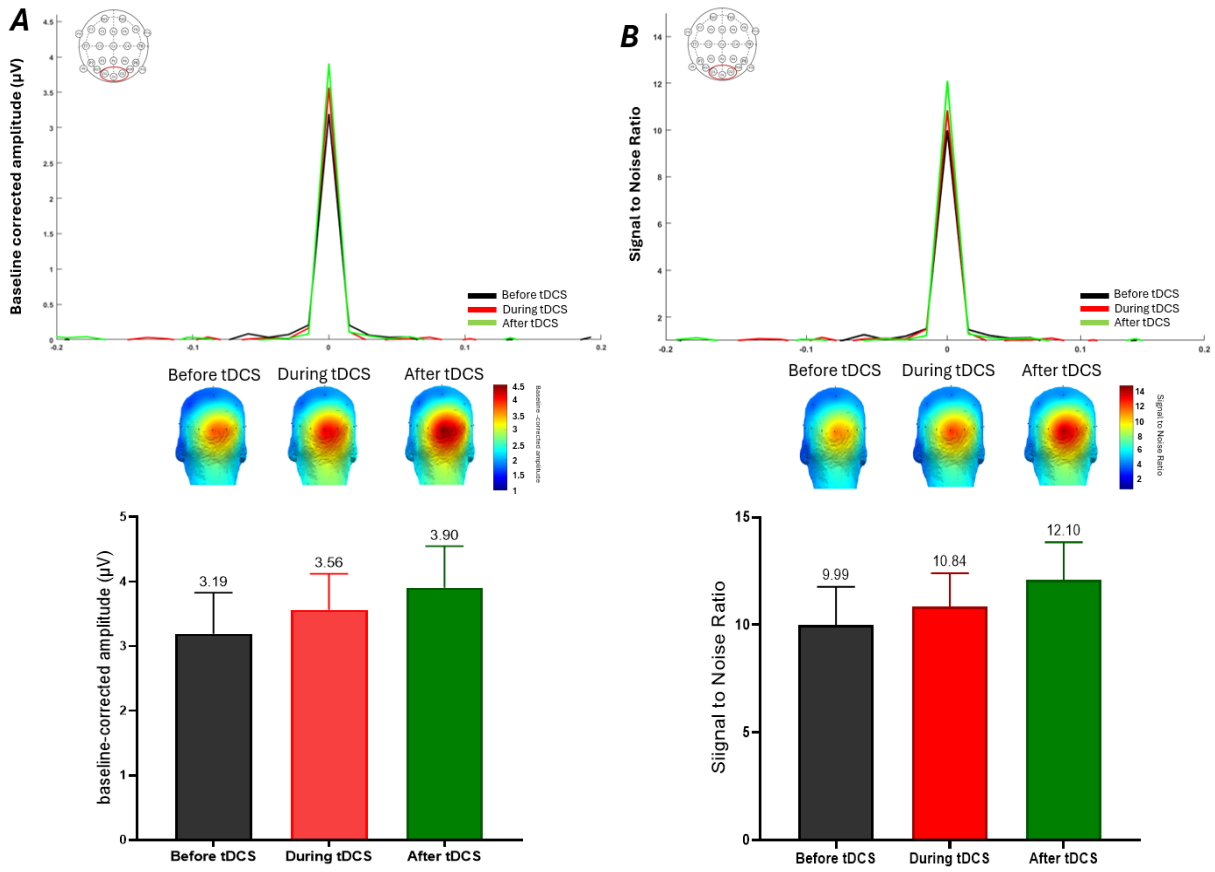

Figure 53. Baseline-corrected amplitudes and SNR of the general visual responses across phases.
Baseline-corrected amplitudes (A) and SNR (B) peaks of the sum of the five general visual frequency (6Hz) harmonics at the right medial occipital (MO) regions before (black), during (red), and after tDCS (green). Above: The spectrum is centered on the frequency bin of interest. 3D scalp map topographies of the general visual response across the three phases. Below, histograms of the baseline-corrected amplitudes and the SNR of the general visual responses across the three experimental phases in the MO regions. Baseline corrected amplitude of the general visual responses increased during and after tDCS in comparison to before tDCS, but no significant neuromodulation was detected (p=0.42 and p=0.11, respectively). Similarly, for the SNR, values increased during and after tDCS in comparison to before tDCS but didn't show any significance (p=0.72 and p=0.14, respectively, repeated measure ANOVA). Bars represent standard mean errors, and the mean is reported on top of each bar.

V. Discussion

V.1. Attenuation of face-selective responses detectability during tDCS in scalp EEG

The quantification of online neuromodulatory effects induced by tDCS has been challenging, largely due to methodological and physiological constraints (Gebodh et al., 2019; Woods et al., 2016b). In this study, we explored, in a unique methodology combining tDCS with scalp EEG recordings and FPVS, the neuromodulatory effects of tDCS on face-selective responses. The periodic nature of the visual stimuli generated frequency-tagged responses (face-selective and general visual responses) isolated in the frequency domain within small frequency bins (1/75 seconds: 0.013 Hz). Therefore, the frequency-tagging method enhanced the robustness of the recorded signals, making them less susceptible to EEG artifacts (Regan, 1989). This robust methodology facilitates a clearer and more reliable interpretation of the neuromodulatory effects of tDCS during and after stimulation.

The electrophysiological responses in the drug-resistant epileptic patients have been simultaneously recorded with intracerebral (iEEG) (reported in chapter **II**) and scalp electrodes (EEG) during FPVS-tDCS experimentation to target face-selective regions (VOTC) and compare tDCS neuromodulatory effects. With iEEG recordings from contacts in the right hemisphere, we observed a clear and statistically significant increase in the face-selective responses during and after stimulation (Chapter II, **Figure 40**). Meanwhile, scalp EEG recordings revealed an overall similar pattern of variation during and after tDCS, which didn't reach any statistical significance. Although intracerebral and scalp EEG signals were recorded simultaneously during the same tDCS experiment (anodal P10, +2mA, 20 minutes) and FPVS paradigm (Face localizer), the differences between their effects arise from methodological discrepancies. While iEEG signals measure the local field potential directly inside the grey matter of the face-selective brain regions with high spatial and temporal resolution, scalp EEG picks up signals from multiple brain sources at a distance from the scalp sensors (Koessler et al., 2015). Additionally, the recorded scalp EEG signals are more attenuated in comparison to iEEG due to the resistive properties of the skull, which aren't well characterized and difficult to accurately estimate during *in vivo* recording, particularly in humans (Koessler et al., 2017). The baseline-corrected amplitude of the face-selective response was attenuated by 6.4-fold on average across phases from the intracerebral to scalp EEG recordings. Moreover, the reduced number of patients included in scalp EEG investigation (n=8) in comparison to those included with iEEG recording (n=11) may have reduced our statistical power.

In parallel to the increasing signal amplitude recorded with scalp EEG electrodes, the SNR significantly decreased during tDCS, reflecting an increase in signal with a proportional rise in

background noise (**supplementary figure S6**). This suggests that tDCS may have modulated both the face-selective response and the surrounding neural or non-neural activity (noise). Although the response remained present, its detection may have been compromised during stimulation due to several methodological constraints associated with combining tDCS, scalp EEG, and iEEG. Despite the implementation of rigorous methodological and experimental controls, some tDCS-induced artifacts remain unavoidable. The tDCS stimulator may have produced broadband inherent artifacts, resulting in a current deviating from the ideal constant DC. Additionally, it may have injected noise from the impedance measurement into the recorded signal during stimulation (Gebodh et al., 2019). These artifacts might have been avoided in phases P1 and P3 (before and after tDCS), as we unplugged the stimulating wire from the tDCS stimulator after ramping but not during the active tDCS phase(P2). Furthermore, due to clinical investigation limitations, some noisy scalp electrodes were positioned near the tDCS stimulating electrode and were subsequently interpolated using the mean amplitude of neighboring electrodes. These findings highlight the importance of considering noise characteristics alongside signal strength when evaluating tDCS-induced neuromodulatory effects.

V.2. Comparison between iEEG results to Scalp EEG

One of the aims of this study is to investigate the correlation between scalp and intracerebral EEG responses during facial categorization, with a particular focus on electrophysiological neuromodulation induced by tDCS. iEEG recordings of the face-selective responses in the right VOTC revealed (chapter **II)** the significant neuromodulatory effect of tDCS, especially on the OCC and the PTL. Based on scalp topographies, five contiguous channels (P8, P10, PO8, Oz, and O2) distributed over the ROT regions were defined as the ROI for investigating face-selective responses. Given their anatomical and functional roles, we could assume that the OCC and the PTL in the VOTC serve as the main brain sources for the face-selective signal recorded by scalp ROT electrodes. Furthermore, utilizing the same recording setup (iEEG and scalp EEG) in epileptic patients during a frequency-tagging approach as the one we used, Jacques et al. (2020) provided a correlational investigation between scalp responses and intracerebral signals. They evidenced the presence of a significant correspondence between the right lateral IOG and four scalp electrodes in ROT regions (PO8, P10, P4, and O2). However, in our study, the right IOG (**Figure 40**, **chapter II**) revealed no significant neuromodulation of the face-selective response during or after tDCS, and its pattern of change across phases didn't align with the one revealed by scalp ROT electrodes. Moreover, scalp EEG recordings reflect a mixture of signals generated from multiple active brain sources, complicating the ability to isolate specific neuronal patterns (volume conductance). Additionally, artifact distortion due to methodological and physiological reasons can influence the signal recording during tDCS, which resulted in the investigation of the tDCS

electrophysiological influence only outside the stimulation period (D. W. Kim et al., 2019; Reinhart et al., 2016; Yang et al., 2014; Lafontaine et al., 2013; Antal, Kincses, et al., 2004).

Combining scalp EEG with tDCS and iEEG electrodes doesn't come without its challenges. Given the unique implantation schema for each patient, depending on their epilepsy profile, some scalp electrodes had to be repositioned to minimize interference with iEEG electrodes, ensure sterility near surgical sites, and reduce infection risks (Barborica et al., 2021). Before the tDCS experiment (day 5 of clinical exploration), conductive gel is reapplied to the scalp electrode, as the quality of the signal is usually degraded underneath the protective sterile surgical head cap. The latter is reapplied over the scalp electrodes before experimenting to minimize infection risks. Interestingly, through the investigation of the epileptiform discharges near skull defects using scalp EEG, MaderJr et al., 2018 revealed the possible modification in the distribution of the EEG voltage on the scalp near skull holes. Although SEEG induced skull holes are very small, slightly exceeding 0.8 mm (diameter of implanted depth electrode), the possibility of a scalp EEG signal distortion related to the implanted electrodes cannot be rejected.

V.3. tDCS disrupts surface synchrony while enhancing deep neural activity

In the aim of investigating tDCS electrophysiology effect on the brain outside of a clinical setting, in a context closer to home-based use, we also performed the same tDCS protocol in 18 healthy controls with only scalp EEG recordings (Torro-Alves et al., 2025, *submitted*). Scalp EEG recordings in healthy controls revealed an important decrease in the SNR and amplitude during tDCS, followed by a significant rebound effect after tDCS, which manifested as an increase in both measures for the face identity response. Although the same tDCS experimental parameters (20 min, +2mA, anode over right occipito-temporal cortex on P10) were applied during a three-phase sham-controlled protocol in both simultaneous iEEG-EEG and only EEG experiments, each study revealed different findings, especially after tDCS.

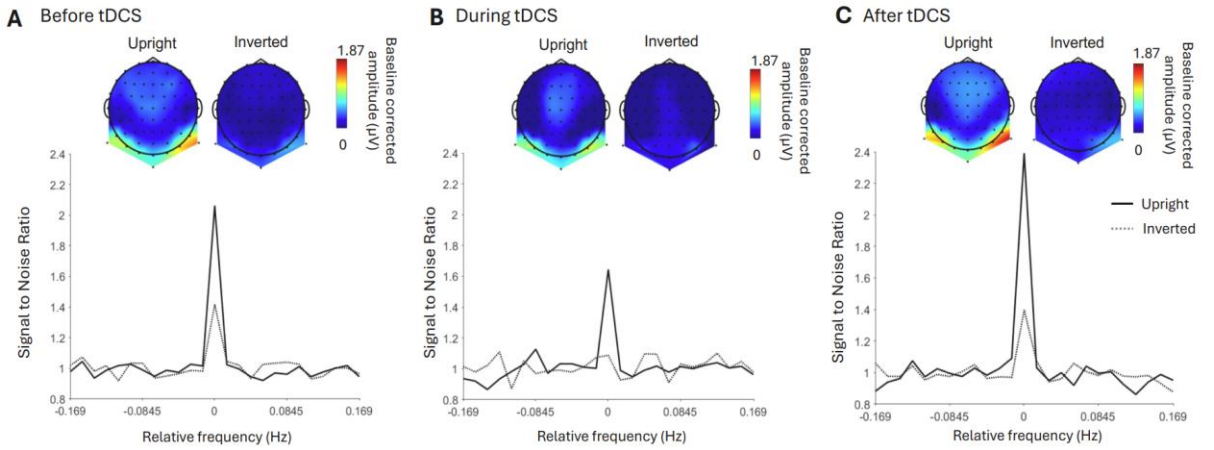

Figure 54. Face-identity discrimination responses at Bilateral OT regions across tDCS phases.
Grand-averaged SNR of the summed response at the first six harmonics of 1.2 Hz, measured bilaterally over occipitotemporal (OT) regions, for upright faces (black solid lines) and inverted faces (grey dotted lines), across three experiential phases: (A) before tDCS, (B) during tDCS, and (C) after tDCS. The frequency spectrum is centered on the target frequency bin. Scalp topographies displayed above each spectrum illustrate the baseline-corrected amplitude response at 1.2 Hz and its harmonics. Adopted from (Torro-Alves et al., 2025, *submitted*)

The difference between these findings can be attributed to the difference in experimental set-up conditions. In our study, patients were evaluated in a clinical setting with a less controlled environment for artifacts during simultaneous iEEG and scalp EEG recording, whereas in Torro-Alves et al. (2025), healthy controls were assessed with scalp EEG only in an EEG laboratory with better control over signal distortions. In addition, a 64-channel EEG cap was used for recording, allowing for a more consistent and standardized placement of the scalp EEG and tDCS electrodes across participants and minimizing variability. In contrast, due to clinical constraints, the 26 scalp EEG electrodes and tDCS electrodes had to be repositioned and adjusted for each patient, depending on their implantation profile, mainly to reduce infection risk. Moreover, the difference in the size of the population included in the study (18 for Torro-Alves et al., 2025 vs 8 in our study) directly influenced our statistical power. Additionally, although both studies used FPVS paradigms related to facial recognition, they differed in their specific focus: the face localizer targeted regions associated with general face-selectivity, whereas the latter focused more on facial identity processing. This distinction may have primed different neural regions, leading to distinct patterns of modulation during the tDCS phase. We can hypothesize that the effective control of experimental set-up and procedures in Torro-Alves et al. (2025), combined with a larger sample size, contributed to a more precise targeting of the VOTC and may explain the significant post-tDCS effects they observed.

In the current literature, the exploration of tDCS electrophysiological effects is mainly limited to offline investigation, i.e., recording brain activity after tDCS, due to the broadband artifacts occurring during tDCS. Recent work of Civile et al. (2020) combined tDCS with simultaneous scalp EEG to investigate the impact of online tDCS on the N170 component for the FIE. In accordance with previous

studies (Civile, 2020, 2019, 2018), their findings demonstrated that anodal tDCS at 1.5mA reduced recognition for upright faces, and consequently the FIE, as evidenced by increased N170 latency and reduced amplitude during stimulation. These findings seem to be in accordance with the anodal tDCS at 2mA during EEG recording and FPVS paradigm from Torro-Alves et al. (2025). The FPVS approach adopted here allows for an automatic, robust, and objective identification of the face identity discrimination response when faces are presented periodically in upright and inverted orientations (**Figure 28, Chapter I**). The differential response between upright and inverted face individuation reflects the FIE, which seemed to be reduced during tDCS (P2) as indicated by the reduction in the amplitude and the SNR of the upright face individuation responses. Civile et al. (2024) argued that tDCS seems to influence the configuration of cognitive processing by increasing the generalization between stimuli and maintaining salience for their common features. Although this theory seems logical during stimulation, it's contradicted by the significant rebound effects perceived after tDCS reported in Alves et al. (2025).

Contrary to our expectations, Torro-Alves et al. (2025) found a reduction in the amplitude and the SNR of the face-identity discrimination response during tDCS. Notably, immediately after tDCS to the occipitotemporal region, the amplitude and the SNR of the face identity response increased significantly. This rebound effect may reflect a transient interference with ongoing neural synchronization during stimulation, followed by a compensatory enhancement in cortical excitability or a network reorganization once the stimulation is stopped. In our study, a partially similar pattern was observed in the scalp EEG data during stimulation. Although the amplitude increases post-stimulation did not reach significance, we found a significant reduction in SNR during tDCS, which might indicate a similar disruption of synchronized neural activity. Interestingly, this effect was not observed with intracerebral recordings, where a significant increase in amplitude both during and after stimulation was present. This discrepancy could be explained by the differences in spatial resolution and sensitivity between local and large-scale networks. Intracerebral electrodes directly capture local excitability changes, while scalp EEG is more susceptible to noise during stimulation. As a result, some of the effects might be masked in the scalp signal during tDCS and only emerge after.

Taken together, these results could suggest that tDCS may transiently disrupt surface-level synchrony (as measured by scalp EEG) while enhancing deeper or more localized neural activity (as measured by iEEG), leading to apparent rebound effects that may depend on the recording method, stimulation timing, and task used. According to the assessment of regional cerebral blood flow (rCBF) during and after tDCS using an arterial spin labeling MRI, anodal tDCS leads to a notable increase in rCBF during stimulation, which persists after stimulation (Zheng et al., 2011). These hemodynamic changes may reflect desynchronization of local neural processing, particularly in the ROT regions close

to the stimulating electrode, receiving the strongest EF. tDCS could locally enhance neural activity in the occipitotemporal regions, resulting in irregular neural firing and disruption of the ongoing neural network. Additionally, the rebound effect observed in scalp EEG recording following stimulation is in accordance with the delayed increase in rCBF, which suggests a reconfiguration of neural activity that depends on the stimulation phase.

V.4. Reconsidering stimulation sites in face recognition: VOTC or DLPFC?

Notably, what differentiates our study and Torro-Alves et al. (2025) from the investigation in Civile et al., 2020, beyond the use of the FPVS approach and frequency domain analysis is the placement of the stimulating electrode at P10, targeting the right VOTC. Several studies (Civile, 2020b, 2020a; 2019; 2018; Lafontaine et al., 2013; Reinhart et al., 2016) have adopted a tDCS montage where the anodal electrode is mainly targeting the right DLPFC for modulating face recognition. This decision seems to be driven by two main methodological and functional aspects.

Firstly, the belief that tDCS-induced EF is diffuse and superficial, thereby cannot reach deeper brain regions in the occipito-temporal cortex, limiting its efficacy in altering its excitability. On the other hand, DLPFC is a superficial frontal area that is easily accessible for targeting with tDCS. However, recent reports from (Louviot et al., 2022) have shown the ability of a low-intensity tDCS using only 2 HD electrodes to target deep brain structures like the hippocampus and the cingulate gyrus close to the VOTC. Additionally, simultaneous scalp and iEEG recordings revealed the major cortical role the IOG (in the VOTC) plays in the generation of the face-evoked N170 when viewing upright and inverted faces (Jacques et al., 2018).

Secondly, the DLPFC plays a critical role in top-down cognitive processes like attention, memory, and decision-making, which are essential when performing face recognition tasks. However, it seems that the type of face recognition paradigms they employed requires not only perceptual encoding of facial features but also integration of other cognitive functions (Civile et al., 2024; Lafontaine et al., 2013; Sanchez et al., 2016; Tian et al., 2024). In this regard, our use of the FPVS paradigm offers a key methodological advantage as it allows for the implicit and periodic presentation of face stimuli, resulting in automatic and frequency-tagged electrophysiological responses that are less affected by task demands or participant attention (Rossion et al., 2015a). Moreover, tDCS and TMS targeting DLPFC revealed valuable insight into its involvement in the processing of different facial aspects like recognition of facial expression (Mattavelli et al., 2013), face selectivity (Mattavelli et al., 2016), and facial trustworthiness (Ferrari et al., 2016). Targeting the VOTC responses induced by the FPVS with tDCS doesn't diminish the importance of the DLPFC in facial processing but allows the use of

a well-adapted method to quantify the electrophysiological effects of tDCS with high sensitivity and specificity.

V.5. Effects of tDCS on the contralateral hemisphere

The contralateral influence of DES has been recently reported (Angelini, Jacques, et al., 2024; Angelini, Volfart, et al., 2024; Volfart et al., 2023) providing evidence of the inter-hemispheric effective connectivity when stimulating a functional face-selective region in the brain. However, we weren't able to replicate these findings when applying a low-intensity tDCS with 2 HD electrodes in our experiment. In contrast, Torro-Alves et al. (2025), using our same tDCS protocol, with the anode over the right OT cortex (P10 scalp EEG position), successfully influenced the face identity discrimination response in the left hemisphere. They reported a decrease in the SNR during tDCS, followed by an important increase after stimulation, i.e., replicating the rebound effect on both left and right occipitotemporal regions. Their findings suggest that the two functional regions, right and left VOTC, under the influence of tDCS, can synchronize their activity to achieve optimal face identification performance. Notably, a TMS study examining the causal role of both right and left STS in facial expression processing found that, although the right STS was more actively involved than the left, effective recognition of facial expressions depended on computations performed in both right and left STS (Sliwinska & Pitcher, 2018). These results from tDCS and TMS studies suggest the potential modulatory influence of a right hemispheric occipitotemporal tDCS on both ipsilateral and contralateral face-selective regions. Indeed, future studies should aim to increase the number of patients evaluated with this protocol and, potentially, the number of scalp electrodes used to capture electrophysiological activity in response to tDCS, in order to strengthen the statistical power and support more robust conclusions.

Notably, the interaction between both right and left occipitotemporal regions and their potential functional synchronization raises an important question concerning left hemispheric stimulation. The occipitotemporal regions in the left hemisphere have been demonstrated to have a crucial role in visual word processing, in particular the visual word form area in the left VOTC (Lochy et al., 2015, 2018; Rossion & Lochy, 2022; Volfart et al., 2021). Despite its substantial contribution to visual word processing, the left VOTC exerts some face discrimination properties: responds to objects and faces, but with less selectivity for faces than the right hemisphere (Jonas et al., 2016). As the left VOTC supports multiple cognitive and perceptual functions (Hagen et al., 2021), its electrical stimulation with tDCS could potentially enhance its performance for face processing, especially for face identification. In contrast, a previous TMS study targeting the face-selective OFA also failed to demonstrate bilateral effects where stimulation of the right OFA significantly influenced discrimination of individual face parts (eyes, nose, mouth), whereas TMS of the left OFA had no effect (Pitcher et al., 2007). Nevertheless, the

objective and robust FPVS approach utilized in this study in combination with a tDCS protocol targeting the left occipitotemporal regions (P9 and FT10 scalp EEG positions) could potentially clarify the doubts regarding this issue.

VI. Perspectives and Conclusion

All in all, combining tDCS with simultaneous iEEG and scalp EEG recording during an FPVS paradigm reinforces the investigation of the online effects of tDCS and allows for the quantification of its electrophysiological impact using frequency-domain analysis. This study represents an initial step toward integrating FPVS paradigms into the study of tDCS-induced neuromodulation and addressing current methodological limitations in scalp EEG. Future work should focus on improving artifact rejection techniques and refining this approach to facilitate clearer and more reliable assessments of tDCS effects on brain activity.

Comparing intracerebral and scalp EEG investigation of tDCS neuromodulatory electrophysiological findings suggests that tDCS may transiently disorganize the cortical network near the stimulation site and simultaneously enhance neural activity in deeper brain regions. However, further investigation of the intracerebral electrophysiological effect of tDCS on face identity discrimination is needed to fully confirm this conclusion. Data from intracerebral investigation have already been collected from 12 drug-resistant epileptic patients performing a face identity FPVS task during tDCS and require further analysis of the scalp EEG and iEEG recordings. Investigating identity discrimination using combined iEEG and tDCS can clarify the neuromodulatory effects of tDCS on local and network levels. Additionally, it could allow the comparison between the impact of tDCS on two closely related aspects of facial cognition: general face discrimination and face identity recognition.

Furthermore, implementing this robust methodology (tDCS with scalp EEG and FPVS) allows the investigation of different cognitive functions, like word recognition. By applying tDCS using an adapted electrode montage targeting the left hemisphere (P9 and FT10), where word recognition is typically lateralized, it allows the investigation of the neuromodulatory effects of tDCS on word processing in the human brain. Notably, as reported in (Hagen et al., 2021) some regions in the left VOTC, i.e., the fusiform gyrus and its surrounding sulci, exhibit an overlap in the representation of faces and words. Targeting these regions with tDCS could help uncover how electrical stimulation modulates category-selective neural responses and whether it differentially affects face and word processing within overlapping cortical regions.

In conclusion, our methodology enables the transition of tDCS findings from invasive intracerebral investigations to non-invasive and user-friendly scalp EEG recordings. Consequently, refinement of this methodology may reduce the reliance on invasive methods for investigating tDCS neuromodulation. Ultimately, this supports the use of non-invasive EEG for monitoring tDCS neuromodulation effects in research and future clinical settings. It also opens the possibility of applying tDCS combined with scalp EEG recording in home-based settings.

VII. Supplementary Materials

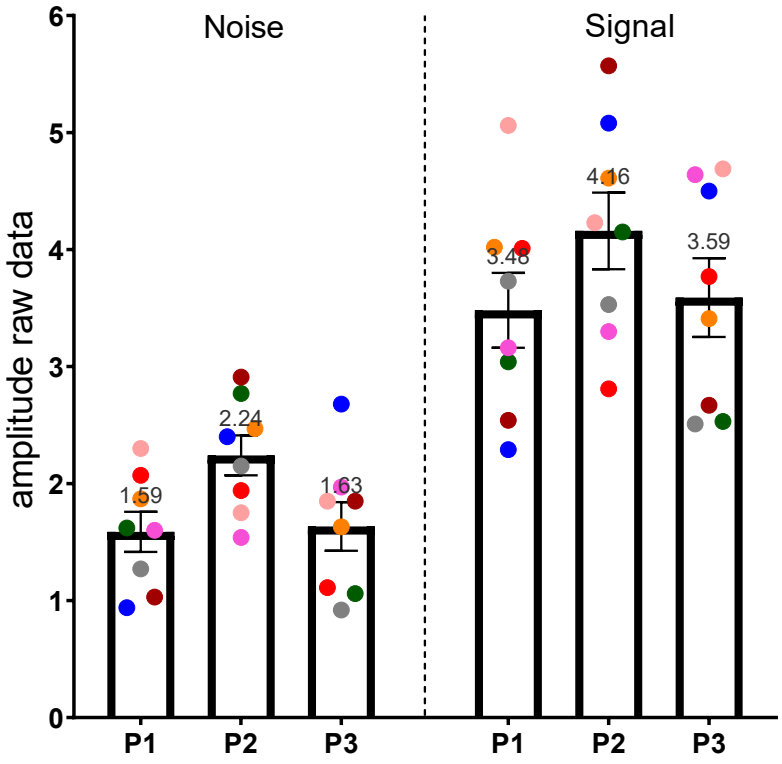

Supplementary Figure S6. Raw EEG signals for both signals and noise across phases.
Average amplitudes of the raw EEG signals amplitude for both signals (i.e., the face-selective responses at 1.2Hz and harmonics) and noise (i.e., the 25 frequency bands surrounding the face-selective responses) before (P1), during (P2), and after tDCS. During tDCS, the noise increases in comparison to before tDCS and follows the same trend of variation of the signal. Each dot represents the average amplitudes for each patient.

Chapter IV: Cognitive EEG Biomarkers recorded with Wireless Neuronaute and Icecap: A frequency-tagging Validation Study

- ***Objective:*** Evaluate the performance of a novel wireless EEG device: Neuronaute® paired with the ultrathin Icecap® for recording cognitive EEG biomarkers.
- ***Methods:*** Two Scalp EEG caps (*Icecap* and *Electrocap*) combined individually with the *Neuronaute* (new EEG acquisition system) and *FPVS,* n= 20 healthy participants.

Highlights

1. Icecap and Electrocap electrode systems demonstrate similar efficiency in detecting cognitive EEG measures (amplitude, SNR, and topographic patterns).
2. Both electrode systems detected evoked EEG responses in a stable and consistent manner, as evidenced by significant inter- and intra-cap correlations.
3. Despite impedance measurement errors (19%) associated with the Neuronaute, Similar impedance values were reported from both electrode systems.
4. Combining FPVS with the Neuronaute-Icecap system offers a reliable, high-quality alternative for electrophysiological research and clinical applications.
5. Potential use of the Neuronaute coupled with the Icecap for EEG acquisition and wireless data transmission in a home-based environment.

The work described in this chapter is under submission as a paper to the Journal of *Clinical Neurophysiology*:

Tabikh, M., David, J., Rossion, B., & Koessler, L. (2025). Cognitive EEG Biomarkers recorded with Wireless Neuronaute and Icecap: A frequency-tagging Validation Study.

I. Introduction

The electroencephalogram, which refers to the recording of the electrical brain activity using electrodes placed on the scalp, is a century-old method (Adrian & Matthews, 1934; Berger, 1929). Although it is well established, it continues to be widely used to assess both normal and abnormal brain functions across different age groups, from development and adulthood, to aging (Regan, 1989). One commonly used approach involves recording stimulus-triggered changes in EEG activity, known as ERPs, which are associated with sensory, motor, or cognitive stimuli. Due to the low SNR of individual EEG responses in the time domain, ERPs are obtained by averaging multiple event-related EEG experimental trials (S. Luck, 2005; Dawson et al., 1951). Since the 1990s and with the digitization of EEG signals, a growing number of systems with different technologies have been developed to record EEG. For cognitive research, high-spatial and high-temporal resolution EEG systems were developed (Gevins et al., 1995). These systems are often non-portable, expensive, and not user-friendly, requiring technical expertise within controlled laboratory environments. Conversely, for easier clinical investigations (i.e., spontaneous EEG recording), wireless, portable, inexpensive, and easy-to-use EEG systems have been developed. However, these systems are rarely validated for cognitive measures analysis and are therefore seldom used for routine cognitive evaluations.

The *Neuronaute*® is a portable medical EEG recording system from *Bioserenity*® (the company that funded the Cifre grant for the first two years of this thesis project, Grant number 2021/0324) that allows wireless data transmission to a storage cloud for remote clinical reviewing. This innovative technology is user-friendly and compatible with several scalp EEG caps, making it an efficient tool for fast patient tuning around and large-scale clinical use in routine EEG. It supports long-term EEG monitoring for up to 72 hours, which is particularly beneficial for managing chronic neurological disorders like epilepsy. The *Icecap®* is an adaptable, disposable, ultrathin, and flexible scalp EEG cap compatible with the Neuronaute system. The single-use cap guarantees routine and long-duration EEG recordings with optimal rapid application (*Neuronaute*, n.d.).

Monitoring the clinical effects of tDCS can be challenging, often requiring sophisticated EEG setups and specialized technical expertise. In the previous chapters, we've addressed these limitations via the simple approach combining scalp EEG-tDCS and FPVS. Hence, the present study evaluates the *Neuronaute*®, an easy-to-use, clinically efficient, and wireless EEG system coupled with an ultrathin *Icecap*®, aiming to provide a practical solution for reliable cognitive electrophysiological measurements. Our primary goal here was to validate this system by characterizing the quality (i.e., amplitude, topography, and SNR) of evoked EEG biomarkers recorded in healthy adults with the

Neuronaute coupled with the Icecap, compared to the Neuronaute coupled with a well-validated EEG cap, the *Electrocap*®, used in clinical research. While this study did not combine tDCS with EEG recordings in a wireless system, it lays the groundwork for such application. Ultimately, the goal is to integrate Neuronaute with tDCS and FPVS in longitudinal, home-based settings; such a capability would be particularly valuable for identifying when the after-effects of tDCS begin to fade and when a new session might be needed. Thereby, it would reduce the need for repeated hospital visits and enable remote monitoring of the neuromodulatory effects of tDCS, particularly during and after stimulation.

To objectively evaluate the performance of the two scalp electrode systems, we rely on the technique of frequency-tagging (FPVS), which consists of presenting a stimulus at a rapid periodic rate and analyzing EEG responses in the frequency domain (SSVEP, Regan, 1966). The characteristics of this robust approach (sensitive, implicit, objective) offer key advantages for EEG-based cognition measures, particularly when comparing populations or validating systems, since it produces high SNR neural responses that can be objectively identified and quantified at the known stimulation frequency in the frequency domain (Norcia et al., 2015; Rossion et al., 2015a; Regan, 1989)(section IX, Chapter **I**).

In the present study, we used a specific rapid oddball paradigm validated over the past decade for measuring (unfamiliar) face identity recognition (original study:(Liu-Shuang et al., 2014a); see also (Rossion et al., 2020) for review;(Hagen et al., 2024)). The face identity discrimination paradigm allows the isolation of the response to a new face identity presented between same face identity images, reflecting high-level visual processing.

II. Main Objectives

The main objective of the study in Chapter **IV** is to investigate the ability of the Neuronaute-Icecap® system to perform effective electrophysiological measurements of cognition through:

(i) Characterize the quality of the evoked EEG responses with the Neuronaute coupled with the Icecap compared to the Neuronaute coupled with the Electrocap.
(ii) Investigate the correlation between the sequences within the same system, as well as the correlation between both systems (Icecap vs Electrocap).
(iii) Compare the recorded impedance and the setting up time for both scalp EEG systems.

III. Materials and Methods

III.1. Participants

Twenty participants (10 males; mean age = 25.2 ± 7.09, range = 20-54) were recruited for this experiment. All participants provided written consent to participate in the study, which was conducted in accordance with the principles outlined in the Declaration of Helsinki and approved by a local ethics committee. They received financial compensation for their participation. Among the participants, only one was left-handed. All participants had normal or corrected-to-normal vision, and none reported a history of neurological, psychiatric, or dermatological disorders.

III.2. EEG Acquisition

III.2.1 Neuronaute: a Wireless EEG System

The Neuronaute® EEG System is a CE 2797 marked Class IIa medical device, as per regulation (EU) 2017/745, and a Class II medical device according to the classification regulation of the Food and Drug Administration (FDA). It allows recordings of up to 24 EEG channels. The Neuronaute® is easy to use, offering wireless transmission of the recorded EEG data to the cloud and real-time notifications, enabling clinicians to monitor recordings remotely, which is particularly beneficial for at-home or remote testing.

EEG recordings were obtained from the Neuronaute® (Ref: 1001-15015-EU) by randomly and sequentially connecting both the Icecap® (see section 2.2.2) and the Electrocap® (see section **2.2.3**). The Neuronaute is composed of a BioAdapter that allows the use of touch-proof electrode connectors that individually record: 24 EEG channels, 1 environmental noise channel, 2 bipolar EMG channels, 1 ECG channel, 2 GND channels, which allow grounding, and 2 REF channels for referencing (**Figure 55**). The BioAdapter can also be connected directly to the Icecap via an adapter (i.e., IceAdapter®). A high-capacity battery that enables recording for up to 72 hours is also attached to the BioAdapter.

Electrophysiological signal was recorded at a sampling rate of 250Hz and transmitted by Wi-Fi via a detachable box that clips onto the terminal (i.e., the Head Module). The EEG signals were visualized in real time on the Neuronaute web platform installed on a tablet device. A notch filter at 50 Hz was applied to visualize the recordings during the experiment. After ending the recording, the data was stored locally on the recorder and then transmitted to the N-CLOUD web platform via Wi-Fi.

To synchronize EEG recordings with the cognitive tasks (i.e., the periodic visual stimuli displayed on a screen), analog triggers were inserted into the Neuronaute recordings via the ECG touch-proof connector electrode. These triggers were generated by a photodiode placed on the screen

that detected the color changes of a square displayed on the screen below the photodiode that went from black to white between each stimulus presentation.

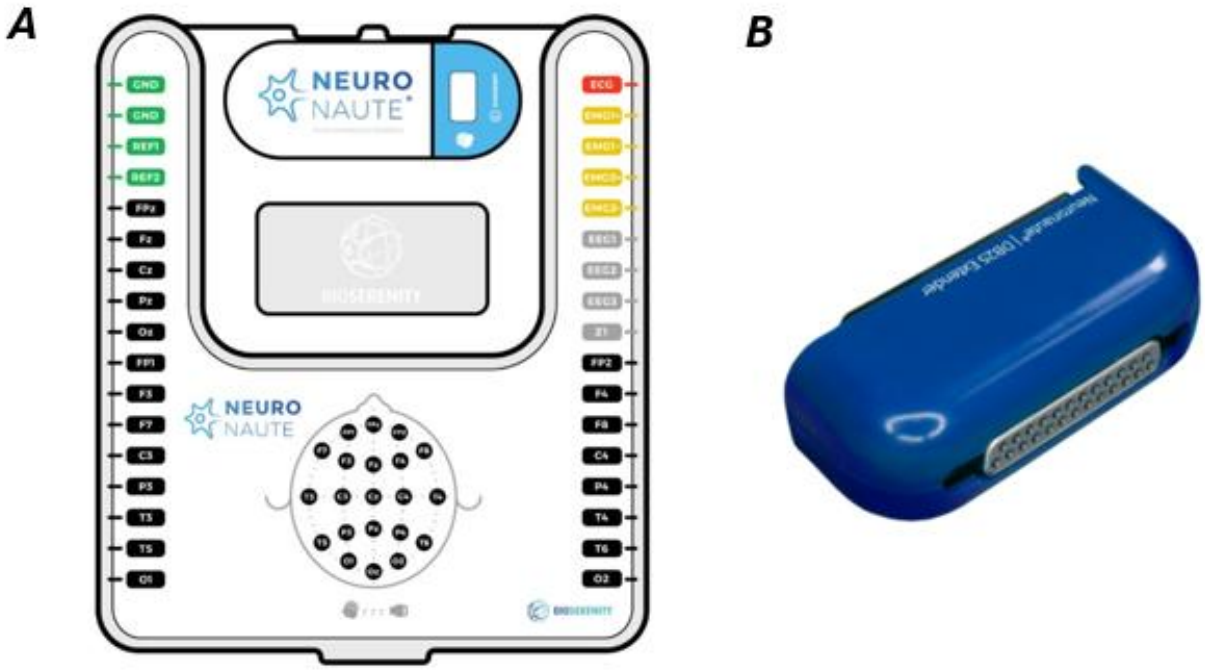

Figure 55. A. Schematic representation of the Neuronaute.
A. The Neuronaute device comprises a BioAdapter terminal equipped with both touch-proof electrode connectors and a dedicated Icecap connector. This setup recorded data from 24 EEG channels referenced to a common reference. ***B.*** Image of the DB25 connector

a. Icecap: An Ultrathin EEG Net

The *Icecap*® is a CE marked class I medical device developed by Bioserenity to be used with the Neuronaute®. The Icecap (Ref: 1001-01010-EU, V2) is an ultrathin, single-use, and non-washable net.

It's made up of flexible copper ribbons that incorporate scalp electrodes coated with a thin layer of silver to optimize electrical impedance. The cap is equipped with 21 electrodes (Fp1, Fp2, F7, F3, Fz, F4, F8, T7, C3, Cz, C4, T8, P7, P3, Pz, P4, P8, O1 and O2. Fpz is built in as the ground channel, and Oz as the reference channel. The Icecap was placed on the scalp surface thanks to four adhesives fixed on the right and left temples, between the eyebrows, and on the neck of the head (**Figure 56A**). Once the Icecap was set up, EEG paste (Elefix V, Nihon Kohden) was applied under each electrode using a standard 20 ml syringe (without a needle). The hair beneath each electrode was carefully parted using either fingers or a plastic syringe. Each electrode was gently pressed to ensure the EEG paste adhered properly to the scalp. Setting up the Icecap took 16 ± 5 minutes on average.

b. Electrocap: a widely clinically used EEG cap

The other cap used in association with the Neuronaute was the standard Electrocap® (Electrocap International, INC, USA). The cap consists of 23 EEG channels (FP1, F3, C3, P3, O1, F7, T7, P7, AFZ, FZ, FT9, P9, FP2, F4, C4, P4, O2, F8, T8, P8, CZ, PZ, FT10, P10) (**Figure 56.B**). AFz electrode is built-in as the reference and ground. Each channel was connected individually to its corresponding touch-proof connector on the Neuronaute BioAdapter.

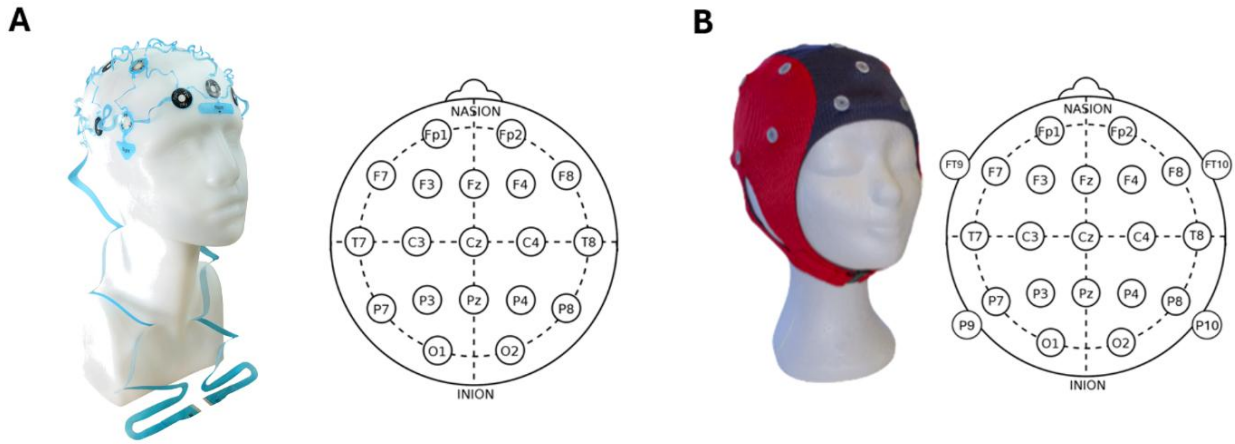

Figure 56. Schematic presentation of both EEG recording caps.
A. The ultrathin Icecap net is equipped with 19 EEG channels. Electrodes are directly included in a flexible copper ribbon and coated with a thin layer of silver. The net is placed on the scalp using several adhesive fixations points: the right and left temples, in between the eyebrows and on the neck of the head. ***B.*** The Electrocap is equipped with 23 EEG channels. Electrodes are made with Ag/AgCl disks. Electrocap is held in place by a chin strap.

Since the Electrocap has more EEG channels than the touch-proof EEG connectors on the BioAdapter, basal temporal electrodes (FT9, FT10, P9 and P10) were inserted into free supplementary touch-proof connectors. For signal processing, these channels were renamed during the analysis process. Setting up the Electrocap took 11 ± 3 minutes on average.

III.3. Fast Periodic Visual Stimulation

To induce well-defined cognitive evoked EEG responses, we used a FVPS paradigm extensively validated in several previous studies performed (e.g.,(Dzhelyova et al., 2019; Vettori, Dzhelyova, et al., 2019; Liu-Shuang et al., 2016, 2014a; see Rossion et al., 2020 for review). It consisted of 25 male and 25 female face images, all unfamiliar to the participants and displaying neutral expressions. The images were cropped to exclude any external features such as hair and ears and were shown on a grey background (**Figure 57A**). They were 290 ± 9 pixels in height and 188 ± 12 pixels in width, with an image resolution of 480 ppi. When viewed from 80 cm from the computer monitor, the stimuli subtended a

visual angle of approximately 5 × 4 degrees. To create inverted faces, the images were flipped vertically along the horizontal axis.

III.4. Experimental Procedures

The EEG-FPVS experiment was conducted in a quiet, dimly lit room. Each participant was tested with both caps (i.e., Electrocap and Icecap) during the same testing session, half of the participants starting with Icecap® and the other half with the Electrocap®. Participants washed and dried their hair in between the testing of the two caps. Scalp electrode impedances were measured and maintained low (i.e., from 5 to 10 kΩ as recommended by the International Federation of Clinical Neurophysiology; Babiloni et al., 2020) for all electrodes on both caps.

After installing the cap, participants were seated in front of a computer screen where the FPVS paradigm was presented. The same face identity image was displayed at a frequency rate of 6 Hz (i.e., 6 images per second) with different identities (randomly selected from the remaining 24 faces in the set) periodically appearing every 7 images, corresponding to a frequency rate of 0.856 Hz (6/7) (i.e., presentation pattern: AAAAAA**B**AAAAAA**C**AAAAAA**D**AA…, see **Figure 57A**). As shown in **Figure 56B**, each sequence started with a 2 to 5-seconds (display of a grey background with a fixation cross, followed by a 2-sec fade-in period where the stimulus contrast gradually increased from zero to full contrast to minimize sudden-onset reactions like blinking.

Then, the stimuli were shown for 60 seconds, ending with a 2-sec fade-out (**Figure 57B**). Stimuli were presented using sinusoidal contrast modulation (Liu-Shuang et al., 2014a; Rossion & Boremanse, 2011). Each presentation cycle lasted 166 msec (i.e., 1000 milliseconds/6) and began with a grey background with the faces appearing and reaching full contrast at 83 ms before decreasing again at the same rate (**Figure 57B**). To minimize low-level effects, stimulus sizes varied between 74% and 120%, with a 2% step. Two sequences were run with the female face stimulus set and two with the male face stimulus set (4 upright condition sequences in total). To further control for low-level visual effects, two additional sequences were run with inverted faces (“inverted condition”). In total, each participant completed with each cap six sequences of 66 seconds each, with randomized sequence order. Considering the unequal number of sequences by condition, analyses of condition effect were run by comparing only the first two Upright sequences (out of four) with the two inverted sequences.

To maintain consistent attention levels throughout the experiment, participants performed an orthogonal cognitive task, being asked to press a response box button whenever the fixation cross at the center of the screen briefly changed color (for 1 second, from blue to red). These color changes occur randomly 10 times per trial. In this study, mean accuracy at detecting the color change were

similar between caps (Icecap: 98.68±3.88%, Electrocap: 98.68±3.05%; F (1.18) =0, p>0.99), and across condition (Up: 98.35±4.09% and Inverted: 99.01±2.73 %; F (1.18) =0,97, p=0.34). Mean correct reaction times (RT) were also similar between caps (Icecap: 0.42±0.06s, Electrocap: 0.42±0.06s; F (1.18) =0.03, p=0.86), and across conditions (Up: 0.43±0.06s and Inverted: 0.42±0.06s; F (1.18) =0.19, p=0.67).

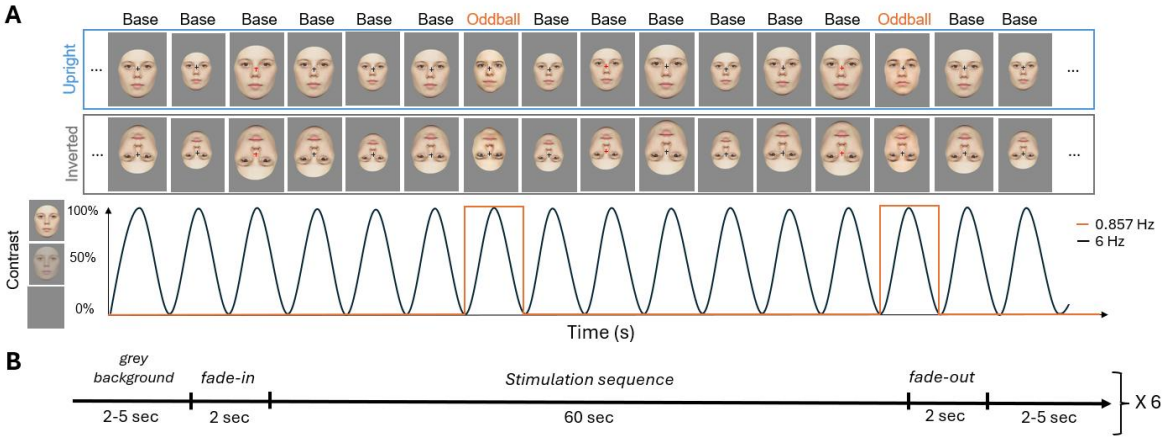

Figure 57. Representation of the experimental design paradigm.
A. The same face identity was presented at a frequency of 6Hz (Base), with a different identity face (Oddball) appearing every seven stimuli. As depicted at the bottom of the figure, stimuli were presented with a sinusoidal modulation, reaching full contrast halfway through the presentation time. Faces were displayed either upright or inverted. A blue cross was centered on the screen, randomly changing color to red. Participants were required to press a button whenever the cross changed color. **B.** Each stimulation sequence began with 2 to 5 seconds of a grey background, followed by a 2-second stimulus fade-in. The main stimulation lasted for 60 seconds, ended with a 2-second fade-out and another 2 to 5 seconds of grey background. Each participant completed 6 sequences.

III.5. EEG Analysis

EEG analyses were conducted using *Letswave 6*, an open-source toolbox (https://www.letswave.org/) operating on MATLAB R2021a (MathWorks, USA). Data processing protocols largely followed established methodologies from prior research (e.g., with the same paradigm; Dzhelyova et al., 2019; Vettori, et al., 2019; Liu-Shuang et al., 2014) but is detailed below.

Two EEG recordings were imported for cap testing for each participant (e, one for each EEG cap). The start of each sequence was determined based on the trigger from the photodiode, which indicated the onset of image presentation within each sequence. The data were filtered by a Fast Fourier Transform (FFT) multi-notch filter with a 0.5 Hz bandwidth to remove electrical noise at 50 Hz and its two harmonics (100 and 150 Hz).

Then, the data were segmented by sequence, covering 2 seconds before and after the sequence (-2 to 64 sec). Eyeblink correction was applied to recordings from both recording systems from participants who exhibited more than 0.2 blinks per second on average during the sequence for at least one recording (Retter & Rossion, 2016) using independent component analysis (ICA). Only one

identifiable component was removed in 8 participants for both recordings. For individual channels with artifacts (one channel for 7 participants for Electrocap recording) interpolation was conducted with linear combination of the three neighboring channels. One epoch was removed from the Electrocap recording of one participant due to excessive noise. All EEG channels were re-referenced to a common average reference using only the 19 electrodes that are common to both caps (i.e., C3, C4, Cz, F3, F4, F7, F8, Fp1, Fp2, Fz, O1, O2, P3, Pz, P4, T7, T8, P7, P8).

Each sequence was then re-segmented to an integer number of 1Hz cycles, with exclusion of fade-in and fade-out stimulation portions. The resulting cropped epochs were 59.64 seconds long corresponding to exactly 14 887 bins in total. Epochs of the same condition were averaged in the time-domain for each participant to increase SNR. Then, Fast Fourier Transform (FFT) was applied, and the amplitude spectra was extracted, with a high frequency resolution of 0.0168 Hz (1/59.54 seconds).

To compare the scalp EEG responses (for both identity discrimination responses and general visual responses) of the two EEG sensor nets, different scalp regions of interest (ROI) (including several electrodes) were defined using visual inspection of the topographical maps from both recording caps (**Figure 58**; see also Rossion et al., 2020). The ROI for identity discrimination EEG responses (at 0.856 Hz and harmonics) included the right and left occipito-temporal regions (P8 and P7 channels, respectively). The ROI for general visual EEG responses (at the base rate 6Hz and harmonics) included the left and right occipital regions (O1 and O2 channels). All these ROI were in accordance with our previous studies that used this cognitive paradigm.

To identify significant responses at the frequency of interest and harmonics, we calculated Z-scores ($Z = (x-\mu \text{ baseline noise}) / \sigma \text{ baseline noise}$; x being the amplitude of the bin of interest) across the average of all electrodes on the FFT spectrum average across individuals for each EEG cap. The baseline noise level was estimated as the average of twenty-two surrounding bins, excluding the immediately adjacent bins (i.e., 10 frequency bins on each side, corresponding to a frequency range of 0.302 Hz).

Responses were considered significant if the Z-score was above 1.64 ($p<.05$, one-tailed, i.e., signal>noise), indicating that the response was significantly larger than the EEG noise estimated in the neighboring frequencies.

To quantify the EEG responses, the significant harmonics of the frequency of interest identified in the previous steps were summed (Retter & Rossion, 2016; Retter, Rossion & Schiltz, 2021). For that, the EEG spectrum was segmented into successive chunks centered on the bin containing the identity discrimination frequency (0.856 Hz, 1.712 Hz, 2.567 Hz, etc.), and chunks of significant harmonics were summed. Each chunk contained 25 bins (i.e., a chunk length of 0.403 Hz). Then, two methods were used to quantify the EEG responses: (1) subtraction of the baseline noise from the signal (corrected amplitude in µV) for quantification, (2) division of the baseline from the signal (signal-to-noise ratio,

SNR) for optimal visualization. Baseline EEG activity was estimated as the average of the twenty-four surrounding bins, excluding the immediately adjacent bins and the local maximum and minimum amplitude bins (i.e., 10 frequency bins on each side). Grand averages were computed to display results at the *Cap* and *Condition* levels.

Finally, to test intra-sequence reliability, the four sequences from the upright condition were divided into two pairs based on their order (odd and even). Specifically, "Pair 1" included sequences 1 and 3, and "Pair 2" included sequences 2 and 4. The analysis was then performed as previously described by averaging the two trials within each pair in the time domain before applying the Fast Fourier Transform (FFT). Only 19 participants were included for this last analysis, as we removed one entire sequence of one participant due to noisy EEG recording.

III.6. Statistical Analysis

First, Student t-test were performed on the average EEG response of all 20 channels to compare the global amplitude of the upright condition response between the two EEG electrode systems.

To compare face identification response amplitudes for upright condition between systems on ROI, two-way repeated measure ANOVA were performed with *Hemisphere* and *Cap* as within subjects' factors. Then, statistical analyses were computed on the amplitude response for each condition (Upright and Inverted) with a three-way mixed ANOVA with the factors *Hemisphere*, *System* and *Condition* as within subjects' factors.

For the general visual frequency, a student t-test was computed to compare response amplitude between systems. When the data did not validate parametric test conditions, Wilcoxon-Mann-Whitney tests were used. Chi-squared tests were used to compare the proportion of significant electrodes between systems.

Finally, to evaluate correlations between and within each EEG system's amplitude response, Pearson correlations were computed for normally distributed data, and Spearman correlations for data violating the assumption of normality. Coefficients of correlation were compared using Z-test.

IV.Results

IV.1. Face Identity Discrimination EEG Responses Across Systems

Clear EEG responses were observed for both EEG electrode systems at the face identity discrimination frequencies (0.856 Hz and harmonics: 1.712 Hz, 2.568 Hz…) during the upright face condition, particularly on both the left and right occipito-temporal electrodes, with a notable right hemispheric dominance (**Figure 58**).

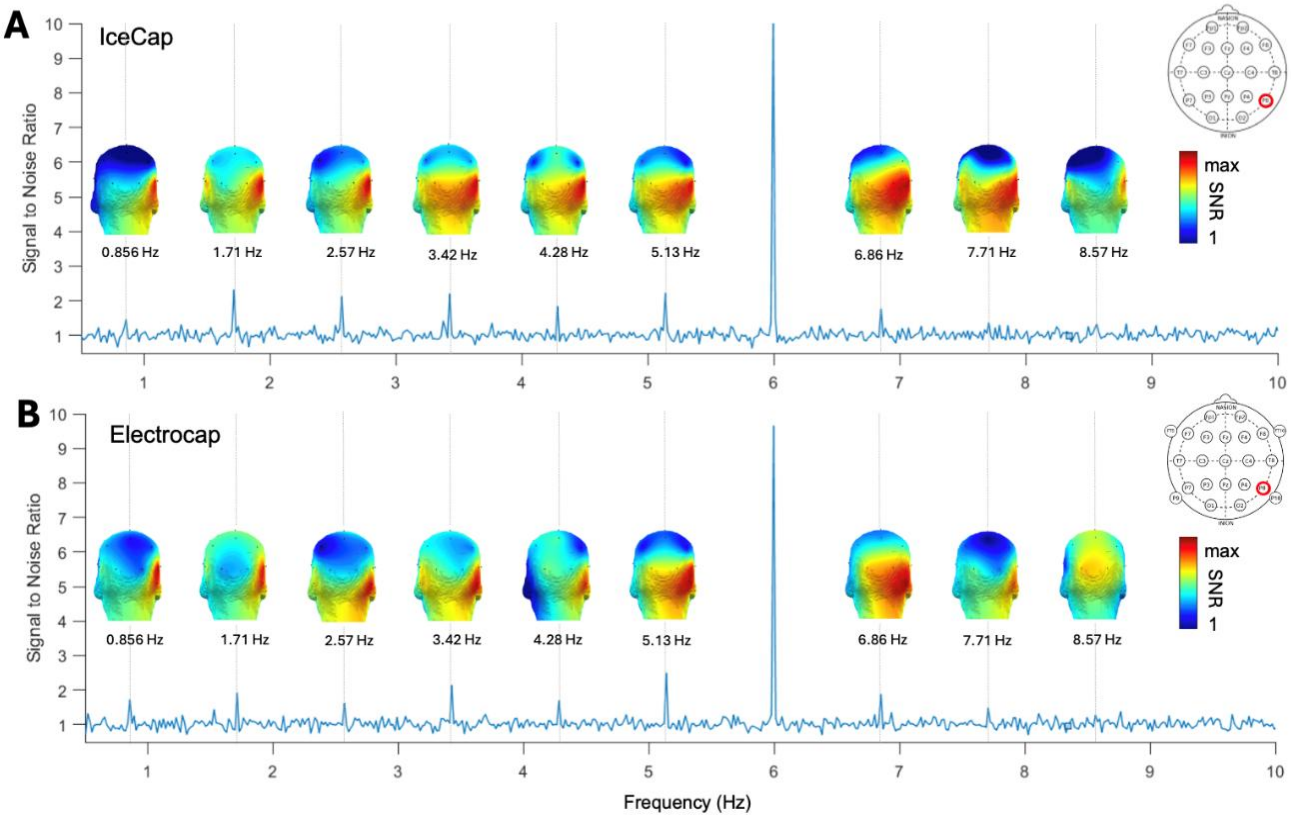

Figure 58. Frequency spectrum of SNR at right occipito-temporal electrode P8 and 3D scalp map topographies. Upright faces condition, at the top for Icecap (A) and at the bottom for Electrocap (B). In this example, for both EEG caps, clear EEG response peaks were observed at the face identity discrimination frequency of 0.856 Hz plus the harmonics (1.712 Hz, 2.568 Hz…), with a notable right hemisphere dominance. The 6 Hz frequency peak corresponds to the general visual response.

Across all electrodes averaged, the amplitude at the fundamental frequency of 0.856 Hz was not significant for both EEG electrodes system (Electrocap: Z=0.87, p=.20; Icecap: Z=-0.14, p=.44). However, significant amplitudes were observed at the second harmonic (1.712 Hz) up until the 9th harmonic for both EEG caps, excluding the 6Hz frequency corresponding to the general visual stimulation frequency (i.e., 1.712 Hz, 2.568 Hz, 3.424 Hz, 4.280 Hz, 5.136 Hz, 6.856 Hz, 7.712 Hz and 8.568 Hz; Z>1.64, p<.05).

Focusing only on P8 electrode, the first harmonic frequency (0.856 Hz) was significant only for the Electrocap (Electrocap: Z= 1.95, p<.05; Icecap: Z=1.10, p=.14), but without any difference between caps (t_{19}=0.05, p=.96). The number of significant harmonics was also consistent across EEG electrode systems, with all the next 9 harmonics of 0.856 Hz being significant.

All the following analyses were run with the sum of the nine harmonics of the 0.856 Hz. For the upright face condition, across the average of all EEG electrodes, no significant difference was observed for the amplitudes of the face identity discrimination response between the two EEG electrode systems (t_{19}=1.11, p=.28).

On the right hemisphere (i.e., P8 electrode), the amplitude for the sum of the 9 harmonics of 0.856 Hz was highly significant for both systems, with a significantly larger response for the Icecap (Icecap: 0.99±0.87 µV, Z=6.98, p<.0001; Electrocap: 0.77±0.72 µV, Z=8.33, p<.0001) (**Figure 59.A**). The average SNR value for the Icecap was 1.79±0.65, ranging from 0.94 to 3.070 and 1.71±0.57 for the Electrocap, ranging from 0.65 to 2.95 (**Supplementary Figure S7**).

On the left hemisphere (i.e., P7 electrode), similarly, both EEG electrode systems showed significant amplitudes of the summed harmonics, also with a significantly larger responses for the Icecap (Icecap: 0.57±0.49 µV, Z=6.35, p<.0001; ElectroCap: 0.48±0.61 µV; Z=5.37, p<.0001) (**Figure 59.B**). The average SNR values for the Icecap was 1.43±0.37, ranging from 0.88 to 2.15 and 1.38±0.46 for the Electrocap, ranging from 0.52 to 2.25 (S**upplementary Figure S7**).

The ANOVA showed no effect of *Cap* ($F_{1,19}$=2.89, p=.11) but a main effect of *Hemisphere* ($F_{1,19}$=5.3, p<.05) with a large amplitude recorded at P8 (right hemisphere, 0.88±0.81 µV) than P7(left hemisphere, 0.52±0.56 µV) as observed on the topographical maps of both caps (**Figure 59C**). There was no significant interaction between *Cap* and *Hemispheres* ($F_{1,19}$=0.65, p=.43).

Since the largest amplitude response was found on lower channel P10 for the Electrocap (0.89±0.63 µV, **Figure 59C**), we also compared its amplitude with channel P8 of the Icecap. There was no significant difference when considering these 2 channels showing the largest response for the respective EEG electrode system configurations (t_{19}=0.81, p=.43, Supp Fig B).

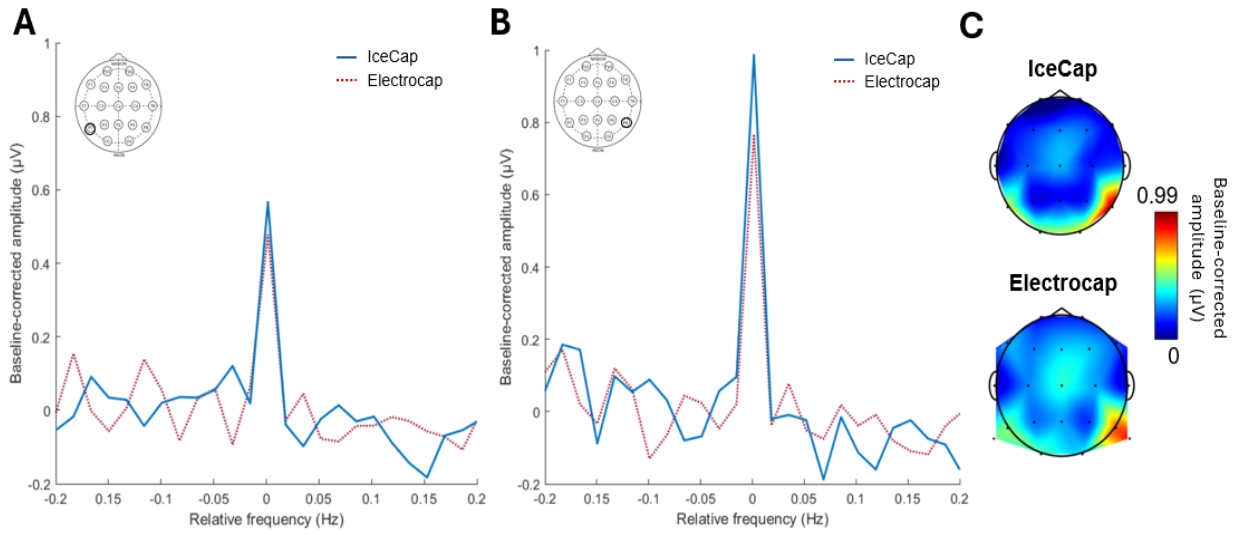

Figure 59. Baseline-corrected amplitudes of the summed harmonics for both caps.
These two graphs are presented for the average of all participants on the left ***(A)*** or right ***(B)*** occipito-temporal region (P7 and P8 electrodes, respectively). The spectrum is centered on the frequency bin of interest. In solid blue line for the Icecap and in dash-dot red line for Electrocap. ***C.*** Scalp map topographies of the corrected amplitude of the face identity discrimination response (0.856 Hz and harmonics) for both caps for the upright condition.

IV.2. Face Identity Discrimination Inversion Effect

For the inverted face condition, no significant responses were found on the average of all channels for any of the caps (Electrocap: Z=0.61, p=.27; Icecap: Z=0.08, p=.47). The response did not even reach significance for the P8 channel (Electrocap: Z=1.31, p=.095; Icecap: Z=1.63, p=.052) but a significant response at P7 was found for the Electrocap only (Z=1.79, p<.05; Icecap: Z=-0.27, p=.40) (**Figure 60**).

A three-way ANOVA computed on the average of the participants on the P8 or the P7 electrodes revealed a significant effect of *Hemisphere* ($F_{1,19}$=9.35, p<.01; P8 0.52±0.72 µV> P7: 0.24±0.50 µV) and *Condition* ($F_{1,19}$=20.54, p<.001, Upright: 0.62±0.65 µV > Inverted: 0.15±0.52 µV), but no main effect of *Cap* ($F_{1,19}$=0.009, p=.92, Icecap: 0.38±0.62 µV, Electrocap: 0.39±0.65 µV).

The interaction between *Hemisphere* and *Cap* was not significant ($F_{1,19}$= 2.912, p=.10). The interaction between *Condition* and *Cap* just failed to reach significance ($F_{1,19}$ = 3.947, p=.06) as the interaction between *Hemisphere* and *Condition* ($F_{1,19}$ = 3.112, p=.09). The three-way interaction of *Hemisphere*, *Cap*, and *Condition* was not significant ($F_{1,19}$=0.006, p=.94).

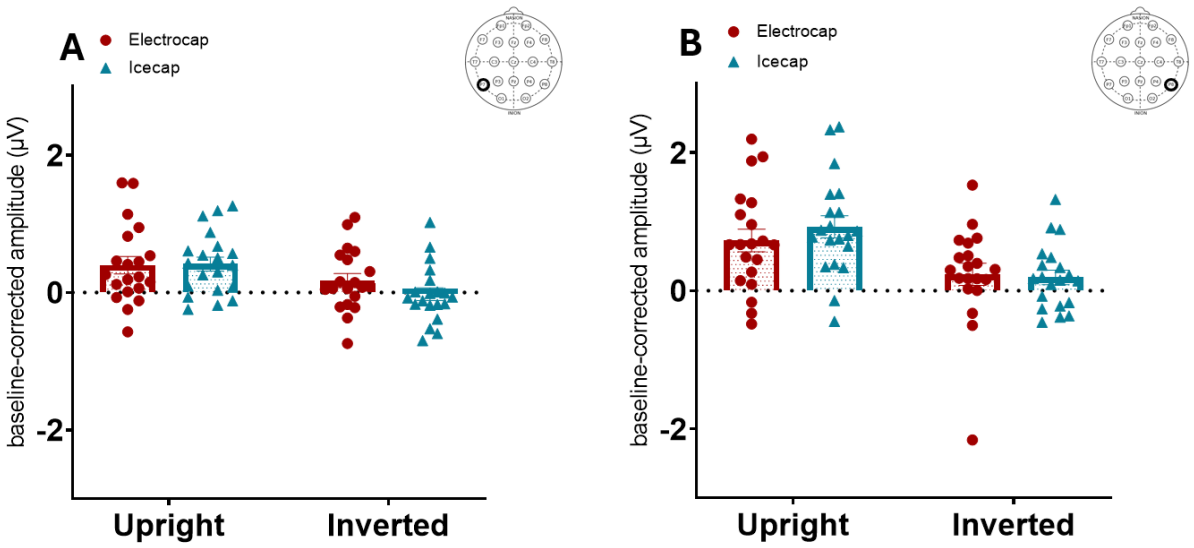

Figure 60. Face identity discrimination inversion effect
Histograms of the baseline-corrected amplitude of face identity discrimination response for both conditions and for both recording caps (Icecap in red circles and Electrocap in blue triangles) for the average of right occipito-temporal ROI (**A**), and left occipito-temporal ROI (**B**). Each dot represents one participant. Bars represent standard deviation to the mean.

IV.3. Face Identity Discrimination at the Individual Level

On averaged amplitudes at P8 and P7 channels together, the number of participants with a significant face identity discrimination response at the individual level was not significantly different between the two caps (Electrocap:14/20, Icecap: 13/20, $\chi 2$=0.0000018, p=.50). Similar results were found when analyzing the P8 and P7 channels individually: P7: 10/20 for Electrocap and 12/20 for Icecap ($\chi 2$ =0.5, p=.24); P8: 15/20 for Electrocap and 13/20 for Icecap ($\chi 2$=0.12, p=.37).

IV.4. Intra And Inter-Cap Reliability

A significant correlation of response amplitude was found between the average amplitude response of face identity discrimination at OT ROI (i.e., average of P7 and P8) of odd upright sequences (i.e., Pair 1: sequences 1 and 3) with the average amplitude response of even upright sequences (i.e., Pair 2: sequences 2 and 4) both for the Icecap (r= 0.48, p=.038) and the Electrocap (r=0.7212, p=.0005). This reflects a stable amplitude response across sequences for both caps. There was no significant difference between these two correlation coefficients (z= 1.1, p=.1357).

Concerning inter-cap reliability, a significant correlation (tested with 4 sequences) was found between face discrimination amplitude response with both caps the Electrocap and Icecap at OT ROI (r=.67, p=.0012) (**Figure 61**).

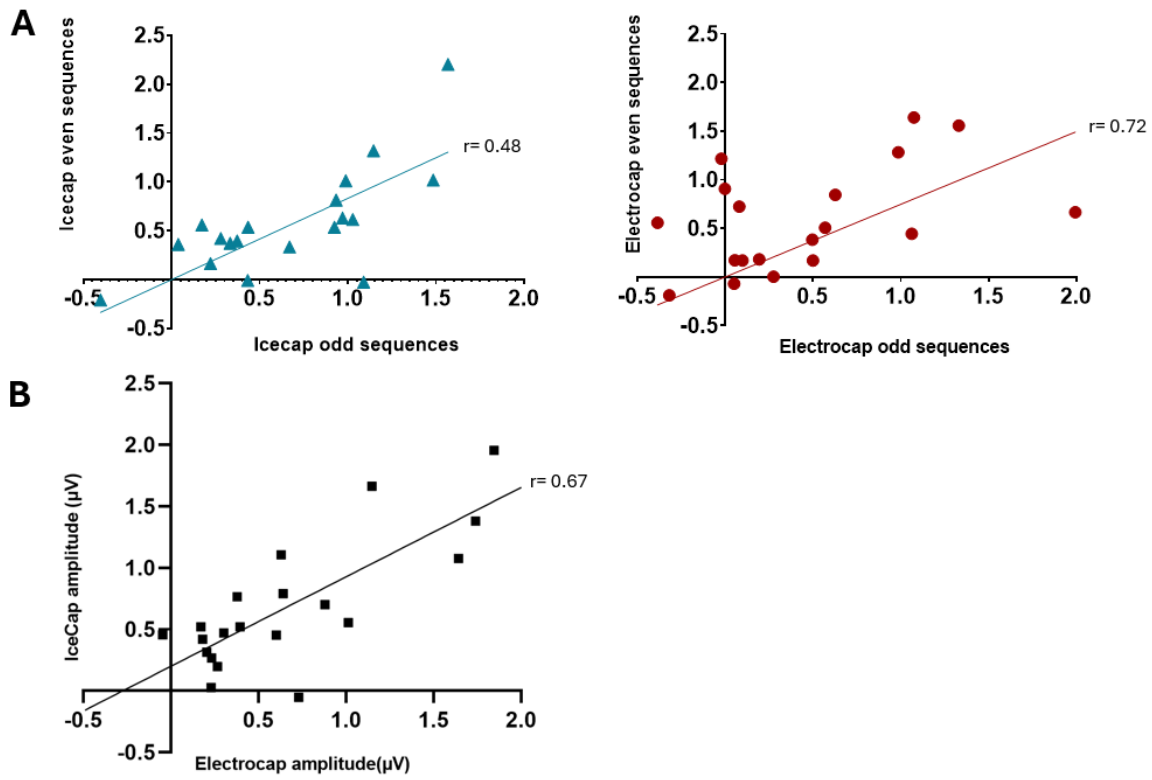

Figure 61. Intra and inter-cap reliability
A. Correlation between amplitude at OT ROI (i.e., average of P7 and P8) between a pair of odd and a pair of even sequences for Icecap, on the left panel and Electrocap on the right panel. ***B.*** Correlation between baseline-corrected amplitude of the two recording caps at OT ROI. The black solid lines represent the regression line.

IV.5. General Visual Base Frequency Response

A high significant amplitude response was observed for both caps in the upright face condition at the general visual base frequency of 6Hz, up to eight harmonics (i.e., 6Hz, 12Hz,18Hz, 24Hz, 30Hz, 36Hz, 42Hz and 48Hz, Zs>2.32, p<.01) across the average of all electrodes. Quantification of the response was therefore computed with the sum of the first eight harmonics.

Scalp map topographies of the general visual base frequency responses revealed high similarities between the caps, with peak amplitude response observed at the O1 and the O2 electrode sites (**Figure 62A**). Statistical analyses of the amplitude response showed no significant effect of *Cap* ($F_{1,19}$=1, p=.33), no significant effect of *Condition* ($F_{1,19}$=3.04, p=.10) or *Hemisphere* (i.e., O1 vs O2, $F_{1,19}$=0.16, p=.69). No significant interaction was found (p>.05). Additionally, base frequency EEG amplitude response was highly correlated between caps at both O1 (r=.66, p=.0015) and O2 channels (r=.74, p=.0002) (**Figure 62**).

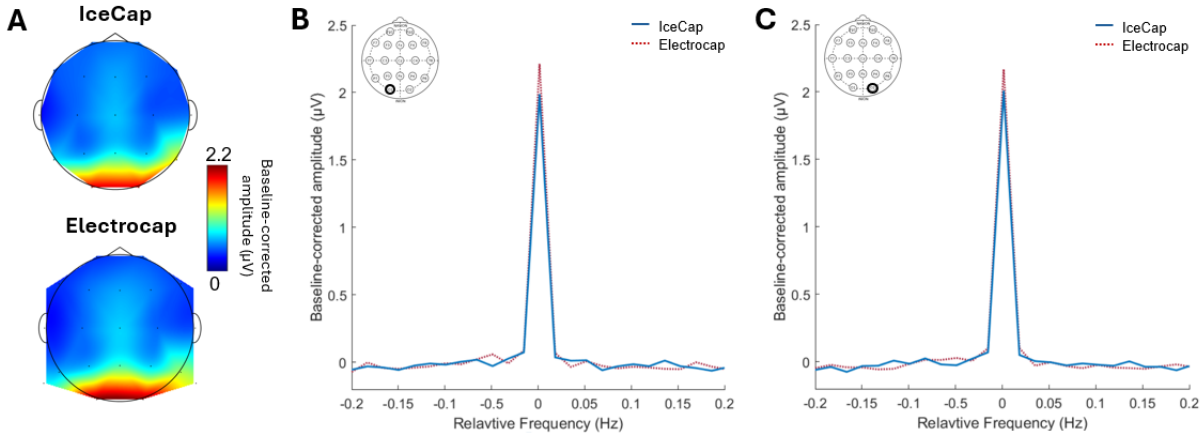

Figure 62. Baseline-corrected amplitudes of the general visual response for both caps.
A. Scalp map topographies of the corrected amplitude of the general visual response (6Hz and harmonics) for both EEG caps. Baseline-corrected amplitude of the sum of the ten first 6Hz harmonics at the right ***(B)*** and the left occipital ROI ***(C).*** The spectrum is centered on the frequency bin of interest. In the solid blue line for Icecap and in the dashed red line for Electrocap.

IV.6. Set Up Time and Comfort

Although no dedicated questionnaire was conducted to assess participants' feedback regarding comfort with both scalp EEG systems, most participants presented a preference towards the ElectroCap. They found it more comfortable, simpler, and easier to adjust and remove after the experiment. They noted that '*the conductive gel was also easier to wash out'*. Meanwhile, the Icecap participants reported an uncomfortable and itching sensation on the scalp, in addition *to feeling that the net is extremely sensitive, making them afraid to move*. It's Elefix V gel, used with Icecap, was described as *very thick, sticky, and difficult to remove, with a strong, oily odor*. In contrast, some participants preferred the Icecap and reported that the *cap's stabilizing straps are more comfortable and unnoticeable on the head, providing good contact with the skin*. The only reported drawback related to the Electrocap was that some participants found the chin straps to be itchy in comparison to the Icecap.

The setup time for both the Icecap and the Electrocap was measured in all 20 subjects. The average setup time for the Icecap was significantly longer than for the Electrocap (Icecap: 16 ± 5 minutes vs Electrocap: 11 ± 3 minutes, p = 0.0002) (**Figure 63**).

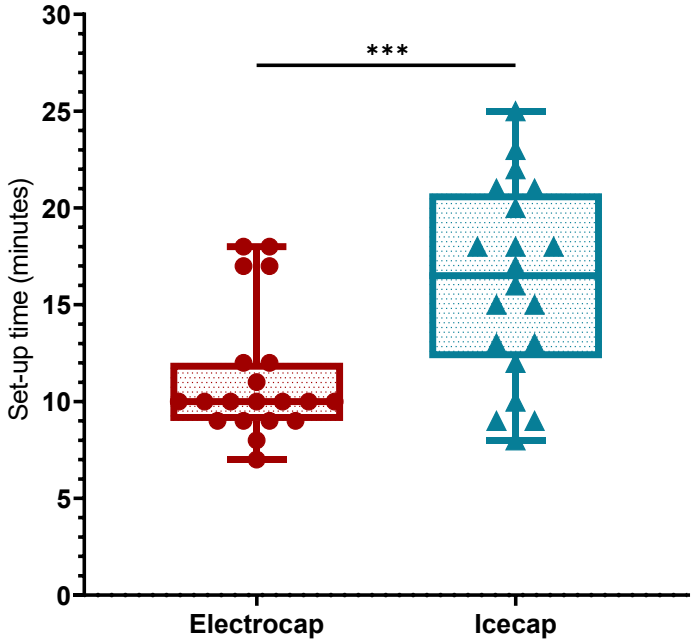

Figure 63. Box plots of setup time for Icecap and Electrocap.
Box plots show the distribution of the averaged setup time (minutes) of the Icecap (blue) and the Electrocap (red) across 20 subjects. The time to set up the Icecap system (16 ± 5 minutes) was significantly greater than for the Electrocap (11 ± 3 minutes; $p < 0.05$).

IV.7. Impedance Measurement

During the impedance measurement before and after the FPVS experiment with each scalp EEG electrode system, a value of "1" indicating measurement failures occurred due to the inability of the Neuronaute to read the impedance. In total for all subjects, 1520 impedance measurements were done (19 electrodes × 4 recordings × 20 subjects) from which 245 measurements were errors (presented the value 1), and 1275 readings were successful. The total percentage of errors is 19% from all 1520 measurements, before and after the experiment, for both caps. Of the 245 errors, 178 (73 %) occurred with the Electrocap and 67 (27 %) with Icecap. As the Neuronaute failed to reliably measure impedance on those electrodes, we were unable to analyze their impedance changes and weren't included for further analysis.

Scalp-electrode impedances remained within the recommended 5–10 kΩ range (International Federation of Clinical Neurophysiology; Babiloni et al., 2020). Notably, the average impedance during and after the FPVS experiment was significantly greater for the Icecap than for the Electrocap (Icecap: 8.55 ± 4.24 kΩ vs Electrocap: 6.51± 2.9 kΩ, $p = 0.03$) (**Figure 64**).

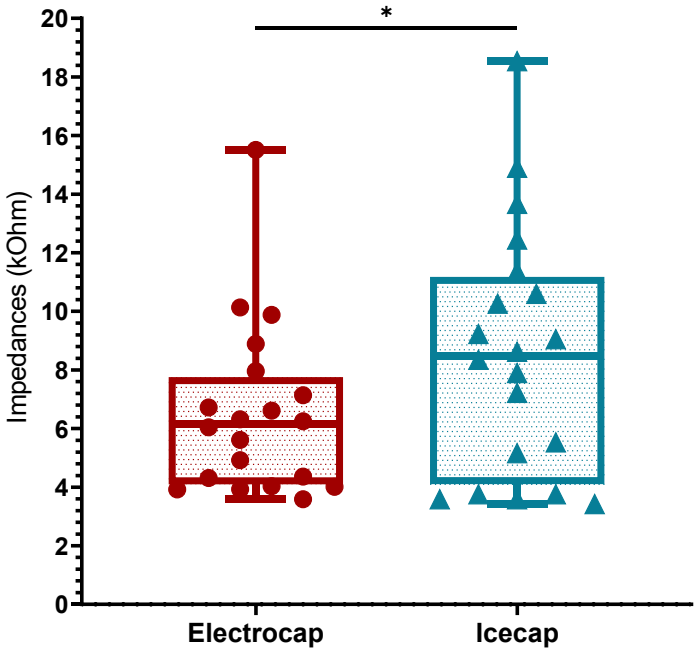

Figure 64. Box plots of scalp-electrodes impedances for Icecap and Electrocap.
Box plots show the distribution of averaged electrode impedances (kΩ) measured during and after the FPVS experiment for the Icecap (blue) and Electrocap (red) across 20 subjects (excluding "1" error readings). Although both systems maintained impedances within the recommended 5–10 kΩ range, the Icecap exhibited a significantly higher average impedance (8.55 ± 4.24 kΩ) compared to the Electrocap (6.51 ± 2.90 kΩ; ; p = 0.03). Each triangle and circle present one participant.

V. Discussion

V.1. Icecap Reveals Comparable Cognitive Evoked EEG Measures to Electrocap

In this study, we showed that the ultrathin Icecap® and wireless Neuronaute® system can accurately and rapidly (i.e., few minutes) record cognitive evoked EEG measures when compared to the well-validated Electrocap system. Similar amplitudes and (high) SNRs were observed for the neural face identity responses, which were localized over the same brain regions, using the two cap systems. In addition, scalp amplitude topographies were comparable across the two EEG electrode systems and participants. In the literature, face identity discrimination EEG responses have been reported in the occipitotemporal regions with a right hemispheric dominance, whether in standard ERP measures (e.g., Caharel et al., 2009; Jacques et al., 2007) or with FPVS (e.g., Liu-Shuang et al., 2016). In our methodological study, the EEG responses were consistently localized over occipito-temporal regions, underscoring the reliability and sensitivity of this method, combining the Neuronaute with FPVS paradigm in assessing face identity processing. This also indicates that the Icecap system provides proper scalp coverage and sufficient inter-electrode distance for cognitive electrophysiological evaluation. The high correlations found in both intra-cap and inter-cap reliability analyses confirm the consistency of evoked potential measurements across systems. This stability underscores the reliability of the recorded responses, regardless of the cap used. Moreover, the significant correlation between Icecap and Electrocap supports the use of the Icecap as a potential alternative for future research while guaranteeing accuracy and reproducibility in electrophysiological studies.

One notable difference between the two scalp EEG caps is the number and distribution of the scalp electrodes: 21 electrodes for Icecap and 24 for Electrocap. Interestingly, the Electrocap included two supplementary electrodes in the lateral occipitotemporal regions (i.e., P10 and P9) (Koessler et al., 2009), known to be highly sensitive to face processing. Despite the lack of a P10 electrode in the Icecap montage, our findings showed a similar amplitude magnitude between P10 for Electrocap and P8 in Icecap for the face discrimination response. Due to the close distance between the two electrodes, it is possible that important electrical activity from the brain sources (e.g. Inferior occipital gyrus, Jacques et al., 2018) responsible for the high amplitude response in P10 , was captured by the neighboring P8 electrode in Icecap. These findings suggest that, even though the Icecap lacks full coverage of the lateral occipitotemporal regions, it is still capable of detecting face-discrimination responses if the electrode is properly placed in key scalp locations. This underscores the ability of minimal scalp EEG montages to capture important cognitive responses, if the electrode placement is accurately targeting the regions of interest. Future studies are required to investigate the accuracy of minimal EEG

montages in comparison to more dense ones, in order to optimize signal quality. Moreover, previous investigations of the FIE using this FPVS paradigm revealed a significant reduction in the face discrimination response between the upright and inverted conditions over the right occipito-temporal regions (Jacques et al., 2020; Liu-Shuang et al., 2014a; Rossion & Boremanse, 2011). These findings are in line with our results obtained from both electrode systems and further provide evidence of the validity of Icecap for measuring the FIE.

V.2. Comfort, Setting Up Time, and Remote Usability of Icecap

Although no proper assessment was conducted, participants reported greater comfort with the Icecap compared to the Electrocap. Indeed, the Electrocap provides a familiar and easy-to-use design, despite some reports of an itching sensation from the chinstraps. However, most participants reported greater comfort with Icecap due to its lightweight, ultrathin, and flexible design. Icecap's ergonomic design can accommodate users across a wide age range without the mechanical constraints of chinstraps or belts, due to its adjustable size, eliminating the need for multiple cap sizes. Nevertheless, dedicated experiments are needed to systematically assess participants' comfort levels for each scalp EEG system and to optimize the Icecap design for better and more comfortable usability.

On the other hand, measuring the setup time for each scalp cap connected to the Neuronaute revealed that Icecap required a significantly longer setup period. These findings can be attributed to Icecap's unfamiliar design and gel application in comparison to the simpler Electrocap. Despite the integrated stabilizing adhesives on the temples, nasion, and inion, Icecap's net structure is highly flexible, which requires great attention to ensure the proper placement of each electrode on the head's surface. Meanwhile, the simple and rigid Electrocap design with prefixed electrodes adapted to the cap size (depending on the head circumference), allows for a more precise electrode localization with easier and more reliable alignment. Additionally, the Icecap uses a very thick and sticky conductive gel that requires careful manual application to each electrode site. Its application and removal are more difficult, especially with longer hair, as it demands the need to manually part the hair near each electrode. In contrast, the thinner and more manageable gel added for each electrode with Electrocap is user-friendly and less time-consuming.

Moreover, to reduce the setup time, several improvements could be considered for the Icecap system. Firstly, replacing the conductive gel with a less thick and more easily applicable formulation facilitates a faster and more efficient application, which increases participants' comfort. Secondly, maintaining the unique quality of flexibility in the Icecap but offering it in multiple sizes (e.g., small, medium, large, x-large), could allow for quicker adaptation to different head shapes and sizes and

minimize the need to overstretch the Icecap. These adjustments could contribute to a more efficient, fast, and participant-friendly setup, ultimately improving the practicality of the Icecap system in both research and clinical environments.

In addition, its single-use design reduces removal setup time for technicians by eliminating the long cleaning process and variable drying periods required with other reusable EEG caps. For home-based applications, it is particularly well-adapted and effective, considering that wireless Neuronaute enables direct transfer of the recorded EEG signals to the secure N-cloud platform. This innovative technology offers fast, automated (thanks to frequency tagging), and remote EEG analysis by reducing onsite data acquisition. This solution differs from conventional ERP analysis in the time domain, which requires manual processing and often-tricky analysis (e.g., amplitude and latency peaks measurement). It is this current approach that's compelling a wider implementation of cognitive evoked potentials in clinical settings, especially outside specialized hospital structures. Such technological integration of wireless EEG acquisition with cloud-based processing remains uncommon in the biomedical field and offers valuable advancement for remote neurophysiological monitoring.

V.3. Assessment of Face Discrimination with FPVS

Notably, ERPs in the time domain typically have a low SNR, requiring a long duration of experimentation (several trials averaged) to achieve a high-quality signal (high SNR) in the time domain, which can be susceptible to participants' fatigue or variability in their attentional states. Additionally, ERPs are highly sensitive to artifacts like eye blinks, muscle activity, and environmental noise, necessitating rigorous preprocessing steps that may distort genuine neural responses (Rousselet et al., 2007). Moreover, ERP peaks such as the P300 or N400 can vary widely between individuals and even within the same individual across sessions due to fluctuations in cognitive state, attention, and noise (Hsin et al., 2025; Holm et al., 2006). Their extraction can be subjective and imposes a significant challenge that contributes to low test–retest reliability. The choice of peak detection methods (e.g., manual vs. automated, amplitude vs. latency measures) can introduce additional variability, as small changes in signal processing parameters can lead to different results. Furthermore, ERPs often exhibit overlapping components, making it difficult to precisely isolate a single peak without contamination from other neural processes. These factors reduce the reproducibility of ERP studies, especially when comparing data across sessions, individuals, or laboratories (Rossion et al., 2020).

To circumvent these issues, in the present study, the use of FPVS offers an objective and sensitive approach to quickly (within a few minutes) obtain robust and repeatable EEG measures (Regan, 1989; Rossion et al., 2020). This approach allowed us to objectively quantify and compare the

EEG measures from the two EEG electrode systems in the frequency domain. The objectivity and sensitivity of this approach stem from the specific predefinition of the response frequency. In fact, it relies on a fixed periodic stimulus frequency that elicits automatic and time-locked neural responses with a high SNR. The latter appears significantly in clear peaks at predefined frequencies when analyzed in the frequency domain, allowing for robust statistical detection without the need for subjective and manual peak extraction (Rossion et al., 2020; Rossion & Boremanse, 2011). Thus, the frequency-tagging method ensures reproducibility, minimizes analysis bias, and provides a sensitive and reliable marker of brain activity. Advanced approaches such as artificial intelligence, machine learning, robust statistical modeling, and individualized peak detection strategies are being explored to further improve the reliability of the approach.

V.4. Impedance Measurement with Icecap and Neuronaute

Errors in impedance measurement occurred as default values, i.e., "1" when recording with both scalp systems. These errors are caused by high impedance values exceeding the device's measurement range or its internal system capacities, which can lead to failed readings and eventually a default error value. We reported a 19% impedance measurement error rate with the Neuronaute system. These findings are consistent with a 20% error rate previously reported by Bioserenity during their quality control testing of the Neuronaute. This high impedance error rate may compromise the quality of the EEG signal by increasing the injected noise and reducing the SNR of the ERP (for time domain analysis), consequently, affecting the detection of neural signals (Kappenman & Luck, 2010). Future work needs to assess this issue by reducing the impedance error and modifying the device's range to accommodate larger measurement ranges.

Impedance errors typically occur when the system cannot reliably measure the electrical contact between the electrode and the scalp. Several factors can contribute to this type of error, such as poor contact between the electrode and the skin due to dry skin, insufficient gel or hair obstruction, electrode displacement, and instability in the hardware connections (Goyal et al., 2022; G. Li et al., 2017). Additionally, the differences in wire connections may directly influence compatibility with the impedance measuring system. Notably, Electrocap, which reported higher error values than Icecap, was connected individually to each touch-proof input electrode connector of the Neuronaute, while the Icecap was directly connected via a dedicated DB-25 connector. A more detailed analysis by Bioserenity is necessary to evaluate whether the DB-25 connector is more reliable for recording than individual touch-proof connections. These errors highlight the importance of optimizing the electrode's placement and connections and improving the system's design to ensure more reliable impedance monitoring and, consequently, higher quality EEG signals.

Although no significant difference was observed between the impedance values measured in the 20 healthy subjects with Electrocap and Icecap, it's important to note that impedance measurements were only considered for electrodes without any default error value i.e., without a value of "1". This technique led to variability in the number of electrodes included in the statistical analysis across subjects and scalp systems, resulting in the underrepresentation of certain electrodes or participants, specifically those with multiple impedance-related errors. This selective exclusion may limit the generalization of the proper impedance values between the two systems, in particular for Electrocap, which presented high impedance error values. These findings imply that although the average impedance may appear similar, the reliability and consistency of its acquisition may differ between scalp systems. This highlights the importance of optimizing the connectivity between the impedance measuring system in the Neuronaute and the scalp EEG caps, especially for Icecap, to improve the quality of data acquisition and eventually reduce noise recordings.

V.5. Future Applications of the Icecap-Neuronaute System

In the near future, these technologies should enable automatic transfer and extraction of EEG biomarkers. Applying artificial intelligence approaches (e.g., large brain models) holds great potential for classifying cognitive EEG measures, as already demonstrated in brain–computer interface research (Cao, 2020; Pfeffer et al., 2024). Additionally, such technology can benefit both clinicians and patients by increasing accessibility and frequency of testing and enabling larger-scale longitudinal EEG monitoring outside the hospital environment. It is important to mention that cognitive ERPs have emerged as powerful neurophysiological tools in clinical settings, providing objective measures of cognitive processing. These electrophysiological markers are particularly valuable for assessing functions such as attention, memory, language processing, and executive function, making them crucial for diagnosing and monitoring neurological and psychiatric disorders (Lascano et al., 2017; Nuwer, 1998). For example, ERP analysis research has shown that cognitive impairments can be detected in Alzheimer's disease (David et al., 2025) , multiple sclerosis (Hardmeier et al., 2014), epilepsy (Zhong et al., 2019), and mental illnesses (Campanella, 2023). They can also serve as predictive markers for awakening from coma (Fischer et al., 2004).

EEG has been instrumental in studying impairments in face and object recognition in conditions such as prosopagnosia and autism spectrum disorder (e.g., Feuerriegel et al., 2015; Vettori et al., 2020; Vettori, Jacques, et al., 2019). EEG has also been used to evaluate language, particularly in patients with dyslexia, aphasia following stroke, or traumatic brain injury (Mehraram et al., 2025; Močilnik et al., 2024; Premeti et al., 2024; Chatelle et al., 2020). It provides insights into lexical, semantic and

syntactic processing deficits, allowing clinicians to track development and recovery and to tailor rehabilitation strategies (Wilson et al., 2012; Kawohl et al., 2010; Frisch et al., 2004).

Beyond their diagnostic utility, ERPs offer significant value in treatment monitoring. In pharmacological studies, EEG alterations have been used to evaluate the efficacy of cognitive-enhancing drugs in disorders such as schizophrenia and major depressive disorder (S. J. Luck et al., 2011). Moreover, neurofeedback and cognitive training interventions have incorporated ERP measures to assess neural plasticity and treatment response, providing a direct link between intervention strategies and changes in brain function (Loriette et al., 2021; Covey et al., 2018)

VI.Conclusion and Perspectives

In conclusion, this study demonstrated the validity and reliability of the new Icecap-Neuronaute system, showing that it is operational and well designed for electrophysiological assessments of cognitive functions, particularly for face identity discrimination. The ergonomic design of the ultrathin cap, the high-quality recording, and the wireless transmission offer promising perspectives for future applications in both clinical and home-based environments.

Investigating electrophysiological responses of various cognitive functions, especially ERPs with scalp EEG recordings for patients and healthy subjects, is a pivotal tool used by clinicians to assess the health of brain activity. It's one of the main methods used for assessing severity, tracking the prognosis, and recovery of different neurological disorders. Furthermore, ERPs offer valuable insights into the functioning of various cognitive processes such as language across different human populations, including individuals with neuropsychological conditions like dyslexia and reading impairments. In this study, healthy controls were tested with two additional FPVS paradigms: the *Words paradigm*, targeting visual word processing (**Figure 65**), and the *Facelocaliser paradigm*, targeting visual face recognition in the human brain (previously mentioned in Chapters 2 and 3, **Figure 29**). The two FPVS paradigms were employed to further validate the capacity of the Icecap-Neuronaute system to record different cognitive measures, as both have been extensively and robustly validated in the literature for eliciting evoked frequency-specific responses in the brain regions associated with their respective cognitive functions (Hagen et al., 2021; Lochy et al., 2015; Rossion et al., 2015a)

Further analysis needs to assess the ability of the Icecap-Neuronaute system to detect EEG biomarkers implicated in the two cognitive functions of the FPVS approaches, by comparing word-

selective (and face-selective) responses recorded with the Icecap with those recorded with the Electrocap. This experimentation would further validate the system's ability to record cognitive evoked ERP, as well as its capacity to capture neural responses associated with distinct cognitive functions across different brain regions.

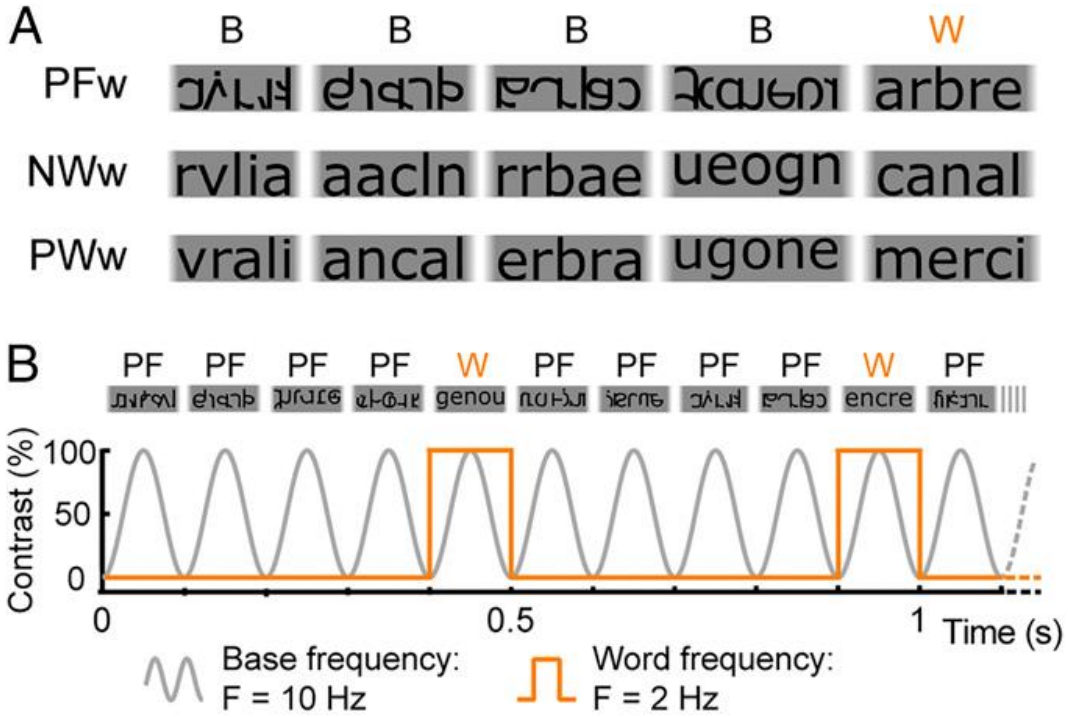

Figure 65. Experimental Words paradigm.
A. In this design, words (w) are inserted into three types of base stimuli (B), creating three experimental conditions: words among pseudo fonts (PFw), among nonwords (NWw), and pseudowords (PWw). **B.** During FPVS paradigm, the sequences (PF, NW, and PW; PFw shown here) are presented rapidly at 10 Hz through a sinusoidal contrast change, with words (W) inserted every 5th item at a frequency of 2 Hz (=10 Hz/5) . Adopted from Lochy et al., 2015.

The innovative characteristic to securely store EEG signals in the N-cloud and wirelessly transmit for analysis opens promising avenues in the medical field for both clinicians and patients. As the biomedical field continues to shift toward home-based solutions, adopting this technique could significantly enhance the accessibility and frequency of EEG testing. In turn, it would support large-scale longitudinal monitoring of brain activity outside of traditional hospital settings.

Notably, implementing the Icecap-Neuronaute system for at-home application requires additional inspection of its recording capabilities. In this initial study, we lay the groundwork for validating the system's ability to record and analyze evoked responses when operated by professionals in a controlled laboratory environment. We compared the two scalp electrode systems, both

connected to Neuronaute, and confirmed Icecap's ability to record and analyze EEG biomarkers. Future work needs to assess the quality of the recording and acquisition performance of the home-targeted Neuronaute system with that of a research-grade instrument, like the Biosemi® EEG system. This investigation has been conducted with the same 20 healthy controls included in the present study, who returned for EEG recordings with the Biosemi system in our laboratory. Such a comparison will enable a validation of the Neuronaute system across multiple characteristics: recording set-up, data acquisition, storage, wireless transmission, analysis, recording, and system quality. Ultimately, it would lay the foundation towards safe and effective home-based EEG monitoring. Indeed, the home-based process requires training the patients to conduct the placement of electrodes on the scalp and manage the acquisition parameters in order to transmit the recordings to the clinicians.

Notably, enabling at-home use of biomedical tools like EEG recording represents a critical step towards expanding the reach of neurotechnological instruments. It paves the way for integrating additional medical technologies into home-based environments, such as transcranial electrical stimulation, offering the possibilities for long-term monitoring and interventions. Nevertheless, this transition from laboratory/clinical controlled settings to home-based environments requires clear guidelines, user-friendly applications, and reliable protocols to enable effective application. The ability to remotely apply therapeutic procedures, collect data, and provide quantitative biomarkers of cognitive function could support earlier diagnosis, better treatment planning, and continuous tracking of therapeutic applications. Ultimately, implementing such technologies could enhance outcomes across a range of neurological and psychiatric conditions like Alzheimer's disorder, Epilepsy, Depression, etc. that may benefit from repeated tDCS sessions and more rapid and objective assessment of disease status.

VII. Supplementary Materials

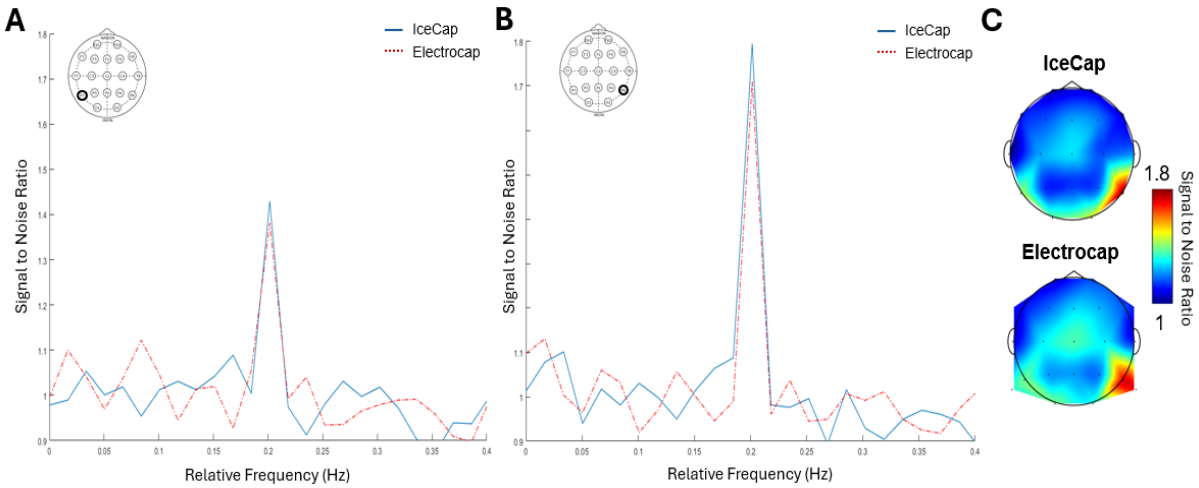

Supplementary Figure S7. SNR of the Summed Harmonics for Both Caps.
These two graphs are presented for the average of all participants on the left (A) or right (B) occipito-temporal region. The spectrum is centered on the frequency bin of interest. In a solid blue line for the Icecap and a dashed-dot red line for Electrocap. (C) Scalp map topographies of the SNR of the face identity discrimination response (0.856 Hz and harmonics) for both caps for the upright condition.

Chapter V: General discussion and Perspectives

tDCS is a widely used NIBS technique, increasingly explored for its therapeutic potential in various neuropsychiatric conditions, particularly in the context of cognitive rehabilitation. By delivering low-intensity electrical current through electrodes placed on the scalp, tDCS can modulate cortical excitability. However, the acute and persisting effects of tDCS are highly dependent on a range of stimulation parameters, including electrode size and placement, current intensity, and duration. Despite the extensive *in vivo* and *in vitro* research, the precise neurophysiological mechanisms underlying tDCS remain incompletely understood, especially regarding its impact on electrophysiological activity. As outlined in **Chapter I**, much of the existing literature relies on limited methodological approaches, primarily scalp EEG recordings and behavioral measures, to investigate tDCS effects, particularly in the domain of visual face processing. These approaches, while valuable, offer only partial insight into the mechanisms and neural dynamics engaged by tDCS.

To overcome these limitations, in this research project, we employed tDCS with a minimally invasive intracerebral EEG recording in drug drug-resistant epileptic patient, as explored in Chapter **II.** We utilized the simultaneous iEEG and scalp EEG provided for clinical monitoring to investigate the correlation between iEEG findings and scalp EEG effects of tDCS, as detailed in Chapter **III**. The FPVS employed simultaneously in each study with iEEG and scalp EEG investigations of tDCS neuromodulation provided a robust and implicit approach for face recognition processing. We finally address the challenging monitoring of electrophysiological tDCS effects, which often require advanced EEG setups and professional supervision. After addressing these challenges in the previous chapters, in Chapter **IV,** we validate the performance of a simple EEG acquisition system combined with FPVS, to pave the way for future applications to track long-term effects of neuromodulation and make it suitable for home-based longitudinal follow-ups. We proceed in this chapter to discuss the different findings from each chapter and discuss their possible future implications.

I. tDCS and Intracerebral Investigation

Ever since the pioneering works of Nitsche and Walter in the early 2000s, the use of tDCS has been increasing, especially for medical and therapeutic applications (Antal et al., 2022; Lefaucheur et al., 2017). The study presented in chapter ***II*** of this thesis manuscript addressed a longstanding gap in the field of tES previously highlighted by Liu et al., 2018, who noted that despite the proliferation of tDCS research, the mechanistic understanding by which weak electric currents influence the human brain remains elusive. Critically, he highlighted the uncertainty in translating mechanistic findings from animal and *in vitro* models to humans, especially regarding whether the attenuated EFs reaching the human brain with conventional protocols can directly affect neurons and their networks. In this study, we bridge the gap between animal and *in vitro* studies with *in vivo* human investigations by providing intracranial human data that supports direct modulation of neuronal activity. Our findings offer evidence in support of electrophysiological efficacy under routine tDCS parameters.

Due to the lack of standardized tDCS parameters among existing studies, it remains unclear which configurations are most effective for inducing lasting neuromodulatory effects in humans (Esmaeilpour et al., 2018). As part of our rationale for exploring the therapeutic potential of tDCS, we adopted well-established parameters commonly used in clinical applications (2mA, 20 minutes) for treating various neurophysiological disorders in humans (Lefaucheur, 2016). In addition to using these parameters, we employed a simple and widely used tDCS configuration to investigate whether a minimalistic montage, supported by a substantial body of literature (Datta et al., 2009 ; Caparelli-Daquer et al., 2012 ; M.-F. Kuo & Nitsche, 2012 ; Villamar et al., 2013 ;Edwards et al.2013 ; Roy et al., 2014; DaSilva et al.,2015 ; Nikolin et al.2015; Alam et al., 2016; Morya et al., 202019 ;u et al., 2021 ; Masina et al., 2021) can effectively induce neuromodulation in the human brain. Specifically, we used small HD ring electrodes instead of conventional sponge electrodes; this choice was motivated by both practical and conceptual considerations: HD electrodes are more compatible with simultaneous iEEG recordings as their compact size facilitates co-registration with depth electrodes. Moreover, this design allows us to test whether neuromodulatory effects can be achieved with minimal electrode configuration (2 small electrodes) and relatively low current intensity. Our findings demonstrate that even low-intensity stimulation over the visual ventral stream can lead to measurable neuromodulation, suggesting that high current amplitudes may not be necessary when focal targeting is optimized.

The general consensus, largely derived from different research methodologies (*in vitro* and *in vivo*) (Gartside, 1968; Radman et al., 2009; Rahman et al., 2017), implies simplified polarity specific tDCS effects, wherein anodal tDCS enhances neuronal excitability and cathodal tDCS leads to the opposite effect (Bhattacharya et al., 2022; Korai et al., 2021; Morya et al., 2019; Yamada & Sumiyoshi, 2021; Rahman et al., 2013; Nitsche, Fricke, et al., 2003; Nitsche, et al., 2003). Our intracerebral findings that showed significant positive neuromodulation with anodal tDCS support the positive neuroenhancement previously reported by cortical oscillations (Antal, Varga, et al., 2004; Bolognini & Diana, 2021), MEP (Baxter et al., 2014; Nitsche & Paulus, 2000), VEP, like the N70 component (Antal et al., 2006), ERPs like the N170 (Civile et al., 2020b; 2018), and the SSVEPs (D. W. Kim et al., 2019). However, it is important to note that in our study, by investigating the effects of tDCS at the level of individual patients and specific regions such as the VOTC, we observed both increases and decreases in neuronal activity. This variability supports a more nuanced and complex understanding of tDCS mechanisms, suggesting that its effects are highly context- and region-dependent. In line with this, several studies have reported contradictory effects of anodal and cathodal tDCS, challenging the conventional assumption that anodal stimulation is purely excitatory and cathodal purely inhibitory (Siebner et al., 2004; Antal et al., 2004; 2006; Accornero et al., 2007; Miniussi et al., 2012; Lafontaine et al., 2013; Mangia et al., 2014; Mancini et al., 2016; Costantino et al., 2017; Bolognini & Diana, 2021). Notably, an *in vitro* investigation explained the possibility of asymmetric and polarity-independent synaptic plasticity following stimulation, indicating that both anodal and cathodal tDCS can result in similar effects in LTP and LTD (Kronberg et al., 2017). Given these findings, future studies should systematically investigate the specific influence of cathodal stimulation and directly compare its effects to those of anodal tDCS, particularly in regions such as the VOTC, where structural and functional heterogeneity may play a critical role in shaping the neuromodulatory outcome.

Furthermore, Esmaeilpour et al., 2018 highlighted that increasing current intensity predicts a linear increase in EF strength; however, it does not necessarily translate to a linear or monotonic enhancement of neurophysiological or behavioral outcomes. Notably, our findings were conducted from averaged responses across all patients, which could have masked inter-individual variabilities in response to tDCS. Morphological brain differences across individuals, such as skull thickness, sulcal depth, or electrode placement, and intra-individual neuroarchitectural complexity within VOTC subregions, characterized by variability in both gyral structures (i.e., antMTG, antMTG, antFG, latFG, medFG, IOG, VMO) and sulcal morphology (i.e., antOTS, antCoS, MFS, CoS, OTS), contribute to the structural and functional heterogeneity of this region and explain the non-uniform EF distribution within VOTC (Holdefer et al., 2006; Miranda et al., 2013). These inter-and intra-variabilities could have

modulated current distribution and ultimately contribute to heterogeneous effects of stimulation, even under standardized stimulation protocols (Vöröslakos et al., 2018; Opitz et al., 2015; Vergallito et al., 2022; L. M. Li et al., 2015)

One session of low-intensity tDCS provides critical and direct evidence of tDCS's ability to induce acute and lasting neurophysiological changes in the human brain. Early *in vitro* and *in vivo* animal studies (Bindman et al., 1962; Creutzfeldt et al., 1962) laid the foundation by demonstrating that weak direct currents can influence cortical neuronal excitability. These studies have shown how EFs lead to sustained polarization of neuronal cell membranes, changes in neuronal firing rates, and transmembrane potential (Korai et al., 2021; Yavari et al., 2018; Rahman et al., 2017; Das et al., 2016; Pelletier & Cicchetti, 2014; Bikson & Rahman, 2013; Nitsche et al., 2008). Our study using direct human iEEG recordings supports these fundamental biophysical principles in the electrophysiology of the human brain during stimulation. Moreover, the lasting effects observed following stimulation in our study appear consistent with neurobiological mechanisms underlying changes in neuronal and synaptic excitability, particularly LTP and LTD. In addition, in the brain, various factors such as the orientation of the EF relative to the spatial arrangement and properties of neuronal compartments (e.g., axons, dendrites, soma) play a critical role in shaping stimulation outcomes (Bikson et al., 2019; Reed & Cohen Kadosh, 2018; Kronberg et al., 2017; Pelletier & Cicchetti, 2014; Monte-Silva et al., 2013; Ranieri et al., 2012; Nitsche & Paulus, 2001). These interactions are further influenced by the cytoarchitectural organization and neural clustering specific to regions within the VOTC, contributing to the variability and complexity of the neuromodulatory effects observed (Grill-Spector et al., 2017;2014b; Weiner et al., 2014, 2014).

Beyond this, our findings also lay the groundwork for identifying the neural electrophysiological changes that may underlie the behavioral outcomes frequently associated with tDCS(Doruk et al., 2014; Masina et al., 2021; Parkin et al., 2019) , especially in the context of facial perception, where it has been linked to reduced FIE (Civile et al., 2024; 2019, 2020b; 2020a) and modulating face discrimination (Wu et al., 2021) and face perception and memory (Barbieri et al., 2016a). To further investigate the relationship between electrophysiological neuromodulation and behavioral outcomes, future studies should incorporate behavioral tasks sensitive to tDCS-induced effects, such as old/new recognition paradigms (Civile, Cooke, et al., 2019, 2020b), face perception task (Barbieri et al., 2016a; Brunyé et al., 2017; Gonzalez-Perez et al., 2019) or the famous face discrimination task (Pisoni et al., 2020; Volfart et al., 2023). Additionally, integrating a longitudinal design with follow-up assessments at multiple time

points post-stimulation (e.g., 30 minutes, 1 hour, and several hours), combining both electrophysiological and behavioral measures could provide a more comprehensive characterization of the temporal evolution and potential persistence of tDCS-induced effects.

In contrast to (Nitsche & Paulus, 2001), our investigation did not aim to determine the minimum tDCS duration required to induce after-effects or long-lasting changes. Rather, it aimed to validate the standard tDCS stimulation duration typically used in clinical and research protocols to assess its behavioral and neurorehabilitation effects in both healthy individuals and patient populations(Renzi et al., 2015; Reinhart et al., 2016; Lefaucheur, 2016; Barbieri et al., 2016a; Manfredi et al., 2017; Gonzalez-Perez et al., 2019; Pisoni et al., 2020). The direct *in vivo* findings confirm prior results indicating that tDCS effects are not restricted to the stimulation period but can persist for minutes to hours if stimulation intensity and duration are sufficient (Bikson et al., 2019; Das et al., 2016, p. 202; Nitsche et al., 2008; Nitsche, 2003; Nitsche & Paulus, 2001; Antal, Kincses, et al., 2004). Thus, the adopted 20-minute duration is well within the established range for inducing persistent electrophysiological after-effects. Moreover, the oversimplified linear relationship between the duration of stimulation and enhanced efficacy has been increasingly challenged. Recent studies suggest that longer stimulation periods don't necessarily enhance tDCS effects or increase their validity and may even reverse or diminish the expected outcomes due to homeostatic mechanisms or non-linear plasticity responses (Yavari et al., 2018; Jamil et al., 2017; Lefaucheur et al., 2017; Monte-Silva et al., 2013).

Therefore, within the framework of this study, implementing a protocol in which the stimulation duration varies, from a few minutes to 30 minutes during a single tDCS session, could help identify the optimal duration that induces maximal tDCS neuromodulation during simulation and the threshold beyond which anodal excitability is abolished. Additionally, combining such protocol with longitudinal electrophysiological exploration of the post-stimulation effect (immediately, a couple of minutes, to hours) could help determine how long the neuromodulatory effects of different stimulation periods persist, and the time required for neural activity to return to baseline. Such an approach also allows the exploration of the most efficient number of sessions and the optimal inter-intervention timing (**Figure 66**).

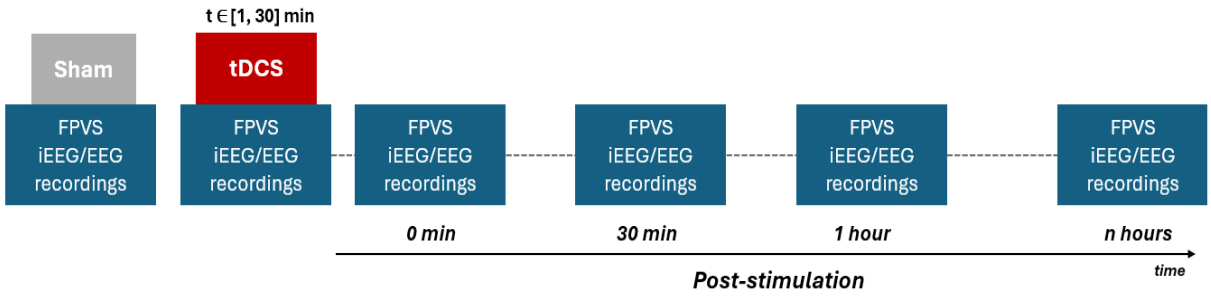

Figure 66. Proposed protocol for Investigating tDCS' duration effects and post-stimulation dynamics.
Schematic representation of the experimental protocol designed to investigate the effects of varying tDCS durations and their post-stimulation impact at several time points. Stimulation durations (t_{stim}) range from 1 to 30 minutes across different sessions, to identify the optimal stimulation time that induces maximal neuromodulation and to determine the threshold beyond which anodal excitability may be reduced. Each stimulation condition is followed by FPVS iEEG/EEG recordings at multiple time points (immediately, 30 minutes, 1 hour, and several hours post-tDCS). .

II. tDCS and Scalp EEG

Working with epilepsy patients provided the unique opportunity to simultaneously record intracerebral as well as scalp EEG activity during tDCS, an approach rarely possible with healthy individuals. Hence, we leveraged simultaneous iEEG-EEG recordings in epileptic patients, combined with HD-tDCS and an FPVS paradigm, to investigate whether similar neuromodulatory effects could be detected across both recording modalities in response to visual recognition. This represents an essential intermediate step towards bridging invasive and noninvasive approaches, allowing us to evaluate whether the neuromodulatory effects observed intracerebrally can also be captured through scalp EEG. Demonstrating this correspondence is a necessary foundation before attempting to replicate and extend these findings into healthy individuals, where only non-invasive tools are available.

The use of small HD-tDCS electrodes seems to be the most suitable option for investigating acute tDCS effects during simultaneous EEG recording, as it allows us to overcome limitations associated with clinical and conventional tDCS setups. Due to their large size, conventional tDCS electrodes generate a diffuse EF that saturates EEG recording amplifiers, making simultaneous acquisition particularly challenging (Diana et al., 2024; Spitoni et al., 2013). However, small HD electrodes used here, which are approximately the same size as standard EEG electrodes, can be placed adjacent to EEG and intracerebral electrodes without any physical obstruction (Baxter et al., 2014; Roy et al., 2014). The HD-tDCS system can mitigate amplifier saturation problems through wider dynamic ranges (Diana et al., 2024).Beyond hardware advantages, HD electrodes can also provide a greater

focused and targeted EF stimulation of specific cortical areas (Faria et al., 2012a; Datta et al., 2009). Moreover, the 4x1 HD montage has been shown to be a valuable tool for simultaneous EEG recording during tDCS, enabling the detection of both acute and lasting changes in broadband cortical synchronization(Roy et al., 2014). Future studies should consider implementing more complex montages, like the 4x1 HD montage combined with scalp EEG, to improve the likelihood of observing important tDCS effects.

One major limitation of our simultaneous tDCS-EEG investigation is the lack of methodologically reliable artifact removal techniques, while several approaches exist, their effectiveness remains limited and inconsistent, particularly during active stimulation(Gebodh et al., 2019). The latter stems from the complex nature of the tDCS-induced artifacts encountered during online EEG recordings that overlap with ongoing neural activity. Despite our attempts at controlling the experimental conditions, running a tDCS experiment in a clinical setup for iEEG recording and video monitoring with limited scalp coverage, limited our ability to minimize or remove some non-inherent artifacts such as myogenic and ocular ones. Regardless of the use of only two HD ring electrodes for tDCS, spectral artifacts were still observed at harmonic frequencies near the stimulating electrode. These rhythmic artifacts could be attributed to a modulation by nonstationary broadband physiological artifacts like cardiac or respiratory distortions, or even to the ongoing impedance measurement by tDCS device (Kohli & Casson, 2019; Gebodh et al., 2019; Noury et al., 2016). Thanks to the FPVS approach implemented in this study that isolated the responses in specific predefined frequencies of interest (Rossion et al., 2015a), the application of temporal filtering to remove tDCS rhythmic artifacts didn't affect the integrity of the neural responses at the target frequencies. This methodological advantage allowed us to reliably quantify both face-selective and general visual responses, even in the presence of low-amplitude stimulation-related noise.

Furthermore, the application of ICA to isolate specific tDCS artifacts was hindered or challenged by the absence of clear, distinguishing features that reliably separate stimulation-related components from neural brain activity. While some IC components displayed scalp topographies consistent with the location of the stimulation electrodes, their temporal characteristics were highly similar, making it difficult to determine which components to remove without risking the distortion of ongoing neural signals. This overlap in features further complicates the use of ICA for artifact correction in concurrent tDCS-EEG recordings, where stimulation-related and neural activities can co-exist within overlapping frequency bands. The lack of objective criteria for artifact removal underscores the limitations of ICA in

concurrent tDCS and EEG. Thus, future studies aiming to understand neuromodulatory effects with online tDCS and EEG in clinical populations could consider combining ICA with a phantom head model (Mancini et al., 2015, 2016; Roy et al., 2014). This method could offer a valuable preliminary assessment of the characteristics of tDCS-induced artifacts and help evaluate the feasibility of the experimental procedure in a clinical setting. Such an approach would also allow for controlled validation of artifact components in the absence of neural activity, potentially improving the identification and removal of stimulation-related signals in patient data.

All in all, the refinement of tDCS artifact removal techniques would facilitate the investigation of correlations between intracerebral and scalp EEG findings, enabling direct comparison between tDCS effects on deep brain regions vs critical surface. Moreover, correlation studies, especially when combined with different cognitive tasks (like learning, memory, and working memory), which are rarely explored due to the challenges of intracerebral implantation, could help bridge the gap between the diverse tDCS effects observed with scalp EEG reported in the literature. Furthermore, the application of adequate artifact correction pipelines combining both experimental and signal-processing strategies would allow the transition from invasive intracerebral investigation to noninvasive scalp EEG recording adequate for most healthy controls.

III. Icecap and Neuronaute

Undeniably, conventional research-grade EEG recording devices have been pivotal tools in the exploration of electrophysiological brain activity, especially for medical purposes. EEG is utilized in monitoring, diagnosing, and treating neurological (Basak et al., 2024)and psychiatric disorders (Newson & Thiagarajan, 2019). In addition, it's become instrumental in exploring cognitive dysfunctions by enabling early identification of neurophysiological biomarkers, supporting prognosis assessment, and ensuring effective implementation of targeted therapies (Alvi et al., 2022).

Following methodological advancements and medical needs, recent enhancements in the EEG field include the development and integration of wireless and portable EEG devices (Casson, 2019). Ideally, these devices would allow the application of the extensive EEG research accumulated over the past century to real-world situations, outside laboratory environments, and without constraints of old equipment. The use of portable EEG devices, similar to the Neuronaute-Icecap system, has been

increasing exponentially in the last fourteen years (He et al., 2023 for review). Various wireless EEG devices are currently available for customers, researchers, and clinical applications. Based on the purpose of their application, they differ in various characteristics: electrode properties (type, placement, number), amplifier, impedance, battery life, and access to real-time data (Niso et al., 2023).

The parameters we reported for the Neuronaute system appear to align with current trends in the wireless EEG market. Most available devices include an average of 18 electrodes, slightly fewer than the 21 included in the Icecap. Moreover, electrode placement and headset design are generally adapted to the system's intended purpose, whether clinical, research-oriented, or consumer-focused. For instance, a limited scalp coverage with fewer electrodes may be sufficient when targeting specific regions, such as the occipital cortex for visual activity. Notably, despite Icecap lacking the P10 temporo-occipital electrode, the face-selective responses were still observed at the nearby P8 electrode.

Additionally, the Neuronaute system seems to provide one of the longest battery lives among wireless EEG devices (i.e., 72 hours). The extended battery life duration enhances devices' portability, as it allows greater mobility and facilitates long-term monitoring (e.g., overnight recordings for sleep monitoring)(Scott et al., 2020). It's also been employed for seizure monitoring in epileptic patients. The current version of the Neuronaute we tested here seems bulky and less suitable for prolonged duration; however, the newest version (Neuronaute+) available for customers is reportedly more compact and allows more portability.

Moreover, some modifications could be proposed to improve the device's usability. Although with the Neuronaute device, the impedances can be checked before and during acquisition, it interrupts ongoing recording. Enhancing the platform to allow simultaneous acquisition and impedance tracking would improve detection and real-time identification of noisy electrodes. Additionally, while the current device enables remote access to acquired recordings, integrating new technologies that allow remote real-time data access would be impactful, especially for long-duration monitoring like sleep studies and seizure detection (Mathewson et al., 2024).

The main aim of developing wireless EEG devices is to allow the remote monitoring of patients' electrophysiological activity, whether in a resting state or during a task. In the present manuscript, we validate the ability of the Neuronaute/Icecap system in recording cognitive visual potentials during fast periodic presentation of images in a research environment. Notably, scientists have urged the adoption

of a multidisciplinary approach including cognitive measures in treating neuropsychiatric disorders (Z. Lu et al., 2025; Jadhav et al., 2022; Sowndhararajan et al., 2018). Providing clinicians with the ability to remotely record and monitor patients' ERPs in response to specific tasks would open new avenues in the medical field (Campanella, 2013).

Integrating a wireless EEG recording system like the Neuronaute with a tDCS device in a controlled home-based environment could expand the accessibility and ecological validity of neurophysiological investigations. With adequate user training, it could enable frequent and flexible testing sessions outside traditional laboratory settings, particularly benefiting patients with neurological or psychiatric conditions. Combining this setup with an FPVS paradigm would allow us to record reliable electrophysiological responses with minimal behavioral demands, making it well-suited for remote monitoring. In this respect, wearable wireless EEG solutions like the Icecap, which prioritize comfort and mobility, alongside accessible tDCS systems, could open new possibilities for clinical and research use by promoting more personalized and continuous assessment of brain activity.

Building on this idea, the next step could be the development of a closed-loop system that not only delivers tDCS but also detects and responds to neural abnormalities in real time. Previous work of Leite et al., 2017, has shown the potential of such systems to monitor brain activity and adjust stimulation parameters accordingly, allowing for more targeted and adaptive interventions. When combined with scalp EEG biomarkers linked to specific neuropsychiatric disorders, this approach could support personalized treatment strategies by identifying abnormal patterns and modulating them dynamically. This type of system could be valuable for long-term management of conditions like epilepsy, depression, or attention disorders, especially if integrated into a user-friendly home-based setup (Vliet et al., 2012). It could also offer new opportunities for researchers to study how brain activity evolves in more natural "everyday life" settings, with direct impact on diagnosis and therapy.

General Conclusion

This research provides the first direct electrophysiological evidence of tDCS-induced neuromodulation within the human brain using intracerebral recordings. he multimodal integration of tDCS with simultaneous iEEG and FPVS in epileptic patients successfully bridged the longstanding gap between animal research with human protocols, offering clear proof of tDCS effects on neural activity in vivo in the human brain. The findings presented in this thesis advance the field by demonstrating that: 1) A low-intensity electric field applied during one session of tDCS can produce significant acute and lasting change in neuronal functions, 2) Only two HD small electrodes can achieve functionally targeting of ongoing evoked neuronal activity in specific face-selective brain regions, 3) Differential patterns of neuromodulation within the middle fusiform gyrus reflect the influence of underlying neuroarchitectural features, 4) validate the effectiveness of standard clinical tDCS parameters (20 min, 2mA) used for clinical therapy, 5) provide foundational electrophysiological evidence underlying the widely reported behavioral effects of tDCS in the literature, 6) FPVS emerges as a robust and reliable paradigm for capturing selective and objective neuromodulatory effects in humans.

Acknowledging the limited accessibility of iEEG recordings, we leveraged simultaneous iEEG–scalp EEG recordings alongside HD-tDCS and FPVS to investigate whether neuromodulatory effects detected intracerebrally are reflected at the scalp level. This unique multimodal approach combining simultaneous iEEG-EEG-tDCS and FPVS allowed us to show: 1) Despite limited sample size and scalp coverage, scalp EEG holds great potential for detecting tDCS neuromodulatory changes observed intracerebrally, 2) Contrary to iEEG recording, the effects of a single tDCS session on scalp-recorded neural signals are transient and reversible, 3) during active stimulation, tDCS transiently modulates both neural signals and background noise, obscuring interpretation of amplitudes tDCS-induced changes, 4) tDCS transiently disorganize the cortical network near the stimulation site while concurrently enhancing neural activity in deeper brain regions.

And finally, with the aim of expanding the methodological potential of applying the tDCS–FPVS approach to accessible, home-based settings, we validated the use of the Neuronaute–Icecap acquisition system for recording cognitive EEG biomarkers. The Neuronaute-FPVS setup revealed: 1) Reliable, significant, and objective electrophysiological measures of face identity discrimination. 2) ergonomic cap design that facilitates user comfort, as well as ease of application and removal, 3)

Wireless transmission of data and remote monitoring underscore the potential for its application in home-based environments.

All in all, we have significantly improved the understanding of the electrophysiological mechanism of tDCS neuromodulation in the human brain. We laid the groundwork for future investigations using a multimodal approach (intracerebral EEG, scalp EEG, FPVS) with tDCS application for both neurorehabilitation in patients and modulating neural activity in healthy individuals. We also provided objective and quantifiable measures of tDCS neuromodulation across different recording scales. The frequency-tagging approach provided a substantial tool for reliably tracking dynamic changes in cognitive processing in targeted brain regions during stimulation. We also provide foundational evidence supporting the use of standard minimal tDCS parameters (2mA, 20 minutes, 2HD electrodes) and establish a framework for future research to apply these protocols or to investigate tDCS effects on diverse cognitive functions.

References

Accornero, N., Li Voti, P., La Riccia, M., & Gregori, B. (2007). Visual evoked potentials modulation during direct current cortical polarization. *Experimental Brain Research*, *178*(2), 261–266. https://doi.org/10.1007/s00221-006-0733-y

Adrian, E. D., & Matthews, B. H. C. (1934). The Berger rhythm: Potential changes from the occipital lobes in man. *Brain*, *57*(4), 355–385. https://doi.org/10.1093/brain/57.4.355

Alam, M., Truong, D. Q., Khadka, N., & Bikson, M. (2016). Spatial and polarity precision of concentric high-definition transcranial direct current stimulation (HD-tDCS). *Physics in Medicine and Biology*, *61*(12), 4506–4521. https://doi.org/10.1088/0031-9155/61/12/4506

Alekseichuk, I., Falchier, A. Y., Linn, G., Xu, T., Milham, M. P., Schroeder, C. E., & Opitz, A. (2019). Electric field dynamics in the brain during multi-electrode transcranial electric stimulation. *Nature Communications*, *10*(1), 2573. https://doi.org/10.1038/s41467-019-10581-7

Allison, T., Puce, A., Spencer, D. D., & McCarthy, G. (1999). Electrophysiological Studies of Human Face Perception. I: Potentials Generated in Occipitotemporal Cortex by Face and Non-face Stimuli. *Cerebral Cortex*, *9*(5), 415–430. https://doi.org/10.1093/cercor/9.5.415

Alonso-Prieto, E., Belle, G. V., Liu-Shuang, J., Norcia, A. M., & Rossion, B. (2013). The 6 Hz fundamental stimulation frequency rate for individual face discrimination in the right occipito-temporal cortex. *Neuropsychologia*, *51*(13), 2863–2875. https://doi.org/10.1016/j.neuropsychologia.2013.08.018

Alvi, A. M., Siuly, S., & Wang, H. (2022). Neurological abnormality detection from electroencephalography data: A review. *Artificial Intelligence Review*, *55*(3), 2275–2312. https://doi.org/10.1007/s10462-021-10062-8

Angelini, L., Jacques, C., Maillard, L., Colnat-Coulbois, S., Rossion, B., & Jonas, J. (2024). Bidirectional and Cross-Hemispheric Modulations of Face-Selective Neural Activity Induced by Electrical Stimulation within the Human Cortical Face Network. *Brain Sciences*, *14*(9), 906. https://doi.org/10.3390/brainsci14090906

Angelini, L., Volfart, A., Jacques, C., Colnat-Coulbois, S., Maillard, L., Rossion, B., & Jonas, J. (2024). Effective connectivity of functional brain regions through concurrent intracerebral electrical stimulation and frequency-tagged visual presentation. *Brain Stimulation*, *17*(3), 726–729. https://doi.org/10.1016/j.brs.2024.05.016

Antal, A., Ambrus, G. G., & Chaieb, L. (2014). The impact of electrical stimulation techniques on behavior. *WIREs Cognitive Science*, *5*(6), 649–659. https://doi.org/10.1002/wcs.1319

Antal, A., Brepohl, N., Poreisz, C., Boros, K., Csifcsak, G., & Paulus, W. (2008). Transcranial Direct Current Stimulation Over Somatosensory Cortex Decreases ExperimentallyInduced Acute Pain Perception. *The Clinical Journal of Pain*, *24*(1), 56. https://doi.org/10.1097/AJP.0b013e318157233b

Antal, A., Ganho-Ávila, A., Assecondi, S., Barbour, T., Bjekić, J., Blumberger, D. M., Bolognini, N., Brunelin, J., Chanes, L., Dale, M., Dubbioso, R., D'Urso, G., Filipcic, I., Filipović, S. R., Hirnstein, M., Konings, F., Langguth, B., Leocani, L., Sorkhabi, M. M., … Baeken, C. (2024). The

consequences of the new European reclassification of non-invasive brain stimulation devices and the medical device regulations pose an existential threat to research and treatment: An invited opinion paper. *Clinical Neurophysiology*, *163*, 280–291. https://doi.org/10.1016/j.clinph.2024.03.039

Antal, A., & Herrmann, C. S. (2016). Transcranial Alternating Current and Random Noise Stimulation: Possible Mechanisms. *Neural Plasticity*, *2016*(1), 3616807. https://doi.org/10.1155/2016/3616807

Antal, A., Kincses, T. Z., Nitsche, M. A., Bartfai, O., & Paulus, W. (2004). Excitability Changes Induced in the Human Primary Visual Cortex by Transcranial Direct Current Stimulation: Direct Electrophysiological Evidence. *Investigative Ophthalmology & Visual Science*, *45*(2), 702–707. https://doi.org/10.1167/iovs.03-0688

Antal, A., Luber, B., Brem, A.-K., Bikson, M., Brunoni, A. R., Cohen Kadosh, R., Dubljević, V., Fecteau, S., Ferreri, F., Flöel, A., Hallett, M., Hamilton, R. H., Herrmann, C. S., Lavidor, M., Loo, C., Lustenberger, C., Machado, S., Miniussi, C., Moliadze, V., … Paulus, W. (2022). Non-invasive brain stimulation and neuroenhancement. *Clinical Neurophysiology Practice*, *7*, 146–165. https://doi.org/10.1016/j.cnp.2022.05.002

Antal, A., Nitsche, M. A., & Paulus, W. (2001). External modulation of visual perception in humans. *Neuroreport*, *12*(16), 3553–3555. https://doi.org/10.1097/00001756-200111160-00036

Antal, A., Nitsche, M. A., & Paulus, W. (2006). Transcranial direct current stimulation and the visual cortex. *Brain Research Bulletin*, *68*(6), 459–463. https://doi.org/10.1016/j.brainresbull.2005.10.006

Antal, A., Terney, D., Kühnl, S., & Paulus, W. (2010). Anodal Transcranial Direct Current Stimulation of the Motor Cortex Ameliorates Chronic Pain and Reduces Short Intracortical Inhibition. *Journal of Pain and Symptom Management*, *39*(5), 890–903. https://doi.org/10.1016/j.jpainsymman.2009.09.023

Antal, A., Terney, D., Poreisz, C., & Paulus, W. (2007). Towards unravelling task-related modulations of neuroplastic changes induced in the human motor cortex. *European Journal of Neuroscience*, *26*(9), 2687–2691. https://doi.org/10.1111/j.1460-9568.2007.05896.x

Antal, A., Varga, E. T., Kincses, T. Z., Nitsche, M. A., & Paulus, W. (2004). Oscillatory brain activity and transcranial direct current stimulation in humans. *NeuroReport*, *15*(8), 1307. https://doi.org/10.1097/01.wnr.0000127460.08361.84

Atkinson, A. P., & Adolphs, R. (2011). The neuropsychology of face perception: Beyond simple dissociations and functional selectivity. *Philosophical Transactions of the Royal Society B: Biological Sciences*, *366*(1571), 1726–1738. https://doi.org/10.1098/rstb.2010.0349

Babiloni, C., Barry, R. J., Başar, E., Blinowska, K. J., Cichocki, A., Drinkenburg, W. H. I. M., Klimesch, W., Knight, R. T., Lopes da Silva, F., Nunez, P., Oostenveld, R., Jeong, J., Pascual-Marqui, R., Valdes-Sosa, P., & Hallett, M. (2020). International Federation of Clinical Neurophysiology (IFCN) – EEG research workgroup: Recommendations on frequency and topographic analysis of resting state EEG rhythms. Part 1: Applications in clinical research studies. *Clinical Neurophysiology*, *131*(1), 285–307. https://doi.org/10.1016/j.clinph.2019.06.234

Barbero, F. M., Calce, R. P., Talwar, S., Rossion, B., & Collignon, O. (2021). *A robust voice-selective response in the human brain as revealed by electrophysiological recordings and fast periodic auditory stimulation* (p. 2021.03.13.435142). bioRxiv. https://doi.org/10.1101/2021.03.13.435142

Barbieri, M., Negrini, M., Nitsche, M. A., & Rivolta, D. (2016a). Anodal-tDCS over the human right occipital cortex enhances the percept ion and memory of both faces and objects. *Neuropsychologia*, *81*, 238–244. PubMed. https://doi.org/10.1016/j.neuropsychologia.2015.12.030

Barbieri, M., Negrini, M., Nitsche, M. A., & Rivolta, D. (2016b). Anodal-tDCS over the human right occipital cortex enhances the perception and memory of both faces and objects. *Neuropsychologia*, *81*, 238–244. https://doi.org/10.1016/j.neuropsychologia.2015.12.030

Barborica, A., Mindruta, I., Sheybani, L., Spinelli, L., Oane, I., Pistol, C., Donos, C., López-Madrona, V. J., Vulliemoz, S., & Bénar, C.-G. (2021). Extracting seizure onset from surface EEG with independent component analysis: Insights from simultaneous scalp and intracerebral EEG. *NeuroImage : Clinical*, *32*, 102838. https://doi.org/10.1016/j.nicl.2021.102838

Basak, M., Maiti, D., & Das, D. (2024). EEG Innovations in Neurological Disorder Diagnostics: A Five-Year Review. *Asian Journal of Research in Computer Science*, *17*(6), 226–249. https://doi.org/10.9734/ajrcos/2024/v17i6470

Batsikadze, G., Moliadze, V., Paulus, W., Kuo, M.-F., & Nitsche, M. A. (2013). Partially non-linear stimulation intensity-dependent effects of direct current stimulation on motor cortex excitability in humans. *The Journal of Physiology*, *591*(7), 1987–2000. https://doi.org/10.1113/jphysiol.2012.249730

Baxter, B. S., Edelman, B., Zhang, X., Roy, A., & He, B. (2014). Simultaneous high-definition transcranial direct current stimulation of the motor cortex and motor imagery. *Annual International Conference of the IEEE Engineering in Medicine and Biology Society. IEEE Engineering in Medicine and Biology Society. Annual International Conference*, *2014*, 454–456. https://doi.org/10.1109/EMBC.2014.6943626

Beaudreau, S. A., & Finger, S. (2006). Medical electricity and madness in the 18th century: The legacies of Benjamin Franklin and Jan Ingenhousz. *Perspectives in Biology and Medicine*, *49*(3), 330–345. https://doi.org/10.1353/pbm.2006.0036

Begemann, M. J., Brand, B. A., Ćurčić-Blake, B., Aleman, A., & Sommer, I. E. (2020). Efficacy of non-invasive brain stimulation on cognitive functioning in brain disorders: A meta-analysis. *Psychological Medicine*, *50*(15), 2465–2486. https://doi.org/10.1017/S0033291720003670

Benninger, D. H., Lomarev, M., Lopez, G., Wassermann, E. M., Li, X., Considine, E., & Hallett, M. (2010). Transcranial direct current stimulation for the treatment of Parkinson's disease. *Journal of Neurology, Neurosurgery & Psychiatry*, *81*(10), 1105–1111. https://doi.org/10.1136/jnnp.2009.202556

Berger, H. (1929). Über das Elektrenkephalogramm des Menschen. *Archiv für Psychiatrie und Nervenkrankheiten*, *87*(1), 527–570. https://doi.org/10.1007/BF01797193

Bhattacharya, A., Mrudula, K., Sreepada, S. S., Sathyaprabha, T. N., Pal, P. K., Chen, R., & Udupa, K. (2022). An Overview of Noninvasive Brain Stimulation: Basic Principles and Clinical

Applications. *Canadian Journal of Neurological Sciences*, *49*(4), 479–492. https://doi.org/10.1017/cjn.2021.158

Biasiucci, A., Franceschiello, B., & Murray, M. M. (2019). Electroencephalography. *Current Biology*, *29*(3), R80–R85. https://doi.org/10.1016/j.cub.2018.11.052

Bikson, M., Brunoni, A. R., Charvet, L. E., Clark, V. P., Cohen, L. G., Deng, Z.-D., Dmochowski, J., Edwards, D. J., Frohlich, F., Kappenman, E. S., Lim, K. O., Loo, C., Mantovani, A., McMullen, D. P., Parra, L. C., Pearson, M., Richardson, J. D., Rumsey, J. M., Sehatpour, P., … Lisanby, S. H. (2018). Rigor and reproducibility in research with transcranial electrical stimulation: An NIMH-sponsored workshop. *Brain Stimulation*, *11*(3), 465–480. https://doi.org/10.1016/j.brs.2017.12.008

Bikson, M., Grossman, P., Thomas, C., Zannou, A. L., Jiang, J., Adnan, T., Mourdoukoutas, A. P., Kronberg, G., Truong, D., Boggio, P., Brunoni, A. R., Charvet, L., Fregni, F., Fritsch, B., Gillick, B., Hamilton, R. H., Hampstead, B. M., Jankord, R., Kirton, A., … Woods, A. J. (2016). Safety of Transcranial Direct Current Stimulation: Evidence Based Update 2016. *Brain Stimulation*, *9*(5), 641–661. https://doi.org/10.1016/j.brs.2016.06.004

Bikson, M., Inoue, M., Akiyama, H., Deans, J. K., Fox, J. E., Miyakawa, H., & Jefferys, J. G. R. (2004). Effects of uniform extracellular DC electric fields on excitability in rat hippocampal slices in vitro. *The Journal of Physiology*, *557*(Pt 1), 175–190. https://doi.org/10.1113/jphysiol.2003.055772

Bikson, M., Paulus, W., Esmaeilpour, Z., Kronberg, G., & Nitsche, M. A. (2019). Mechanisms of Acute and After Effects of Transcranial Direct Current Stimulation. In H. Knotkova, M. A. Nitsche, M. Bikson, & A. J. Woods (Eds.), *Practical Guide to Transcranial Direct Current Stimulation: Principles, Procedures and Applications* (pp. 81–113). Springer International Publishing. https://doi.org/10.1007/978-3-319-95948-1_3

Bikson, M., & Rahman, A. (2013). Origins of specificity during tDCS: Anatomical, activity-selective, and input-bias mechanisms. *Frontiers in Human Neuroscience*, *7*. https://doi.org/10.3389/fnhum.2013.00688

Bikson, M., Rahman, A., & Datta, A. (2012). Computational Models of Transcranial Direct Current Stimulation. *Clinical EEG and Neuroscience*, *43*(3), 176–183. https://doi.org/10.1177/1550059412445138

Bindman, L. J., Lippold, O. C. J., & Redfearn, J. W. T. (1962). Long-lasting Changes in the Level of the Electrical Activity of the Cerebral Cortex produced by Polarizing Currents. *Nature*, *196*(4854), 584–585. https://doi.org/10.1038/196584a0

Bindman, L. J., Lippold, O. C. J., & Redfearn, J. W. T. (1964). The action of brief polarizing currents on the cerebral cortex of the rat (1) during current flow and (2) in the production of long-lasting after-effects. *The Journal of Physiology*, *172*(3), 369–382.

Boggio, P. S., Ferrucci, R., Mameli, F., Martins, D., Martins, O., Vergari, M., Tadini, L., Scarpini, E., Fregni, F., & Priori, A. (2012). Prolonged visual memory enhancement after direct current stimulation in Alzheimer's disease. *Brain Stimulation*, *5*(3), 223–230. https://doi.org/10.1016/j.brs.2011.06.006

Boggio, P. S., Nunes, A., Rigonatti, S. P., Nitsche, M. A., Pascual-Leone, A., & Fregni, F. (2007). Repeated sessions of noninvasive brain DC stimulation is associated with motor function improvement in stroke patients. *Restorative Neurology and Neuroscience*, *25*(2), 123–129.

Bolognini, N., & Diana, L. (2021). Multimodal Association of tDCS with Electroencephalography. In A. R. Brunoni, M. A. Nitsche, & C. K. Loo (Eds.), *Transcranial Direct Current Stimulation in Neuropsychiatric Disorders: Clinical Principles and Management* (pp. 107–126). Springer International Publishing. https://doi.org/10.1007/978-3-030-76136-3_7

Bradley, C., Nydam, A. S., Dux, P. E., & Mattingley, J. B. (2022). State-dependent effects of neural stimulation on brain function and cognition. *Nature Reviews. Neuroscience*, *23*(8), 459–475. https://doi.org/10.1038/s41583-022-00598-1

Brunyé, T. T., Moran, J. M., Holmes, A., Mahoney, C. R., & Taylor, H. A. (2017). Non-invasive brain stimulation targeting the right fusiform gyrus selectively increases working memory for faces. *Brain and Cognition*, *113*, 32–39. https://doi.org/10.1016/j.bandc.2017.01.006

Caharel, S., d'Arripe, O., Ramon, M., Jacques, C., & Rossion, B. (2009). Early adaptation to repeated unfamiliar faces across viewpoint changes in the right hemisphere: Evidence from the N170 ERP component. *Neuropsychologia*, *47*(3), 639–643. https://doi.org/10.1016/j.neuropsychologia.2008.11.016

Caharel, S., & Rossion, B. (2021). The N170 is Sensitive to Long-term (Personal) Familiarity of a Face Identity. *Neuroscience*, *458*, 244–255. https://doi.org/10.1016/j.neuroscience.2020.12.036

Campanella, S. (2013). Why it is time to develop the use of cognitive event-related potentials in the treatment of psychiatric diseases. *Neuropsychiatric Disease and Treatment*, *9*, 1835–1845. https://doi.org/10.2147/NDT.S53687

Campanella, S. (2023). The potential utility of evoked potentials in the treatment of mental illnesses. *Psychoradiology*, *3*, kkad024. https://doi.org/10.1093/psyrad/kkad024

Cao, Z. (2020). A review of artificial intelligence for EEG-based brain−computer interfaces and applications. *Brain Science Advances*, *6*(3), 162–170. https://doi.org/10.26599/BSA.2020.9050017

Caparelli-Daquer, E. M., Zimmermann, T. J., Mooshagian, E., Parra, L. C., Rice, J. K., Datta, A., Bikson, M., & Wassermann, E. M. (2012). A pilot study on effects of 4×1 High-Definition tDCS on motor cortex excitability. *2012 Annual International Conference of the IEEE Engineering in Medicine and Biology Society*, 735–738. https://doi.org/10.1109/EMBC.2012.6346036

Caspers, J., Zilles, K., Eickhoff, S. B., Schleicher, A., Mohlberg, H., & Amunts, K. (2013). Cytoarchitectonical analysis and probabilistic mapping of two extrastriate areas of the human posterior fusiform gyrus. *Brain Structure & Function*, *218*(2), 511–526. https://doi.org/10.1007/s00429-012-0411-8

Cassidy, S. M., Robertson, I. H., & O'Connell, R. G. (2012). Retest reliability of event-related potentials: Evidence from a variety of paradigms. *Psychophysiology*, *49*(5), 659–664. https://doi.org/10.1111/j.1469-8986.2011.01349.x

Casson, A. J. (2019). Wearable EEG and beyond. *Biomedical Engineering Letters*, *9*(1), 53–71. https://doi.org/10.1007/s13534-018-00093-6

Chatelle, C., Rosenthal, E. S., Bodien, Y. G., Spencer-Salmon, C. A., Giacino, J. T., & Edlow, B. L. (2020). EEG Correlates of Language Function in Traumatic Disorders of Consciousness. *Neurocritical Care*, *33*(2), 449–457. https://doi.org/10.1007/s12028-019-00904-3

Chhatbar, P. Y., Kautz, S. A., Takacs, I., Rowland, N. C., Revuelta, G. J., George, M. S., Bikson, M., & Feng, W. (2018). Evidence of transcranial direct current stimulation-generated electric fields at subthalamic level in human brain in vivo. *Brain Stimulation*, *11*(4), 727–733. https://doi.org/10.1016/j.brs.2018.03.006

Ciullo, V., Spalletta, G., Caltagirone, C., Banaj, N., Vecchio, D., Piras, F., & Piras, F. (2021). Transcranial Direct Current Stimulation and Cognition in Neuropsychiatric Disorders: Systematic Review of the Evidence and Future Directions. *The Neuroscientist: A Review Journal Bringing Neurobiology, Neurology and Psychiatry*, *27*(3), 285–309. https://doi.org/10.1177/1073858420936167

Civile, C., Cooke, A., Liu, X., McLaren, R., Elchlepp, H., Lavric, A., Milton, F., & McLaren, I. P. L. (2019). The effect of tDCS on recognition depends on stimulus generalization: Neuro-stimulation can predictably enhance or reduce the face inversion effect. *Journal of Experimental Psychology: Animal Learning and Cognition*. https://www.academia.edu/40447563/The_effect_of_tDCS_on_recognition_depends_on_stimulus_generalization_Neuro_stimulation_can_predictably_enhance_or_reduce_the_face_inversion_effect

Civile, C., Cooke, A., Liu, X., McLaren, R., Elchlepp, H., Lavric, A., Milton, F., & McLaren, I. P. L. (2020a). The effect of tDCS on recognition depends on stimulus generalization: Neuro-stimulation can predictably enhance or reduce the face inversion effect. *Journal of Experimental Psychology: Animal Learning and Cognition*, *46*(1), 83–98. https://doi.org/10.1037/xan0000232

Civile, C., Cooke, A., Liu, X., McLaren, R., Elchlepp, H., Lavric, A., Milton, F., & McLaren, I. P. L. (2020b). The effect of tDCS on recognition depends on stimulus generalization: Neuro-stimulation can predictably enhance or reduce the face inversion effect. *Journal of Experimental Psychology: Animal Learning and Cognition*, *46*(1), 83–98. https://doi.org/10.1037/xan0000232

Civile, C., McLaren, R., & McLaren, I. P. L. (2018). How we can change your mind: Anodal tDCS to Fp3 alters human stimulus representation and learning. *Neuropsychologia*, *119*, 241–246. https://doi.org/10.1016/j.neuropsychologia.2018.08.019

Civile, C., Obhi, S. S., & McLaren, I. P. L. (2019). The role of experience-based perceptual learning in the face inversion effect. *Vision Research*, *157*, 84–88. https://doi.org/10.1016/j.visres.2018.02.010

Civile, C., Waguri, E., & McLaren, I. P. L. (2024). Using transcranial direct current stimulation (tDCS) to selectively modulate the face inversion effect and N170 event-related potentials. *Perception*, *53*(2), 125–142. https://doi.org/10.1177/03010066231215909

Civile, C., Waguri, E., Quaglia, S., Wooster, B., Curtis, A., McLaren, R., Lavric, A., & McLaren, I. P. L. (2020a). Testing the effects of transcranial direct current stimulation (tDCS) on the face inversion effect and the N170 event-related potentials (ER Ps) component. *Neuropsychologia*, *143*, 107470. PubMed. https://doi.org/10.1016/j.neuropsychologia.2020.107470

Civile, C., Waguri, E., Quaglia, S., Wooster, B., Curtis, A., McLaren, R., Lavric, A., & McLaren, I. P. L. (2020b). Testing the effects of transcranial direct current stimulation (tDCS) on the face inversion effect and the N170 event-related potentials (ERPs) component. *Neuropsychologia*, *143*, 107470. https://doi.org/10.1016/j.neuropsychologia.2020.107470

Costantino, A. I., Titoni, M., Bossi, F., Premoli, I., Nitsche, M. A., & Rivolta, D. (2017). Preliminary Evidence of "Other-Race Effect"-Like Behavior Induced by Cathodal-tDCS over the Right Occipital Cortex, in the Absence of Overall Effects on Face/Object Processing. *Frontiers in Neuroscience*, *11*, 661. https://doi.org/10.3389/fnins.2017.00661

Covey, T. J., Shucard, J. L., Benedict, R. H., Weinstock-Guttman, B., & Shucard, D. W. (2018). Improved cognitive performance and event-related potential changes following working memory training in patients with multiple sclerosis. *Multiple Sclerosis Journal - Experimental, Translational and Clinical*, *4*(1), 2055217317747626. https://doi.org/10.1177/2055217317747626

Creutzfeldt, O. D., Fromm, G. H., & Kapp, H. (1962). Influence of transcortical d-c currents on cortical neuronal activity. *Experimental Neurology*, *5*(6), 436–452. https://doi.org/10.1016/0014-4886(62)90056-0

Das, S., Holland, P., Frens, M. A., & Donchin, O. (2016). Impact of Transcranial Direct Current Stimulation (tDCS) on Neuronal Functions. *Frontiers in Neuroscience*, *10*, 550. https://doi.org/10.3389/fnins.2016.00550

DaSilva, A. F., Truong, D. Q., DosSantos, M. F., Toback, R. L., Datta, A., & Bikson, M. (2015). State-of-art neuroanatomical target analysis of high-definition and conventional tDCS montages used for migraine and pain control. *Frontiers in Neuroanatomy*, *9*, 89. https://doi.org/10.3389/fnana.2015.00089

DaSilva, A. F., Volz, M. S., Bikson, M., & Fregni, F. (2011). Electrode Positioning and Montage in Transcranial Direct Current Stimulation. *Journal of Visualized Experiments : JoVE*, *51*, 2744. https://doi.org/10.3791/2744

Datta, A., Bansal, V., Diaz, J., Patel, J., Reato, D., & Bikson, M. (2009). Gyri-precise head model of transcranial direct current stimulation: Improved spatial focality using a ring electrode versus conventional rectangular pad. *Brain Stimulation*, *2*(4), 201-207.e1. https://doi.org/10.1016/j.brs.2009.03.005

Datta, A., Elwassif, M., Battaglia, F., & Bikson, M. (2008). Transcranial current stimulation focality using disc and ring electrode configurations: FEM analysis. *Journal of Neural Engineering*, *5*(2), 163–174. https://doi.org/10.1088/1741-2560/5/2/007

David, J., Quenon, L., Hanseeuw, B., Ivanoiu, A., Volfart, A., Koessler, L., & Rossion, B. (2025). An objective and sensitive electrophysiological marker of word semantic categorization impairment in Alzheimer's disease. *Clinical Neurophysiology*, *170*, 98–109. https://doi.org/10.1016/j.clinph.2024.12.018

Dawson, R. E., Webster, J. E., & Gurdjian, E. S. (1951). *Serial Electroencephalography in Acute Head Injuries*. https://doi.org/10.3171/jns.1951.8.6.0613

Diana, L., Casati, C., Melzi, L., Bianchi Marzoli, S., & Bolognini, N. (2024). The effects of occipital and parietal tDCS on chronic visual field defects after brain injury. *Frontiers in Neurology*, *15*. https://doi.org/10.3389/fneur.2024.1340365

Dmochowski, J. P., Datta, A., Bikson, M., Su, Y., & Parra, L. C. (2011). Optimized multi-electrode stimulation increases focality and intensity at target. *Journal of Neural Engineering*, *8*(4), 046011. https://doi.org/10.1088/1741-2560/8/4/046011

Doruk, D., Gray, Z., Bravo, G. L., Pascual-Leone, A., & Fregni, F. (2014). Effects of tDCS on executive function in Parkinson's disease. *Neuroscience Letters*, *582*, 27–31. https://doi.org/10.1016/j.neulet.2014.08.043

Dzhelyova, M., Jacques, C., Dormal, G., Michel, C., Schiltz, C., & Rossion, B. (2019). High test-retest reliability of a neural index of rapid automatic discrimination of unfamiliar individual faces. *Visual Cognition*, *27*(2), 127–141. https://doi.org/10.1080/13506285.2019.1616639

Edwards, D., Cortes, M., Datta, A., Minhas, P., Wassermann, E. M., & Bikson, M. (2013). Physiological and modeling evidence for focal transcranial electrical brain stimulation in humans: A basis for high-definition tDCS. *NeuroImage*, *74*, 266–275. https://doi.org/10.1016/j.neuroimage.2013.01.042

Esmaeilpour, Z., Marangolo, P., Hampstead, B. M., Bestmann, S., Galletta, E., Knotkova, H., & Bikson, M. (2018). Incomplete evidence that increasing current intensity of tDCS boosts outcomes. *Brain Stimulation*, *11*(2), 310–321. https://doi.org/10.1016/j.brs.2017.12.002

Esmaeilpour, Z., Milosevic, M., Azevedo, K., Khadka, N., Navarro, J., Brunoni, A., Popovic, M. R., Bikson, M., & Fonoff, E. T. (2017). Proceedings #21. Intracranial voltage recording during transcranial direct current stimulation (tDCS) in human subjects with validation of a standard model. *Brain Stimulation: Basic, Translational, and Clinical Research in Neuromodulation*, *10*(4), e72–e75. https://doi.org/10.1016/j.brs.2017.04.114

Faria, P., Fregni, F., Sebastião, F., Dias, A. I., & Leal, A. (2012a). Feasibility of focal transcranial DC polarization with simultaneous EE G recording: Preliminary assessment in healthy subjects and human epil epsy. *Epilepsy & Behavior: E&B*, *25*(3), 417–425. PubMed. https://doi.org/10.1016/j.yebeh.2012.06.027

Faria, P., Fregni, F., Sebastião, F., Dias, A. I., & Leal, A. (2012b). Feasibility of focal transcranial DC polarization with simultaneous EEG recording: Preliminary assessment in healthy subjects and human epilepsy. *Epilepsy & Behavior: E&B*, *25*(3), 417–425. https://doi.org/10.1016/j.yebeh.2012.06.027

Ferrari, C., Lega, C., Vernice, M., Tamietto, M., Mende-Siedlecki, P., Vecchi, T., Todorov, A., & Cattaneo, Z. (2016). The Dorsomedial Prefrontal Cortex Plays a Causal Role in Integrating Social Impressions from Faces and Verbal Descriptions. *Cerebral Cortex*, *26*(1), 156–165. https://doi.org/10.1093/cercor/bhu186

Ferrucci, R., Bortolomasi, M., Vergari, M., Tadini, L., Salvoro, B., Giacopuzzi, M., Barbieri, S., & Priori, A. (2009). Transcranial direct current stimulation in severe, drug-resistant major depression. *Journal of Affective Disorders*, *118*(1–3), 215–219. https://doi.org/10.1016/j.jad.2009.02.015

Feuerriegel, D., Churches, O., Hofmann, J., & Keage, H. A. D. (2015). The N170 and face perception in psychiatric and neurological disorders: A systematic review. *Clinical Neurophysiology*, *126*(6), 1141–1158. https://doi.org/10.1016/j.clinph.2014.09.015

Filmer, H. L., Mattingley, J. B., & Dux, P. E. (2020). Modulating brain activity and behaviour with tDCS: Rumours of its death have been greatly exaggerated. *Cortex*, *123*, 141–151. https://doi.org/10.1016/j.cortex.2019.10.006

Fischer, C., Luauté, J., Adeleine, P., & Morlet, D. (2004). Predictive value of sensory and cognitive evoked potentials for awakening from coma. *Neurology*, *63*(4), 669–673. https://doi.org/10.1212/01.wnl.0000134670.10384.e2

Flöel, A. (2014). tDCS-enhanced motor and cognitive function in neurological diseases. *NeuroImage*, *85 Pt 3*, 934–947. https://doi.org/10.1016/j.neuroimage.2013.05.098

Fregni, F., Gimenes, R., Valle, A. C., Ferreira, M. J. L., Rocha, R. R., Natalle, L., Bravo, R., Rigonatti, S. P., Freedman, S. D., Nitsche, M. A., Pascual-Leone, A., & Boggio, P. S. (2006). A randomized, sham-controlled, proof of principle study of transcranial direct current stimulation for the treatment of pain in fibromyalgia. *Arthritis and Rheumatism*, *54*(12), 3988–3998. https://doi.org/10.1002/art.22195

Frisch, S., Hahne, A., & Friederici, A. D. (2004). Word category and verb–argument structure information in the dynamics of parsing. *Cognition*, *91*(3), 191–219. https://doi.org/10.1016/j.cognition.2003.09.009

Fritsch, B., Reis, J., Martinowich, K., Schambra, H. M., Ji, Y., Cohen, L. G., & Lu, B. (2010). Direct Current Stimulation Promotes BDNF-Dependent Synaptic Plasticity: Potential Implications for Motor Learning. *Neuron*, *66*(2), 198–204. https://doi.org/10.1016/j.neuron.2010.03.035

Gangemi, A., Colombo, B., & Fabio, R. A. (2021). Effects of short- and long-term neurostimulation (tDCS) on Alzheimer's disease patients: Two randomized studies. *Aging Clinical and Experimental Research*, *33*(2), 383–390. https://doi.org/10.1007/s40520-020-01546-8

Gartside, I. B. (1968). Mechanisms of sustained increases of firing rate of neurons in the rat cerebral cortex after polarization: Reverberating circuits or modification of synaptic conductance? *Nature*, *220*(5165), 382–383. https://doi.org/10.1038/220382a0

Gebodh, N., Esmaeilpour, Z., Adair, D., Chelette, K., Dmochowski, J., Woods, A. J., Kappenman, E. S., Parra, L. C., & Bikson, M. (2019). Inherent Physiological Artifacts In EEG During tDCS. *NeuroImage*, *185*, 408–424. https://doi.org/10.1016/j.neuroimage.2018.10.025

Gevins, A., Leong, H., Smith, M. E., Le, J., & Du, R. (1995). Mapping cognitive brain function with modern high-resolution electroencephalography. *Trends in Neurosciences*, *18*(10), 429–436. https://doi.org/10.1016/0166-2236(95)94489-R

Gonzalez-Perez, M., Wakui, E., Thoma, V., Nitsche, M. A., & Rivolta, D. (2019). Transcranial alternating current stimulation (tACS) at 40 Hz enhances face and object perception. *Neuropsychologia*, *135*, 107237. https://doi.org/10.1016/j.neuropsychologia.2019.107237

Goyal, K., Borkholder, D. A., & Day, S. W. (2022). Dependence of Skin-Electrode Contact Impedance on Material and Skin Hydration. *Sensors (Basel, Switzerland)*, *22*(21), 8510. https://doi.org/10.3390/s22218510

Grill-Spector, K., & Weiner, K. S. (2014a). The functional architecture of the ventral temporal cortex and its role in categorization. *Nature Reviews. Neuroscience*, *15*(8), 536–548. https://doi.org/10.1038/nrn3747

Grill-Spector, K., & Weiner, K. S. (2014b). The functional architecture of the ventral temporal cortex and its role in categorization. *Nature Reviews. Neuroscience*, *15*(8), 536–548. https://doi.org/10.1038/nrn3747

Grill-Spector, K., Weiner, K. S., Kay, K., & Gomez, J. (2017). The Functional Neuroanatomy of Human Face Perception. *Annual Review of Vision Science*, *3*, 167–196. https://doi.org/10.1146/annurev-vision-102016-061214

Guidetti, M., Arlotti, M., Bocci, T., Bianchi, A. M., Parazzini, M., Ferrucci, R., & Priori, A. (2022). Electric Fields Induced in the Brain by Transcranial Electric Stimulation: A Review of In Vivo Recordings. *Biomedicines*, *10*(10), Article 10. https://doi.org/10.3390/biomedicines10102333

Hagen, S., Jacques, C., Maillard, L., Colnat-Coulbois, S., Rossion, B., & Jonas, J. (2020). Spatially Dissociated Intracerebral Maps for Face- and House-Selective Activity in the Human Ventral Occipito-Temporal Cortex. *Cerebral Cortex (New York, N.Y.: 1991)*, *30*(7), 4026–4043. https://doi.org/10.1093/cercor/bhaa022

Hagen, S., Laguesse, R., & Rossion, B. (2024). Extensive Visual Training in Adulthood Reduces an Implicit Neural Marker of the Face Inversion Effect. *Brain Sciences*, *14*(2), 146. https://doi.org/10.3390/brainsci14020146

Hagen, S., Lochy, A., Jacques, C., Maillard, L., Colnat-Coulbois, S., Jonas, J., & Rossion, B. (2021). Dissociated face- and word-selective intracerebral responses in the human ventral occipito-temporal cortex. *Brain Structure & Function*, *226*(9), 3031–3049. https://doi.org/10.1007/s00429-021-02350-4

Halgren, E., Baudena, P., Heit, G., Clarke, J. M., Marinkovic, K., & Clarke, M. (1994). Spatio-temporal stages in face and word processing. I. Depth-recorded potentials in the human occipital, temporal and parietal lobes [corrected]. *Journal of Physiology, Paris*, *88*(1), 1–50. https://doi.org/10.1016/0928-4257(94)90092-2

Hardmeier, M., Hatz, F., Naegelin, Y., Hight, D., Schindler, C., Kappos, L., Seeck, M., Michel, C. M., & Fuhr, P. (2014). Improved Characterization of Visual Evoked Potentials in Multiple Sclerosis by Topographic Analysis. *Brain Topography*, *27*(2), 318–327. https://doi.org/10.1007/s10548-013-0318-6

Hassanzahraee, M., Nitsche, M. A., Zoghi, M., & Jaberzadeh, S. (2020). Determination of anodal tDCS intensity threshold for reversal of corticospinal excitability: An investigation for induction of counter-regulatory mechanisms. *Scientific Reports*, *10*(1), 16108. https://doi.org/10.1038/s41598-020-72909-4

Haxby, J. V., Hoffman, E. A., & Gobbini, M. I. (2000). The distributed human neural system for face perception. *Trends in Cognitive Sciences*, *4*(6), 223–233. https://doi.org/10.1016/s1364-6613(00)01482-0

He, C., Chen, Y.-Y., Phang, C.-R., Stevenson, C., Chen, I.-P., Jung, T.-P., & Ko, L.-W. (2023). Diversity and Suitability of the State-of-the-Art Wearable and Wireless EEG Systems Review. *IEEE Journal of Biomedical and Health Informatics*, *27*(8), 3830–3843. https://doi.org/10.1109/JBHI.2023.3239053

Holdefer, R. N., Sadleir, R., & Russell, M. J. (2006). Predicted current densities in the brain during transcranial electrical stimulation. *Clinical Neurophysiology*, *117*(6), 1388–1397. https://doi.org/10.1016/j.clinph.2006.02.020

Holm, A., Ranta-aho, P. O., Sallinen, M., Karjalainen, P. A., & Müller, K. (2006). Relationship of P300 single-trial responses with reaction time and preceding stimulus sequence. *International Journal of Psychophysiology*, *61*(2), 244–252. https://doi.org/10.1016/j.ijpsycho.2005.10.015

Hopkins, C. D. (2009). Electrical Perception and Communication. In L. R. Squire (Ed.), *Encyclopedia of Neuroscience* (pp. 813–831). Academic Press. https://doi.org/10.1016/B978-008045046-9.01827-1

Hordacre, B., Moezzi, B., & Ridding, M. C. (2018). Neuroplasticity and network connectivity of the motor cortex following stroke: A transcranial direct current stimulation study. *Human Brain Mapping*, *39*(8), 3326–3339. https://doi.org/10.1002/hbm.24079

Horvath, J. C., Forte, J. D., & Carter, O. (2015a). Evidence that transcranial direct current stimulation (tDCS) generates little-to-no reliable neurophysiologic effect beyond MEP amplitude modulation in healthy human subjects: A systematic review. *Neuropsychologia*, *66*, 213–236. https://doi.org/10.1016/j.neuropsychologia.2014.11.021

Horvath, J. C., Forte, J. D., & Carter, O. (2015b). Quantitative Review Finds No Evidence of Cognitive Effects in Healthy Populations From Single-session Transcranial Direct Current Stimulation (tDCS). *Brain Stimulation*, *8*(3), 535–550. https://doi.org/10.1016/j.brs.2015.01.400

Hoy, K. E., Bailey, N. W., Arnold, S. L., & Fitzgerald, P. B. (2015). The effect of transcranial Direct Current Stimulation on gamma activity and working memory in schizophrenia. *Psychiatry Research*, *228*(2), 191–196. https://doi.org/10.1016/j.psychres.2015.04.032

Hsin, C.-H., Lee, C.-Y., & Tsao, Y. (2025). Exploring N400 Predictability Effects During Sustained Speech Comprehension: From Listening-Related Fatigue to Speech Enhancement Evaluation. *Ear and Hearing*, *46*(4), 922. https://doi.org/10.1097/AUD.0000000000001635

Huang, Y., Liu, A. A., Lafon, B., Friedman, D., Dayan, M., Wang, X., Bikson, M., Doyle, W. K., Devinsky, O., & Parra, L. C. (2017). Measurements and models of electric fields in the in vivo human brain during transcranial electric stimulation. *eLife*, *6*, e18834. https://doi.org/10.7554/eLife.18834

Huang, Y., & Parra, L. C. (2019). Can transcranial electric stimulation with multiple electrodes reach deep targets? *Brain Stimulation*, *12*(1), 30–40. https://doi.org/10.1016/j.brs.2018.09.010

Islam, N., Aftabuddin, M., Moriwaki, A., Hattori, Y., & Hori, Y. (1995). Increase in the calcium level following anodal polarization in the rat brain. *Brain Research*, *684*(2), 206–208. https://doi.org/10.1016/0006-8993(95)00434-R

Jacques, C., d'Arripe, O., & Rossion, B. (2007). The time course of the inversion effect during individual face discrimination. *Journal of Vision*, *7*(8), 3. https://doi.org/10.1167/7.8.3

Jacques, C., Jonas, J., Maillard, L., Colnat-Coulbois, S., Koessler, L., & Rossion, B. (2018). The inferior occipital gyrus is a major cortical source of the face-evoked N170: Evidence from simultaneous scalp and intracerebral human recordings. *Human Brain Mapping*, *40*(5), 1403–1418. https://doi.org/10.1002/hbm.24455

Jacques, C., Jonas, J., Maillard, L., Colnat-Coulbois, S., Koessler, L., & Rossion, B. (2019). The inferior occipital gyrus is a major cortical source of the face-evoked N170: Evidence from

simultaneous scalp and intracerebral human recordings. *Human Brain Mapping*, *40*(5), 1403–1418. https://doi.org/10.1002/hbm.24455

Jacques, C., Jonas, J., Maillard, L., Colnat-Coulbois, S., Rossion, B., & Koessler, L. (2020). Fast periodic visual stimulation to highlight the relationship between human intracerebral recordings and scalp electroencephalography. *Human Brain Mapping*, *41*(9), 2373–2388. https://doi.org/10.1002/hbm.24952

Jacques, C., Retter, T. L., & Rossion, B. (2016). A single glance at natural face images generate larger and qualitatively different category-selective spatio-temporal signatures than other ecologically-relevant categories in the human brain. *NeuroImage*, *137*, 21–33. https://doi.org/10.1016/j.neuroimage.2016.04.045

Jacques, C., Rossion, B., Volfart, A., Brissart, H., Colnat-Coulbois, S., Maillard, L., & Jonas, J. (2020). The neural basis of rapid unfamiliar face individuation with human intracerebral recordings. *NeuroImage*, *221*, 117174. https://doi.org/10.1016/j.neuroimage.2020.117174

Jadhav, C., Kamble, P., Mundewadi, S., Jaiswal, N., Mali, S., Ranga, S., Suvvari, T. K., & Rukadikar, A. (2022). Clinical applications of EEG as an excellent tool for event related potentials in psychiatric and neurotic disorders. *International Journal of Physiology, Pathophysiology and Pharmacology*, *14*(2), 73–83.

Jamil, A., Batsikadze, G., Kuo, H., Labruna, L., Hasan, A., Paulus, W., & Nitsche, M. A. (2017). Systematic evaluation of the impact of stimulation intensity on neuroplastic after-effects induced by transcranial direct current stimulation. *The Journal of Physiology*, *595*(4), 1273–1288. https://doi.org/10.1113/JP272738

Jonas, J., Descoins, M., Koessler, L., Colnat-Coulbois, S., Sauvée, M., Guye, M., Vignal, J.-P., Vespignani, H., Rossion, B., & Maillard, L. (2012). Focal electrical intracerebral stimulation of a face-sensitive area causes transient prosopagnosia. *Neuroscience*, *222*, 281–288. https://doi.org/10.1016/j.neuroscience.2012.07.021

Jonas, J., Jacques, C., Liu-Shuang, J., Brissart, H., Colnat-Coulbois, S., Maillard, L., & Rossion, B. (2016). A face-selective ventral occipito-temporal map of the human brain with intracerebral potentials. *Proceedings of the National Academy of Sciences of the United States of America*, *113*(28), E4088-4097. https://doi.org/10.1073/pnas.1522033113

Jonas, J., & Rossion, B. (2021). Intracerebral electrical stimulation to understand the neural basis of human face identity recognition. *European Journal of Neuroscience*, *54*(1), 4197–4211. https://doi.org/10.1111/ejn.15235

Jonas, J., Rossion, B., Brissart, H., Frismand, S., Jacques, C., Hossu, G., Colnat-Coulbois, S., Vespignani, H., Vignal, J.-P., & Maillard, L. (2015). Beyond the core face-processing network: Intracerebral stimulation of a face-selective area in the right anterior fusiform gyrus elicits transient prosopagnosia. *Cortex*, *72*, 140–155. https://doi.org/10.1016/j.cortex.2015.05.026

Jonas, J., Rossion, B., Krieg, J., Koessler, L., Colnat-Coulbois, S., Vespignani, H., Jacques, C., Vignal, J.-P., Brissart, H., & Maillard, L. (2014). Intracerebral electrical stimulation of a face-selective area in the right inferior occipital cortex impairs individual face discrimination. *NeuroImage*, *99*, 487–497. https://doi.org/10.1016/j.neuroimage.2014.06.017

Kabakov, A. Y., Muller, P. A., Pascual-Leone, A., Jensen, F. E., & Rotenberg, A. (2012). Contribution of axonal orientation to pathway-dependent modulation of excitatory

transmission by direct current stimulation in isolated rat hippocampus. *Journal of Neurophysiology*, *107*(7), 1881–1889. https://doi.org/10.1152/jn.00715.2011

Kanwisher, N., McDermott, J., & Chun, M. M. (1997). The Fusiform Face Area: A Module in Human Extrastriate Cortex Specialized for Face Perception. *The Journal of Neuroscience*, *17*(11), 4302–4311. https://doi.org/10.1523/JNEUROSCI.17-11-04302.1997

Kappenman, E. S., & Luck, S. J. (2010). The effects of electrode impedance on data quality and statistical significance in ERP recordings. *Psychophysiology*, *47*(5), 888–904. https://doi.org/10.1111/j.1469-8986.2010.01009.x

Kar, K., Duijnhouwer, J., & Krekelberg, B. (2017). Transcranial Alternating Current Stimulation Attenuates Neuronal Adaptation. *Journal of Neuroscience*, *37*(9), 2325–2335. https://doi.org/10.1523/JNEUROSCI.2266-16.2016

Kawohl, W., Bunse, S., Willmes, K., Hoffrogge, A., Buchner, H., & Huber, W. (2010). Semantic event-related potential components reflect severity of comprehension deficits in aphasia. *Neurorehabilitation and Neural Repair*, *24*(3), 282–289. https://doi.org/10.1177/1545968309348311

Kekic, M., Boysen, E., Campbell, I. C., & Schmidt, U. (2016). A systematic review of the clinical efficacy of transcranial direct current stimulation (tDCS) in psychiatric disorders. *Journal of Psychiatric Research*, *74*, 70–86. https://doi.org/10.1016/j.jpsychires.2015.12.018

Kessler, S. K., Turkeltaub, P. E., Benson, J. G., & Hamilton, R. H. (2012). Differences in the experience of active and sham transcranial direct current stimulation. *Brain Stimulation*, *5*(2), 155–162. https://doi.org/10.1016/j.brs.2011.02.007

Kho, S. K., Keeble, D., Wong, H. K., & Estudillo, A. J. (2023). Null effect of anodal and cathodal transcranial direct current stimulation (tDCS) on own- and other-race face recognition. *Social Neuroscience*, 1–14. https://doi.org/10.1080/17470919.2023.2263924

Kim, D. W., Kim, E., Lee, C., & Im, C. H. (2019). Can Anodal Transcranial Direct Current Stimulation Increase Steady-State Visual Evoked Potential Responses? *Journal of Korean Medical Science*, *34*(43), e285. https://doi.org/10.3346/jkms.2019.34.e285

Kim, J. J., Crespo-Facorro, B., Andreasen, N. C., O'Leary, D. S., Zhang, B., Harris, G., & Magnotta, V. A. (2000). An MRI-based parcellation method for the temporal lobe. *NeuroImage*, *11*(4), 271–288. https://doi.org/10.1006/nimg.2000.0543

Koessler, L., Cecchin, T., Colnat-Coulbois, S., Vignal, J.-P., Jonas, J., Vespignani, H., Ramantani, G., & Maillard, L. G. (2015). Catching the invisible: Mesial temporal source contribution to simultaneous EEG and SEEG recordings. *Brain Topography*, *28*(1), 5–20. https://doi.org/10.1007/s10548-014-0417-z

Koessler, L., Colnat-Coulbois, S., Cecchin, T., Hofmanis, J., Dmochowski, J. P., Norcia, A. M., & Maillard, L. G. (2017). In-vivo measurements of human brain tissue conductivity using focal electrical current injection through intracerebral multicontact electrodes. *Human Brain Mapping*, *38*(2), 974–986. https://doi.org/10.1002/hbm.23431

Koessler, L., Louviot, S., Dmochowski, J., Vignal, J.-P., Jonas, J., Colnat-Coulbois, S., Tyvaert, L., & Maillard, L. (2023). Transcranial direct current stimulation reduces intracerebrally-recorded

epileptic seizures and behavioral disturbances. *Brain Stimulation*, *16*(2), 667–669. https://doi.org/10.1016/j.brs.2023.03.040

Koessler, L., Maillard, L., Benhadid, A., Vignal, J. P., Felblinger, J., Vespignani, H., & Braun, M. (2009). Automated cortical projection of EEG sensors: Anatomical correlation via the international 10-10 system. *NeuroImage*, *46*(1), 64–72. https://doi.org/10.1016/j.neuroimage.2009.02.006

Kohli, S., & Casson, A. J. (2019). Removal of Gross Artifacts of Transcranial Alternating Current Stimulation in Simultaneous EEG Monitoring. *Sensors*, *19*(1), Article 1. https://doi.org/10.3390/s19010190

Korai, S. A., Ranieri, F., Di Lazzaro, V., Papa, M., & Cirillo, G. (2021). Neurobiological After-Effects of Low Intensity Transcranial Electric Stimulation of the Human Nervous System: From Basic Mechanisms to Metaplasticity. *Frontiers in Neurology*, *12*. https://www.frontiersin.org/article/10.3389/fneur.2021.587771

Kraft, A., Roehmel, J., Olma, M. C., Schmidt, S., Irlbacher, K., & Brandt, S. A. (2010). Transcranial direct current stimulation affects visual perception measured by threshold perimetry. *Experimental Brain Research*, *207*(3–4), 283–290. https://doi.org/10.1007/s00221-010-2453-6

Kronberg, G., Bridi, M., Abel, T., Bikson, M., & Parra, L. C. (2017). Direct Current Stimulation Modulates LTP and LTD: Activity Dependence and Dendritic Effects. *Brain Stimulation*, *10*(1), 51–58. https://doi.org/10.1016/j.brs.2016.10.001

Kuo, H.-I., Bikson, M., Datta, A., Minhas, P., Paulus, W., Kuo, M.-F., & Nitsche, M. A. (2013). Comparing cortical plasticity induced by conventional and high-definition 4 × 1 ring tDCS: A neurophysiological study. *Brain Stimulation*, *6*(4), 644–648. https://doi.org/10.1016/j.brs.2012.09.010

Kuo, M.-F., & Nitsche, M. A. (2012). Effects of transcranial electrical stimulation on cognition. *Clinical EEG and Neuroscience*, *43*(3), 192–199. https://doi.org/10.1177/1550059412444975

Kuo, M.-F., Paulus, W., & Nitsche, M. A. (2008). Boosting Focally-Induced Brain Plasticity by Dopamine. *Cerebral Cortex*, *18*(3), 648–651. https://doi.org/10.1093/cercor/bhm098

Lafon, B., Henin, S., Huang, Y., Friedman, D., Melloni, L., Thesen, T., Doyle, W., Buzsáki, G., Devinsky, O., Parra, L. C., & A. Liu, A. (2017). Low frequency transcranial electrical stimulation does not entrain sleep rhythms measured by human intracranial recordings. *Nature Communications*, *8*(1), 1199. https://doi.org/10.1038/s41467-017-01045-x

Lafon, B., Rahman, A., Bikson, M., & Parra, L. C. (2017). Direct Current Stimulation Alters Neuronal Input/Output Function. *Brain Stimulation*, *10*(1), 36–45. https://doi.org/10.1016/j.brs.2016.08.014

Lafontaine, M. P., Théoret, H., Gosselin, F., & Lippé, S. (2013). Transcranial direct current stimulation of the dorsolateral prefrontal cortex modulates repetition suppression to unfamiliar faces: An ERP study. *PloS One*, *8*(12), e81721. https://doi.org/10.1371/journal.pone.0081721

Lascano, A. M., Lalive, P. H., Hardmeier, M., Fuhr, P., & Seeck, M. (2017). Clinical evoked potentials in neurology: A review of techniques and indications. *Journal of Neurology, Neurosurgery & Psychiatry*, *88*(8), 688–696. https://doi.org/10.1136/jnnp-2016-314791

Lefaucheur, J.-P. (2016). A comprehensive database of published tDCS clinical trials (2005-2016). *Neurophysiologie Clinique = Clinical Neurophysiology*, *46*(6), 319–398. https://doi.org/10.1016/j.neucli.2016.10.002

Lefaucheur, J.-P., Antal, A., Ahdab, R., Ciampi de Andrade, D., Fregni, F., Khedr, E. M., Nitsche, M., & Paulus, W. (2008). The use of repetitive transcranial magnetic stimulation (rTMS) and transcranial direct current stimulation (tDCS) to relieve pain. *Brain Stimulation*, *1*(4), 337–344. https://doi.org/10.1016/j.brs.2008.07.003

Lefaucheur, J.-P., Antal, A., Ayache, S. S., Benninger, D. H., Brunelin, J., Cogiamanian, F., Cotelli, M., De Ridder, D., Ferrucci, R., Langguth, B., Marangolo, P., Mylius, V., Nitsche, M. A., Padberg, F., Palm, U., Poulet, E., Priori, A., Rossi, S., Schecklmann, M., … Paulus, W. (2017). Evidence-based guidelines on the therapeutic use of transcranial direct current stimulation (tDCS). *Clinical Neurophysiology: Official Journal of the International Federation of Clinical Neurophysiology*, *128*(1), 56–92. https://doi.org/10.1016/j.clinph.2016.10.087

Leite, J., Morales-Quezada, L., Carvalho, S., Thibaut, A., Doruk, D., Chen, C.-F., Schachter, S. C., Rotenberg, A., & Fregni, F. (2017). Surface EEG-Transcranial Direct Current Stimulation (tDCS) Closed-Loop System. *International Journal of Neural Systems*, *27*(6), 1750026. https://doi.org/10.1142/S0129065717500265

Li, G., Wang, S., & Duan, Y. Y. (2017). Towards gel-free electrodes: A systematic study of electrode-skin impedance. *Sensors and Actuators B: Chemical*, *241*, 1244–1255. https://doi.org/10.1016/j.snb.2016.10.005

Li, L. M., Uehara, K., & Hanakawa, T. (2015). The contribution of interindividual factors to variability of response in transcranial direct current stimulation studies. *Frontiers in Cellular Neuroscience*, *9*, 181. https://doi.org/10.3389/fncel.2015.00181

Li, L. M., Violante, I. R., Leech, R., Ross, E., Hampshire, A., Opitz, A., Rothwell, J. C., Carmichael, D. W., & Sharp, D. J. (2018). Brain state and polarity dependent modulation of brain networks by transcranial direct current stimulation. *Human Brain Mapping*, *40*(3), 904–915. https://doi.org/10.1002/hbm.24420

Liebetanz, D., Nitsche, M. A., Tergau, F., & Paulus, W. (2002). Pharmacological approach to the mechanisms of transcranial DC-stimulation-induced after-effects of human motor cortex excitability. *Brain*, *125*(10), 2238–2247. https://doi.org/10.1093/brain/awf238

Liu, A., Vöröslakos, M., Kronberg, G., Henin, S., Krause, M. R., Huang, Y., Opitz, A., Mehta, A., Pack, C. C., Krekelberg, B., Berényi, A., Parra, L. C., Melloni, L., Devinsky, O., & Buzsáki, G. (2018). Immediate neurophysiological effects of transcranial electrical stimulation. *Nature Communications*, *9*(1), 5092. https://doi.org/10.1038/s41467-018-07233-7

Liu, J., Harris, A., & Kanwisher, N. (2010). Perception of Face Parts and Face Configurations: An fMRI Study. *Journal of Cognitive Neuroscience*, *22*(1), 203–211. https://doi.org/10.1162/jocn.2009.21203

Liu-Shuang, J., Norcia, A. M., & Rossion, B. (2014a). An objective index of individual face discrimination in the right occi pito-temporal cortex by means of fast periodic oddball

stimulation. *Neuropsychologia*, *52*, 57–72. PubMed. https://doi.org/10.1016/j.neuropsychologia.2013.10.022

Liu-Shuang, J., Norcia, A. M., & Rossion, B. (2014b). An objective index of individual face discrimination in the right occipito-temporal cortex by means of fast periodic oddball stimulation. *Neuropsychologia*, *52*, 57–72. https://doi.org/10.1016/j.neuropsychologia.2013.10.022

Liu-Shuang, J., Torfs, K., & Rossion, B. (2016). An objective electrophysiological marker of face individualisation impairment in acquired prosopagnosia with fast periodic visual stimulation. *Neuropsychologia*, *83*, 100–113. https://doi.org/10.1016/j.neuropsychologia.2015.08.023

Lochy, A., Jacques, C., Maillard, L., Colnat-Coulbois, S., Rossion, B., & Jonas, J. (2018). Selective visual representation of letters and words in the left ventral occipito-temporal cortex with intracerebral recordings. *Proceedings of the National Academy of Sciences*, *115*(32), E7595–E7604. https://doi.org/10.1073/pnas.1718987115

Lochy, A., Van Belle, G., & Rossion, B. (2015). A robust index of lexical representation in the left occipito-temporal cortex as evidenced by EEG responses to fast periodic visual stimulation. *Neuropsychologia*, *66*, 18–31. https://doi.org/10.1016/j.neuropsychologia.2014.11.007

Lopez-Quintero, S. V., Datta, A., Amaya, R., Elwassif, M., Bikson, M., & Tarbell, J. M. (2010). DBS-relevant electric fields increase hydraulic conductivity of in vitro endothelial monolayers. *Journal of Neural Engineering*, *7*(1), 016005. https://doi.org/10.1088/1741-2560/7/1/016005

Loriette, C., Ziane, C., & Ben Hamed, S. (2021). Neurofeedback for cognitive enhancement and intervention and brain plasticity. *Revue Neurologique*, *177*(9), 1133–1144. https://doi.org/10.1016/j.neurol.2021.08.004

Louviot, S., Dmochowski, J., Jonas, J., Maillard, L., Colnat-Coulbois, S., Tyvaert, L., & Koessler, L. (2019, February 25). *A human in-vivo evaluation of roast using simultaneous intracerebral electrical stimulations and scalp EEG*. 3rd International Brain Stimulation Conference. https://doi.org/10.1016/j.brs.2018.12.075

Louviot, S., Tyvaert, L., Maillard, L. G., Colnat-Coulbois, S., Dmochowski, J., & Koessler, L. (2022). Transcranial Electrical Stimulation generates electric fields in deep human brain structures. *Brain Stimulation*, *15*(1), 1–12. https://doi.org/10.1016/j.brs.2021.11.001

Lu, H., Liu, Q., Guo, Z., Zhou, G., Zhang, Y., Zhu, X., & Wu, S. (2020). Modulation of Repeated Anodal HD-tDCS on Attention in Healthy Young Adults. *Frontiers in Psychology*, *11*. https://doi.org/10.3389/fpsyg.2020.564447

Lu, Z., Guo, J., Sun, J., Sun, Y., Zhang, Y., Zhang, Y., Liao, Y., Kang, Z., Feng, X., Zhao, G., Yuan, R., Zhu, Y., & Yue, W. (2025). The event-related potential components across psychiatric disorders: A systematic review and network meta-analysis. *Molecular Psychiatry*, 1–10. https://doi.org/10.1038/s41380-025-03062-5

Luck, S. (2005). An Introduction to The Event-Related Potential Technique. In *Cambridge*.

Luck, S. J., Mathalon, D. H., O'Donnell, B. F., Hämäläinen, M. S., Spencer, K. M., Javitt, D. C., & Uhlhaas, P. J. (2011). A Roadmap for the Development and Validation of Event-Related Potential Biomarkers in Schizophrenia Research. *Biological Psychiatry*, *70*(1), 28–34. https://doi.org/10.1016/j.biopsych.2010.09.021

MaderJr, E. C., Miller, D., Toler, J. M., & Olejniczak, P. W. (2018). Focal Epileptiform Discharges Can Mimic Electrode Artifacts When Recorded on the Scalp Near a Skull Defect. *Journal of Investigative Medicine High Impact Case Reports*, *6*, 2324709618795305. https://doi.org/10.1177/2324709618795305

Maillard, L., Vignal, J.-P., Gavaret, M., Guye, M., Biraben, A., McGonigal, A., Chauvel, P., & Bartolomei, F. (2004). Semiologic and Electrophysiologic Correlations in Temporal Lobe Seizure Subtypes. *Epilepsia*, *45*(12), 1590–1599. https://doi.org/10.1111/j.0013-9580.2004.09704.x

Mancini, M., Brignani, D., Conforto, S., Mauri, P., Miniussi, C., & Pellicciari, M. C. (2016). Assessing cortical synchronization during transcranial direct current stimulation: A graph-theoretical analysis. *NeuroImage*, *140*, 57–65. https://doi.org/10.1016/j.neuroimage.2016.06.003

Mancini, M., Pellicciari, M. C., Brignani, D., Mauri, P., De Marchis, C., Miniussi, C., & Conforto, S. (2015). Automatic artifact suppression in simultaneous tDCS-EEG using adaptive filtering. *Annual International Conference of the IEEE Engineering in Medicine and Biology Society. IEEE Engineering in Medicine and Biology Society. Annual International Conference*, *2015*, 2729–2732. https://doi.org/10.1109/EMBC.2015.7318956

Manfredi, M., Proverbio, A. M., Gonçalves Donate, A. P., Macarini Gonçalves Vieira, S., Comfort, W. E., De Araújo Andreoli, M., & Boggio, P. S. (2017). tDCS application over the STG improves the ability to recognize and appreciate elements involved in humor processing. *Experimental Brain Research*, *235*(6), 1843–1852. https://doi.org/10.1007/s00221-017-4932-5

Mangia, A. L., Pirini, M., & Cappello, A. (2014). Transcranial direct current stimulation and power spectral parameters: A tDCS/EEG co-registration study. *Frontiers in Human Neuroscience*, *8*. https://doi.org/10.3389/fnhum.2014.00601

Masina, F., Arcara, G., Galletti, E., Cinque, I., Gamberini, L., & Mapelli, D. (2021). Neurophysiological and behavioural effects of conventional and high definition tDCS. *Scientific Reports*, *11*(1), 7659. https://doi.org/10.1038/s41598-021-87371-z

Mathewson, K. E., Kuziek, J. P., Scanlon, J. E. M., & Robles, D. (2024). The moving wave: Applications of the mobile EEG approach to study human attention. *Psychophysiology*, *61*(9), e14603. https://doi.org/10.1111/psyp.14603

Mattavelli, G., Pisoni, A., Romero Lauro, L. J., Marino, B. F., Bonomi, M., Rosanova, M., & Papagno, C. (2019). TMS-EEG approach unveils brain mechanisms underlying conscious and unconscious face perception. *Brain Stimulation*, *12*(4), 1010–1019. https://doi.org/10.1016/j.brs.2019.02.022

Mattavelli, G., Rosanova, M., Casali, A. G., Papagno, C., & Romero Lauro, L. J. (2013). Top-down interference and cortical responsiveness in face processing: A TMS-EEG study. *NeuroImage*, *76*, 24–32. https://doi.org/10.1016/j.neuroimage.2013.03.020

Mattavelli, G., Rosanova, M., Casali, A. G., Papagno, C., & Romero Lauro, L. J. (2016). Timing of emotion representation in right and left occipital region: Evidence from combined TMS-EEG. *Brain and Cognition*, *106*, 13–22. https://doi.org/10.1016/j.bandc.2016.04.009

McCaig, C. D., Rajnicek, A. M., Song, B., & Zhao, M. (2005). Controlling cell behavior electrically: Current views and future potential. *Physiological Reviews*, *85*(3), 943–978. https://doi.org/10.1152/physrev.00020.2004

Mehraram, R., Kries, J., De Clercq, P., Vandermosten, M., & Francart, T. (2025). EEG reveals brain network alterations in chronic aphasia during natural speech listening. *Scientific Reports*, *15*(1), 2441. https://doi.org/10.1038/s41598-025-86192-8

Milne-Ives, M., Duun-Henriksen, J., Blaabjerg, L., Mclean, B., Shankar, R., & Meinert, E. (2023). At home EEG monitoring technologies for people with epilepsy and intellectual disabilities: A scoping review. *Seizure: European Journal of Epilepsy*, *110*, 11–20. https://doi.org/10.1016/j.seizure.2023.05.007

Miniussi, C., Brignani, D., & Pellicciari, M. C. (2012). Combining transcranial electrical stimulation with electroencephalography: A multimodal approach. *Clinical EEG and Neuroscience*, *43*(3), 184–191. https://doi.org/10.1177/1550059412444976

Miranda, P. C., Mekonnen, A., Salvador, R., & Ruffini, G. (2013). The electric field in the cortex during transcranial current stimulation. *NeuroImage*, *70*, 48–58. https://doi.org/10.1016/j.neuroimage.2012.12.034

Močilnik, V., Rutar Gorišek, V., Sajovic, J., Pretnar Oblak, J., Drevenšek, G., & Rogelj, P. (2024). Integrating EEG and Machine Learning to Analyze Brain Changes during the Rehabilitation of Broca's Aphasia. *Sensors (Basel, Switzerland)*, *24*(2), 329. https://doi.org/10.3390/s24020329

Monai, H., Ohkura, M., Tanaka, M., Oe, Y., Konno, A., Hirai, H., Mikoshiba, K., Itohara, S., Nakai, J., Iwai, Y., & Hirase, H. (2016). Calcium imaging reveals glial involvement in transcranial direct current stimulation-induced plasticity in mouse brain. *Nature Communications*, *7*(1), 11100. https://doi.org/10.1038/ncomms11100

Monte-Silva, K., Kuo, M.-F., Hessenthaler, S., Fresnoza, S., Liebetanz, D., Paulus, W., & Nitsche, M. A. (2013). Induction of Late LTP-Like Plasticity in the Human Motor Cortex by Repeated Non-Invasive Brain Stimulation. *Brain Stimulation*, *6*(3), 424–432. https://doi.org/10.1016/j.brs.2012.04.011

Monte-Silva, K., Kuo, M.-F., Liebetanz, D., Paulus, W., & Nitsche, M. A. (2010). Shaping the optimal repetition interval for cathodal transcranial direct current stimulation (tDCS). *Journal of Neurophysiology*, *103*(4), 1735–1740. https://doi.org/10.1152/jn.00924.2009

Morya, E., Monte-Silva, K., Bikson, M., Esmaeilpour, Z., Biazoli, C. E., Fonseca, A., Bocci, T., Farzan, F., Chatterjee, R., Hausdorff, J. M., da Silva Machado, D. G., Brunoni, A. R., Mezger, E., Moscaleski, L. A., Pegado, R., Sato, J. R., Caetano, M. S., Sá, K. N., Tanaka, C., … Okano, A. H. (2019). Beyond the target area: An integrative view of tDCS-induced motor cortex modulation in patients and athletes. *Journal of NeuroEngineering and Rehabilitation*, *16*(1), 141. https://doi.org/10.1186/s12984-019-0581-1

Neuronaute. (n.d.). BioSerenity. Retrieved May 7, 2025, from https://bioserenity.com/fr/neuronaute/

Newson, J. J., & Thiagarajan, T. C. (2019). EEG Frequency Bands in Psychiatric Disorders: A Review of Resting State Studies. *Frontiers in Human Neuroscience*, *12*, 521. https://doi.org/10.3389/fnhum.2018.00521

Niemann, F., Shahbabaie, A., Paßmann, S., Riemann, S., Malinowski, R., Kocataş, H., Caisachana Guevara, L. M., Abdelmotaleb, M., Antonenko, D., Blankenburg, F., Fischer, R., Hartwigsen, G., Li, S.-C., Nitsche, M. A., Thielscher, A., Timmann, D., Fromm, A., Hayek, D., Hubert, A.-K., … Meinzer, M. (2024). Neuronavigated Focalized Transcranial Direct Current Stimulation Administered During Functional Magnetic Resonance Imaging. *Journal of Visualized Experiments: JoVE*, *213*. https://doi.org/10.3791/67155

Nikolin, S., Loo, C. K., Bai, S., Dokos, S., & Martin, D. M. (2015). Focalised stimulation using high definition transcranial direct current stimulation (HD-tDCS) to investigate declarative verbal learning and memory functioning. *NeuroImage*, *117*, 11–19. https://doi.org/10.1016/j.neuroimage.2015.05.019

Niso, G., Romero, E., Moreau, J. T., Araujo, A., & Krol, L. R. (2023). Wireless EEG: A survey of systems and studies. *NeuroImage*, *269*, 119774. https://doi.org/10.1016/j.neuroimage.2022.119774

Nitsche, M. A., & Bikson, M. (2017). Extending the parameter range for tDCS: Safety and tolerability of 4 mA stimulation. *Brain Stimulation*, *10*(3), 541–542. https://doi.org/10.1016/j.brs.2017.03.002

Nitsche, M. A., Cohen, L. G., Wassermann, E. M., Priori, A., Lang, N., Antal, A., Paulus, W., Hummel, F., Boggio, P. S., Fregni, F., & Pascual-Leone, A. (2008). Transcranial direct current stimulation: State of the art 2008. *Brain Stimulation*, *1*(3), 206–223. https://doi.org/10.1016/j.brs.2008.06.004

Nitsche, M. A., Fricke, K., Henschke, U., Schlitterlau, A., Liebetanz, D., Lang, N., Henning, S., Tergau, F., & Paulus, W. (2003). Pharmacological modulation of cortical excitability shifts induced by transcranial direct current stimulation in humans. *The Journal of Physiology*, *553*(Pt 1), 293–301. https://doi.org/10.1113/jphysiol.2003.049916

Nitsche, M. A., Liebetanz, D., Schlitterlau, A., Henschke, U., Fricke, K., Frommann, K., Lang, N., Henning, S., Paulus, W., & Tergau, F. (2004). GABAergic modulation of DC stimulation-induced motor cortex excitability shifts in humans. *The European Journal of Neuroscience*, *19*(10), 2720–2726. https://doi.org/10.1111/j.0953-816X.2004.03398.x

Nitsche, M. A., Müller-Dahlhaus, F., Paulus, W., & Ziemann, U. (2012). The pharmacology of neuroplasticity induced by non-invasive brain stimulation: Building models for the clinical use of CNS active drugs. *The Journal of Physiology*, *590*(19), 4641–4662. https://doi.org/10.1113/jphysiol.2012.232975

Nitsche, M. A., Nitsche, M. S., Klein, C. C., Tergau, F., Rothwell, J. C., & Paulus, W. (2003). Level of action of cathodal DC polarisation induced inhibition of the human motor cortex. *Clinical Neurophysiology: Official Journal of the International Federation of Clinical Neurophysiology*, *114*(4), 600–604. https://doi.org/10.1016/s1388-2457(02)00412-1

Nitsche, M. A., & Paulus, W. (2000). Excitability changes induced in the human motor cortex by weak transcranial direct current stimulation. *The Journal of Physiology*, *527*(Pt 3), 633–639. https://doi.org/10.1111/j.1469-7793.2000.t01-1-00633.x

Nitsche, M. A., & Paulus, W. (2001). Sustained excitability elevations induced by transcranial DC motor cortex stimulation in humans. *Neurology*, *57*(10), 1899–1901. https://doi.org/10.1212/wnl.57.10.1899

Nitsche, M. A., Seeber, A., Frommann, K., Klein, C. C., Rochford, C., Nitsche, M. S., Fricke, K., Liebetanz, D., Lang, N., Antal, A., Paulus, W., & Tergau, F. (2005). Modulating parameters of excitability during and after transcranial direct current stimulation of the human motor cortex. *The Journal of Physiology*, *568*(1), 291–303. https://doi.org/10.1113/jphysiol.2005.092429

Norcia, A. M., Appelbaum, L. G., Ales, J. M., Cottereau, B. R., & Rossion, B. (2015). The steady-state visual evoked potential in vision research: A review. *Journal of Vision*, *15*(6), 4. https://doi.org/10.1167/15.6.4

Noury, N., Hipp, J. F., & Siegel, M. (2016). Physiological processes non-linearly affect electrophysiological recordings during transcranial electric stimulation. *NeuroImage*, *140*, 99–109. https://doi.org/10.1016/j.neuroimage.2016.03.065

Nuwer, M. R. (1998). Fundamentals of evoked potentials and common clinical applications today. *Electroencephalography and Clinical Neurophysiology*, *106*(2), 142–148. https://doi.org/10.1016/s0013-4694(97)00117-x

O'Connell, N. E., Cossar, J., Marston, L., Wand, B. M., Bunce, D., Moseley, G. L., & Souza, L. H. D. (2012). Rethinking Clinical Trials of Transcranial Direct Current Stimulation: Participant and Assessor Blinding Is Inadequate at Intensities of 2mA. *PLOS ONE*, *7*(10), e47514. https://doi.org/10.1371/journal.pone.0047514

Ohn, S. H., Park, C.-I., Yoo, W.-K., Ko, M.-H., Choi, K. P., Kim, G.-M., Lee, Y. T., & Kim, Y.-H. (2008). Time-dependent effect of transcranial direct current stimulation on the enhancement of working memory. *Neuroreport*, *19*(1), 43–47. https://doi.org/10.1097/WNR.0b013e3282f2adfd

Opitz, A., Falchier, A., Yan, C.-G., Yeagle, E. M., Linn, G. S., Megevand, P., Thielscher, A., Deborah A., R., Milham, M. P., Mehta, A. D., & Schroeder, C. E. (2016). Spatiotemporal structure of intracranial electric fields induced by transcranial electric stimulation in humans and nonhuman primates. *Scientific Reports*, *6*(1), 31236. https://doi.org/10.1038/srep31236

Opitz, A., Paulus, W., Will, S., Antunes, A., & Thielscher, A. (2015). Determinants of the electric field during transcranial direct current stimulation. *NeuroImage*, *109*, 140–150. https://doi.org/10.1016/j.neuroimage.2015.01.033

O'Shea, J., & Walsh, V. (2007). Transcranial magnetic stimulation. *Current Biology*, *17*(6), R196–R199. https://doi.org/10.1016/j.cub.2007.01.030

Palmisano, A., Chiarantoni, G., Bossi, F., Conti, A., D'Elia, V., Tagliente, S., Nitsche, M. A., & Rivolta, D. (2023). Face pareidolia is enhanced by 40 Hz transcranial alternating current stimulation (tACS) of the face perception network. *Scientific Reports*, *13*, 2035. https://doi.org/10.1038/s41598-023-29124-8

Paredes-Aragon, E., AlKhaldi, N. A., Ballesteros-Herrera, D., & Mirsattari, S. M. (2022). Stereo-Encephalographic Presurgical Evaluation of Temporal Lobe Epilepsy: An Evolving Science. *Frontiers in Neurology*, *13*, 867458. https://doi.org/10.3389/fneur.2022.867458

Parent, A. (2004). Giovanni Aldini: From animal electricity to human brain stimulation. *The Canadian Journal of Neurological Sciences. Le Journal Canadien Des Sciences Neurologiques*, *31*(4), 576–584. https://doi.org/10.1017/s0317167100003851

Park, A. S., & Thompson, B. (2024). Non-invasive brain stimulation and vision rehabilitation: A clinical perspective. *Clinical and Experimental Optometry*, *107*(6), 594–602. https://doi.org/10.1080/08164622.2024.2349565

Parkin, B. L., Bhandari, M., Glen, J. C., & Walsh, V. (2019). The physiological effects of transcranial electrical stimulation do not apply to parameters commonly used in studies of cognitive neuromodulation. *Neuropsychologia*, *128*, 332–339. https://doi.org/10.1016/j.neuropsychologia.2018.03.030

Paulus, W., Nitsche, M. A., & Antal, A. (2016). Application of Transcranial Electric Stimulation (tDCS, tACS, tRNS). *European Psychologist*. https://econtent.hogrefe.com/doi/10.1027/1016-9040/a000242

Pelletier, S. J., & Cicchetti, F. (2014). Cellular and molecular mechanisms of action of transcranial direct current stimulation: Evidence from in vitro and in vivo models. *The International Journal of Neuropsychopharmacology*, *18*(2), pyu047. https://doi.org/10.1093/ijnp/pyu047

Peterchev, A. V., Wagner, T. A., Miranda, P. C., Nitsche, M. A., Paulus, W., Lisanby, S. H., Pascual-Leone, A., & Bikson, M. (2012). Fundamentals of transcranial electric and magnetic stimulation dose: Definition, selection, and reporting practices. *Brain Stimulation*, *5*(4), 435–453. https://doi.org/10.1016/j.brs.2011.10.001

Petti, M., Astolfi, L., Masciullo, M., Clausi, S., Pichiorri, F., Cincotti, F., Mattia, D., & Molinari, M. (2017). Transcranial cerebellar direct current stimulation: Effects on brain resting state oscillatory and network activity. *Annual International Conference of the IEEE Engineering in Medicine and Biology Society. IEEE Engineering in Medicine and Biology Society. Annual International Conference*, *2017*, 4359–4362. https://doi.org/10.1109/EMBC.2017.8037821

Pfeffer, M. A., Ling, S. S. H., & Wong, J. K. W. (2024). Exploring the frontier: Transformer-based models in EEG signal analysis for brain-computer interfaces. *Computers in Biology and Medicine*, *178*, 108705. https://doi.org/10.1016/j.compbiomed.2024.108705

Pilloni, G., Vogel-Eyny, A., Lustberg, M., Best, P., Malik, M., Walton-Masters, L., George, A., Mirza, I., Zhovtis, L., Datta, A., Bikson, M., Krupp, L., & Charvet, L. (2022). Tolerability and feasibility of at-home remotely supervised transcranial direct current stimulation (RS-tDCS): Single-center evidence from 6,779 sessions. *Brain Stimulation*, *15*(3), 707–716. https://doi.org/10.1016/j.brs.2022.04.014

Pisoni, A., Sperandeo, P. R., Romero Lauro, L. J., & Papagno, C. (2020). The Role of the Left and Right Anterior Temporal Poles in People Naming and Recognition. *Neuroscience*, *440*, 175–185. https://doi.org/10.1016/j.neuroscience.2020.05.040

Pitcher, D. (2024). Face Processing and TMS. In E. M. Wassermann, A. V. Peterchev, U. Ziemann, S. H. Lisanby, H. R. Siebner, & V. Walsh (Eds.), *The Oxford Handbook of Transcranial Stimulation: Second Edition* (p. 0). Oxford University Press. https://doi.org/10.1093/oxfordhb/9780198832256.013.27

Pitcher, D., Duchaine, B., & Walsh, V. (2014). Combined TMS and fMRI Reveal Dissociable Cortical Pathways for Dynamic and Static Face Perception. *Current Biology*, *24*(17), 2066–2070. https://doi.org/10.1016/j.cub.2014.07.060

Pitcher, D., Japee, S., Rauth, L., & Ungerleider, L. G. (2017). The Superior Temporal Sulcus Is Causally Connected to the Amygdala: A Combined TBS-fMRI Study. *The Journal of Neuroscience: The Official Journal of the Society for Neuroscience*, *37*(5), 1156–1161. https://doi.org/10.1523/JNEUROSCI.0114-16.2016

Pitcher, D., Walsh, V., & Duchaine, B. (2011). The role of the occipital face area in the cortical face perception network. *Experimental Brain Research*, *209*(4), 481–493. https://doi.org/10.1007/s00221-011-2579-1

Pitcher, D., Walsh, V., Yovel, G., & Duchaine, B. (2007). TMS Evidence for the Involvement of the Right Occipital Face Area in Early Face Processing. *Current Biology*, *17*(18), 1568–1573. https://doi.org/10.1016/j.cub.2007.07.063

Polanía, R., Nitsche, M. A., & Paulus, W. (2011). Modulating functional connectivity patterns and topological functional organization of the human brain with transcranial direct current stimulation. *Human Brain Mapping*, *32*(8), 1236–1249. https://doi.org/10.1002/hbm.21104

Powell, T. Y., Boonstra, T. W., Martin, D. M., Loo, C. K., & Breakspear, M. (2014). Modulation of Cortical Activity by Transcranial Direct Current Stimulation in Patients with Affective Disorder. *PLoS ONE*, *9*(6), e98503. https://doi.org/10.1371/journal.pone.0098503

Premeti, A., Bucci, M. P., Heidlmayr, K., Vigneron, P., & Isel, F. (2024). Neurodynamics of selected language processes involved in word reading: An EEG study with French dyslexic adults. *Journal of Neurolinguistics*, *71*, 101201. https://doi.org/10.1016/j.jneuroling.2024.101201

Priori, A. (2003). Brain polarization in humans: A reappraisal of an old tool for prolonged non-invasive modulation of brain excitability. *Clinical Neurophysiology*, *114*(4), 589–595. https://doi.org/10.1016/S1388-2457(02)00437-6

Priori, A., Berardelli, A., Rona, S., Accornero, N., & Manfredi, M. (1998). Polarization of the human motor cortex through the scalp. *NeuroReport*, *9*(10), 2257.

Puce, A., Allison, T., Gore, J. C., & McCarthy, G. (1995). Face-sensitive regions in human extrastriate cortex studied by functional MRI. *Journal of Neurophysiology*, *74*(3), 1192–1199. https://doi.org/10.1152/jn.1995.74.3.1192

Radman, T., Ramos, R. L., Brumberg, J. C., & Bikson, M. (2009). Role of cortical cell type and morphology in subthreshold and suprathreshold uniform electric field stimulation *in vitro*. *Brain Stimulation*, *2*(4), 215-228.e3. https://doi.org/10.1016/j.brs.2009.03.007

Radman, T., Su, Y., An, J. H., Parra, L. C., & Bikson, M. (2007). Spike Timing Amplifies the Effect of Electric Fields on Neurons: Implications for Endogenous Field Effects. *Journal of Neuroscience*, *27*(11), 3030–3036. https://doi.org/10.1523/JNEUROSCI.0095-07.2007

Rahman, A., Lafon, B., Parra, L. C., & Bikson, M. (2017). Direct current stimulation boosts synaptic gain and cooperativity in vitro. *The Journal of Physiology*, *595*(11), 3535–3547. https://doi.org/10.1113/JP273005

Rahman, A., Reato, D., Arlotti, M., Gasca, F., Datta, A., Parra, L. C., & Bikson, M. (2013). Cellular effects of acute direct current stimulation: Somatic and synaptic terminal effects. *The Journal of Physiology*, *591*(10), 2563–2578. https://doi.org/10.1113/jphysiol.2012.247171

Ranieri, F., Podda, M. V., Riccardi, E., Frisullo, G., Dileone, M., Profice, P., Pilato, F., Di Lazzaro, V., & Grassi, C. (2012). Modulation of LTP at rat hippocampal CA3-CA1 synapses by direct current stimulation. *Journal of Neurophysiology*, *107*(7), 1868–1880. https://doi.org/10.1152/jn.00319.2011

Reato, D., Bikson, M., & Parra, L. C. (2015). Lasting modulation of in vitro oscillatory activity with weak direct current stimulation. *Journal of Neurophysiology*, *113*(5), 1334–1341. https://doi.org/10.1152/jn.00208.2014

Reato, D., Rahman, A., Bikson, M., & Parra, L. C. (2013). Effects of weak transcranial alternating current stimulation on brain activity—A review of known mechanisms from animal studies. *Frontiers in Human Neuroscience*, *7*, 687. https://doi.org/10.3389/fnhum.2013.00687

Reato, D., Salvador, R., Bikson, M., Opitz, A., Dmochowski, J., & Miranda, P. C. (2019). Principles of Transcranial Direct Current Stimulation (tDCS): Introduction to the Biophysics of tDCS. In H. Knotkova, M. A. Nitsche, M. Bikson, & A. J. Woods (Eds.), *Practical Guide to Transcranial Direct Current Stimulation: Principles, Procedures and Applications* (pp. 45–80). Springer International Publishing. https://doi.org/10.1007/978-3-319-95948-1_2

Reed, T., & Cohen Kadosh, R. (2018). Transcranial electrical stimulation (tES) mechanisms and its effects on cortical excitability and connectivity. *Journal of Inherited Metabolic Disease*, *41*(6), 1123–1130. https://doi.org/10.1007/s10545-018-0181-4

Regan, D. (1966). Some characteristics of average steady-state and transient responses evoked by modulated light. *Electroencephalography and Clinical Neurophysiology*, *20*(3), 238–248. https://doi.org/10.1016/0013-4694(66)90088-5

Regan, D. (1974). Electrophysiological evidence for colour channels in human pattern vision. *Nature*, *250*(5465), 437–439. https://doi.org/10.1038/250437a0

Regan, D. (1989). *Human Brain Electrophysiology: Evoked Potentials and Evoked Magnetic Fields in Science and Medicine*. Elsevier.

Reinhart, R. M. G., Cosman, J. D., Fukuda, K., & Woodman, G. F. (2017). Using transcranial direct-current stimulation (tDCS) to understand cognitive processing. *Attention, Perception & Psychophysics*, *79*(1), 3–23. https://doi.org/10.3758/s13414-016-1224-2

Reinhart, R. M. G., Xiao, W., McClenahan, L. J., & Woodman, G. F. (2016). Electrical Stimulation of Visual Cortex Can Immediately Improve Spatial Vision. *Current Biology: CB*, *26*(14), 1867–1872. https://doi.org/10.1016/j.cub.2016.05.019

Renzi, C., Ferrari, C., Schiavi, S., Pisoni, A., Papagno, C., Vecchi, T., Antal, A., & Cattaneo, Z. (2015). The role of the occipital face area in holistic processing involved in face detection and discrimination: A tDCS study. *Neuropsychology*, *29*(3), 409–416. https://doi.org/10.1037/neu0000127

Retter, T. L., & Rossion, B. (2016). Uncovering the neural magnitude and spatio-temporal dynamics of natural image categorization in a fast visual stream. *Neuropsychologia*, *91*, 9–28. https://doi.org/10.1016/j.neuropsychologia.2016.07.028

Retter, T. L., Rossion, B., & Schiltz, C. (2021). Harmonic Amplitude Summation for Frequency-tagging Analysis. *Journal of Cognitive Neuroscience*, *33*(11), 2372–2393. https://doi.org/10.1162/jocn_a_01763

Rosburg, T., Ludowig, E., Dümpelmann, M., Alba-Ferrara, L., Urbach, H., & Elger, C. E. (2010). The effect of face inversion on intracranial and scalp recordings of event-related potentials. *Psychophysiology*, *47*(1), 147–157. https://doi.org/10.1111/j.1469-8986.2009.00881.x

Rossion, B. (2014). Understanding individual face discrimination by means of fast periodic visual stimulation. *Experimental Brain Research*, *232*(6), 1599–1621. https://doi.org/10.1007/s00221-014-3934-9

Rossion, B., & Boremanse, A. (2011). Robust sensitivity to facial identity in the right human occipito-temporal cortex as revealed by steady-state visual-evoked potentials. *Journal of Vision*, *11*(2), 16. https://doi.org/10.1167/11.2.16

Rossion, B., & Caharel, S. (2011). ERP evidence for the speed of face categorization in the human brain: Disentangling the contribution of low-level visual cues from face perception. *Vision Research*, *51*(12), 1297–1311. https://doi.org/10.1016/j.visres.2011.04.003

Rossion, B., Gauthier, I., Tarr, M. J., Despland, P., Bruyer, R., Linotte, S., & Crommelinck, M. (2000). The N170 occipito-temporal component is delayed and enhanced to inverted faces but not to inverted objects: An electrophysiological account of face-specific processes in the human brain. *Neuroreport*, *11*(1), 69–74. https://doi.org/10.1097/00001756-200001170-00014

Rossion, B., Hanseeuw, B., & Dricot, L. (2012). Defining face perception areas in the human brain: A large-scale factorial fMRI face localizer analysis. *Brain and Cognition*, *79*(2), 138–157. https://doi.org/10.1016/j.bandc.2012.01.001

Rossion, B., Jacques, C., & Jonas, J. (2018). Mapping face categorization in the human ventral occipitotemporal cortex with direct neural intracranial recordings. *Annals of the New York Academy of Sciences*. https://doi.org/10.1111/nyas.13596

Rossion, B., Jacques, C., & Jonas, J. (2023). Intracerebral Electrophysiological Recordings to Understand the Neural Basis of Human Face Recognition. *Brain Sciences*, *13*(2), Article 2. https://doi.org/10.3390/brainsci13020354

Rossion, B., Jacques, C., & Jonas, J. (2024). The anterior fusiform gyrus: The ghost in the cortical face machine. *Neuroscience & Biobehavioral Reviews*, *158*, 105535. https://doi.org/10.1016/j.neubiorev.2024.105535

Rossion, B., & Lochy, A. (2022). Is human face recognition lateralized to the right hemisphere due to neural competition with left-lateralized visual word recognition? A critical review. *Brain Structure & Function*, *227*(2), 599–629. https://doi.org/10.1007/s00429-021-02370-0

Rossion, B., & Michel, C. (2018). Normative accuracy and response time data for the computerized Benton Facial Recognition Test (BFRT-c). *Behavior Research Methods*, *50*(6), 2442–2460. https://doi.org/10.3758/s13428-018-1023-x

Rossion, B., Retter, T. L., & Liu-Shuang, J. (2020). Understanding human individuation of unfamiliar faces with oddball fast periodic visual stimulation and electroencephalography. *The European Journal of Neuroscience*, *52*(10), 4283–4344. https://doi.org/10.1111/ejn.14865

Rossion, B., Torfs, K., Jacques, C., & Liu-Shuang, J. (2015a). Fast periodic presentation of natural images reveals a robust face-sel ective electrophysiological response in the human brain. *Journal of Vision*, *15*(1), 18. Silverchair. https://doi.org/10.1167/15.1.18

Rossion, B., Torfs, K., Jacques, C., & Liu-Shuang, J. (2015b). Fast periodic presentation of natural images reveals a robust face-selective electrophysiological response in the human brain. *Journal of Vision*, *15*(1), 18. https://doi.org/10.1167/15.1.18

Rousselet, G. A., Husk, J. S., Bennett, P. J., & Sekuler, A. B. (2007). Single-trial EEG dynamics of object and face visual processing. *NeuroImage*, *36*(3), 843–862. https://doi.org/10.1016/j.neuroimage.2007.02.052

Roy, A., Baxter, B., & He, B. (2014). High-Definition Transcranial Direct Current Stimulation Induces Both Acute and Persistent Changes in Broadband Cortical Synchronization: A Simultaneous tDCS–EEG Study. *IEEE Transactions on Biomedical Engineering*, *61*(7), 1967–1978. https://doi.org/10.1109/TBME.2014.2311071

Ruhnau, P., Rufener, K. S., Heinze, H.-J., & Zaehle, T. (2018). Sailing in a sea of disbelief: In vivo measurements of transcranial electric stimulation in human subcortical structures. *Brain Stimulation: Basic, Translational, and Clinical Research in Neuromodulation*, *11*(1), 241–243. https://doi.org/10.1016/j.brs.2017.09.015

Russo, R., Wallace, D., Fitzgerald, P. B., & Cooper, N. R. (2013). Perception of Comfort During Active and Sham Transcranial Direct Current Stimulation: A Double Blind Study. *Brain Stimulation*, *6*(6), 946–951. https://doi.org/10.1016/j.brs.2013.05.009

Salado, A. L., Koessler, L., De Mijolla, G., Schmitt, E., Vignal, J.-P., Civit, T., Tyvaert, L., Jonas, J., Maillard, L. G., & Colnat-Coulbois, S. (2018). sEEG is a Safe Procedure for a Comprehensive Anatomic Exploration of the Insula: A Retrospective Study of 108 Procedures Representing 254 Transopercular Insular Electrodes. *Operative Neurosurgery*, *14*(1), 1. https://doi.org/10.1093/ons/opx106

Salimpour, Y., Liu, C.-C., Webber, W. R., Mills, K. A., & Anderson, W. S. (2017). Subdural recordings from an awake human brain for measuring current intensity during transcranial direct current stimulation. *2017 39th Annual International Conference of the IEEE Engineering in Medicine and Biology Society (EMBC)*, 1110–1113. https://doi.org/10.1109/EMBC.2017.8037023

Sanchez, A., Vanderhasselt, M.-A., Baeken, C., & De Raedt, R. (2016). Effects of tDCS over the right DLPFC on attentional disengagement from positive and negative faces: An eye-tracking study. *Cognitive, Affective, & Behavioral Neuroscience*, *16*(6), 1027–1038. https://doi.org/10.3758/s13415-016-0450-3

San-Juan, D., Espinoza López, D. A., Vázquez Gregorio, R., Trenado, C., Fernández-González Aragón, M., Morales-Quezada, L., Hernandez Ruiz, A., Hernandez-González, F., Alcaraz-Guzmán, A., Anschel, D. J., & Fregni, F. (2017). Transcranial Direct Current Stimulation in Mesial Temporal Lobe Epilepsy and Hippocampal Sclerosis. *Brain Stimulation*, *10*(1), 28–35. https://doi.org/10.1016/j.brs.2016.08.013

San-juan, D., Morales-Quezada, L., Orozco Garduño, A. J., Alonso-Vanegas, M., González-Aragón, M. F., Espinoza López, D. A., Vázquez Gregorio, R., Anschel, D. J., & Fregni, F. (2015). Transcranial Direct Current Stimulation in Epilepsy. *Brain Stimulation*, *8*(3), 455–464. https://doi.org/10.1016/j.brs.2015.01.001

Sarmiento, C. I., San-Juan, D., & Prasath, V. B. S. (2016). Letter to the Editor: Brief history of transcranial direct current stimulation (tDCS): from electric fishes to microcontrollers. *Psychological Medicine*, *46*(15), 3259–3261. https://doi.org/10.1017/S0033291716001926

Scott, H., Lack, L., & Lovato, N. (2020). A systematic review of the accuracy of sleep wearable devices for estimating sleep onset. *Sleep Medicine Reviews*, *49*, 101227. https://doi.org/10.1016/j.smrv.2019.101227

Sergent, J., Ohta, S., & MacDonald, B. (1992). Functional neuroanatomy of face and object processing. A positron emission tomography study. *Brain: A Journal of Neurology*, *115 Pt 1*, 15–36. https://doi.org/10.1093/brain/115.1.15

Siebner, H. R., Lang, N., Rizzo, V., Nitsche, M. A., Paulus, W., Lemon, R. N., & Rothwell, J. C. (2004). Preconditioning of low-frequency repetitive transcranial magnetic stimulation with transcranial direct current stimulation: Evidence for homeostatic plasticity in the human motor cortex. *The Journal of Neuroscience: The Official Journal of the Society for Neuroscience*, *24*(13), 3379–3385. https://doi.org/10.1523/JNEUROSCI.5316-03.2004

Sliwinska, M. W., & Pitcher, D. (2018). TMS demonstrates that both right and left superior temporal sulci are important for facial expression recognition. *NeuroImage*, *183*, 394–400. https://doi.org/10.1016/j.neuroimage.2018.08.025

Solomons, C. D., & Shanmugasundaram, V. (2020). Transcranial direct current stimulation: A review of electrode characteristics and materials. *Medical Engineering & Physics*, *85*, 63–74. https://doi.org/10.1016/j.medengphy.2020.09.015

Sowndhararajan, K., Kim, M., Deepa, P., Park, S. J., & Kim, S. (2018). Application of the P300 Event-Related Potential in the Diagnosis of Epilepsy Disorder: A Review. *Scientia Pharmaceutica*, *86*(2), Article 2. https://doi.org/10.3390/scipharm86020010

Spitoni, G. F., Di Russo, F., Cimmino, R. L., Bozzacchi, C., & Pizzamiglio, L. (2013). Modulation of spontaneous alpha brain rhythms using low-intensity transcranial direct-current stimulation. *Frontiers in Human Neuroscience*, *7*. https://doi.org/10.3389/fnhum.2013.00529

Stagg, C. J., Antal, A., & Nitsche, M. A. (2018). Physiology of Transcranial Direct Current Stimulation. *The Journal of ECT*, *34*(3), 144. https://doi.org/10.1097/YCT.0000000000000510

Stagg, C. J., & Nitsche, M. A. (2011). Physiological basis of transcranial direct current stimulation. *The Neuroscientist: A Review Journal Bringing Neurobiology, Neurology and Psychiatry*, *17*(1), 37–53. https://doi.org/10.1177/1073858410386614

Tabikh, M., Quetu, T., Maillard, L., Colnat-Coulbois, S., Rossion, B., & Koessler, L. (2025). Transcranial direct current stimulation neuromodulates intracranial cognitive evoked activity in humans. *Proceedings of the National Academy of Sciences*, *122*(23), e2416541122. https://doi.org/10.1073/pnas.2416541122

Talairach, J., & Bancaud, J. (1973). Stereotaxic Approach to Epilepsy. Methodology of Anatomo-Functional Stereotaxic Investigations. In H. Krayenb□hl, P. E. Maspes, & W. H. Sweet (Eds.), *Progress in Neurological Surgery* (Vol. 5, pp. 297–354). S. Karger AG. https://doi.org/10.1159/000394343

Tian, Y., Tan, C., Tan, J., Yang, L., & Tang, Y. (2024). Top-down modulation of DLPFC in visual search: A study based on fMRI and TMS. *Cerebral Cortex*, *34*(2). https://doi.org/10.1093/cercor/bhad540

Torro-Alves, N., Davis, J., Tabikh, M., Menzer, Y., Rossion, B., & KOESSLER, L. (2025). Objective Neural Face Recognition Neuromodulation within a Single Transcranial Direct Current Stimulation Session. *Submitted to Brain Stimulation*.

Truong, D. Q., & Bikson, M. (2018). Physics of Transcranial Direct Current Stimulation Devices and Their History. *The Journal of ECT*, *34*(3), 137–143. https://doi.org/10.1097/YCT.0000000000000531

van Vliet, M., Robben, A., Chumerin, N., Manyakov, N. V., Combaz, A., & Van Hulle, M. M. (2012). Designing a brain-computer interface controlled video-game using consumer grade EEG hardware. *2012 ISSNIP Biosignals and Biorobotics Conference: Biosignals and Robotics for Better and Safer Living (BRC)*, 1–6. https://doi.org/10.1109/BRC.2012.6222186

Vergallito, A., Feroldi, S., Pisoni, A., & Romero Lauro, L. J. (2022). Inter-Individual Variability in tDCS Effects: A Narrative Review on the Contribution of Stable, Variable, and Contextual Factors. *Brain Sciences*, *12*(5), Article 5. https://doi.org/10.3390/brainsci12050522

Vettori, S., Dzhelyova, M., Van der Donck, S., Jacques, C., Steyaert, J., Rossion, B., & Boets, B. (2019). Reduced neural sensitivity to rapid individual face discrimination in autism spectrum disorder. *NeuroImage: Clinical*, *21*, 101613. https://doi.org/10.1016/j.nicl.2018.101613

Vettori, S., Dzhelyova, M., Van der Donck, S., Jacques, C., Steyaert, J., Rossion, B., & Boets, B. (2020). Frequency-Tagging Electroencephalography of Superimposed Social and Non-Social Visual Stimulation Streams Reveals Reduced Saliency of Faces in Autism Spectrum Disorder. *Frontiers in Psychiatry*, *11*. https://doi.org/10.3389/fpsyt.2020.00332

Vettori, S., Jacques, C., Boets, B., & Rossion, B. (2019). Can the N170 Be Used as an Electrophysiological Biomarker Indexing Face Processing Difficulties in Autism Spectrum Disorder? *Biological Psychiatry: Cognitive Neuroscience and Neuroimaging*, *4*(3), 321–323. https://doi.org/10.1016/j.bpsc.2018.07.015

Villamar, M. F., Volz, M. S., Bikson, M., Datta, A., Dasilva, A. F., & Fregni, F. (2013). Technique and considerations in the use of 4x1 ring high-definition transcranial direct current stimulation (HD-tDCS). *Journal of Visualized Experiments: JoVE*, *77*, e50309. https://doi.org/10.3791/50309

Volfart, A., Jonas, J., Maillard, L., Busigny, T., Rossion, B., & Brissart, H. (2020). Typical visual unfamiliar face individuation in left and right mesial temporal epilepsy. *Neuropsychologia*, *147*, 107583. https://doi.org/10.1016/j.neuropsychologia.2020.107583

Volfart, A., Rice, G. E., Lambon Ralph, M. A., & Rossion, B. (2021). Implicit, automatic semantic word categorisation in the left occipito-temporal cortex as revealed by fast periodic visual stimulation. *NeuroImage*, *238*, 118228. https://doi.org/10.1016/j.neuroimage.2021.118228

Volfart, A., Rossion, B., Yan, X., Angelini, L., Maillard, L., Colnat-Coulbois, S., & Jonas, J. (2023). Intracerebral electrical stimulation of the face-selective right lateral fusiform gyrus transiently impairs face identity recognition. *Neuropsychologia*, *190*, 108705. https://doi.org/10.1016/j.neuropsychologia.2023.108705

Vöröslakos, M., Takeuchi, Y., Brinyiczki, K., Zombori, T., Oliva, A., Fernández-Ruiz, A., Kozák, G., Kincses, Z. T., Iványi, B., Buzsáki, G., & Berényi, A. (2018). Direct effects of transcranial electric stimulation on brain circuits in rats and humans. *Nature Communications*, *9*(1), Article 1. https://doi.org/10.1038/s41467-018-02928-3

Wang, C. S.-M., Chang, W.-H., Yang, Y.-K., & Cheng, K.-S. (2023). Comparing Transcranial Direct Current Stimulation (tDCS) with Other Non-Invasive Brain Stimulation (NIBS) in the Treatment of Alzheimer's Disease: A Literature Review. *Journal of Medical and Biological Engineering*, *43*(4), 362–375. https://doi.org/10.1007/s40846-023-00810-2

Weiner, K. S., Golarai, G., Caspers, J., Chuapoco, M. R., Mohlberg, H., Zilles, K., Amunts, K., & Grill-Spector, K. (2014). The mid-fusiform sulcus: A landmark identifying both cytoarchitectonic and functional divisions of human ventral temporal cortex. *NeuroImage*, *84*, 453–465. https://doi.org/10.1016/j.neuroimage.2013.08.068

Weiner, K. S., & Grill-Spector, K. (2015). The evolution of face processing networks. *Trends in Cognitive Sciences*, *19*(5), 240–241. https://doi.org/10.1016/j.tics.2015.03.010

Willis, M. L., Costantino, A. I., Nitsche, M. A., Palermo, R., & Rivolta, D. (2019). Anodal tDCS and High-Frequency tRNS Targeting the Occipitotemporal Cortex Do Not Always Enhance Face Perception. *Frontiers in Neuroscience*, *13*, 78. https://doi.org/10.3389/fnins.2019.00078

Wilson, K. R., O'Rourke, H., Wozniak, L. A., Kostopoulos, E., Marchand, Y., & Newman, A. J. (2012). Changes in N400 topography following intensive speech language therapy for individuals with aphasia. *Brain and Language*, *123*(2), 94–103. https://doi.org/10.1016/j.bandl.2012.06.005

Wolkenstein, L., & Plewnia, C. (2013). Amelioration of Cognitive Control in Depression by Transcranial Direct Current Stimulation. *Biological Psychiatry*, *73*(7), 646–651. https://doi.org/10.1016/j.biopsych.2012.10.010

Woods, A. J., Antal, A., Bikson, M., Boggio, P. S., Brunoni, A. R., Celnik, P., Cohen, L. G., Fregni, F., Herrmann, C. S., Kappenman, E. S., Knotkova, H., Liebetanz, D., Miniussi, C., Miranda, P. C., Paulus, W., Priori, A., Reato, D., Stagg, C., Wenderoth, N., & Nitsche, M. A. (2016a). A technical guide to tDCS, and related non-invasive brain stimulation tools. *Clinical Neurophysiology*, *127*(2), 1031–1048. https://doi.org/10.1016/j.clinph.2015.11.012

Woods, A. J., Antal, A., Bikson, M., Boggio, P. S., Brunoni, A. R., Celnik, P., Cohen, L. G., Fregni, F., Herrmann, C. S., Kappenman, E. S., Knotkova, H., Liebetanz, D., Miniussi, C., Miranda, P. C., Paulus, W., Priori, A., Reato, D., Stagg, C., Wenderoth, N., & Nitsche, M. A. (2016b). A technical guide to tDCS, and related non-invasive brain stimulation tools. *Clinical Neurophysiology: Official Journal of the International Federation of Clinical Neurophysiology*, *127*(2), 1031–1048. https://doi.org/10.1016/j.clinph.2015.11.012

Wu, D., Zhang, P., Liu, N., Sun, K., & Xiao, W. (2021). Effects of High-Definition Transcranial Direct Current Stimulation Over the Left Fusiform Face Area on Face View Discrimination Depend on the Individual Baseline Performance. *Frontiers in Neuroscience*, *15*. https://doi.org/10.3389/fnins.2021.704880

Wyler, A. R., Ojemann, G. A., Lettich, E., & Ward, A. A. (1984). Subdural strip electrodes for localizing epileptogenic foci. *Journal of Neurosurgery*, *60*(6), 1195–1200. https://doi.org/10.3171/jns.1984.60.6.1195

Yamada, Y., & Sumiyoshi, T. (2021). Neurobiological Mechanisms of Transcranial Direct Current Stimulation for Psychiatric Disorders; Neurophysiological, Chemical, and Anatomical Considerations. *Frontiers in Human Neuroscience*, *15*. https://doi.org/10.3389/fnhum.2021.631838

Yang, L.-Z., Zhang, W., Shi, B., Yang, Z., Wei, Z., Gu, F., Zhang, J., Cui, G., Liu, Y., Zhou, Y., Zhang, X., & Rao, H. (2014). Electrical Stimulation over Bilateral Occipito-Temporal Regions Reduces N170 in the Right Hemisphere and the Composite Face Effect. *PLOS ONE*, *9*(12), e115772. https://doi.org/10.1371/journal.pone.0115772

Yavari, F., Jamil, A., Mosayebi Samani, M., Vidor, L. P., & Nitsche, M. A. (2018). Basic and functional effects of transcranial Electrical Stimulation (tES)—An introduction. *Neuroscience & Biobehavioral Reviews*, *85*, 81–92. https://doi.org/10.1016/j.neubiorev.2017.06.015

Yovel, G. (2016). Neural and cognitive face-selective markers: An integrative review. *Neuropsychologia*, *83*, 5–13. https://doi.org/10.1016/j.neuropsychologia.2015.09.026

Zanotto, V., Boscariol, P., Gasparetto, A., Lanzutti, A., Vidoni, R., Di Lorenzo, N., Gallina, P., Via, A. D., & Rossi, A. (2011). A Master-Slave Haptic System for Neurosurgery. *Applied Bionics and Biomechanics*, *8*(2), 819689. https://doi.org/10.3233/ABB-2011-0026

Zheng, X., Alsop, D. C., & Schlaug, G. (2011). Effects of Transcranial Direct Current Stimulation (tDCS) on Human Regional Cerebral Blood Flow. *NeuroImage*, *58*(1), 26–33. https://doi.org/10.1016/j.neuroimage.2011.06.018

Zhong, R., Li, M., Chen, Q., Li, J., Li, G., & Lin, W. (2019). The P300 Event-Related Potential Component and Cognitive Impairment in Epilepsy: A Systematic Review and Meta-analysis. *Frontiers in Neurology*, *10*. https://doi.org/10.3389/fneur.2019.00943

Zorowitz, S., & Niv, Y. (2023). Improving the Reliability of Cognitive Task Measures: A Narrative Review. *Biological Psychiatry: Cognitive Neuroscience and Neuroimaging*, *8*(8), 789–797. https://doi.org/10.1016/j.bpsc.2023.02.004

Appendix

Transcranial direct current stimulation neuromodulates intracranial cognitive evoked activity in humans.

Tabikh M, Quetu T, Maillard L, Colnat-Coulbois S, Rossion B, Koessler L. Transcranial direct current stimulation neuromodulates intracranial cognitive evoked activity in humans. Proc Natl Acad Sci U S A. 2025 Jun 10;122(23):e2416541122.

Doi: 10.1073/pnas.2416541122. Epub 2025 Jun 3. PMID: 40460123; PMCID: PMC12168024.

PNAS RESEARCH ARTICLE | NEUROSCIENCE OPEN ACCESS

Transcranial direct current stimulation neuromodulates intracranial cognitive evoked activity in humans

Mireille Tabikh[a], Tom Quetu[a], Louis Maillard[a,b], Sophie Colnat-Coulbois[a,c], Bruno Rossion[a,b], and Laurent Koessler[a,d,1]

Affiliations are included on p. 10.

Edited by Helen Mayberg, Icahn School of Medicine at Mount Sinai, New York, NY; received September 24, 2024; accepted April 15, 2025

Transcranial direct current stimulation (tDCS) is an easy to use, noninvasive brain stimulation technique that gained prominence for its potential in cognitive rehabilitation. Electroencephalography (EEG), which records electrical brain activity with a high temporal resolution, is well suited to quantify tDCS-induced neuromodulation in humans. However, most studies relying on scalp EEG recordings or event-related potentials showed low reliability and only indirect correlations. Here, we combined intracranial EEG (iEEG) recordings with a sham-controlled tDCS experiment during fast periodic visual stimulation. Anodal (+2 mA) tDCS was applied over the right occipito-temporal cortex for 20 min using two small ring high-definition electrodes. Through the analysis of iEEG signals of 947 intracerebral contacts in 11 drug-resistant epileptic patients, we quantified the neuromodulation of iEEG cognitive evoked responses during (P2 phase) and after (P3 phase) tDCS by comparison to a control phase before tDCS (P1 phase). Significant neuromodulations of face-selective iEEG activity in anterior & posterior temporal lobe and in the occipital lobe were found, with amplitude increases of 3% and 4%, 16% and 13%, and 36% and 33%, during and after tDCS, respectively. Interestingly, despite a unique tDCS session, the face-selective neuromodulation in the right visual occipito-temporal cortex remained significant ($P = 0.015$) after tDCS (P3 vs. P1). This iEEG study demonstrates that using low intensity tDCS and small ring electrodes can induce significant electrophysiological effects on a selective cognitive function in humans.

transcranial direct current stimulation | neuromodulation | human in vivo | intracranial EEG recording | cognitive evoked activity

Significance

A sham-controlled transcranial direct current stimulation (tDCS) experiment was performed simultaneously with intracranial electroencephalographic recording (iEEG) and fast periodic visual stimulation (FPVS) in epileptic patients. General visual and face-selective iEEG responses evoked by FPVS were quantified before, during, and after a single session of anodal tDCS performed over the right posterior temporal lobe (PTL) using small ring electrodes. Significant amplitude increases of face-selective iEEG responses were observed during tDCS, whereas weak neuromodulation occurred on general visual responses. The neuromodulations were observed in the PTL. Finally, and interestingly, the neuromodulation remained after a single tDCS session. This study shows that objective, selective, and significant neuromodulation can be obtained using small electrodes and low intensity with tDCS.

The development of noninvasive brain stimulation (NIBS) techniques has opened new avenues for cognitive rehabilitation in neurological and psychiatric diseases. Among these techniques, transcranial direct current stimulation (tDCS) stands out from other techniques for its potential to modulate neural activity using low-intensity currents and its ability to be used at home with very little inexpensive equipment (1). tDCS is based on injecting a low-intensity direct current (few milliamps) onto the scalp's surface, for several minutes in one or several sessions, using two or more scalp electrodes (for recent review see ref. 2). Since the 2000s, the use of tDCS as an alternative (or complementary) treatment for different neurological, psychiatric, and cognitive disorders has increased exponentially [for review see ref. 3 in neurological disease, (4) in psychiatric disease].

Despite its promising effects in humans, tDCS effects have long been questioned due to the lack of evidence demonstrating the current's ability to pass through the highly resistive skull and to reach brain tissue (5–7). Recently, human in vivo studies using low-intensity NIBS simultaneously combined with intracranial electroencephalographic (iEEG) recordings have shown that significant electric fields (EF) can reach cortical brain structures as well as deep medial brain structures (such as the hippocampi, cingulate gyri, and the amygdalae) (8). The current's propagation from scalp to cortical brain structures in humans is one of the fundamental steps needed to obtain an electrophysiological modulation of brain activity. The second step, that has yet to be investigated, concerns the low-intensity current's ability to modulate the electrophysiological cortical activity in the human brain supporting cognitive functions.

At this level, the precise quantification of electrophysiological modulation due to tDCS remains unknown in humans. This lack of electrophysiological evidence supports interpretation of tDCS effects as placebo or indirect (e.g., metabolic) effects. Objective electrophysiological quantifications have never been performed previously due to methodological constraints, especially the scarcity of access to iEEG recordings, the only reference method for direct recording of cortical brain sources with high spatial and temporal resolution. A number of previous studies combined scalp EEG recordings with tDCS during cognitive

Author contributions: M.T., B.R., and L.K. designed research; M.T. and T.Q. performed research; M.T. and L.K. analyzed data; L.M. and S.C.-C. included patients and review the manuscript; B.R. review the manuscript; and M.T.and L.K. wrote the paper.

The authors declare no competing interest.

This article is a PNAS Direct Submission.

Copyright © 2025 the Author(s). Published by PNAS. This open access article is distributed under Creative Commons Attribution License 4.0 (CC BY).

[1]To whom correspondence may be addressed. Email: laurent.koessler@cnrs.fr.

This article contains supporting information online at https://www.pnas.org/lookup/suppl/doi:10.1073/pnas.2416541122/-/DCSupplemental.

Published June 3, 2025.

Downloaded from https://www.pnas.org by 92.184.124.201 on December 16, 2025 from IP address 92.184.124.201.

tasks, but several methodological drawbacks led to controversial results (9, 10). In particular, nonphysiological artifacts [different to physiological artifacts i.e., interaction between the stimulation and the biological tissues (11)] on scalp EEG signals during tDCS induce challenging denoising processes (12, 13) and unprecise characterization of the electrophysiological effects (14, 15).

Here, we circumvent these issues by simultaneously combining sham-controlled tDCS with iEEG recording during fast periodic visual stimulation (FPVS). FPVS, of "frequency-tagging," is an approach that generates electrophysiological activity responses at known periodic frequencies with high signal-to-noise ratio (SNR), objectivity, and robust test–retest results (16, 17). Since the neural activity of interest can be confined to small (known) frequency bins, it is largely immune to tDCS artifacts (*SI Appendix*, Fig. S1), making this approach particularly well-suited to perform an intracerebral evaluation of neuromodulation characteristics of the periodically evoked iEEG responses (in terms of amplitude, SNR, and spatial distribution). In the present study, the noise amplitude remains stable (i.e., no increase between P1, P2, and P3 phases) and weak (2 to 3 times less than the signal amplitude) during tDCS.

iEEG recordings were obtained through minimally invasive procedure of intracerebral implantation, which does not significantly alter the volume conduction of the head [no current leakage; (18)], offers the ability to investigate electrophysiological neuromodulation during tDCS without artifacts in iEEG signals. In addition, iEEG permits to investigate deep, intermediate, and superficial cortical brain sources which is relevant to sampling large cognitive networks. In the present study, the ventral occipito-temporal cortex (VOTC) was investigated as it contains a highly functional and distributed network that is often explored in epileptic patients (19).

The well-validated FPVS paradigm used here is based on presenting nonface images of different object categories (e.g., animals, plants, houses, …) at a rapid rate of six images per second, i.e., at a frequency of 6 Hz. Images of human faces are inserted every 5th image (i.e., 6 Hz/5 = 1.2 Hz). The presentation of (nonface and face) images at 6 Hz elicits neural responses in the cerebral cortex at the same frequency as image presentation (i.e., at 6 Hz and harmonics: 12 Hz, 18 Hz, etc.) called general visual responses. Furthermore, if face images reliably elicit differential responses, these face-selective responses appear at 1.2 Hz (and harmonics: 2.4 Hz, 3.6 Hz, etc.) (19–21). Due to the periodicity of the FPVS, both types of evoked responses (general visual and face-selective) can be quantified in the frequency domain of the iEEG recording (20). Each FPVS phase contained two successive FPVS sessions (three phases with two sessions each i.e., six FPVS sessions) and each phase was performed before (sham; Phase P1), during (Phase P2), and after (sham; Phase P3) tDCS.

The main objective of this study was to quantify the intracranial electrophysiological effects induced by anodal (+2 mA) tDCS, performed over the right occipito-temporal lobe, on both general visual and face-selective iEEG evoked responses. Then, the issue of anatomical tDCS specificity was investigated by quantifying the intracranial electrophysiological effects in the three main anatomo-functional brain regions of the VOTC.

Results

Sham-controlled tDCS experiments were prospectively performed in 11 drug-resistant epileptic patients. The experiment contained three consecutive phases of iEEG recordings: P1 with sham tDCS during FPVS; P2 with +2 mA tDCS applied over the right VOTC (P10 electrode position) for 10 min (resting state period), followed by 10 min of active tDCS during FPVS (i.e., 20 min of tDCS in all); P3 with sham tDCS during FPVS. Active tDCS was blinded to the patients (Fig. 1*A*). FVPS in this paradigm elicits two types of responses: a general visual response, at 6 Hz and its harmonics, common to both face and nonface images, and a face-selective response, at 1.2 Hz and its harmonics, which reflects a response specific to face stimuli (Fig. 1 *B*–*D*). Patients' attention before, during, and after tDCS remained optimal showing no significant changes in either response accuracies (100% in P1, P2, P3) and response times (mean values for P1: 0.46 s, P2: 0.48 s, P3: 0.47 s; $P = 0.35$).

In our population, a total of 90 intracranial electrodes were implanted in the right hemisphere, each electrode containing 5 to 18 contacts for independent recording of the local field potential (947 contacts in total). Then, iEEG contacts within the right hemisphere (where face-selectivity is the predominant; 21, 22) were investigated. All iEEG contacts in this study were selected because they recorded significant iEEG evoked responses during previous FPVS sessions (same cognitive paradigm i.e., objects and faces) performed during the week of patients' iEEG investigation.

TDCS Significantly Neuromodulates Face Selective Responses. Among 453 iEEG contacts in the right hemisphere (Fig. 2*A*), 260 and 302 iEEG contacts which showed significant general visual and face-selective iEEG responses were used to compute the means and the SEM of these two kinds of neural responses, respectively (Fig. 2 *B* and *C*).

For general visual responses, the averaged baseline-corrected amplitudes and SEM recorded during phases P1, P2, and P3 were 4.09 ± 0.40, 4.15 ± 0.40, and 4.30 ± 0.41 μV, respectively. No significant baseline-corrected amplitude difference was found between the different phases (Fig. 3). The SNR values were 3.85, 3.78, and 3.93 during P1, P2, and P3, respectively (*SI Appendix*, Fig. S2).

For face-selective responses, the average baseline-corrected amplitudes recorded during the three phases (before, during, and after tDCS) were 9.79 ± 1.07, 11.07 ± 1.19 (i.e., +13%), and 10.73 ± 1.17 μV (i.e., +10%), respectively. A significant difference was found between P2 and P1 ($P < 0.001$) and between P3 and P1 ($P < 0.001$, Repeated measures ANOVA) (Fig. 3). The SNR values were 3.28, 3.37, and 3.49 during P1, P2, and P3, respectively (*SI Appendix*, Fig. S2).

Then, a more restrained iEEG analysis was performed using only the iEEG contacts located in the right VOTC.

For general visual responses, the average baseline-corrected amplitudes recorded from 147 contacts during phases P1, P2, and P3 were 6.22 ± 0.64, 6.24 ± 0.64, and 6.56 ± 0.69 μV, respectively. No significant baseline-corrected amplitude difference was observed between the different phases. The SNR values during the three phases were 4.91, 4.66, and 4.93, respectively.

For face-selective visual responses, the average baseline-corrected amplitudes recorded from 181 contacts during phases P1, P2, and P3 were 13.49 ± 1.62, 15.15 ± 1.77 (i.e., +12% with respect to P1), and 14.85 ± 1.76 μV (i.e., +10% with respect to P1), respectively. A significant baseline-corrected amplitude difference was found between P2 and P1 ($P = 0.002$) and between P3 and P1. ($P = 0.003$, Repeated measures ANOVA). The values of the SNR during the three respective phases were 3.83, 3.84, and 3.88, respectively (Fig. 3 and *SI Appendix*, Fig. S2).

HD Electrodes Spatially Targeted Posterior Temporal Lobe (PTL). To investigate the spatial targeting of tDCS, 328 iEEG contacts in the VOTC for both iEEG responses were classified

Downloaded from https://www.pnas.org by 92.184.124.201 on December 16, 2025 from IP address 92.184.124.201.

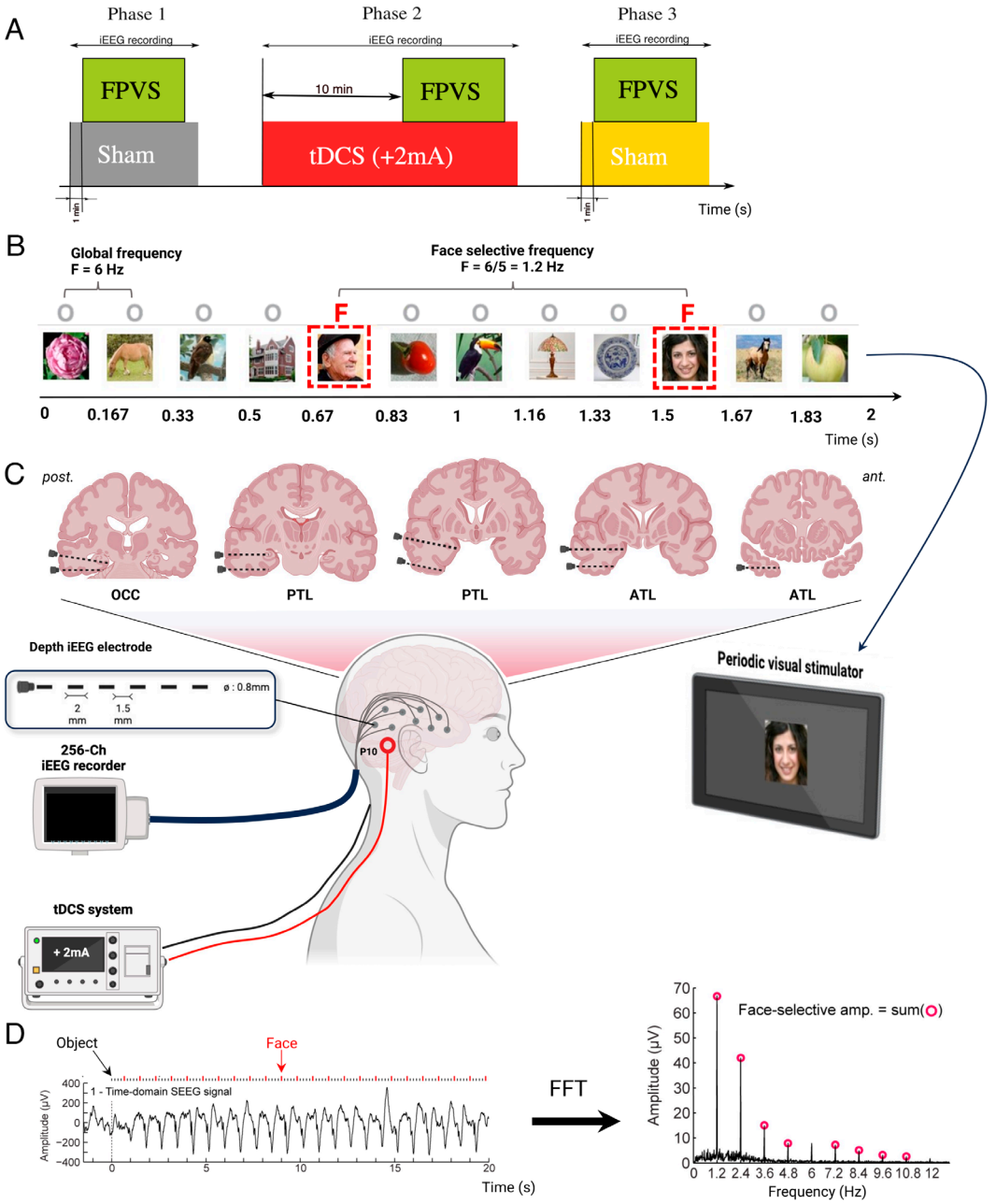

Fig. 1. Overview of the combined iEEG-FPVS-tDCS protocol. (*A*) Timeline of the experiment with the three different phases of FPVS-iEEG sessions performed before, during, and after tDCS. (*B*) The FPVS paradigm. Images of objects were presented by sinusoidal contrast modulation at a rate of six stimuli per second (6 Hz). In the periodic condition, a different face image was presented every five stimuli (i.e., appearing at the frequency of 6/5 = 1.2 Hz). (*C*) Schematic view of the patient's setting during the protocol. An average of eight iEEG multicontact electrodes were implanted in the VOTC from posterior (OCC) to anterior regions (ATL). (*D*) iEEG signal analysis. FFT was applied to iEEG signals in the time domain, with amplitude and SNR spectra extracted for all iEEG contacts. Here, face-selective and general visual amplitude responses (peaks) can be seen at 1.2 Hz and its harmonics (red dots) and 6 Hz plus its harmonic (12 Hz), respectively. Thanks to the duration of each FVPS session (71 s), the frequency resolution of the signal analysis is very high (i.e., 0.0141 Hz). iEEG; intracranial electroencephalography; FPVS: fast periodic visual stimulation; OCC: occipital; PTL: posterior temporal lobe; ATL: anterior temporal lobe; VOTC: ventral occipito-temporal cortex; FFT: Fast Fourier Transform.

into three brain regions of interest (ROI): anterior temporal lobe (ATL), PTL, and occipital lobe (OCC) (Fig. 4*A*). This anatomical classification was previously defined in a previous iEEG study of the face-selective brain regions (21). The average EF values were respectively 0.29 ± 0.36 V/m, 0.17 ± 0.11 V/m and 0.22 ± 0.24 V/m in OCC, PTL, and ATL, respectively. In the inferior occipital gyrus (IOG), the average EF values were 0.38 ± 0.43 V/m (*SI Appendix*, Table S5). The baseline-corrected amplitudes and SNR of the iEEG evoked responses (both general visual and face-selective responses) located in each ROI were computed in each of the three phases of this study.

For general visual responses, the baseline-corrected amplitudes for the iEEG contacts located in the ATL (n = 91) were 3.8 ± 0.47, 3.76 ± 0.43, and 3.94 ± 0.44 μV during the three phases P1, P2, and P3, respectively. In the PTL (n = 40), the values were 9.05 ± 1.40, 9.08 ± 1.37, and 9.56 ± 1.44 μV, during the three phases P1, P2, and P3, respectively. Finally, the highest iEEG evoked responses were found in the OCC (n = 16) with 12.92 ± 3.09, 13.28 ± 3.34, and 13.95 ± 3.36 μV during the P1, P2, and P3, respectively. Despite an increasing trend, no significant change was found between the difference phases (Fig. 4*B*). The mean SNR values of the general visual responses were 3.65, 3.53, and 3.66

Downloaded from https://www.pnas.org by 92.184.124.201 on December 16, 2025 from IP address 92.184.124.201.

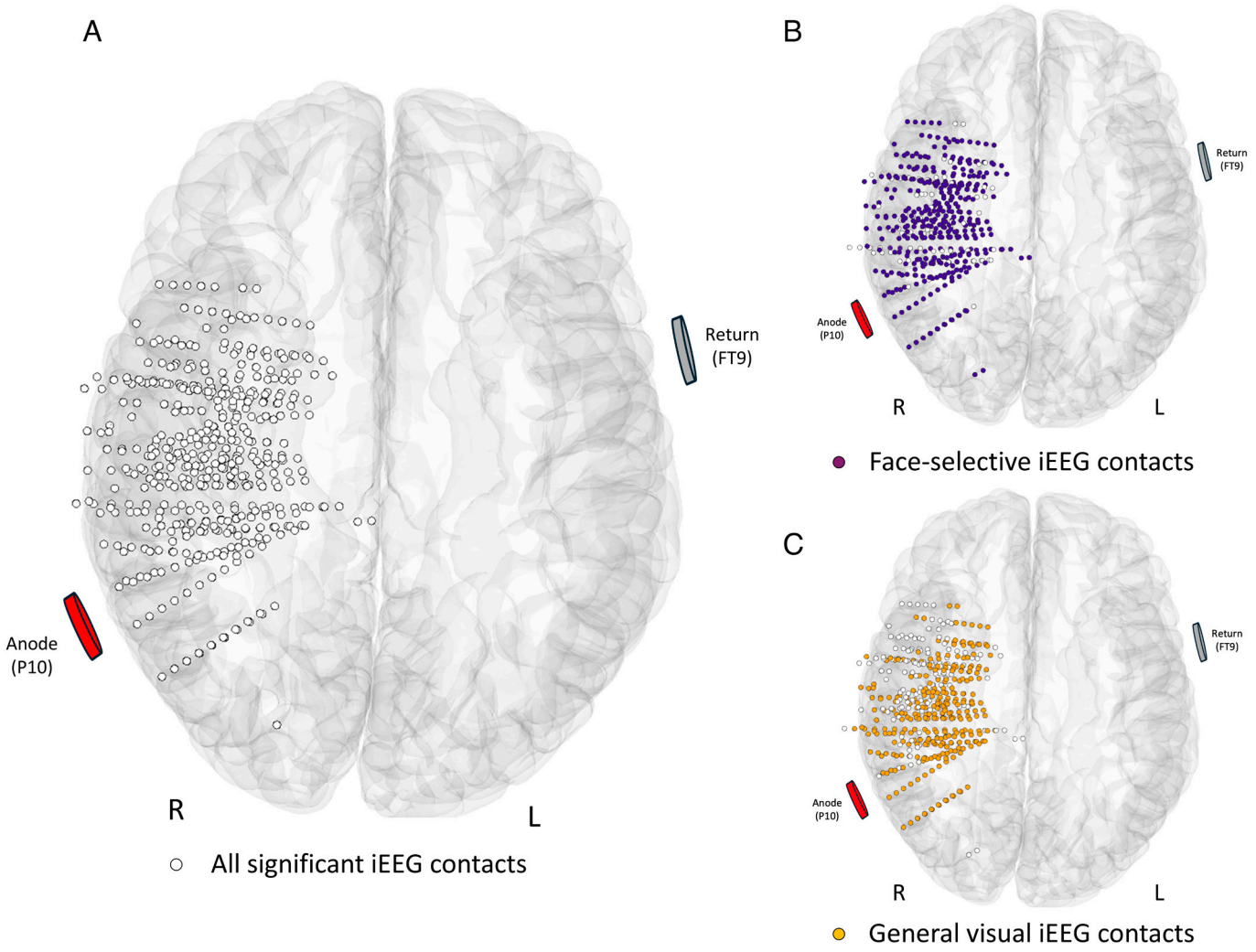

Fig. 2. Spatial distribution of the iEEG contacts and the HD-ring tDCS electrodes in the MNI space (ventral view). (*A*) Maps of all significant iEEG recording contacts (n = 452) in the right hemisphere across the 11 individual brains displayed in the MNI space using transparent reconstructed cortical surface of the Colin27 brain. Each circle represents a single iEEG contact. For visualization purposes, individual contacts are displayed larger than their actual size (2 mm in length). (*B* and *C*) The same display for the iEEG contacts showing face-selective (n = 302; violet circles) and general visual (n = 260; orange circles) responses, respectively.

in the ATL, 5.96, 5.41, and 5.88 in the PTL, and 9.40, 9.19, and 9.80 in the OCC for phases P1, P2, and P3, respectively (*SI Appendix*, Fig. S3).

For face-selective responses, the baseline-corrected amplitudes for the iEEG contacts located in the ATL (n = 114) were 9.79 ± 1.20, 10.16 ± 1.23 (i.e., +4% with respect to P1) and 10.05 ± 1.22 μV (i.e., +3% with respect to P1), during the three phases P1, P2, and P3, respectively (no significant amplitude change). At the opposite, in the PTL (n = 51), the baseline corrected amplitudes were 21.43 ± 4.82, 24.83 ± 5.14 (i.e., +16% with respect to P1) and 24.15 ± 5.14 μV (i.e., +13% with respect to P1) during the three phases, respectively. The amplitude of the face-selective responses significantly varied from P1 to P2 i.e., during the tDCS (P = 0.003), as well as from P1 to P3 i.e., after the tDCS (P = 0.015) (Fig. 4*B*). In the OCC (n = 16), the baseline corrected amplitudes were 14.55 ± 3.56, 19.86 ± 5.41 (i.e., +36% with respect to P1), and 19.41 ± 5.24 μV (i.e., +33% with respect to P1) during the three phases, respectively. The variation of the amplitudes between P2 and P1 and between P3 and P1 showed a trend toward increase. The mean SNR values of the face-selective responses were 3.52, 3.55, and 3.48 in the ATL, 4.22, 4.32, and 4.44 in the PTL and 4.77, 4.36, and 4.91 in the OCC, during the three phases, respectively. (*SI Appendix*, Fig. S3).

Discussion

Significant Neuromodulation Using Low-Intensity, -Duration, and -Resolution TDCS Configuration. Quantifying the intracerebral neuromodulation induced by NIBS in humans in vivo has not been performed before due to methodological and clinical constraints. Here, we overcame these constraints with simultaneous combination of tDCS with iEEG and FPVS. FVPS and iEEG were used as reference methods since they allow objective measurement of (frequency-tagged) brain activities directly within different brain sources organized in a sparse cognitive network and away from the stimulating scalp electrodes that generate electrical artifacts. In addition, the implementation of a sham-controlled experiment with iEEG recordings reduced placebo effects and allowed for a thorough investigation of the different tDCS phases (before, during, and after tDCS). The observed intracerebral neuromodulation was obtained in patients with preserved face perception abilities (23) and in cognitive brain networks similar to those previously mapped (21).

Despite setting tDCS parameters at a common intensity (2 mA), duration (20 min), and using a small number of electrodes (two small HD ring electrodes), tDCS significantly modulated the evoked iEEG responses. Deliberately, these parameters have not been optimized to study tDCS effects under the most frequent

Downloaded from https://www.pnas.org by 92.184.124.201 on December 16, 2025 from IP address 92.184.124.201.

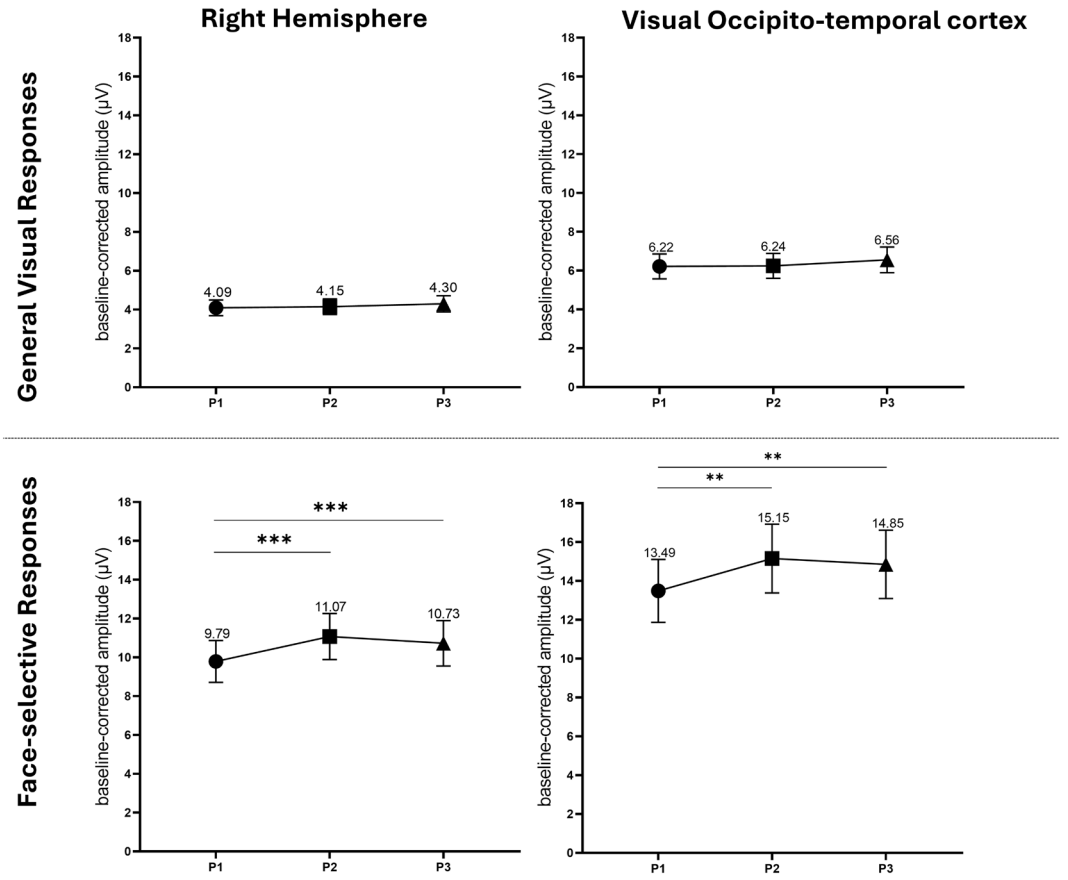

Fig. 3. Neuromodulation of iEEG general visual (on the *Top*) and face-selective (on the *Bottom*) responses across the three phases of the tDCS experiment (before, P1; during, P2; after, P3) in the right hemisphere (*Left* column) and in the right visual occipito-temporal cortex (*Right* column). Averaged baseline-corrected amplitudes and SE of the mean of the iEEG evoked responses were computed during the three different phases for the 11 patients. In the right hemisphere, 260 and 302 iEEG contacts were used to compute the average baseline-corrected amplitudes whereas 147 and 181 contacts were selected for the general visual responses and the face-selective responses, respectively. Face-selective responses were significantly neuromodulated during (P2) and after (P3) tDCS ($P < 0.001$). In contrast, no significant neuromodulation was observed for the general visual responses. Graphs for SNR analysis are presented in *SI Appendix*, Fig. S2. Phases: Black circles: P1 (sham, before tDCS); Black squares: P2 (active, during tDCS); Black triangles: P3 (sham, after tDCS).

conditions encountered in research and clinical uses (24) and consequently, provide findings that would be broadly beneficial to the field. The quantification of iEEG neuromodulation in terms of amplitude showed significant but moderate increases (from 10 to 36%) which could be related to these routine tDCS parameters set in the study. Considering that neuromodulation is related to the intracerebral EF induced within the targeted brain network, one method to obtain a stronger EF, and consequently stronger neuromodulation, could be to increase tDCS intensity. In a combined NIBS-iEEG investigation, we demonstrate a direct linear relationship between the tDCS intensity and the measured intracerebral EF in humans. When tDCS intensity is doubled, the EF is also doubled (8). Yet, increasing the intensity is not without its constraints and dangers. For safety and tolerability considerations, increasing tDCS intensity (e.g., from 2 to 4 mA) can be facilitated by using larger electrodes like pads, which distribute the current over a broader area, or by employing a configuration of multiple small HD electrodes, which enhance focality (25). Considering the promising results of computational studies with high definition tDCS (26), this method should potentially achieve greater neuromodulation. Our original study which used small HD ring electrodes, instead of the more commonly used large sponges or pads, is also a first step in demonstrating that significant neuromodulation can be obtained using small ring electrodes despite the lack of an HD configuration. In the presurgical context of iEEG investigation, small HD electrodes are well suited to be positioned alongside the iEEG electrodes. This ergonomic aspect, along with their efficiency in distributing currents in the head tissues, is important to highlight, especially for broader clinical use.

Finally, the iEEG neuromodulation induced by tDCS in the posterior and OCC during our face-perception tasks could objectively explain the behavioral (27, 28) and scalp EEG (14, 15) changes and increases observed after tDCS in some studies.

Significant Neuromodulation Remained After a Single-tDCS Session. In this study, a single 20-min tDCS session was assigned for each participant. Despite this minimal procedure, interestingly, significant face-selective electrophysiological neuromodulation remained after the tDCS session. This finding confirms results showing that tDCS altered cortical excitability for approximately 1 h poststimulation, as demonstrated through scalp EEG evoked potential analysis (29, 30). Here, the iEEG aftereffects were measured immediately following the tDCS session (within a few minutes). The absence of longer investigation (e.g., 1 h or even more after the tDCS) was due to clinical reasons, specifically the removal of iEEG electrodes just after the experiment when clinical investigation was finished. Performing tDCS experiment earlier in the week is not feasible in the iEEG context because tDCS could disorganize the surrounding epileptic brain networks and therefore, bias the clinical diagnosis of epilepsy.

In a recent review (7), the main conclusion was the lack of evidence of cognitive effects in healthy populations (n = 59 analyses) resulting from a single session of tDCS. This apparent tDCS

Downloaded from https://www.pnas.org by 92.184.124.201 on December 16, 2025 from IP address 92.184.124.201.

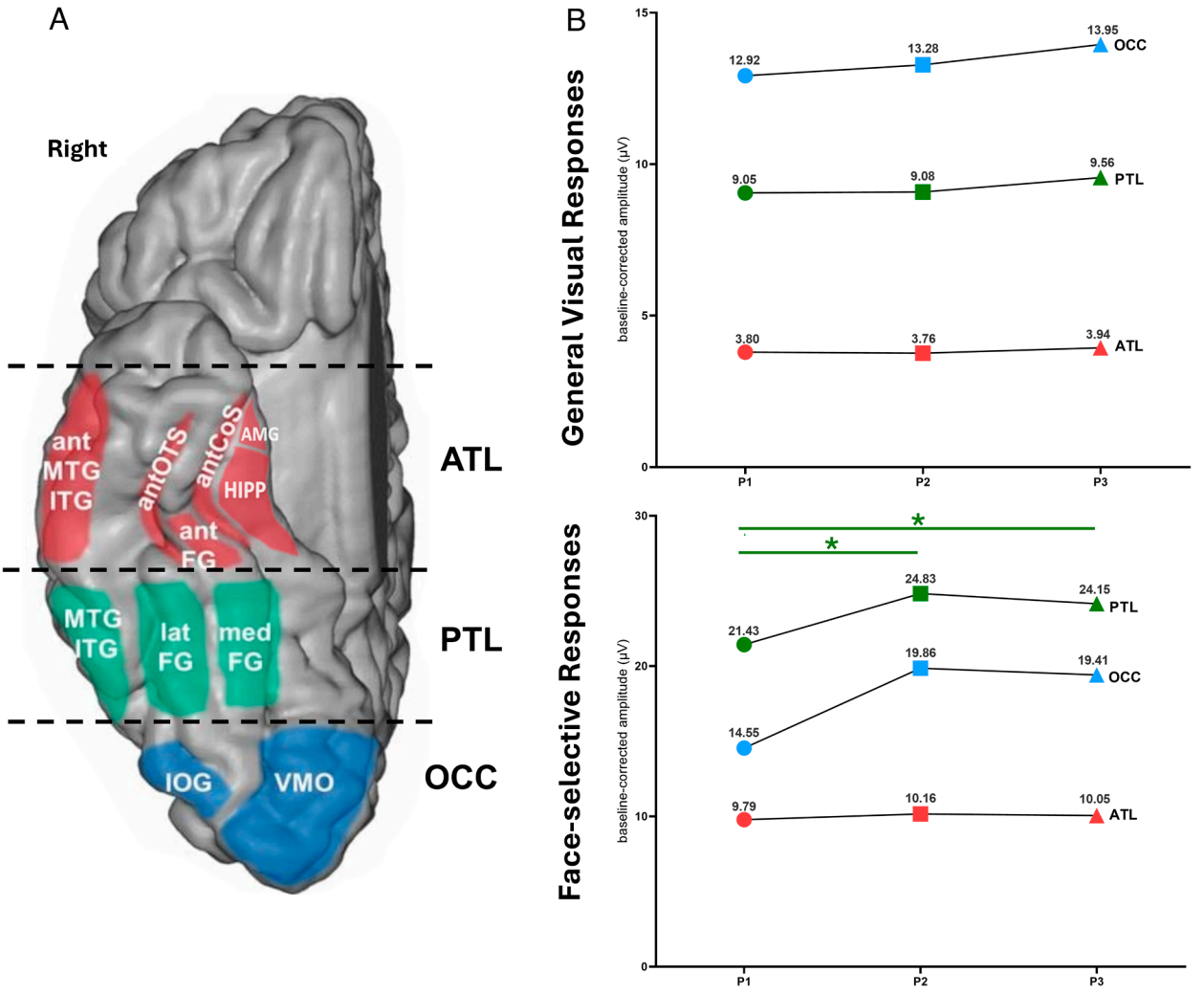

Fig. 4. Neuromodulation of iEEG general visual and face-selective in the right VOTC. (*A*) Schematic anatomical view of each brain region of interest in the right VOTC. Brain regions are depicted over the right ventral surface of the Colin27 brain, although the iEEG responses were recorded by intracerebral contacts inside these regions. Three main regions (ATL in red, PTL in green, and OCC in blue) were defined to compare the spatial neuromodulation. (*B*) Baseline corrected amplitudes (mean; µV) of the general visual and the face-selective iEEG responses in the three ROIs during the three phases. A significant difference in the baseline-corrected amplitudes of the iEEG responses was observed in the PTL during the tDCS (P2) and maintained afterward (P3) in comparison to before tDCS (P1) ($P = 0.003$ & $P = 0.015$, respectively; repeated measure ANOVA). VOTC: ventral occipito-temporal cortex, ATL: Anterior Temporal Lobe, PTL: Posterior Temporal Lobe, OCC: Occipital Lobe. Colored circles: P1 (sham, before tDCS); colored squares: P2 (active, during tDCS); colored triangles: P3 (sham, after tDCS).

inefficacy should not be interpreted as a unique single-session issue because several other parameters such as the investigated brain cognitive networks (language, memory, executive functions, …), the control conditions, and the tDCS parameters (montage, duration, and intensity) were very different from one study to another and not fully controlled. Here, our finding using robust methodology, which provides electrophysiological evidence of tDCS effects, opens insights on the link between electrophysiological and behavioral neuromodulation. Indeed, the electrophysiological changes (i.e., the amplitude increases in the different brain regions of the VOTC) observed in our study are probably not strong enough to induce behavioral changes. Nevertheless, two important points must be made. First, the absence of behavioral changes after a single-session must not lead to the conclusion that tDCS is ineffective. Second, our results show that the low, or even null, cognitive effects could be primarily related to methodological aspects i.e., too moderate neuromodulation using common tDCS parameters.

For therapeutic purposes, more long-lasting aftereffects are desirable. Animal studies indicate that repeating DC stimulation during the aftereffects of an initial session enhances its efficacy (31, 32). Nonetheless, repeated induction of plasticity might also trigger homeostatic counteracting mechanisms (33). Two options were investigated in the literature to induce long-lasting effects. First, extending the duration of stimulation or increasing its intensity, both of which have been employed in clinical settings (34–36). The alternative method to extend tDCS aftereffects is through the repetition of tDCS sessions. Empirically, repetitive tDCS has been shown to produce cumulative effects when administered once daily in humans (37, 38).

This innovative combination of tDCS with iEEG recordings will be ideally suited to investigate this additional challenge i.e., the impact of tDCS parameters (like intensity, montage, duration, and repetition) on human cognition. This tDCS-iEEG-FPVS approach should provide effective technical guidelines to enhance a specific cognitive network.

Functional Targeting and Specific Neuromodulation. Through the analysis of frequency-tagged iEEG responses, we demonstrate that tDCS has an electrophysiological impact only on face-selective responses and not on general visual iEEG responses. This finding was made possible by a FPVS paradigm providing two distinct

Downloaded from https://www.pnas.org by 92.184.124.201 on December 16, 2025 from IP address 92.184.124.201.

types of cognitive responses in the same experiment. The specificity of the neuromodulation induced by tDCS can be explained by the functional targeting of the VOTC, a region known to be critical for face processing. Since the FPVS task demands rapid (i.e., single glance) recognition of faces, the face-selective neural networks in the VOTC were more heavily engaged during the task.

This task-specific engagement of face-selective circuits likely made them more responsive to the effects of tDCS, which modulated their excitability in a task-dependent manner. In contrast, the broader visual networks involved in general visual processing were less engaged by this task, and therefore, less affected by the neuromodulation. Thus, the combined effects of functional targeting and increased neural engagement during face-selective processing could explain why tDCS specifically modulated face-selective responses with less influence on the general visual responses.

In the present study, a P10 (anode)—FT9 (return) tDCS montage was used specifically to target the right occipito-temporal cortex. The choice of the anodal P10 position was driven by previous scalp EEG studies that showed strong face-selective responses in this occipito-temporal scalp region using the same FPVS paradigm (20). Brain structures in the PTL of the VOTC were significantly impacted by tDCS but the largest amplitude neuromodulation was observed in the OCC, where face-selective activity ("occipital face area") is typically localized according to the literature (39–42) and where a high EF magnitude was observed. The lack of significance in the OCC during and after tDCS is likely due to insufficient statistical power, as there were fewer iEEG contacts in this region (clinical constraints) compared to the ATL and PTL. Considering the same range and non-null-averaged EF values observed in our different ROI (0.14 to 0.40 V/m, *SI Appendix*, Table S5), the contribution of indirect neuromodulations [i.e., physiologically evoked neuromodulations in the highly connected VOTC; (43)] cannot be observed here. Indeed, to investigate this specific question, at least one ROI with significant iEEG responses and zero EF value would exist inside the brain network. In the present study, all ROI were under the influence (more or less strongly) of the induced EFs.

The small HD ring electrodes have the advantage of allowing a precise placement over the right occipito-temporal region without touching the iEEG electrodes that need to be protected (asepsis reasons). The right occipito-temporal cortex was targeted in this experiment because it holds one of the crucial nodes of the cortical face-selective network as shown with neuroimaging [EEG: (39), TMS: (40) and fMRI: (41)] and using direct intracerebral electrical stimulations (42). This original tDCS montage, with only two small HD ring electrodes, allows for significant neuromodulation. It is evidence showing that this montage can yield effective results. Usually, small ring electrodes are used in HD-tDCS with a montage of 4 × 1 i.e., one center-anode or -cathode and four return electrodes around. In the present study, it is interesting to note that HD electrodes can also be used in a "conventional" tDCS montage with only two electrodes.

Additionally, the small HD ring electrodes were certainly the key element to precisely target face-selective responses in the IOG with a sufficient EF. Computational studies with 4 × 1 HD montage demonstrated that small ring electrodes can focus and increase the intracerebral EF on the brain target compared to a bipolar sponge montage (44).

The face-selective electrophysiological neuromodulation is also crucial and important evidence of "functional targeting" that considers that cognitive brain networks already activated by a task become more sensitive to direct constant current stimulation (45, 46). An in vitro study showed that only synapses already experiencing plasticity would be influenced by DCS, while inactive synapses remained unmodulated (47). The dependence of tDCS on brain state has been mainly investigated using noninvasive neuroimaging [e.g.: scalp EEG (48) and fMRI (49)]. Our results provide the first evidence of functional targeting in humans using intracranial EEG recordings.

In conclusion, the current evidence provided by this intracerebral investigation in humans represents the first milestone demonstrating the ability of tDCS to induce objective, selective, and significant electrophysiological effects. Using this original method of simultaneous tDCS-iEEG-FPVS, future research could address important questions to define the most effective tDCS parameters for achieving the highest electrophysiological neuromodulation and, ultimately, sustainable behavioral changes.

Materials and Methods

Participants. Eleven patients (six females; mean age: 31 ± 8 y) with focal drug-resistant epilepsy were prospectively included in this sham-controlled tDCS study. All patients provided written consent to take part in the study, which was conducted according to the principles expressed in the declaration of Helsinki and approved by a national ethics committee (Comité de Protection des Personnes Sud-Ouest et Outre Mer 4) certified by the French Ministry of Health (Institutional Review Board: IORG0009855). They were informed of the side effects of tDCS (tingling sensation, headache, etc.), and were instructed to report any discomfort during the experiment.

Their standard presurgical evaluation included neuropsychological tests and long-term (5-d period) high-resolution EEG video recordings combined with electrical source imaging analysis, positron emission tomography and high-resolution MRI. All participants had normal to corrected-to-normal vision and performed the Benton Face Recognition Test (50) before the iEEG exploration, with an average score of 43.3 ± 4.2 (10 patients had a Benton score above 39 of 54, reflecting normal performance in matching individual faces, and one patient had a score below 39 of 54, reflecting mild impairment). To identify the epileptogenic zone and the surrounding functional brain regions, patients were implanted with intracranial multicontact electrodes (iEEG) in the Epilepsy Unit of the University Hospital of Nancy. In all patients, iEEG allowed for the delineation of a single and spatially limited epileptogenic zone. Due to the right hemispheric dominance of face-perception, participants with at least one iEEG electrode implanted in the right hemisphere were included in this study.

Transcranial Electrical Stimulation. Before the tDCS experiment, a session of transcranial alternating current stimulation (0.5 mA, 2 min, 7 Hz, P10-FT9 montage) was performed to measure the EF in the different brain ROI. The EF was obtained by calculating the gradient of the voltage measured on each contact of a same iEEG electrode (for detailed information about the EF calculation, see ref. 8).

Sham-controlled anodal tDCS experiments were performed before the iEEG electrode removal (i.e., the last day of the iEEG investigation). This timing was decided to avoid tDCS aftereffects during the iEEG investigation which could influence the diagnosis (e.g., brain network instability). TDCS was performed using 2 HD-ring electrodes (12 mm external diameter; Soterix Medical®, New York, NY).

Both were inserted in an electrode-holder (24 mm diameter) filled with a conductive gel, creating a 4.52 cm^2 stimulation area on the scalp for each electrode. The impedances were measured before tDCS stimulation and were always less than or equal to 5 kΩ during the active stimulation.

According to the HD electrodes' geometry, the current densities generated on site were 0.44 $mA.cm^{-2}$ for +2 mA intensity. The stimulation was delivered through these electrodes using a multichannel TES stimulator MxN-9 (Soterix Medical®, New York, NY). To target the VOTC, the anodal electrode was placed on the P10 scalp position and the common electrode on the FT9 scalp position (51).

Two sham sessions were performed before (P1 phase) and after (P3 phase) tDCS in combination with FVPS (Fig. 5). During the sham stimulations, amplitude increased from 0 to 2 mA within the first 30 s, followed immediately by a decrease from 2 mA to 0 over the subsequent 30 s. The active anodal tDCS session (Phase 2)

Downloaded from https://www.pnas.org by 92.184.124.201 on December 16, 2025 from IP address 92.184.124.201.

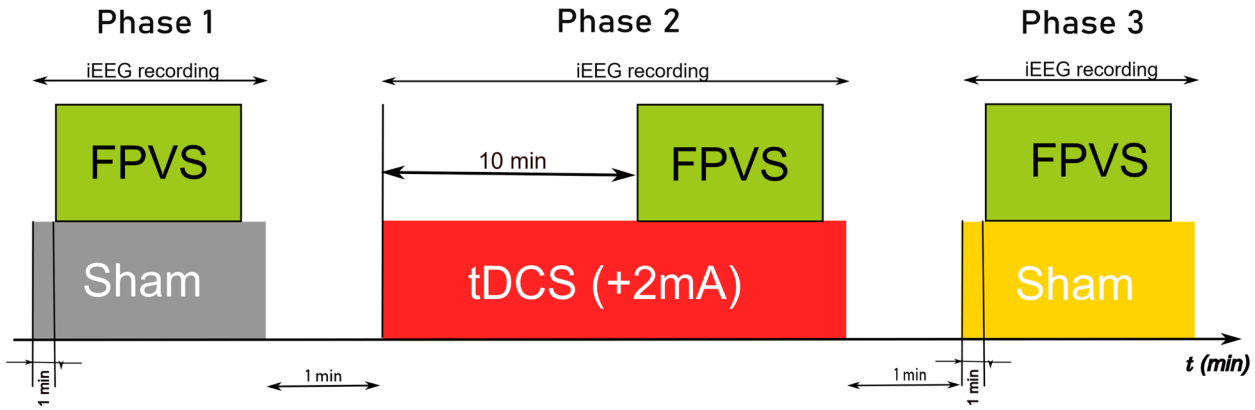

Fig. 5. Design of the study protocol with tDCS, FPVS, and iEEG. During phase 1 (P1) and phase 3 (P3) a sham-tDCS session was performed during FPVS. Between them, phase 2 (P2) was performed with 10 min of active +2 mA tDCS alone, followed by 10 min of active tDCS during FPVS. IEEG recordings recorded brain activity during the three phases.

was performed at +2 mA (P10) for 20 min (with common parameters as outlined in ref. 3. Considering that it could take from 5 to 10 min of tDCS to produce persistent changes inside the brain, FPVS started in phase P2 after 10 min of active anodal tDCS (3, 52). Consequently, the P2 session consisted of 10 min of active tDCS alone, followed by 10 min of concurrent tDCS and FPVS.

FPVS.

Stimuli. 200 natural images of various nonface objects from 14 nonface categories were used (cats, dogs, vegetables, horses, flowers, birds, fruits, phones...) in addition to 50 natural images of human faces. Each image showcased an unsegmented object or face near the center, varying in size, viewpoint, lighting, and background. All images were standardized for mean pixel luminance and contrast. The same stimuli were used by ref. 21 to find the face-selective ventral occipito-temporal map of the human brain with intracerebral potentials.

Procedure. Participants were shown continuous sequences with highly variable natural images of objects at a frequency of 6 Hz through sinusoidal contrast modulation. Highly variable natural images of faces presented periodically were presented every fifth image (i.e., at 1.2 Hz = 6/5 Hz) (Fig. 6). Participants were unaware of the periodicity of the faces. A sequence lasted 79 s, including 75 s of stimulation (i.e., 90 images of human face and 360 images of natural objects) at full contrast flanked by 2 s of fade-in and 2 s of fade-out, where contrast gradually increased or decreased, respectively. This extended duration of the sequence results in a high-frequency resolution (i.e., 71 s so 0.0141 Hz), enabling the isolation of the specific response within a narrow frequency range, significantly improving its SNR. The FPVS paradigm was repeated two times during each phase (i.e., 2 sessions * 3 phases = 6 sessions in all). Throughout the sequences, participants were directed to maintain their gaze on a persistent small blue cross positioned at the center of the stimuli. Their task was only to identify brief color changes (from blue to red) in this central fixation cross, lasting 500 ms.

Intracranial EEG.

Recording. For each patient, an individual stereotactic implantation plan was defined according to the presurgical evaluation and epileptogenic zone localization hypotheses. Under general anesthesia, the iEEG electrodes (0.8 mm-diameter, from 5 to 18 Platinum/Iridium contacts with 2 mm length separated by 1.5 mm insulator; Dixi Medical®, Besançon, France) were implanted according to a standard stereotactic procedure (53). The iEEG electrodes were inserted through a screw (2.45 mm-diameter) and secured with a tight seal to prevent cerebrospinal fluid leak. Immediately after the implantation, patients underwent a postoperative CT-scan.

Using a coregistration of the CT-scan with the preoperation high-resolution MRI (voxel-based registration; SPM 8 toolbox for Matlab; MathWorks, Natick, MA), the anatomical positions of each electrode's contacts were localized, and potential surgical complications were inspected. Due to the minimally invasive procedure used for iEEG investigation, anatomical structures were not displaced in the intracranial volume (no cerebrospinal fluid leakage and no brain swelling) and MRI-Computed Tomography coregistration can be assumed as very precise (<1 mm). IEEG signals were recorded with a 256-channel (2 × 128 channels) amplifier with a 1 kHz sampling rate (LTM256, Micromed, Mogliano, Italy). The Fpz scalp electrode was set as the reference electrode for the recording and a bipolar montage was then computed for each patient. Among 947 iEEG contacts, 67 iEEG contacts showed saturated amplitude during tDCS (Phase P2) so that they were excluded from the analysis. No significant general visual or face-selective iEEG responses were found in these contacts before the tDCS, so their exclusion did not change the results.

Anatomical localization. The 3D position of each iEEG contact was automatically detected in the individual CT-scan [60] and visually defined using patients' MRI-CT coregistration. Each individual brain was subdivided into different brain ROI using individual anatomical landmarks (i.e., gyri and sulci) instead of normalizing all brains which can blur the individuality of anatomical organization. IEEG contacts were then localized according to these brain ROI and grouped by anatomical localization across all participants. The VOTC was parcellated according

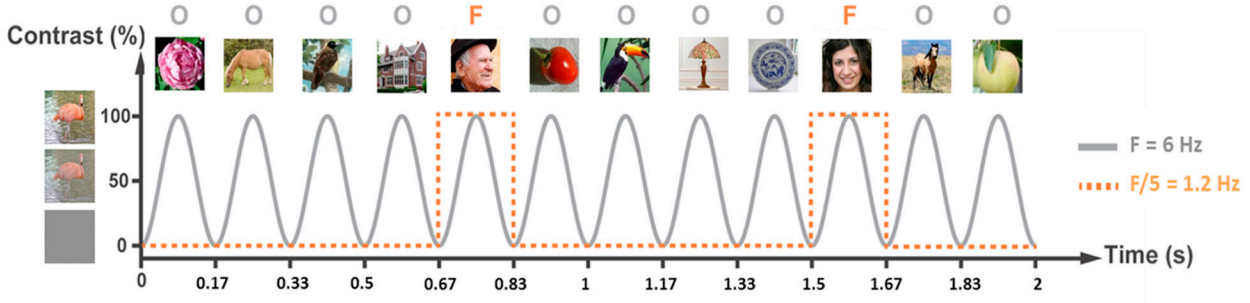

Fig. 6. FPVS used in this tDCS-iEEG experiment. Images of objects were presented by sinusoidal contrast modulation at a rate of six stimuli per second (6 Hz). In the periodic condition shown here, a different face image was presented every five stimuli (i.e., appearing at the frequency of 6/5 = 1.2 Hz). This stimulation sequence recruits ventral occipito-temporal brain regions and therefore obtains iEEG general visual and face-selective evoked responses.

Downloaded from https://www.pnas.org by 92.184.124.201 on December 16, 2025 from IP address 92.184.124.201.

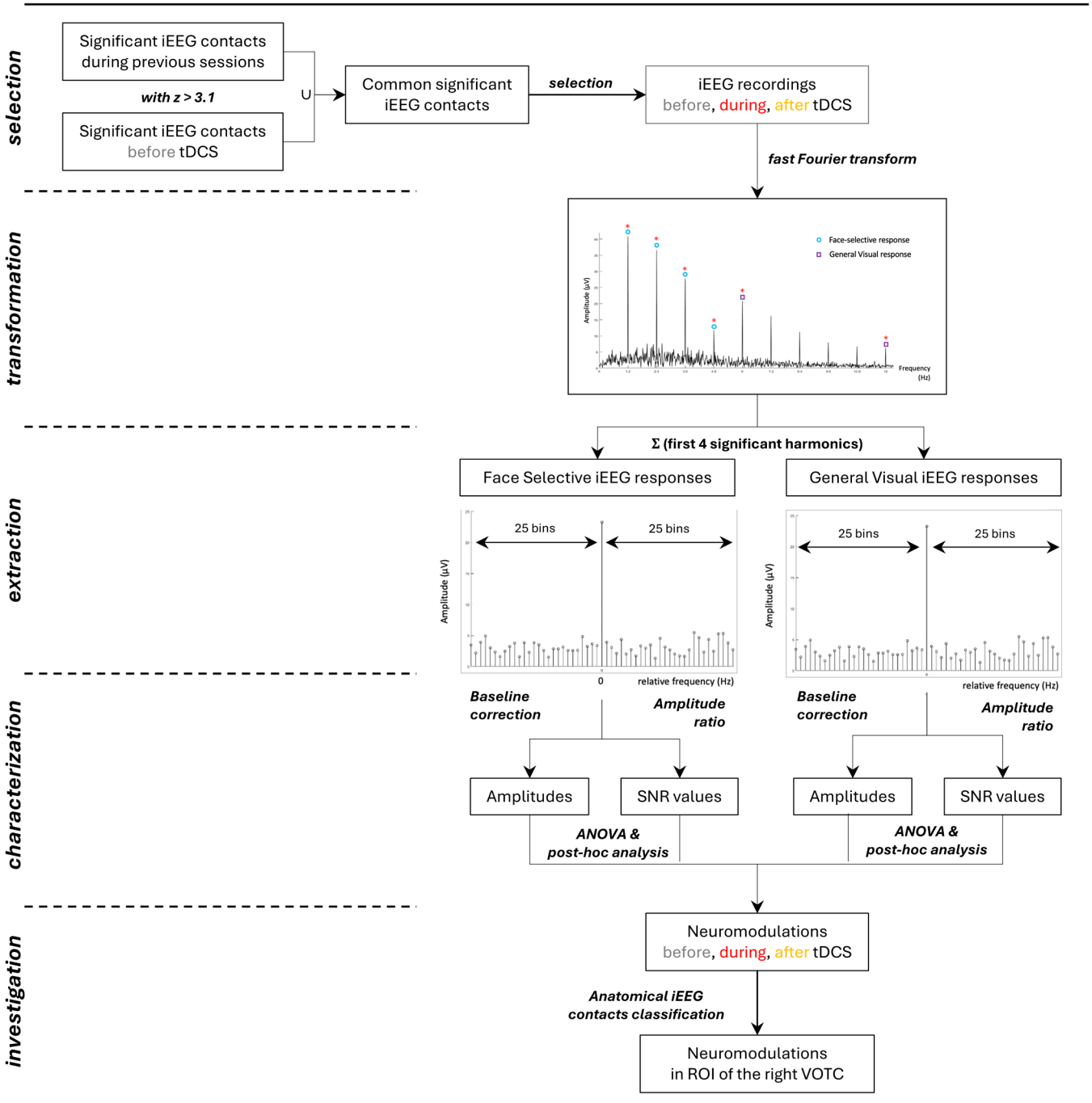

Fig. 7. Overview of the iEEG data analysis. Raw iEEG signals were analyzed in the frequency domain after FFT. A baseline correction was applied to extract the iEEG response amplitudes. SNR was also estimated. Then, ANOVA tests with post hoc comparisons were used to compare the results before, during, and after the tDCS and across the different ROI.

to the atlas of Kim et al. (54). The VOTC sulci were used as mesio-lateral landmarks (especially collateral sulcus and occipito-temporal sulcus) and MR coronal planes gave landmarks for antero-posterior brain structures.

Spectral analysis. Data segments of iEEG signals corresponding to the FPVS sequences were selected (79-s segments, −2 to +81 s) from the recordings. In our main data analyses, we refrained from conducting artifact rejection procedures since intracerebral artifacts, primarily stemming from epileptic spikes, along with electro-oculographic and electromyographic activities (attributable to our use of a prefrontal scalp electrode as the reference electrode for most patients), exhibit a more extensive distribution across the frequency spectrum compared to the specific frequencies of interest: 1.2 and 6 Hz, and their corresponding harmonics. The 79 s data segments were cropped to contain an integer number of 1.2-Hz cycles beginning 2 s after the onset of the sequence (right at the end of the fade-in period) until ∼77 s, before stimulus fade-out (90 face cycles ∼75 s). Sequences were averaged in the time domain separately for each participant. A fast Fourier transform (FFT) was applied on these averaged segments (see all raw amplitude spectrum in *SI Appendix*, Fig. S4), then the amplitude spectra were extracted for all intracerebral contacts (Fig. 7).

Extraction of iEEG evoked responses. The FPVS sessions applied in this study allows us to identify and separate two different types of iEEG responses: i) a general visual iEEG response occurring at the base stimulation frequency (6 Hz) and its harmonics, as well as ii) a face-selective iEEG response at 1.2 Hz and its harmonics. Significant face- selective responses at the face stimulation frequency (1.2 Hz) and its harmonics (2.4, 3.6 Hz, etc.) were detected by transforming the frequency spectra to z scores. The z scores were computed as the difference between amplitude at each frequency bin and the mean amplitude of the corresponding

Downloaded from https://www.pnas.org by 92.184.124.201 on December 16, 2025 from IP address 92.184.124.201.

48 surrounding bins (25 bins on each side, i.e., 50 bins, but excluding the two bins directly adjacent to the bin of interest, i.e., 48 bins) divided by the SD of amplitudes in the corresponding 48 surrounding bins. A contact was considered as face-selective if the z score of the iEEG response was >3.1 (i.e., $P < 0.001$, one-tailed: signal > noise) for at least one of the first four face-selective frequency harmonics in the periodic condition (1.2, 2.4, 3.6, or 4.8 Hz). The same procedure was performed to extract significant general visual responses at 6 Hz and its harmonics (18, 24, 30 Hz) (Fig. 7).

Characterization of iEEG evoked responses. Baseline-corrected amplitudes were calculated as the difference between the amplitude at each frequency bin and the mean of 48 corresponding surrounding bins (25 bins on each side, i.e., 50 bins, but excluding the two bins directly adjacent to the bin of interest, so, 48 bins). The general visual and the face-selective iEEG responses were then quantified at each iEEG contact as the sum of the baseline-subtracted amplitude across harmonics. Face-selective responses were quantified as the sum of the baseline-subtracted amplitudes at the face-selective frequency harmonics from the 1st until the 4th (1.2 until 4.8 Hz). General visual responses were similarly quantified by summing the amplitudes from the 1st until the 4th base frequency harmonics (six until 24 Hz). Therefore, for each iEEG contact, we obtained two amplitude values that respectively represented the overall face-selective response and the overall general visual response during each of the three phases (before, during, and after tDCS) for the condition tested. Finally, SNR spectra were calculated as the ratio between the amplitude at each frequency bin and the average of the corresponding 48 surrounding bins (Fig. 7).

Intracranial Neuromodulation Investigation.

Selection of iEEG contacts. To compare the iEEG neuromodulation before, during, and after tDCS, selective iEEG contacts (i.e., contacts that recorded iEEG evoked responses for either general or face-selective responses) were selected. To do so, during the 2 d leading up to the tDCS experiment (D-2 and D-1), two sessions of FPVS were performed without tDCS using the same paradigm as the one used in this study. The analysis of the iEEG signals during D-2 and D-1 led to the identification of a set of iEEG contacts in the right hemisphere that exhibited statistically significant general visual and face-selective responses. Due to the robustness of the FPVS approach in this protocol (20), this set of iEEG contacts was assigned to our study to compute the mean and SEM of the amplitudes and the SNR during the three phases (Fig. 7).

Neuromodulation according to the time phases. To characterize the tDCS effect over time, means and SEM baseline-corrected amplitudes and SNR of iEEG evoked responses recorded in all the contacts in the right hemisphere, and then in the VOTC. These calculations were performed for both face-selective and general visual responses during P1, P2, and P3 phases. Repeated measure ANOVA tests with post hoc comparisons were performed with the null hypothesis that tDCS has no effect on the iEEG evoked responses [i.e., no baseline-corrected amplitude (or SNR) differences between the iEEG responses] for both general and face-selective responses across the different phases of the experiment (alpha risk: 0.05) (Fig. 7).

Neuromodulation according to the anatomy. To investigate the tDCS effect on the different regions of the VTOC and therefore investigate the spatial targeting of the small ring electrodes, the VOTC was divided into three brain ROI using the anatomo-functional classification from ref. 21: ATL, anterior temporal lobe; PTL, posterior temporal lobe; OCC, occipital lobe. Means and SEM baseline-corrected amplitudes and SNR of iEEG evoked responses recorded in the contacts of the different ROI. Statistical comparisons were performed using repeated measure ANOVA tests with post hoc comparisons with the null hypothesis that intracranial neuromodulation will be the same in all ROI (Fig. 7).

Data, Materials, and Software Availability. Anonymized iEEG data (amplitude and SNR values) data have been deposited in (55).

ACKNOWLEDGMENTS. We express our deepest gratitude to the patients for their involvement in the study. M.T. was supported by a CIFRE grant (Bioserenity Company; Grant number 2021/0324) and ANR eTECH_NEURO.

Author affiliations: [a]Ingenierie Moleculaire, Cellulaire et Physiopathologie, UMR7365, CNRS and University of Lorraine, Nancy F-54000, France; [b]Epilepsy surgery unit, Neurology Department, University Hospital of Nancy, Nancy F-54000, France; [c]Epilepsy surgery unit, Neurosurgery Department, University Hospital of Nancy, Nancy F-54000, France; and [d]Bioserenity, Paris F-75013, France

1. G. Pilloni *et al.*, Tolerability and feasibility of at-home remotely supervised transcranial direct current stimulation (RS-tDCS): Single-center evidence from 6,779 sessions. *Brain Stimul.* **15**, 707–716 (2022).
2. A. J. Woods *et al.*, A technical guide to tDCS, and related non-invasive brain stimulation tools. *Clin. Neurophysiol.* **127**, 1031–1048 (2016).
3. J.-P. Lefaucheur *et al.*, Evidence-based guidelines on the therapeutic use of transcranial direct current stimulation (tDCS). *Clin. Neurophysiol.* **128**, 56–92 (2017).
4. V. Ciullo *et al.*, Transcranial direct current stimulation and cognition in neuropsychiatric disorders: Systematic review of the evidence and future directions. *Neuroscientist* **27**, 285–309 (2021).
5. J. C. Horvath, J. D. Forte, O. Carter, Evidence that transcranial direct current stimulation (tDCS) generates little-to-no reliable neurophysiologic effect beyond MEP amplitude modulation in healthy human subjects: A systematic review. *Neuropsychologia* **66**, 213–236 (2015).
6. B. L. Parkin, M. Bhandari, J. C. Glen, V. Walsh, The physiological effects of transcranial electrical stimulation do not apply to parameters commonly used in studies of cognitive neuromodulation. *Neuropsychologia* **128**, 332–339 (2019).
7. J. C. Horvath, J. D. Forte, O. Carter, Quantitative review finds no evidence of cognitive effects in healthy populations from single-session transcranial direct current stimulation (tDCS). *Brain Stimul.* **8**, 535–550 (2015).
8. S. Louviot *et al.*, Transcranial electrical stimulation generates electric fields in deep human brain structures. *Brain Stimul.* **15**, 1–12 (2022).
9. S. K. Kho, D. Keeble, H. K. Wong, A. J. Estudillo, Null effect of anodal and cathodal transcranial direct current stimulation (tDCS) on own- and other-race face recognition. *Soc. Neurosci.* **18**, 393–406 (2023), 10.1080/17470919.2023.2263924.
10. M. L. Willis, A. I. Costantino, M. A. Nitsche, R. Palermo, D. Rivolta, Anodal tDCS and high-frequency tRNS targeting the occipitotemporal cortex do not always enhance face perception. *Front. Neurosci.* **13**, 78 (2019).
11. N. Gebodh *et al.*, Inherent physiological artifacts in EEG during tDCS. *Neuroimage* **185**, 408–424 (2019).
12. M. Mancini *et al.*, Automatic artifact suppression in simultaneous tDCS-EEG using adaptive filtering. *Annu. Int. Conf. IEEE Eng. Med. Biol. Soc.* **2015**, 2729–2732 (2015).
13. P. Faria, F. Fregni, F. Sebastião, A. I. Dias, A. Leal, Feasibility of focal transcranial DC polarization with simultaneous EEG recording: Preliminary assessment in healthy subjects and human epilepsy. *Epilepsy Behav.* **25**, 417–425 (2012).
14. D. W. Kim, E. Kim, C. Lee, C. H. Im, Can anodal transcranial direct current stimulation increase steady-state visual evoked potential responses? *J. Korean Med. Sci.* **34**, e285 (2019).
15. C. Civile *et al.*, Testing the effects of transcranial direct current stimulation (tDCS) on the face inversion effect and the N170 event-related potentials (ERPs) component. *Neuropsychologia* **143**, 107470 (2020).
16. B. Rossion, Understanding individual face discrimination by means of fast periodic visual stimulation. *Exp. Brain Res.* **232**, 1599–1621 (2014).
17. J. Liu-Shuang, A. M. Norcia, B. Rossion, An objective index of individual face discrimination in the right occipito-temporal cortex by means of fast periodic oddball stimulation. *Neuropsychologia* **52**, 57–72 (2014).
18. L. Koessler *et al.*, Catching the invisible: Mesial temporal source contribution to simultaneous EEG and SEEG recordings. *Brain Topogr.* **28**, 5–20 (2015).
19. B. Rossion, C. Jacques, J. Jonas, Intracerebral electrophysiological recordings to understand the neural basis of human face recognition. *Brain Sci.* **13**, 354 (2023).
20. B. Rossion, K. Torfs, C. Jacques, J. Liu-Shuang, Fast periodic presentation of natural images reveals a robust face-selective electrophysiological response in the human brain. *J. Vision* **15**, 18 (2015).
21. J. Jonas *et al.*, A face-selective ventral occipito-temporal map of the human brain with intracerebral potentials. *Proc. Natl. Acad. Sci. U.S.A.* **113**, E4088–E4097 (2016).
22. A. Puce, T. Allison, J. C. Gore, G. McCarthy, Face-sensitive regions in human extrastriate cortex studied by functional MRI. *J. Neurophysiol.* **74**, 1192–1199 (1995).
23. A. Volfart *et al.*, Typical visual unfamiliar face individuation in left and right mesial temporal epilepsy. *Neuropsychologia* **147**, 107583 (2020).
24. J.-P. Lefaucheur, A comprehensive database of published tDCS clinical trials (2005–2016). *Neurophysiol. Clin.* **46**, 319–398 (2016).
25. M. A. Nitsche, M. Bikson, Extending the parameter range for tDCS: Safety and tolerability of 4 mA stimulation. *Brain Stimul.* **10**, 541–542 (2017).
26. M. Alam, D. Q. Truong, N. Khadka, M. Bikson, Spatial and polarity precision of concentric high-definition transcranial direct current stimulation (HD-tDCS). *Phys. Med. Biol.* **61**, 4506–4521 (2016).
27. A. Pisoni, P. R. Sperandeo, L. J. Romero Lauro, C. Papagno, The role of the left and right anterior temporal poles in people naming and recognition. *Neuroscience* **440**, 175–185 (2020).
28. M. Gonzalez-Perez, E. Wakui, V. Thoma, M. A. Nitsche, D. Rivolta, Transcranial alternating current stimulation (tACS) at 40 Hz enhances face and object perception. *Neuropsychologia* **135**, 107237 (2019).
29. M. A. Nitsche, W. Paulus, Sustained excitability elevations induced by transcranial DC motor cortex stimulation in humans. *Neurology* **57**, 1899–1901 (2001).
30. M. A. Nitsche *et al.*, Level of action of cathodal DC polarization induced inhibition of the human motor cortex. *Clin. Neurophysiol.* **114**, 600–604 (2003).
31. L. J. Bindman, O. C. J. Lippold, J. W. T. Redfearn, The action of brief polarizing currents on the cerebral cortex of the rat (1) during current flow and (2) in the production of long-lasting after-effects. *J. Physiol.* **172**, 369–382 (1964).
32. I. B. Gartside, Mechanisms of sustained increases of firing rate of neurons in the rat cerebral cortex after polarization: Reverberating circuits or modification of synaptic conductance? *Nature* **220**, 382–383 (1968).
33. H. R. Siebner *et al.*, Preconditioning of low-frequency repetitive transcranial magnetic stimulation with transcranial direct current stimulation: Evidence for homeostatic plasticity in the human motor cortex. *J. Neurosci.* **24**, 3379–3385 (2004).
34. R. Ferrucci *et al.*, Transcranial direct current stimulation in severe, drug-resistant major depression. *J. Affect. Disord.* **118**, 215–219 (2009).

Downloaded from https://www.pnas.org by 92.184.124.201 on December 16, 2025 from IP address 92.184.124.201.

35. F. Fregni *et al.*, A randomized, sham-controlled, proof of principle study of transcranial direct current stimulation for the treatment of pain in fibromyalgia. *Arthritis Rheum.* **54**, 3988–3998 (2006).
36. S. H. Ohn *et al.*, Time-dependent effect of transcranial direct current stimulation on the enhancement of working memory. *Neuroreport* **19**, 43–47 (2008).
37. P. S. Boggio *et al.*, Repeated sessions of noninvasive brain DC stimulation is associated with motor function improvement in stroke patients. *Restor. Neurol. Neurosci.* **25**, 123–129 (2007).
38. K. Monte-Silva, M.-F. Kuo, D. Liebetanz, W. Paulus, M. A. Nitsche, Shaping the optimal repetition interval for cathodal transcranial direct current stimulation (tDCS). *J. Neurophysiol.* **103**, 1735–1740 (2010).
39. C. Jacques *et al.*, The inferior occipital gyrus is a major cortical source of the face-evoked N170: Evidence from simultaneous scalp and intracerebral human recordings. *Hum. Brain Mapp.* **40**, 1403–1418 (2019).
40. D. Pitcher, V. Walsh, G. Yovel, B. Duchaine, TMS evidence for the involvement of the right occipital face area in early face processing. *Curr. Biol.* **17**, 1568–1573 (2007).
41. J. Liu, A. Harris, N. Kanwisher, Perception of face parts and face configurations: An fMRI study. *J. Cogn. Neurosci.* **22**, 203–211 (2010).
42. J. Jonas *et al.*, Intracerebral electrical stimulation of a face-selective area in the right inferior occipital cortex impairs individual face discrimination. *NeuroImage* **99**, 487–497 (2014).
43. L. Angelini *et al.*, Bidirectional and cross-hemispheric modulations of face-selective neural activity induced by electrical stimulation within the human cortical face network. *Brain Sci.* **14**, 906 (2024).
44. M. F. Villamar *et al.*, Technique and considerations in the use of 4x1 ring high-definition transcranial direct current stimulation (HD-tDCS). *J. Vis. Exp.* **77**, e50309 (2013), 10.3791/50309.
45. M. Bikson, A. Rahman, Origins of specificity during tDCS: Anatomical, activity-selective, and input-bias mechanisms. *Front. Hum. Neurosci.* **7**, 688 (2013).
46. C. Bradley, A. S. Nydam, P. E. Dux, J. B. Mattingley, State-dependent effects of neural stimulation on brain function and cognition. *Nat. Rev. Neurosci.* **23**, 459–475 (2022).
47. G. Kronberg, M. Bridi, T. Abel, M. Bikson, L. C. Parra, Direct current stimulation modulates LTP and LTD: Activity dependence and dendritic effects. *Brain Stimul.* **10**, 51–58 (2017).
48. M. Petti *et al.*, Transcranial cerebellar direct current stimulation: Effects on brain resting state oscillatory and network activity. *Annu. Int. Conf. IEEE Eng. Med. Biol. Soc.* **2017**, 4359–4362 (2017).
49. L. M. Li *et al.*, Brain state and polarity-dependent modulation of brain networks by transcranial direct current stimulation. *Hum. Brain Mapp.* **40**, 904–915 (2018).
50. B. Rossion, C. Michel, Normative accuracy and response time data for the computerized Benton Facial Recognition Test (BFRT-c). *Behav. Res. Methods* **50**, 2442–2460 (2018).
51. L. Koessler *et al.*, Automated cortical projection of EEG sensors: Anatomical correlation via the International 10–10 system. *Neuroimage* **46**, 64–72 (2009).
52. M. Barbieri, M. Negrini, M. A. Nitsche, D. Rivolta, Anodal-tDCS over the human right occipital cortex enhances the perception and memory of both faces and objects. *Neuropsychologia* **81**, 238–244 (2016).
53. A. L. Salado *et al.*, sEEG is a safe procedure for a comprehensive anatomic exploration of the insula: A retrospective study of 108 procedures representing 254 transopercular insular electrodes. *Oper. Neurosurg.* **14**, 1–8 (2018).
54. J. J. Kim *et al.*, An MRI-based parcellation method for the temporal lobe. *Neuroimage* **11**, 271–288 (2000).
55. M. Tabikh *et al.*, Data from "Intracranial evoked EEG activities recorded before, during and after tDCS in humans." Mendeley Data. https://doi.org/10.17632/25z97kkndg.1. Deposited 19 May 2025.

Downloaded from https://www.pnas.org by 92.184.124.201 on December 16, 2025 from IP address 92.184.124.201.